



This is to certify that the

dissertation entitled

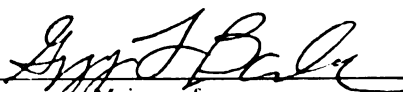
**SYNTHESIS, MODELING AND CHARACTERIZATION OF
ETHYLENE OXIDE-SEGMENTED MICROBLOCK
COPOLYMERS**

presented by

Yiyan Chen

has been accepted towards fulfillment
of the requirements for

Ph. D. degree in Chemistry


Major professor

Date 8/18/99

LIBRARY
Michigan State
University

PLACE IN RETURN BOX to remove this checkout from your record.
TO AVOID FINES return on or before date due.
MAY BE RECALLED with earlier due date if requested.

DATE DUE	DATE DUE	DATE DUE
<hr/>	<hr/>	<hr/>
<hr/>	<hr/>	<hr/>
<hr/>	<hr/>	<hr/>
<hr/>	<hr/>	<hr/>
<hr/>	<hr/>	<hr/>

SYNTHESIS.
ETHYLENE OXIDE

In p

**SYNTHESIS, MODELING AND CHARACTERIZATION OF
ETHYLENE OXIDE-SEGMENTED MICROBLOCK COPOLYMERS**

By

Yiyan Chen

A DISSERTATION

Submitted to
Michigan State University
In partial fulfillment of the requirements
for the degree of

DOCTOR OF PHILOSOPHY

Department of Chemistry

1999

We synthesized a
A block is either an
containing a single dou
polyethylene oxide (PEO)
hydrophilic. The polymer
alkenyl-substituted
length is 98,000. Different
the length of PEO segment
PEO segments become
of crystallization and m
polymer segments, the p
systems.

To understand the
the generic structure
parts of the model com
depends with odd vari

ABSTRACT

SYNTHESIS, MODELING AND CHARACTERIZATION OF ETHYLENE OXIDE- SEGMENTED MICROBLOCK COPOLYMERS

By

Yiyan Chen

We synthesized and characterized a series of $(AB)_n$ microblock copolymers where the A block is either an exact length linear alkyl segment or a linear alkyl segment containing a single double bond, and the B block is an exact length segment of polyethylene oxide (PEO). Thus the A block is hydrophobic, and the B block is hydrophilic. The polymers were prepared in high yields by metathesis polymerization of α,ω -alkenyl-substituted PEOs. The polymers had number average molecular weights as high as 98,000. Differential scanning calorimetry shows that the polymer T_g s increase as the length of PEO segments increase when PEO segments is short, and level off when PEO segments become longer. Above T_g , the polymers exhibit a complicated sequence of crystallization and melting transitions. Because of the amphiphilic nature of the polymer segments, the polymers have good solubility in a variety of polar and nonpolar solvents.

To understand the properties of the $(AB)_n$ polymers, a series of model compounds with the generic structure $H(CH_2)_x(OCH_2CH_2)_yO(CH_2)_xH$ were synthesized. The melting points of the model compounds show an odd-even effect when $x \leq 12$ and $y \leq 6$, with compounds with odd values of y having higher melting points than oligomers with even

ness of γ . This effect

appears in the oligomer

compounds when ethylene

enhance the PEO segment

compounds for study the

We also found that

are two kinds of structure

stable, and another has

long alkyl chains. Most

relation of crystallization

from zigzag conformation

derived from melt crystallization

of helical conformation

Other analogs can also

be a strategy for incorporating

long segment lengths to

systems can be expected

structure as the parent poly

values of y . This effect can be traced to a planar trans conformation for the PEO segments in the oligomers. Unsaturated polymers follow the same trend as the model compounds when ethylene oxide segment is short while saturated polymers follow the trend once the PEO segment is ≥ 3 , which validates the use of these compounds as model compounds for study the polymers.

We also found that crystalline model compounds with seven ethylene oxide units have two kinds of structures: an extended planar zigzag form throughout the whole molecule, and another having a helical ethylene oxide segment flanked by two planar zigzag alkyl chains. More importantly, these conformations can be controlled by the selection of crystallization method. Samples crystallized from polar solvents give the planar zigzag conformation while samples crystallized from nonpolar solvent or fast quenched from melt crystallize in a structure with planar conformations for alkyl chains and a helical conformation for ethylene oxide segment. The structures of the saturated polymer analogs can also be manipulated in the similar manner. This result points to a general strategy for incorporating stable crystalline polymer sub-units into materials. By using segment lengths that correspond to multiples of the polymer unit cell, such segments can be expected to self-assemble into crystalline sub-units that have the same structure as the parent polymer.

To my family

I wish to express

gratitude assistance thro

academic mentor and a g

would also like to thank

Chia-Kong Chang and Ke

Bar group members: Ju

Ma Mao Gao, Micah, C

zifan for making my S

I also enjoyed the

summer skiing and snow

trough only once a year.

supporting me throughout

I want to thank m

Kevin Fakai Chen for his

help my parents (withou

the degree), my brother

arrangement.

ACKNOWLEDGEMENTS

I wish to express my deep appreciation to Professor Gregory L. Baker for his guidance, assistance throughout the course of this research. He has been an excellent academic mentor and a good friend, to whom I can always consult on a lot of issues. I would also like to thank Professor Babak Borhan, Thomas Pinnavaia, Gary Blanchard, Chi-Kwong Chang and Kris Berglund for their guidance and assistance. My thanks to all Baker group members: Jun Qiao (my big Shi1 Xong1), Jun Hou, Jingpin, Sue, Cory, Tara, Mao, Gao, Micah, Chun, JB, Tianqi, Kirk (sorry to leave you so much work), Erin and Fadi for making my 5 years stay in the lab a memorable one.

I also enjoyed the life in Michigan — friendly people, cold winter and cool summer (skiing and swimming), good environment (fishing, gardening, golfing — though only once a year). I like to thank the Department of Chemistry for continuously supporting me throughout the graduate study.

I want to thank my wife Yi for her constant love and support, my naughty son Kevin Fakai Chen for his sacrifice to be away from parents at his very young age. I thank my parents (without your push, I don't know when I would finally start to pursue this degree), my brother and my parents in law for their love, expectation and encouragement.

LIST OF FIGURES

LIST OF SCHEMES.....

LIST OF TABLES

INTRODUCTION.....

I. General

II. Block copolymer pr

1. Phase separation a

2. Crystallization of

III. Multiple thermal tra

1. General phase sep

2. Lamellae thicken

3. Polymorphism.....

IV. Synthesis of (AB)_n

1. Chain polymeriza

2. Ionic living polym

3. Step copolymeriza

4. Metathesis polym

5. Comparison of d
copolymers.....

V. Target molecules in

TABLE OF CONTENTS

LIST OF FIGURES	x
LIST OF SCHEMES.....	xvii
LIST OF TABLES	xix
INTRODUCTION.....	1
I. General	1
II. Block copolymer properties	3
1. Phase separation and morphology.....	3
2. Crystallization of polymers.....	13
III. Multiple thermal transitions for polymers.....	17
1. General phase separated cases	18
2. Lamellae thickening and thinning.....	20
3. Polymorphism	22
IV. Synthesis of (AB) _n block Copolymers	26
1. Chain polymerization.....	26
2. Ionic living polymerization.....	32
3. Step copolymerization.....	36
4. Metathesis polymerization	38
5. Comparison of different polymerization methods for obtaining (AB) _n copolymers.....	47
V. Target molecules in this research	48

VI Several polymers

1. Polyethylene and

2. C₆E₅ nonionic su

3. Microblock copolymers
polyethylene

4. Fluorocarbon-hy

RESULTS

I. Synthesis and purification

1. Acronyms for the

2. Exact length oligomers

3. Triblock amphiphilic

4. Monomers

5. Polymers

II. Properties of triblock

1. Thermal behavior

2. Powder X-ray diffraction

3. Spectroscopic characterization

III. Properties of unsaturated

1. Physical properties

2. Morphologies of unsaturated

3. Spectroscopic characterization

4. Thermal behavior of unsaturated

5. XRD of unsaturated

IV. Properties of saturated

1. Physical properties

VI. Several polymers directly related to this project	50
1. Polyethylene and polyethylene oxide	50
2. C_xE_y nonionic surfactants and $C_xEO_yC_x$ amphiphilic triblock oligomers.....	55
3. Microblock copolymers containing oligothioethylene, oligoethylene and oligooxyethylene	59
4. Fluorocarbon-hydrocarbon microblock copolymers.....	63
RESULTS.....	68
I. Synthesis and purification	68
1. Acronyms for the compounds in this research.....	68
2. Exact length oligoethylene glycols	69
3. Triblock amphiphilic oligomers—model compounds	71
4. Monomers	72
5. Polymers.....	76
II. Properties of triblock oligomers $C_xEO_yC_x$	80
1. Thermal behavior	80
2. Powder X-ray diffraction	97
3. Spectroscopic characterizations	115
III. Properties of unsaturated $(AB)_n$ microblock copolymers $(C_x\pi C_xEO_y)_n$	122
1. Physical properties	122
2. Morphologies of unsaturated polymers.....	124
3. Spectroscopic characterizations	130
4. Thermal behavior of the unsaturated polymers.....	132
5. XRD of unsaturated polymers.....	147
IV. Properties of saturated $(AB)_n$ polymers $(C_xEO_y)_n$	153
1. Physical properties	153

2. Morphology of s
3. Thermal behavior
4. Spectroscopic char
5. XRD results for s

DISCUSSION

I. Synthesis and purifi

1. Synthesis of exac
2. Monomer purifica
3. Polarity changes

II. Structure and proper

1. ABA oligomers C
2. ABA oligomers C
3. ABA oligomers C
4. Melting trends and

III. Structure and proper

1. Melting point trend
2. Polymer structure c
3. Multiple thermal tr

IV. Comparison to other

EXPERIMENTAL

1. General details

1. Thermal characteriz
2. Solvents

2. Morphology of saturated polymers	154
3. Thermal behavior of the saturated polymers.....	158
4. Spectroscopic characterization.....	166
5. XRD results for saturated polymers.....	168
DISCUSSION	171
I. Synthesis and purification	171
1. Synthesis of exact length ethylene glycols	171
2. Monomer purification	173
3. Polarity changes of the compounds in this research	174
4. Polymerization details.....	179
II. Structure and properties of triblock oligomers.....	183
1. ABA oligomers $C_xEO_yC_x$ with $y \leq 6$	183
2. ABA oligomers $C_xEO_yC_x$ with $y = 7$	184
3. ABA oligomers $C_xEO_yC_x$ with $y > 7$	195
4. Melting trends and odd-even effects in triblock oligomers	199
III. Structure and properties of $(AB)_n$ microblock copolymers.....	205
1. Melting point trend compared to the triblock oligomers	205
2. Polymer structure controls	207
3. Multiple thermal transitions of the polymers.....	213
IV. Comparison to other structurally similar $(AB)_n$ copolymers.....	214
EXPERIMENTAL	217
I. General details.....	217
1. Thermal characterization of model compounds and polymers	218
2. Solvents.....	219

3. Argon

4. Sodium mirrors

5. Celite and alumina

II. Synthesis of chemical compounds

1. Synthesis of ethyl acetate

2. Ethylene glycol

3. Exact length ethyl acetate

4. Model compounds

5. General procedures

6. Schrock's molybdenum

7. General procedures

8. General procedures

III. Number of compounds

APPENDIX

BIBLIOGRAPHY

3. Argon	220
4. Sodium mirrors	220
5. Celite and alumina packed funnel for monomer purification	221
II. Synthesis of chemicals in this project	221
1. Synthesis of ethylene glycol oligomer ditosylates	221
2. Ethylene glycol oligomer monotritylates and ditritylates	223
3. Exact length ethylene glycol oligomers	226
4. Model compound syntheses	228
5. General procedure for monomer syntheses and purification	236
6. Schrock's molybdenum catalyst	242
7. General procedure for the synthesis of ethylene oxide-segmented polymers....	243
8. General procedure for preparation of saturated polymers	249
III. Number of compounds	251
APPENDIX	252
BIBLIOGRAPHY	277

Figure 1. Morphologies

Figure 2. Schematic phase

Figure 3. Morphology n

Figure 4. PEO crystallize

Figure 5. Structures of p

Figure 6. Solid state struc

Figure 7. Conformation o

Figure 8. Structures of d

Figure 9. Solid state pac

Figure 10. Monomer pur

Figure 11. DSC heating

Figure 12. DSC heating

Figure 13. DSC heating

Figure 14. DSC heating

Figure 15. DSC heating

Figure 16. DSC heating

Figure 17. DSC heating

Figure 18. Types of DSC

Figure 19. Melting point

Figure 20. DSC heating

Figure 21. DSC heating

the indicated time.....

LIST OF FIGURES

Figure 1. Morphologies of block copolymers	5
Figure 2. Schemetic phase diagram of a typical block copolymer.....	5
Figure 3. Morphology model of thermoplastic rubber	9
Figure 4. PEO crystallized with integer chain folding at different temperature	16
Figure 5. Structures of polyethylene oxide and linear polyethylene	52
Figure 6. Solid state structure of surfactants C_xEO_y	58
Figure 7. Conformation of triblock oligomer $C_{10}ES_2C_{10}$	62
Figure 8. Structures of diblock oligomers F_nH_m	62
Figure 9. Solid state packing of polymer $(CH_2CH_2CF_2CF_2)_n$	67
Figure 10. Monomer purification set-up	75
Figure 11. DSC heating and cooling scans of triblock oligomer $C_{14}EO_3C_{14}$	82
Figure 12. DSC heating scans of triblock oligomers $C_6EO_yC_6$	83
Figure 13. DSC heating scans of triblock oligomers $C_8EO_yC_8$	84
Figure 14. DSC heating scans of triblock oligomers $C_{10}EO_yC_{10}$	85
Figure 15. DSC heating scans of triblock oligomers $C_{12}EO_yC_{12}$	86
Figure 16. DSC heating scans of triblock oligomers $C_{14}EO_yC_{14}$	87
Figure 17. DSC heating scans of triblock oligomers $C_{16}EO_yC_{16}$	88
Figure 18. Types of DSC endotherm peaks seen for triblock oligomers	89
Figure 19. Melting point and heat of fusion measured by DSC.....	89
Figure 20. DSC heating scans of triblock oligomers $C_xEO_7C_x$	94
Figure 21. DSC heating scans of triblock oligomers $C_{14}EO_7C_{14}$ annealed at 35 °C for the indicated time.....	95

Figure 22. DSC heating
different solutions...

Figure 23. Low angle X

Figure 24. Wide angle X

Figure 25. Low angle p

Figure 26. Wide angle p

Figure 27. Low angle p

Figure 28. Wide angle p

Figure 29. Low angle p

Figure 30. Wide angle p
methods.....

Figure 31. Low angle p
Crystal obtained by fl.
the periods of time as

Figure 32. Wide angle p
Crystal obtained by fl.
the periods of time as

Figure 33. Low angle p
crystallization at 41.5

Figure 34. Wide angle p
crystallization at 41.5
stored at room temper

Figure 35. Powder XRD

Figure 36. IR spectrum o

Figure 37. IR spectra of (

Figure 38. Raman spectra
methanol (top).....

Figure 39. Raman spectra
cell and stored at room
indicated in the figure

Figure 22. DSC heating scans of triblock oligomers $C_{14}EO_7C_{14}$ crystallized from different solutions.	96
Figure 23. Low angle XRD for $C_{16}EO_3C_{16}$	98
Figure 24. Wide angle XRD for $C_{16}EO_3C_{16}$	99
Figure 25. Low angle powder XRD of triblock oligomers $C_{14}EO_yC_{14}$	100
Figure 26. Wide angle powder XRD of triblock oligomers $C_{14}EO_yC_{14}$	101
Figure 27. Low angle powder XRD of triblock oligomers $C_xEO_{14}C_x$	102
Figure 28. Wide angle powder XRD of triblock oligomers $C_xEO_{14}C_x$	103
Figure 29. Low angle powder XRD of $C_{14}EO_7C_{14}$ crystallized by different methods.	108
Figure 30. Wide angle powder XRD of $C_{14}EO_7C_{14}$ crystallized by different methods.....	109
Figure 31. Low angle powder XRD of $C_{14}EO_7C_{14}$ crystallized by different methods. Crystal obtained by flash quenching from melt, then holding at room temperature for the periods of time as indicated.	110
Figure 32. Wide angle powder XRD of $C_{14}EO_7C_{14}$ crystallized by different methods. Crystal obtained by flash quenching from melt, then holding at room temperature for the periods of time as indicated.	111
Figure 33. Low angle powder XRD of $C_{14}EO_7C_{14}$ crystals obtained by isothermal crystallization at 41.5 °C.	112
Figure 34. Wide angle powder XRD of $C_{14}EO_7C_{14}$ crystals obtained by isothermal crystallization at 41.5 °C. Bottom: crystal tested right after obtained, Top: crystal stored at room temperature for two months.....	113
Figure 35. Powder XRD evolution of $C_{14}EO_7C_{14}$ annealed at 35°C.....	114
Figure 36. IR spectrum of $C_{14}EO_3C_{14}$	117
Figure 37. IR spectra of $C_{14}EO_7C_{14}$ crystallized from hexanes (bottom) and methanol (top) solutions.	118
Figure 38. Raman spectra of $C_{14}EO_7C_{14}$ crystallized from hexanes (bottom) and methanol (top).....	119
Figure 39. Raman spectra of $C_{14}EO_7C_{14}$. Samples were obtained by quenching from the melt, and stored at room temperature. Spectra were taken at the time intervals indicated in the figure.	120

Figure 40. Raman spectra of the melt, and stored melt, indicated in the figure.

Figure 41. Micrographs of cross-polarized light.

Figure 42. Micrographs of cross-polarized light.

Figure 43. Micrographs of cross-polarized light.

Figure 46. Micrographs.

Figure 44. Micrographs of $(C_8\pi C_8EO)_{10}$ in polarized light.

Figure 45. Micrographs of $(C_8\pi C_8EO)_{14}$ in polarized light.

Figure 47. Low frequency different methods.

Figure 48. DSC heating melt.

Figure 49. DSC heating melt.

Figure 50. DSC heating melt.

Figure 51. DSC heating melt.

Figure 52. DSC heating histories.

Figure 53. DSC heating histories.

Figure 54. DSC heating histories.

Figure 40. Raman spectra of $C_{14}EO_{14}C_{14}$. Samples were obtained by quenching from the melt, and stored at room temperature. Spectra were taken at the time intervals indicated in the figure.	121
Figure 41. Micrographs of polymers $(C_8\pi C_8EO_6)_n$ (left) and $(C_9\pi C_9EO_6)_n$ (right) under cross-polarized light	126
Figure 42. Micrographs of polymers $(C_8\pi C_8EO_7)_n$ (left) and $(C_9\pi C_9EO_7)_n$ (right) under cross-polarized light	126
Figure 43. Micrographs of polymers $(C_8\pi C_8EO_8)_n$ (left) and $(C_9\pi C_9EO_8)_n$ (right) under cross-polarized light	127
Figure 46. Micrographs of polymers $(C_8\pi C_8EO_7)_n$ under non-crosspolarized light. ...	127
Figure 44. Micrographs of polymers $(C_3\pi C_3EO_{10})_n$ (upper left), $(C_4\pi C_4EO_{10})_n$ (upper right), $(C_8\pi C_8EO_{10})_n$ (lower left), and $(C_9\pi C_9EO_{10})_n$ (lower right) under cross-polarized light.	128
Figure 45. Micrographs of polymers $(C_3\pi C_3EO_{14})_n$ (upper left), $(C_4\pi C_4EO_{14})_n$ (upper right), $(C_8\pi C_8EO_{14})_n$ (lower left), and $(C_9\pi C_9EO_{14})_n$ (lower right) under cross-polarized light.	129
Figure 47. Low frequency region IR for polymer $(C_9\pi C_9EO_7)_n$ crystallized using different methods.	131
Figure 48. DSC heating scans of polymer $(C_3\pi C_3EO_7)_n$ after flash quenched from the melt.	135
Figure 49. DSC heating scans of polymer $(C_4\pi C_4EO_7)_n$ after flash quenched from the melt.	136
Figure 50. DSC heating scans of polymer $(C_8\pi C_8EO_7)_n$ after flash quenched from the melt.	137
Figure 51. DSC heating scans of polymer $(C_9\pi C_9EO_7)_n$ after flash quenched from the melt.	138
Figure 52. DSC heating scans of polymer $(C_3\pi C_3EO_6)_n$ with different crystallization histories.....	139
Figure 53. DSC heating scans of polymer $(C_3\pi C_3EO_7)_n$ with different crystallization histories.....	140
Figure 54. DSC heating scans of polymer $(C_3\pi C_3EO_8)_n$ with different crystallization histories.....	141

Figure 55. DSC heating
histories.....

Figure 56. DSC heating
histories.....

Figure 57. DMA and D
are DMA results for

Figure 58. Low angle X
crystallization condi

Figure 59. Wide angle X
crystallization condi

Figure 60. DSC of poly
quenched from the m
were performed.....

Figure 61. XRD of poly

Figure 62. Micrographs
polarized light.....

Figure 63. Micrographs o
different band widths

Figure 64. Micrographs o
($C_{12}EO_{14}$)_n (lower left

Figure 65. DSC heating s

Figure 66. DSC heating s
histories.....

Figure 67. DSC heating s
histories.....

Figure 68. DSC heating s
histories.....

Figure 69. DSC heating s
histories.....

Figure 70. DSC heating s
histories.....

Figure 71. IR spectra of p

Figure 55. DSC heating scans of polymer $(C_3\pi C_3EO_{10})_n$ with different crystallization histories.....	142
Figure 56. DSC heating scans of polymer $(C_3\pi C_3EO_{14})_n$ with different crystallization histories.....	143
Figure 57. DMA and DSC of polymer $(C_4\pi C_4EO_3)_n$ heating scans. The bottom 3 traces are DMA results for the a sample in a parallel plate geometry.	146
Figure 58. Low angle XRD of polymer $(C_9\pi C_9EO_7)_n$ samples prepared using different crystallization conditions.....	149
Figure 59. Wide angle XRD of polymer $(C_9\pi C_9EO_7)_n$ samples prepared using different crystallization conditions.....	150
Figure 60. DSC of polymer $(C_4\pi C_4EO_5)_n$ heating and cooling at 10 °C/min after flash quenched from the melt. Arrows indicate the temperatures where XRD experiments were performed.....	151
Figure 61. XRD of polymer $(C_4\pi C_4EO_5)_n$ as a function of temperature.....	152
Figure 62. Micrographs of polymers $(C_{10}EO_6)_n$ (left) and $(C_{10}EO_7)_n$ (right) under cross-polarized light.	156
Figure 63. Micrographs of polymers $(C_{10}EO_7)_n$ under cross-polarized light showing different band widths.	156
Figure 64. Micrographs of polymers $(C_{10}EO_8)_n$ (upper left), $(C_{10}EO_{10})_n$ (upper right), $(C_{10}EO_{14})_n$ (lower left), and $(C_{20}EO_7)_n$ (lower right) under cross-polarized light. .	157
Figure 65. DSC heating scans of polymers $(C_{10}EO_y)_n$ after flash quenching.....	160
Figure 66. DSC heating scans of polymers $(C_{10}EO_6)_n$ with different crystallization histories.....	161
Figure 67. DSC heating scans of polymers $(C_{10}EO_7)_n$ with different crystallization histories.....	162
Figure 68. DSC heating scans of polymers $(C_{10}EO_8)_n$ with different crystallization histories.....	163
Figure 69. DSC heating scans of polymers $(C_{10}EO_{10})_n$ with different crystallization histories.....	164
Figure 70. DSC heating scans of polymers $(C_{10}EO_{14})_n$ with different crystallization histories.....	165
Figure 71. IR spectra of polymer $(C_{20}EO_7)_n$ crystallized with different solvents.	167

Figure 72. DSC of poly
quenched from the m
were performed in a

Figure 73. XRD of poly
20 are diffract

Figure 74. Estimated s
Numbers in the inset

Figure 75. Triblock olig
PEO conformations

Figure 76. Triblock olig

Figure 77. Raman spectr

Figure 78. Triblock olig
crystallization. Top

Figure 79. Oligomer C₁₄

Figure 80. D-spacings of
the calculated end-to-

Figure 81. Raman spectr

Figure 82. Melting point
values.

Figure 83. Bending of th
and C-O-C.

Figure 84. Percent heat o
oligomers C₈EO, C₈

Figure 85. Melting point
polymers.

Figure 86. Packing of un
conformation.

Figure 87. Comparison o

Figure 88. Packing mode

Figure 89. DSC heating

Figure 72. DSC of polymer $(C_{10}EO_5)_n$ heating and cooling at 10 °C/min after flash quenched from the melt. Arrows indicated are temperatures where XRD experiments were performed in addition to –178 and –130 °C.	169
Figure 73. XRD of polymer $(C_{10}EO_5)_n$ as a function of temperature. Note: peaks at 31.7° 2 θ are diffraction from NaCl impurity.....	170
Figure 74. Estimated solubility parameters of unsaturated polymers $(C_x\pi C_xEO_y)_n$. Numbers in the inset are x values.	178
Figure 75. Triblock oligomer $C_{16}EO_3C_{16}$ calculated end to end distance with different PEO conformations.....	185
Figure 76. Triblock oligomer $C_{16}EO_3C_{16}$ with lamellar structure.....	186
Figure 77. Raman spectra comparison between $C_{14}EO_7C_{14}$ and PEO.	187
Figure 78. Triblock oligomer $C_{14}EO_7C_{14}$ structures obtained from solvent crystallization. Top: from methanol. Bottom: from hexane.	188
Figure 79. Oligomer $C_{14}EO_7C_{14}$ solvent crystallization mechanism.....	190
Figure 80. D-spacings of oligomer $C_{14}EO_yC_{14}$ measured by powder XRD compared to the calculated end-to-end distances.	197
Figure 81. Raman spectra comparison between triblock oligomer and PEO.....	198
Figure 82. Melting points of $C_xEO_yC_x$ triblock oligomers. Numbers in the inset are x values.	202
Figure 83. Bending of the triblock oligomers caused by the angle difference in C-C-C and C-O-C.....	203
Figure 84. Percent heat of fusion deviation versus numbers of ethylene oxide units for oligomers $C_8EO_yC_8$ (top) and $C_{14}EO_yC_{14}$ (bottom).	204
Figure 85. Melting points vs. numbers of ethylene oxide units of triblock oligomers and polymers.	206
Figure 86. Packing of unsaturated polymers $(C_9\pi C_9EO_y)_n$ with a planar zigzag PEO conformation.....	211
Figure 87. Comparison of model compound $C_{14}EO_7C_{14}$ and polymers $(C_9\pi C_9EO_y)_n$	211
Figure 88. Packing model of unsaturated polymers $(C_9\pi C_9EO_y)_n$ in crystalline state.	212
Figure 89. DSC heating scans of triblock oligomers $C_xEO_2C_x$	253

Figure 90. DSC heating

Figure 91. DSC heating

Figure 92. DSC heating

Figure 93. DSC heating

Figure 94. DSC heating

Figure 95. DSC heating

Figure 96. DSC heating

Figure 97. DSC heating
histories.....

Figure 98. DSC heating
histories.....

Figure 99. DSC heating
histories.....

Figure 100. DSC heating
histories.....

Figure 101. DSC heating
histories.....

Figure 102. DSC heating
histories.....

Figure 103. DSC heating
histories.....

Figure 104. DSC heating
histories.....

Figure 105. DSC heating
histories.....

Figure 106. DSC heating
histories.....

Figure 107. DSC heating
histories.....

Figure 90. DSC heating scans of triblock oligomers $C_xEO_3C_x$	254
Figure 91. DSC heating scans of triblock oligomers $C_xEO_4C_x$	255
Figure 92. DSC heating scans of triblock oligomers $C_xEO_5C_x$	256
Figure 93. DSC heating scans of triblock oligomers $C_xEO_6C_x$	257
Figure 94. DSC heating scans of triblock oligomers $C_xEO_8C_x$	258
Figure 95. DSC heating scans of triblock oligomers $C_xEO_{10}C_x$	259
Figure 96. DSC heating scans of triblock oligomers $C_xEO_{14}C_x$	260
Figure 97. DSC heating scans of polymer $(C_4\pi C_4EO_6)_n$ with different crystallization histories.....	261
Figure 98. DSC heating scans of polymer $(C_4\pi C_4EO_7)_n$ with different crystallization histories.....	262
Figure 99. DSC heating scans of polymer $(C_4\pi C_4EO_8)_n$ with different crystallization histories.....	263
Figure 100. DSC heating scans of polymer $(C_4\pi C_4EO_{10})_n$ with different crystallization histories.....	264
Figure 101. DSC heating scans of polymer $(C_4\pi C_4EO_{14})_n$ with different crystallization histories.....	265
Figure 102. DSC heating scans of polymer $(C_8\pi C_8EO_6)_n$ with different crystallization histories.....	266
Figure 103. DSC heating scans of polymer $(C_8\pi C_8EO_7)_n$ with different crystallization histories.....	267
Figure 104. DSC heating scans of polymer $(C_8\pi C_8EO_8)_n$ with different crystallization histories.....	268
Figure 105. DSC heating scans of polymer $(C_8\pi C_8EO_{10})_n$ with different crystallization histories.....	269
Figure 106. DSC heating scans of polymer $(C_8\pi C_8EO_{14})_n$ with different crystallization histories.....	270
Figure 107. DSC heating scans of polymer $(C_9\pi C_9EO_6)_n$ with different crystallization histories.....	271

Figure 108. DSC heating
histories.....

Figure 109. DSC heating
histories.....

Figure 110. DSC heating
histories.....

Figure 111. DSC heating
histories.....

Figure 112. DSC heating
histories.....

Figure 108. DSC heating scans of polymer $(C_9\pi C_9EO_7)_n$ with different crystallization histories.....	272
Figure 109. DSC heating scans of polymer $(C_9\pi C_9EO_8)_n$ with different crystallization histories.....	273
Figure 110. DSC heating scans of polymer $(C_9\pi C_9EO_{10})_n$ with different crystallization histories.....	274
Figure 111. DSC heating scans of polymer $(C_9\pi C_9EO_{14})_n$ with different crystallization histories.....	275
Figure 112. DSC heating scans of polymer $(C_{20}EO_7)_n$ with different crystallization histories.....	276

Scheme 1. Syn and ant

Scheme 2. Synthesis of
and derivatives

Scheme 3. Functional p
isocyanate is

Scheme 4. Sequential a

Scheme 5. Synthesis of
methyl methacryla

Scheme 6. Synthesis of

Scheme 7. Synthesis of

Scheme 8. Synthesis of

Scheme 9. Synthesis of

Scheme 10. Ring-open

Scheme 11. Acyclic d

Scheme 12. Synthesis
along the backbone

Scheme 13. Generaliz

Scheme 14. Ring ope

Scheme 15. ADMET

Scheme 16. Target (

Scheme 17. Synthesi

Scheme 18. Synthesi

Scheme 19. Synthesi

LIST OF SCHEMES

Scheme 1. Syn and anti conformations for polymer 12	25
Scheme 2. Synthesis of derivatives of α -olefin maleic anhydride alternating copolymers and derivatives	30
Scheme 3. Functional polymers from N-substituted poly(maleimide- <i>alt</i> -isopropenyl isocyanate)s	31
Scheme 4. Sequential anionic polymerization of styrene and isoprene	33
Scheme 5. Synthesis of poly[methyl methacrylate- <i>b</i> -styrene- <i>b</i> -butadiene- <i>b</i> -styrene- <i>b</i> -methyl methacrylate] pentablock copolymer.	34
Scheme 6. Synthesis of typical telechelic polymer.....	35
Scheme 7. Synthesis of polyamideurethanes	37
Scheme 8. Synthesis of styrene-ethylene oxide (AB) _n copolymers.....	37
Scheme 9. Synthesis of σ - π conjugated alternating silylene-diacetylene copolymer.....	37
Scheme 10. Ring-opening metathesis polymerization (ROMP).....	39
Scheme 11. Acyclic diene metathesis (ADMET) polymerization.....	39
Scheme 12. Synthesis of unsaturated polymer with perfectly alternating substituents along the backbone	43
Scheme 13. Generalized metathesis copolymerization scheme.....	43
Scheme 14. Ring opening copolymerization of macromonomers	44
Scheme 15. ADMET copolymerization to poly[(hexamethyltrisiloxanediyl)-butenylen].....	46
Scheme 16. Target (AB) _n microblock copolymers	49
Scheme 17. Synthesis of microblock copolymers containing thioethylene segments.....	61
Scheme 18. Synthesis of triblock oligomers CH ₃ (CH ₂) ₉ (SCH ₂ CH ₂) _y S(CH ₂) ₉ CH ₃	61
Scheme 19. Synthesis of triblock oligomer F _n H _m F _n	65

Scheme 20. Synthesis of
hydrocarbon segment

Scheme 21. Examples of

Scheme 22. Synthesis of

Scheme 23. Synthesis of

Scheme 24. Synthesis of

Scheme 25. Synthesis of

Scheme 26. Synthesis of

Scheme 27. Synthesis of

Scheme 28. Isomerization

Scheme 29. Back-biting

Scheme 20. Synthesis of microblock copolymers containing fluorocarbon and hydrocarbon segments	65
Scheme 21. Examples of acronyms for compounds	68
Scheme 22. Synthesis of exact length oligoethylene glycols	70
Scheme 23. Synthesis of oligoethylene glycol ditosylates	70
Scheme 24. Synthesis of triblock oligomers $C_xEO_yC_x$	74
Scheme 25. Synthesis of monomers $\pi C_xEO_yC_x\pi$	74
Scheme 26. Synthesis of unsaturated polymers $(C_x\pi C_xEO_y)_n$	77
Scheme 27. Synthesis of saturated polymers from unsaturated polymers $(C_x\pi C_xEO_y)_n$	77
Scheme 28. Isomerization of $\pi C_2EO_yC_2\pi$ double bonds	180
Scheme 29. Back-biting for polymer degradation	180

Table 1. Combinations

Table 2. Eluents for pu-
chromatography

Table 3. Monomers π C

Table 4. Solvents used

Table 5. Summary of the
oligomers C_nEO_m

Table 6. Melting points

Table 7. Heats of fusion

Table 8. d-spacings (Å)
segments

Table 9. d-spacings (Å)
segments

Table 10. Molecular weights

Table 11. Glass transitions
(C_nEO_m)_n

Table 12. Melting transitions

Table 13. Comparison of
polymers ($C_{2n-2}EO_n$)

Table 14. T_g and T_m s of

Table 15. Solubility parameters
(C_nEO_m)_n

Table 16. Calculated and
kJ/mol

LIST OF TABLES

Table 1. Combinations of $\text{TrEO}_x\text{H} + \text{TsEO}_y\text{Ts}$ used in the synthesis of EO_{2x+y}	71
Table 2. Eluents for purification of monomers $(\pi\text{C}_x\text{EO}_y\text{C}_x\pi)$ by column chromatography	73
Table 3. Monomers $\pi\text{C}_x\text{EO}_y\text{C}_x\pi$ polymerizable by ADMET polymerization.....	78
Table 4. Solvents used for precipitating polymers $(\text{C}_x\pi\text{C}_x\text{EO}_y)_n$	79
Table 5. Summary of the types of DSC endotherms observed for ABA triblock oligomers $\text{C}_x\text{EO}_y\text{C}_x$	81
Table 6. Melting points ($^{\circ}\text{C}$) of ABA triblock oligomers $\text{C}_x\text{EO}_y\text{C}_x$	91
Table 7. Heats of fusion (J/g) of ABA triblock oligomers $\text{C}_x\text{EO}_y\text{C}_x$	92
Table 8. d-spacings (\AA) for triblock oligomers $(\text{C}_{14}\text{EO}_y\text{C}_{14})$ with tetradecyl alkyl segments.	104
Table 9. d-spacings (\AA) for triblock oligomers $(\text{C}_x\text{EO}_{14}\text{C}_x)$ with tetradecaethylene oxide segments.	104
Table 10. Molecular weights and PDI values of unsaturated polymers $(\text{C}_x\pi\text{C}_x\text{EO}_y)_n$. ^a	123
Table 11. Glass transition temperatures ($^{\circ}\text{C}$) of the unsaturated polymers $(\text{C}_x\pi\text{C}_x\text{EO}_y)_n$	133
Table 12. Melting transition temperatures ($^{\circ}\text{C}$) of polymers $(\text{C}_x\pi\text{C}_x\text{EO}_y)_n$	144
Table 13. Comparison of the molecular weights and polydispersities of the hydrogenated polymers $(\text{C}_{2x+2}\text{EO}_y)_n$ and their unsaturated precursors $(\text{C}_x\pi\text{C}_x\text{EO}_y)_n$	154
Table 14. T_g and T_m s of saturated polymers. ($^{\circ}\text{C}$).....	159
Table 15. Solubility parameters $\delta [(\text{cal}/\text{cm}^3)^{1/2}]$ of unsaturated polymers $(\text{C}_x\pi\text{C}_x\text{EO}_y)_n$	177
Table 16. Calculated and measured heats of fusion* for $\text{C}_x\text{EO}_y\text{C}_x$ oligomers. (kJ/mol).....	201

1 General

Block copolymers
that has led to important
the bulk form, as there
the attention from
commercialization of the

Block copolymers
terminally connected se-
ments. For block copo-
lymers, sequential arrangement
of block copolymers with
different segments.

By combining two
methods, one only obtains copolymers
simultaneously, it also gives
basic physical concepts
polymer blend, the poly-
mer blend of microns can
polymer blend is usually

INTRODUCTION

I. General

Block copolymers exhibit a fascinating range of microstructures and properties, which has led to important applications as adhesives, compatibilizers, emulsifiers, and in their bulk form, as thermoplastic elastomers. Therefore, block copolymers continue to draw attention from scientists and engineers more than three decades after commercialization of this class of materials.

Block copolymers are macromolecules comprised of chemically dissimilar, terminally connected segments. Each segment is a homopolymer chain with many repeat units. For block copolymers with two different types of segments A and B, their sequential arrangement can vary from AB structures containing two segments, to ABA block copolymers with three segments, to multiblock $(AB)_n$ systems possessing many segments.

By combining two or more chemically dissimilar segments in one molecule, one not only obtains copolymers that combine the properties of individual segments, but more importantly, it also gives rise to properties not found in simple polymer blends. The basic physical concept that underlines these characteristics is phase separation. In a polymer blend, the polymer phase separates at a macroscopic level. Domains larger than hundreds of microns can easily be seen under microscope. Therefore, the properties of a polymer blend is usually a simple combination the homopolymer properties. In the block

polymer case, phase

size. Phase separa

ra properties. For ex

trained with styrene

usually depend on the

factor and thermody

discussed in more detail.

The most comm

polymers, formed by

between the two phases

morphologies can be co

between the blocks and

interaction between the

and many properties of

applications of block co

for two blocks with m

This leads to triblock

polymers, they have

effectively couple the b

range of properties availa

Due to the pre

nanomolecular chain, th

that in ABA polymers.

copolymer case, phase separation is at the molecular level, generally on the order of the block size. Phase separation at this level can lead to new polymer morphologies and thus new properties. For example, both thermoplastic elastomers and toughened rubbers can be realized with styrene-butadiene block copolymers.¹ The properties of these materials crucially depend on their morphology, both in the molten and solid state. Their phase behavior and thermodynamics are particularly important to understand. They will be discussed in more detail in the following section.

The most commonly encountered block copolymers are amorphous AB diblock copolymers, formed by joining two homopolymers at a single point. The interface between the two phases is defined by the link between the A and B blocks, and different morphologies can be obtained by varying the magnitude of the chemical interactions between the blocks and the ratio of the lengths of the two blocks. Since there is only one connection between the two blocks, this kind of block copolymer is the simplest to study and many properties of AB block copolymers have been elucidated to date. Many applications of block copolymers, for example thermoplastic elastomers, require more than two blocks with more connecting sites (this topic will be discussed in detail later). This leads to triblock and even multiblock copolymers. Compared to diblock copolymers, they have more than one chemical linking point making it possible to effectively couple the behaviors of different phase separated domains, and expand the range of properties available from block copolymers.

Due to the presence of a greater number of physical junction sites per macromolecular chain, the polymer segment length in $(AB)_n$ polymers can be shorter than in ABA polymers to achieve the same properties, which could be an important

feature for processing
 reduced in the $(AB)_n$ S
 AB or ABA systems.
 likely that such materi
 ze $(AB)_n$ microblo
 characterization of (A
 polyethylene oxide (P
 linear alkyl segment c

II. Block copolymer

1. Phase separation

When two poly
 and phase separate. T
 energy change for mix

$$\Delta G_{\text{mix}} = \Delta H_{\text{mix}}$$

Polymers have
 weight. Therefore, a s
 sufficient to produce a
 polymer phase separati
 driving force for each
 these dispersions in w
 opaque.

feature for processing. Since the size of the phase-separated domains can be greatly reduced in the $(AB)_n$ system, it is easier to obtain a more 'homogeneous' material than in AB or ABA systems. Because the size of the micro-domain can be reduced, it is more likely that such materials have high optical clarity. The polymers studied in this research are $(AB)_n$ microblock copolymers. In particular, we studied the synthesis and characterization of $(AB)_n$ copolymers where the B blocks are exact length segments of polyethylene oxide (PEO) and the A block is an exact length linear alkyl segment or a linear alkyl segment containing a single double bond.

II. Block copolymer properties

1. Phase separation and morphology

When two polymeric materials are mixed, the great majority are highly unmixable and phase separate. This is a direct consequence of the well-known relationship for free energy change for mixing (ΔG_{mix}) given by equation 1:

$$\Delta G_{mix} = \Delta H_{mix} - T\Delta S_{mix} \quad \text{eq. 1}$$

Polymers have a very small entropy of mixing (ΔS_{mix}) due to their high molecular weight. Therefore, a slightly positive enthalpy (ΔH_{mix}) due to endothermic mixing is sufficient to produce a positive free energy change, thus resulting in incompatibility (i.e., polymer phase separation). This incompatibility of the blend components provides a driving force for each to aggregate in separate phases. These two-phase systems are coarse dispersions in which the particles are usually large enough to make the blends opaque.

If two polymer
 separation may be initiated
 aggregate, but the domains
 blocks. In addition, the
 limits. The relationship
 AB block system is
 that N_{AB} is the degree of
 Flory-Huggins parameter¹ re-

The Flory-Huggins

$$\chi = \Delta H_{mix} / kTN$$

where N_A is the number of
 segment B. χ is a dimensionless
 for two blocks.

Microphase-separation
 block copolymer composition
 number of monomer units
 of A in a B-matrix are favorable
 For larger values of N_A , the
 they are arranged in a hexagonal
 under essentially symmetric
 oriented and the A-blocks

If two polymeric species are coupled by a chemical link, macroscopic phase separation may be inhibited. As shown in **Figure 1**,^{2,3} the A and B segments still segregate, but the domains have dimensions corresponding to the size of the single blocks. In addition, the domains have a uniform size, and can form ordered mesoscopic lattices. The relationship of morphology to the relative composition of the A block in a AB diblock system is shown in **Figure 2**.² In the figure, ϕ_A is the volume fraction of A block, N_{AB} is the degree of polymerization of the diblock copolymer and χ is the Florry-Huggins parameter⁴ reflecting the interaction properties of the two blocks.

The Florry Huggins parameter χ is defined as

$$\chi = \Delta H_{mix} / kTN_A v_B \quad \text{eq. 2}$$

where N_A is the number of repeat units in segment A and v_B is the volume fraction of segment B. χ is a dimensionless parameter and it reflects the interaction properties of the two blocks.

Microphase-separation leads to different classes of structures that depend on the block copolymer composition. For very small ϕ_A , i.e. $N_A \ll N_B$ (where N_A and N_B are the number of monomer units in the A and B components respectively), spherical inclusions of A in a B-matrix are formed, and they set up a body-centered cubic lattice (**Figure 1a**). For larger values of N_A , (but still $N_A < N_B$), the A-domains have a cylindrical shape and they are arranged in a hexagonal lattice (**Figure 1b**). Layered lattices (**Figure 1d**) form under essentially symmetrical conditions, i.e. $N_A \approx N_B$. Then, for $N_A > N_B$, the phases are inverted and the A-blocks now constitute the continuous matrix.

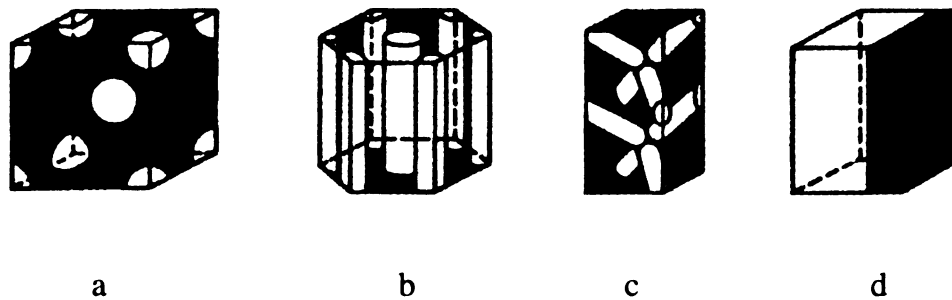


Figure 1. Morphologies of AB block copolymers. White portions represent block A, while dark portions represent block B of the AB polymer.

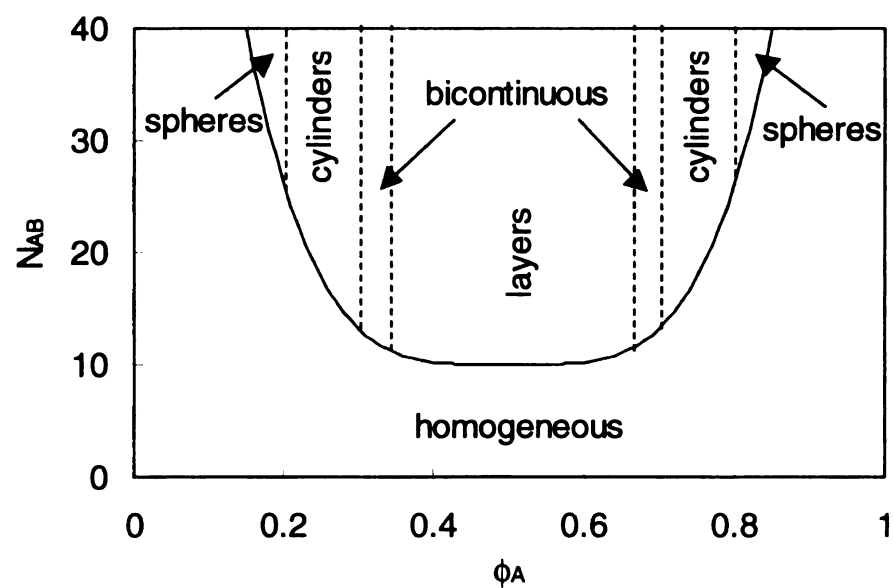


Figure 2. Schematic phase diagram of a typical block copolymer

In addition to
structures occur under
example, presented
structure. 5.6 Hexagon
structure known as a
exists in a narrow range
theoretical calculations
the strong segregation limit

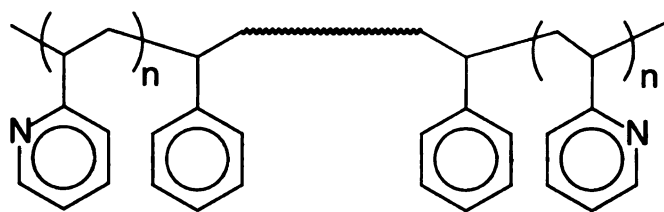
The structures discussed
However, most triblock
phase behavior. For instance
vinylpyridine), **1**, has a
fraction ranges from 0.2



When more blocks
phase behavior is expected
Matsuzaki¹⁴ reported a
styrene-2-vinylpyridine

In addition to lattices composed of spheres, cylinders and layers, periodic structures occur under special conditions, where both phases are continuous. One example, presented in **Figure 1c**, is an ordered bicontinuous double diamond structure.^{5,6} Hexagonally perforated layers (HPL)⁷⁻⁹ and a second bicontinuous cubic structure known as a $Ia\bar{3}d$ /gyroid^{7,10,11} were recently found. These microstructures exist in a narrow range of N_A/N_B , between the cylindrical and lamellar phases, and theoretical calculations show that they are not stable relative to lamellae and cylinders in the strong segregation limit.¹²

The structures discussed above are mainly derived from AB diblock copolymers. However, most triblock or multiblock copolymers also phase separate and exhibit similar phase behavior. For instance, the triblock copolymer poly(2-vinylpyridine-*b*-styrene-*b*-2-vinylpyridine), **1**, has an alternating lamellar structure when the polystyrene volume fraction ranges from 0.28 to 0.58.¹³



1

When more blocks are restrained in the same polymer chain, more complicated phase behavior is expected and new morphologies are discovered. Matsushita and co-workers¹⁴ reported a tricontinuous double-diamond structure formed from styrene-isoprene-2-vinylpyridine triblock copolymer **2**. A knitting pattern in polystyrene-*b*-

polyethylene-*co*-buty

by Sadler's research

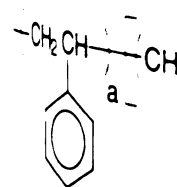
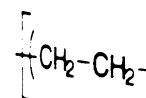
co-butene-*b*-methyl

molecular weights of

morphologies.¹⁶ At

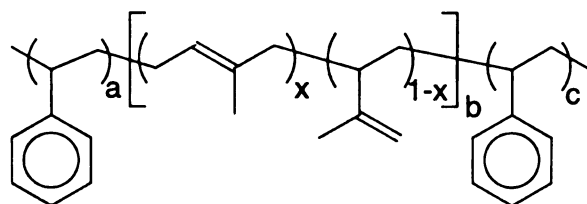
quaters dispersed in

mp

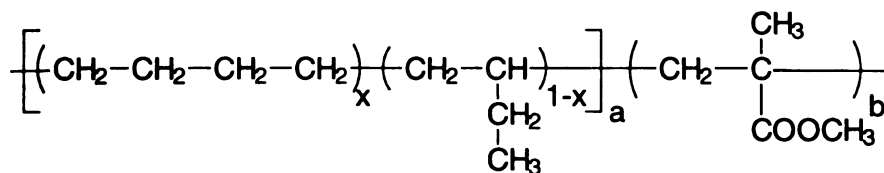


The morphology
less frequently reported
Since the block lengths
number *n* is much larger

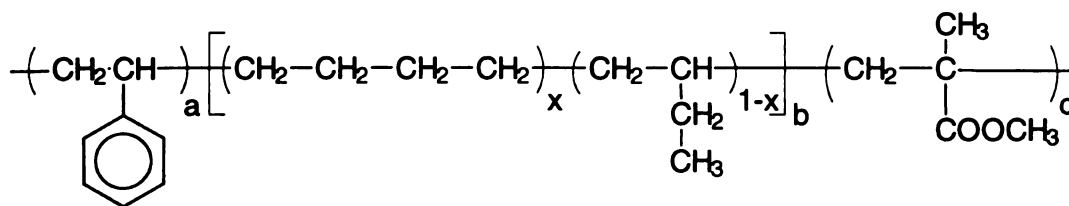
poly(ethylene-*co*-butylene)-*b*-poly(methylmethacrylate) triblock copolymers **3** was found by Stadler's research group.¹⁵ The morphology of well-defined poly(styrene-*b*-ethylene-*co*-1-butene-*b*-methyl methacrylate) (P(S-*b*-EB-*b*-MMA)) triblock copolymers **4** of molecular weights of approximately 2×10^5 has been shown to have new ordered morphologies.¹⁶ At a low EB content (6 wt%), the triblock copolymer shows PS cylinders dispersed in a PMMA matrix. The cylinders are covered with small isolated EB rings.



2



3



4

The morphologies of microblock (AB)_n copolymers where n is large are much less frequently reported, however, phase separation does occur in many cases.^{17,18} Since the block lengths for this kind of polymers are much smaller and the repeating number n is much larger, the polymers show more complexity and their study requires

more powerful equipment

type $n = 1, 2, 3, 4$ with

to have alternating layers

at mean-field principles

microstructural dimension

multiblock copolymer

copolymers with the same

radially mixed) in

thermodynamic incompatibility

separation less favorable

the copolymer molecule

becomes more energetic

Diagram shown in **Figure**

more powerful equipment. Styrene(S)-isoprene(I) multiblock copolymers **5** of the $(S_xI_y)_n$ type ($n = 1, 2, 3, 4$) with total polystyrene volume fractions of about 0.5 were also found to have alternating lamellar structures.¹⁹ Theoretical models based on confined-chain and mean-field principles were used to elucidate the fundamental relationships between microstructural dimensions and molecular characteristics in microphase-separated multiblock copolymers in the strong-segregation limit.²⁰ For $(AB)_n$ multiblock copolymers with the same molecular weight, an increase in n increases the homogeneous (residually mixed) interphase volume fraction, thereby decreasing the extent of thermodynamic incompatibility between the A and B blocks and making microphase separation less favorable. If, on the other hand, the block lengths are held constant and the copolymer molecular weight is allowed to vary with n , microphase separation becomes more energetically favored as n is increased, which is consistent with the phase diagram shown in **Figure 2**.

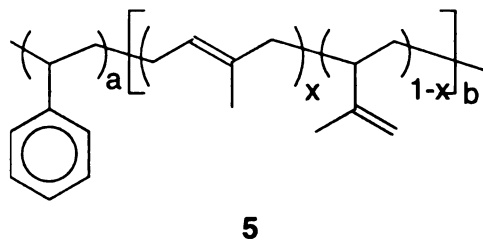




Figure 3

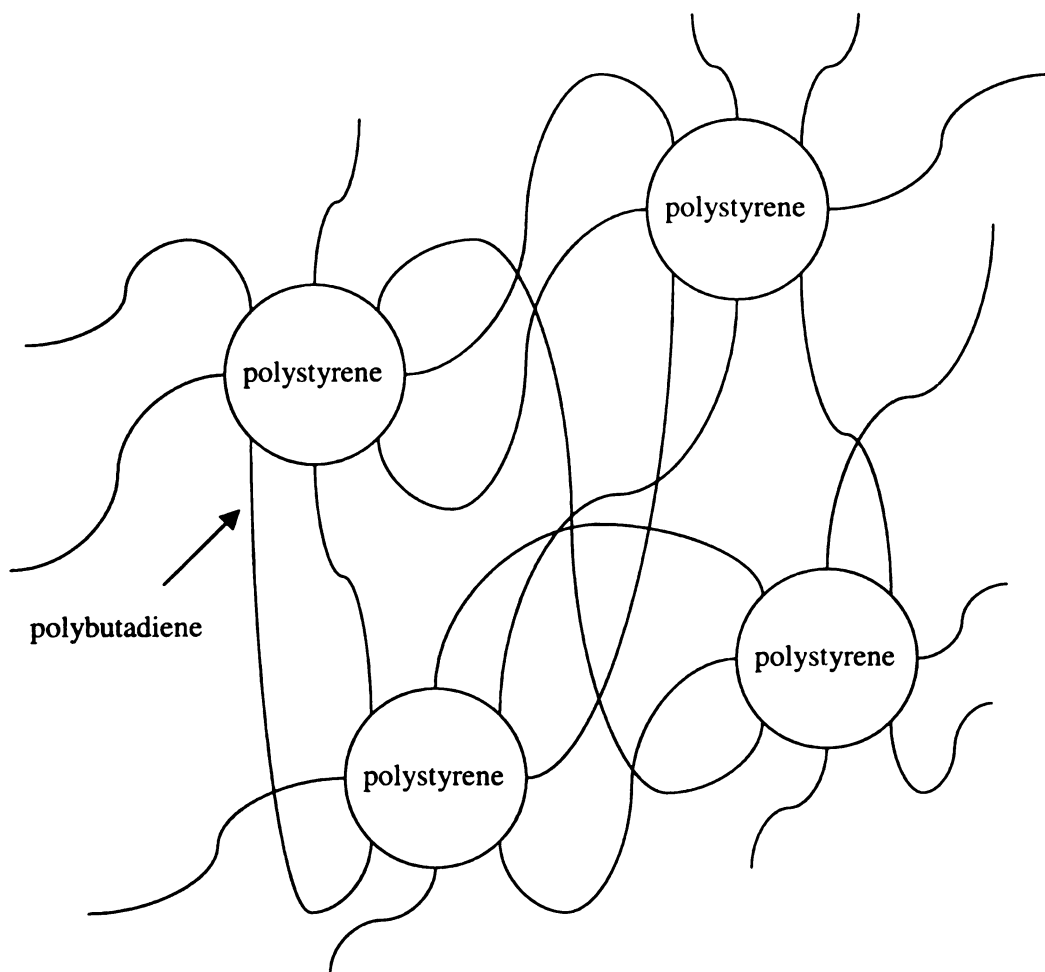


Figure 3. Morphology model of thermoplastic rubber

Phase separation

properties. The most

before, styrene/butadi-

enized rubbers. P

while the T_g for pol

polystyrene is a hard

shown in **Figure 3-21** t

two domains. The n

serve as physical cross

like an ordinary rubb

permanent, these cross

possible at temperature

material is therefore te

triblock copolymers are

the soft block is chemi

More advanced

reported. For example

organizing forces such

entropy. The resulting

few nanometers in LC

and even micrometers

have demonstrated the

mushroom-shaped sup

Phase separation can be used to generate useful materials with designed properties. The most common application is as thermoplastic elastomers. As mentioned before, styrene/butadiene copolymers can form both thermoplastic elastomers and toughened rubbers. Polystyrene has a glass transition temperature, T_g , of about 110 °C while the T_g for polybutadiene is about -100 °C. Therefore, at room temperature, polystyrene is a hard glassy block while the polybutadiene is a soft rubbery block. As shown in **Figure 3**²¹ for a PS-PB-PS triblock system, the blocks phase separate and form two domains. The morphological domains formed by association of the hard blocks serve as physical cross-linking and reinforcement sites, and the bulk material behaves like an ordinary rubber. In contrast to ordinary rubber where the cross-links are permanent, these cross-linking sites are thermally reversible, i.e. melt processing is possible at temperatures above the T_g or T_m (melting point) of the hard block, and the material is therefore termed a thermoplastic elastomer. It is not hard to see that AB diblock copolymers are incapable of producing network structures, since only one end of the soft block is chemically linked to a hard segment domain.

More advanced structural designs based on phase separation have also been reported. For example, spontaneously organizing systems can be tailored by balancing organizing forces such as chemical incompatibility with others such as conformational entropy. The resulting materials spontaneously organize on length scales ranging from a few nanometers in LC phases to hundreds of nanometers in phase-separated structures, and even micrometers in length for surface-segregated materials. Stupp and coworkers have demonstrated the best example of this kind of manipulation in their design of a mushroom-shaped supramolecule.²² The triblock polymer **6** used for this assembly

ness of styrene, is

ments, spontaneous

separation of the two

important roles in the

symmetric packing

etching upper and

respectively. The sup

macromolecular cluste

consists of styrene, isoprene, and a rod-like block based on rigid aromatic rings. In these materials, spontaneous noncentrosymmetric organization was reported. Both microphase separation of the two coil blocks and the crystallization of the rod component played important roles in the selection of the unusual shape of the aggregate. This leads to asymmetric packing of the units, which form micrometer-sized plate-like objects exhibiting upper and lower surfaces that have hydrophobic and hydrophilic character, respectively. The supramolecule assembly can also be chemically cross-linked to form macromolecular clusters.²³



$$n+m=9$$

6

2 Crystallization

Like many s

because of the dispers

are different from s

produce structures w

separated by disorder

nature of crystalline

of ultra-thin slices of

beats with the a

entanglements in the

one Therefore, crys

can be stretched and

entanglements, which

non-crystallizable ch

edgroups, chemical

conformations whic

accumulated in the

small molecules, and

of extended chains o

over a very long ran

Polymers us

formed by nucleatio

spherulites orient p

2. Crystallization of polymers

Like many small molecules, some polymers can be crystallized. However, because of the dispersion in molecular weight and chain entanglements, polymer crystals are different from small molecules. When polymers are cooled from their melts, they produce structures which are only partially crystalline. Layer-like crystallites are separated by disordered regions which leads to another kind of two-phase system—a mixture of crystalline and amorphous phases. Transmission electron microscopic studies of ultra-thin slices of polyethylene (PE) crystals show that the lamellar crystalline phase coexists with the amorphous phase.²⁴ Polymer crystallization requires that the entanglements in the melt be resolved, which is unlikely to be completed within the given time. Therefore, crystallization is preceded by demixing, whereby chain sequences which can be stretched and incorporated into a growing crystal are separated from chains near entanglements, which can only be excluded and shifted into the amorphous regions. The non-crystallizable chain parts of a polymer are not only entanglements, but also include endgroups, chemical perturbations like short chain branches, or specific local conformations which oppose transformation into a uniform chain. They all become accumulated in the amorphous parts of a partially crystalline polymer. Compared to small molecules, another major difference of polymer crystals is that they rarely consist of extended chains of whole polymer molecules. Because it is hard to achieve ordering over a very long range, the polymer chains in polymer crystals often are folded.

Polymers usually crystallize as spherical crystals, or spherulites. Spherulites are formed by nucleation followed by even radial growth.²⁵ The polymer chains inside the spherulites orient perpendicular to the radius vector in most polymers. Vaughan and

Basen²⁶ showed the
aggregate of layers.
stable spherical growth
spherulites exhibit a

In many cases
They are called banded
polarized optical micrographs
addition to the Maltese cross
polyethylene oxide
spherulites. The reason for the
certain length scale
discussion and has been

As small as
equilibrium, it is in
from the melt and
thermodynamics.
maximum growth rate
limited mobility of
partially crystalline
a memory of the temperature
cooling rates,^{31,32}
growth from a melt

Bassett²⁶ showed that the center of the crystal spherulite is sheaf-like and formed by an aggregate of layers. On further growth, they become curved, and finally establish a stable spherical growth surface. When examined using polarized optical microscopy, spherulites exhibit a characteristic Maltese cross pattern of light extinction.

In many cases, spherulites with constantly spaced concentric rings are observed. They are called banded spherulites. For example, a polyethylene crystal observed with a polarized optical microscope shows light extinctions along circles in a periodic manner in addition to the Maltese cross.²⁶ Other polymers such as poly(ϵ -caprolactone),²⁷ and polyethylene oxide²⁸ (PEO) crystallized under certain conditions, also show banded spherulites. The reason for this behavior is that the crystallites periodically twist on a certain length scale. The mechanism leading to this special texture is still under discussion and has not yet been clarified.

As small molecule system states are mainly governed by thermodynamic equilibrium, it is important to note that structure formation for polymers crystallizing from the melt are governed more by kinetic criteria rather than by equilibrium thermodynamics. The structure which develops at a given temperature is that with the maximum growth rate rather than the structure with the lowest free energy because of the limited mobility of the polymer chains. Being kinetically controlled, structures of partially crystalline samples are always strongly affected by thermal processing and show a memory of the thermal history, i.e. the temperatures and times of crystallization,^{29,30} cooling rates,^{31,32} etc. **Figure 4** shows a nice illustration of PEO ($M_n = 6000$) crystal growth from a melt. The rate of crystal growth, as indicated by the radius of spherulite

increment over time

increase in growth rate

relationship of the

expressed with empir

$$u = A \cdot \exp \frac{1}{T}$$

where A and

melting temperature.

crystallization rate. S

fully extended chains

case is shown in the

is caused by a change

comprised of once-f

lower melting point

stable extended cha

preferentially leads t

twice-folded chain cr

growth rate incremen

In the contin

temperature T is inv

and melting temperat

$$d_g(T) = \frac{B}{T_m - T}$$

increment over time, is plotted against the crystallization temperature. The expected increase in growth rate with super cooling is seen over the entire temperature range. The relationship of the spherulite growth rate to the crystallization temperature can be expressed with empirical equations:²

$$u = A \bullet \exp\left(\frac{B_0}{T_m - T}\right) \quad \text{eq. 3}$$

where A and B_0 are constants for a given polymer, and T_m is the equilibrium melting temperature. Therefore, the lower the crystallization temperature, the faster the crystallization rate. Since the molecular weight is low, it is possible to grow crystals with fully extended chains at a temperature close to the equilibrium melting temperature. This case is shown in the far right region of **Figure 4**. A break at 59.5 °C is observed, which is caused by a change in crystal structure. Crystals formed in this part of the curve are comprised of once-folded chains rather than extended molecules. These crystals have a lower melting point and a higher Gibbs free energy than the thermodynamically most stable extended chain form. However, the crystal growth rate is higher which preferentially leads to the formation of this once-folded form. On further cooling, the twice-folded chain crystal is formed preferentially and so on until a relatively continuous growth rate increment is reached.

In the continuous growth regime, the crystallite thickness d_c at crystallization temperature T is inversely proportional to the difference of crystallization temperature and melting temperature, as indicated in equation 4,² where B_1 and B_2 are constants.

$$d_c(T) = \frac{B_1}{T_m - T} + B_2 \quad \text{eq. 4}$$

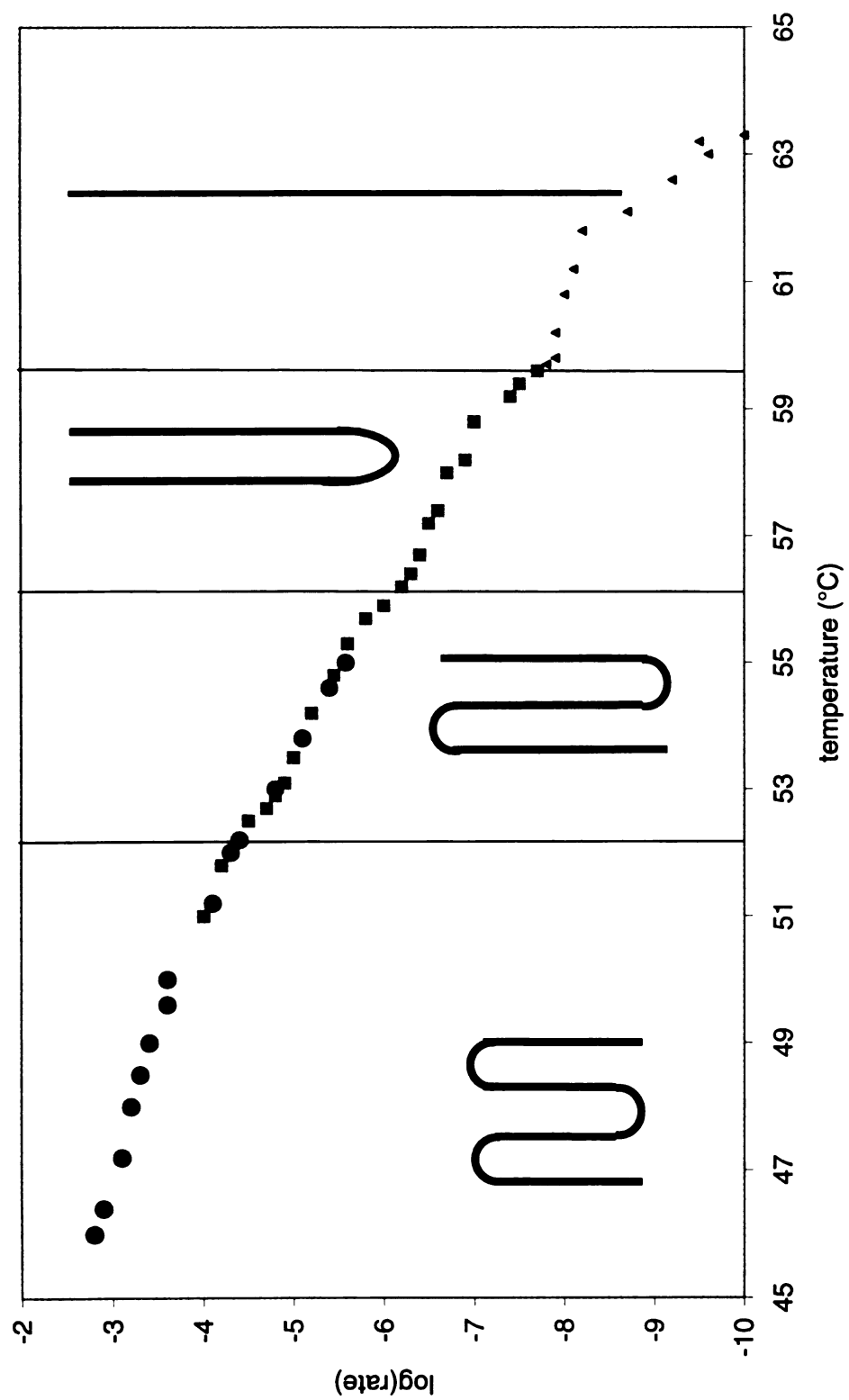


Figure 4. PEO crystallized with integer chain folding at different temperature.

Many well-d
include crystallinity
since it would exp
copolymers. For sim
AB block combinatio
blocks can crystallize
block would be expect
in the homopolymers
structures bearing the
completely different
crystallization, one a
substantially perturb
from amorphous AB
an important role in
will be shown in the

III. Multiple the

When a blo
technique such as
Analysis (DMA), th
can show two T_g 's
crystallization trans.

Many well-defined block copolymers are partially crystalline. Being able to include crystallinity as a design element in block copolymers is particularly attractive since it would expand the range of properties that can be obtained from block copolymers. For simplicity, we can think in terms of two limiting types of crystallizable AB block combinations: copolymers with one crystallizable block, and those where both blocks can crystallize. For copolymers where both the A and B blocks are long, each block would be expected to phase separate and crystallize in the same crystal structure as in the homopolymers. Copolymers where one or both blocks are short would form new structures bearing the characteristic structure of the homopolymer for each block, or form completely different structures. Because of the large ΔH_{fus} associated with crystallization, one also would expect that the formation of crystalline phases would substantially perturb the copolymer microstructures compared to those typically obtained from amorphous AB copolymers. In particular, crystallization kinetics is likely to play an important role in defining the block copolymer morphology. A couple of examples will be shown in the following sections.

III. Multiple thermal transitions for polymers

When a block copolymer is characterized by a scanning thermal analysis technique such as Differential Scanning Calorimetry (DSC) or Dynamic Mechanical Analysis (DMA), they often show multiple transitions. For example, diblock copolymers can show two T_g 's based on their degree of phase separation or show several melting-crystallization transitions during a DSC heating scan. These properties can be classified

into three categories
polymorphism.

1. General phase

When the two
relatively large sea
homopolymers. For
segmented copolymer
glassy poly(arylene ether)
are used to analyze
corresponding to each
nature of the material.
the polysulphone is a
the composition of the
copolymer. $(AB)_n$ type
= 2000 and various

two T_g 's because of the
linked in one molecule
polyolefin blocks in
oligomers indicating d
the T_g of the PET block

Polymers with
backbone also show m
unlike semiflexible

into three categories: phase separation, lamellar thickening and thinning, and polymorphism.

1. General phase separated cases

When the two blocks of a diblock copolymer strongly phase separate on a relatively large scale, the two polymer blocks have properties similar to the pure homopolymers. For example, the structure-property relationship of perfectly alternating segmented copolymers **7** based on soft poly(dimethylsiloxane) (PDMS) segments and glassy poly(arylene ether sulphone) hard segments, have been studied.³³ DMA and DSC were used to analyze the copolymer properties. Isolated thermal transitions corresponding to each block were observed, which is a good indication of the two-phase nature of the material. The soft PDMS segments have T_g s near $-115\text{ }^{\circ}\text{C}$ while the T_g of the polysulphone is around $150\text{ }^{\circ}\text{C}$. The T_g associated with the hard phase depends on the composition of the copolymer and increases with the polysulphone block length in the copolymer. (AB)_n type multi-block polymers **8** with soft segments of polybutadiene ($M_n = 2000$) and various lengths of poly(ethylene terephthalate) (PET) hard segments show two T_g s because of the strongly incompatible blocks.³⁴ However, as they are chemically linked in one molecule, their T_g s are also affected by each other. The T_g s of the polyolefin blocks in these copolymers are all higher than that of their pure homopolymers indicating decreased chain mobility for the polyolefin in the copolymer, while the T_g of the PET block is lower than that of pure PET homopolymer.

Polymers with pendent side chains that are chemically different relative to the backbone also show multiple thermal transitions caused by phase separation. A series of comblike semiflexible polymers **9**, in which the alkyl side chains were located

non-symmetrically or

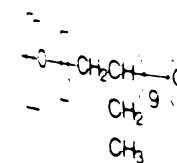
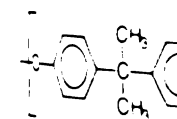
hexyl, octyl, dodecyl

chain melting above

for polymers with 1.

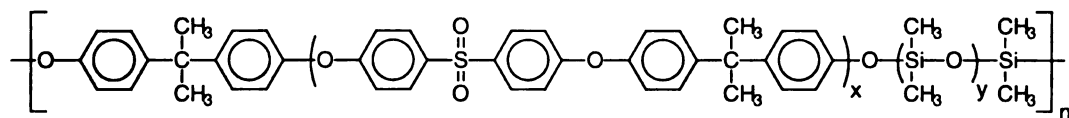
side chains also show

packing patterns.

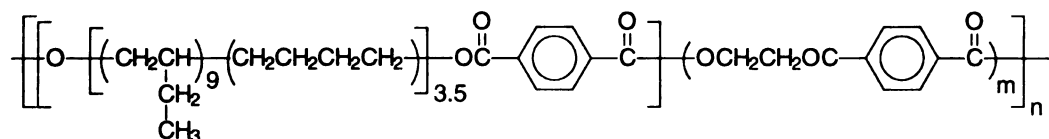


CH₃

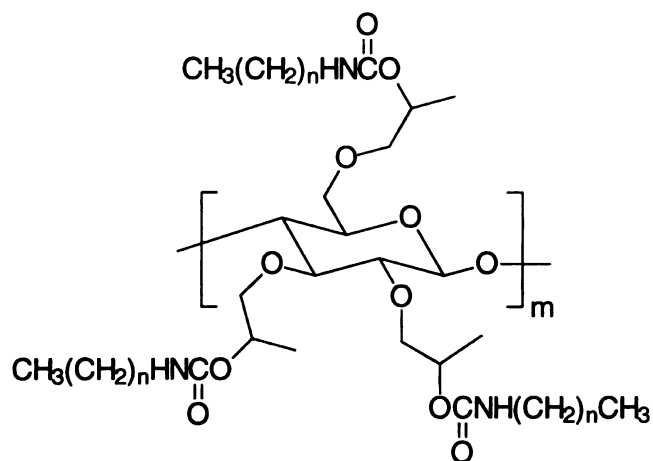
nonsymmetrically on the ring, were synthesized by reacting hydroxypropylcellulose with hexyl, octyl, dodecyl, and octadecyl isocyanates.³⁵ Besides a transition for the main chain melting above 100 °C, DSC experiments showed side-chain melting around 50 °C for polymers with 12 and 18 carbons in the pendant groups. The sample with 18-carbon side chains also show multiple melting transitions that correspond to different side chain packing patterns.



7



8



$n = 5, 7, 11, 17$

9

With shorter
and merge. Hashino
styrene-isoprene tapes
variation along the
mechanical response
occurred both at the
was predictable for the
peaks in the mechanical
shortened and finally
or phase separation is
predicted by the Fox

$$\frac{1}{T_c} = \frac{M}{T_{c1}} +$$

Where T_{c1} and
two blocks, and M , a

2 Lamellae thickness

As mentioned
crystals with different
crystallizable polymers
melting behavior based

The crystallinity
with one crystallizable

With shorter block lengths, the copolymer thermal transitions gradually get closer and merge. Hashimoto and coworkers³⁶ synthesized two series of styrene-butadiene and styrene-isoprene tapered block copolymers and investigated the effects of compositional variation along the main chain on microdomain structures and on linear dynamic mechanical responses. As the segments became shorter, mixing of unlike segments occurred both at the interphase boundary and inside the domains. The thermal behavior was predictable for this kind of system. The two T_g s, as indicated by the loss modulus peaks in the mechanical spectrum, gradually approached each other as the block lengths shortened and finally coalesced. At this point, the block copolymer is a one-phase system or phase separation is only on a very small scale. The T_g of the block copolymer can be predicted by the Fox equation:⁴

$$\frac{1}{T_g} = \frac{M_1}{T_{g1}} + \frac{M_2}{T_{g2}} \quad \text{eq. 5}$$

Where T_{g1} and T_{g2} are the glass transition temperature of the homopolymer of the two blocks, and M_1 and M_2 are the weight fractions of the two blocks.

2. Lamellae thickening and thinning

As mentioned before, PEO samples crystallized at different temperatures can give crystals with different lamellar thickness due to chain folding. When PEO or other crystallizable polymers are incorporated in block copolymers, they often still show multi-melting behavior based on chain folding.

The crystallization of oxyethylene/oxybutylene (E/B) diblock copolymers **10**, with one crystallizable E block and one noncrystallizable B block, has been studied by

simultaneous small

(WAXS), low-frequ

block phase separa

based on the crysta

compare to the me

symmetric triblock c

PEO has been studie

PEO block copolyme

the crystallization of

the transition temper

swelling of the lamell

Chain folding

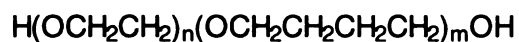
homopolymers. An

triblock copolymers

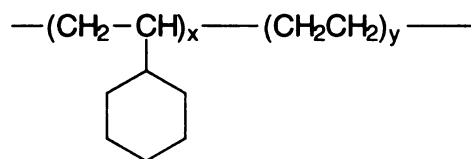
the chain-folded PE

which has been

simultaneous small angle X-ray scattering (SAXS) and wide angle X-ray scattering (WAXS), low-frequency Raman spectroscopy, and DSC.^{37,38} It was shown that the two blocks phase separate and the PEO block crystallizes in once to multiply folded structures based on the crystallization conditions, while the oxybutylene block is slightly stretched compare to the melt. The phase behavior of a low molecular weight ($M_w = 6000$) symmetric triblock copolymer of poly(ethylene oxide) and poly(isobutylene), PEO-PIB-PEO, has been studied using small-angle neutron scattering and TEM.³⁹ This PEO-PIB-PEO block copolymer forms an ordered lamellar phase at low temperatures induced by the crystallization of the PEO segment in a helical conformation with a single fold. Near the transition temperature, 45 °C, the PEO chains unfold, giving rise to significant swelling of the lamellae.



10



11

Chain folding in block copolymers does not always follow the pattern seen for homopolymers. An unusual chain folding pattern for polyethylene has been reported in diblock copolymers of poly(vinyl cyclohexane-*b*-polyethylene) **11**.⁴⁰ The orientation of the chain-folded PE stems was parallel to the lamellar interfaces, unlike the chain folding which has been observed in semicrystalline homopolymers and proposed for

semicrystalline dith
pendicular to the
to the influence of t
glassy amorphous la

3. Polymorphis

In many case
thickening. Instead
the polymer crystals
of behavior.

Polyurethane
oldest and most used
thermogram, depend
include the T_g and e
variation in the T_g o
indicator of the degra
the disordering proce
Seymour *et al.* 43,44
limited short-range
microcrystallites of
continuously by anne
endotherm until it me

semicrystalline diblock copolymers where the crystallized chains align roughly perpendicular to the lamellar interfaces. The unusual chain folding observed is attributed to the influence of topological constraints on the PE blocks which crystallize within the glassy amorphous lamellar microdomains.

3. Polymorphism

In many cases, multiple thermal transitions are not the result of simple lamellar thickening. Instead, several kinds of crystal forms can exist in one polymer sample, i.e. the polymer crystals exhibit polymorphism. Here we show several examples of this kind of behavior.

Polyurethanes are a large family of very important materials that are probably the oldest and most used block copolymers.²¹ Several transitions can be observed in a DSC thermogram, depending on the nature of the solid-state structure of the sample. These include the T_g s and endothermic meltings of crystalline and paracrystalline domains. The variation in the T_g of the soft matrix in segmented polyurethanes can be used as an indicator of the degree of microphase separation.^{41,42} The endotherms associated with the disordering process of the urethane domains depend strongly upon thermal history. Seymour *et al.*^{43,44} demonstrated that these endotherms correspond to domains of limited short-range order (with lower melting points), long-range domains and microcrystallites of the hard segments. Short-range ordering can be improved continuously by annealing as evidenced by a consistent upward temperature shift of the endotherm until it merges with the highest endotherm.

Both the po
involving H-bonding
a planar arrangement
being less favored.
can also be seen.

In addition to
cells of different c
example, wide-angle
influence of the com
different vinyl alcoh
cooling rates, 45
homopolymers, poly
cooling rate have b
copolymers. For sa
obtained for copoly
VA respectively) w
quenched from the
observed for these p
unit cell was continu
by the continuous ch
copolymers which is
melting temperatures

Both the polyamides and polyurethanes are similar in that they can form crystals involving H-bonding. One can think of different kinds of H-bonding arrangements, with a planar arrangement being the most stable, and out of plane intermolecular H-bonding being less favored. Distinct thermal transitions due to different H-bonding arrangements can also be seen.

In addition to size-related polymorphs, polymers that crystallize in different unit cells or different chain conformations also cause multiple thermal transitions. For example, wide-angle X-ray diffraction (WAXS) measurements were used to study the influence of the composition and thermal history on the type of lattice developed in three different vinyl alcohol-ethylene, VAE, copolymers crystallized from the melt at various cooling rates.⁴⁵ The results were compared with those of the corresponding homopolymers, poly(vinyl alcohol) and low-density polyethylene. Both composition and cooling rate have been found to determine the crystalline structure of these VAE copolymers. For samples slowly crystallized from the melt, a monoclinic lattice is obtained for copolymers VAE71 and VAE68 (with compositions of 71 and 68 mol % VA, respectively) while orthorhombic lattices were found for the same samples when quenched from the melt. One unusual structure conversion phenomenon was also observed for these polymers. As monitored by WAXS, the crystal with orthorhombic unit cell was continuously converted to the crystal with monoclinic unit cell as indicated by the continuous change of the lattice angle β . The polymorphism exhibited by these copolymers which is unusual. Moreover, it seems that there are no differences in the melting temperatures between the two crystalline modifications.

Poly(hexamethyleneterephthalate)

conjugated and non-

of this polymer reve

β -forms (mp 151 °C)

triclinic. In all three

that maximizes π - π

group relative to the

is in a syn conforma

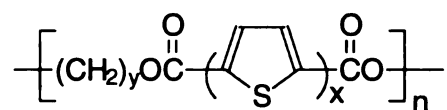
The transformation t

161 °C, γ -form to m

strong π - π interactio

of the phase transfor

Poly(hexamethylene-2,2'-bithiophene-5,5'-dicarboxylate), **12**, has alternating conjugated and nonconjugated segments. X-ray fiber diffraction and DSC investigations of this polymer reveal the existence of three polymorphs.⁴⁶ Both α - (mp ~ 125 °C) and β -forms (mp 151 °C) belong to the monoclinic system, while the γ -form (mp 172 °C), is triclinic. In all three forms the bithiophene dicarboxylate group is confined to a plane that maximizes π - π -conjugation; however, with different orientations of the carbonyl group relative to the sulfur atom (as shown in **Scheme 1**, in the α - and β -forms, S-C-C=O is in a syn conformation (left), while in the γ -form, S-C-C=O is in an anti conformation). The transformation temperatures are as follows: α - to β -form, 130 - 150 °C; β - to γ -form, 161 °C; γ -form to mesophase, 172 °C; and mesophase to isotropic, around 185 °C. The strong π - π interaction between aromatic planes is believed to be the main driving force of the phase transformations.

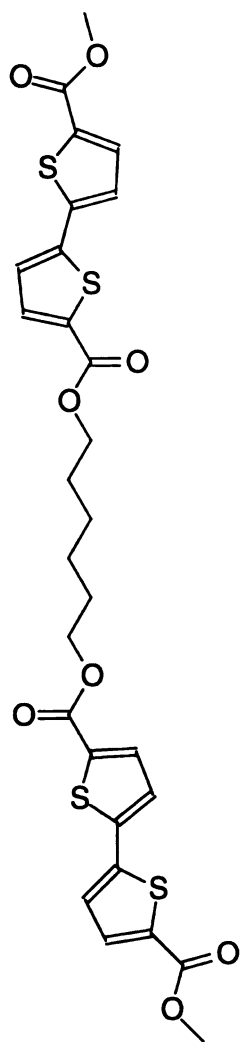


12

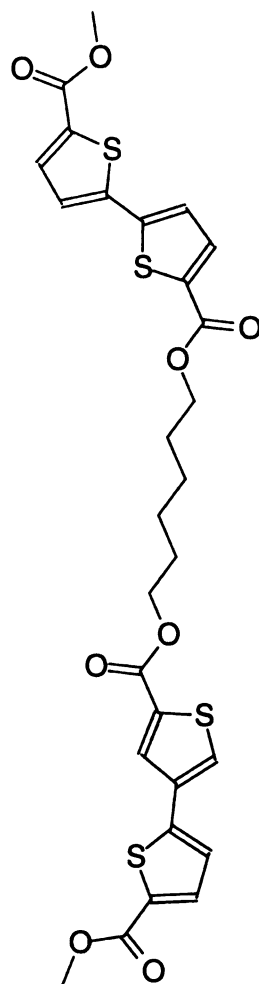
Scheme 1. Syn



Scheme 1. Syn and anti conformations for polymer **12**



syn



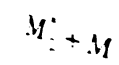
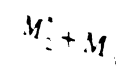
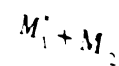
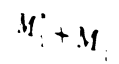
anti

IV. Synthesis of

Synthesis of
years. While the sy
well developed, the
copolymers. Summ
polymers that are re

1. Chain polym

Consider a c
After initiation, the
propagating end and
the asterisk represe
depending on the p
is dependent only o
are possible. Monoc
 M_1 or one ending



IV. Synthesis of (AB)_n Block Copolymers

Synthesis of block copolymers has been a challenge to polymer chemists for years. While the synthetic methods for preparing AB block copolymers are relatively well developed, there are fewer synthetic routes that yield well-defined (AB)_n block copolymers. Summarized below are some of the methods used in the synthesis of (AB)_n polymers that are related to this project.

1. Chain polymerization

Consider a chain polymerization with two kinds of monomers, M₁ and M₂.⁴⁷ After initiation, there are two types of propagating species—one with M₁ at the propagating end and the other with M₂. These can be represented by M₁^{*} and M₂^{*} where the asterisk represents a radical, a carbocation, or a carbanion as the propagating species depending on the particular case. Assuming that the reactivity of the propagating species is dependent only on the monomer unit at the end of the chain, four propagation reactions are possible. Monomers M₁ and M₂ can each add either to a propagating chain ending in M₁ or one ending in M₂ as follows,



where k_{11} is

monomer M_1 , k_{12} is

and so on. Through

$$F_1 = \frac{r_1 f_1}{r_1 f_1 + 1}$$

where

$$r_1 = \frac{k_{11}}{k_{12}}$$

$$r_2 = \frac{k_{22}}{k_{21}}$$

$$f_1 = 1 - f_2$$

and

$$F_2 = 1 - F_1$$

r_1 is the reactivity ratio of monomer 1 ending in monomer 1 to a chain ending in monomer 2 respectively. r_2 is the reactivity ratio of monomer 2 ending in monomer 2 to a chain ending in monomer 1 respectively. f_1 and f_2 are the mole fractions of monomers 1 and 2 in the monomer mixture. F_1 and F_2 are the mole fractions of monomers 1 and 2 in the copolymer. Alternating copolymers are formed when $r_1 = r_2 = 1$.

Alternating copolymers are formed when $r_1 = r_2 = 1$. In this case, the copolymer has a regular alternating sequence of monomers 1 and 2. The copolymer is formed by the alternating addition of monomers 1 and 2 to the growing chain.

where k_{11} is the rate constant for a propagating chain ending in M_1 adding to monomer M_1 , k_{12} is that for a propagating chain ending in M_1 adding to monomer M_2 , and so on. Through derivation,⁴⁷ one can obtain equation 10

$$F_1 = \frac{r_1 f_1^2 + f_1 f_2}{r_1 f_1^2 + 2 f_1 f_2 + r_2 f_2^2} \quad \text{eq. 10}$$

where

$$r_1 = \frac{k_{11}}{k_{12}} \quad \text{eq. 11}$$

$$r_2 = \frac{k_{22}}{k_{21}} \quad \text{eq. 12}$$

$$f_1 = 1 - f_2 = \frac{[M_1]}{[M_1] + [M_2]} \quad \text{eq. 13}$$

and

$$F_1 = 1 - F_2 = \frac{d[M_1]}{d[M_1] + d[M_2]} \quad \text{eq. 14}$$

r_1 is the relative rate for the addition of monomer 1 and monomer 2 to a chain ending in monomer 1, r_2 is the relative rate for the addition of monomer 2 and monomer 1 to a chain ending in monomer 2. f_1 and f_2 are the mole fraction of monomer 1 and monomer 2 respectively, and F_1 and F_2 reflect the composition (mole fraction) of the two monomers in the polymer. The case relevant to $(AB)_n$ microblock copolymers is alternating copolymerization.

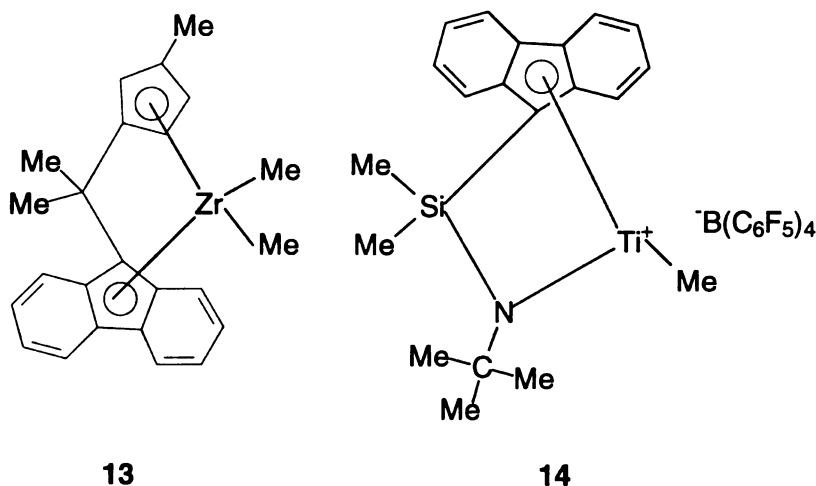
Alternating copolymers, where each block is just one monomer unit long (usually two chain atoms), is an extreme case of a microblock copolymer. Strictly speaking, these

are not block polymers.
 properties. However,
 grafted long side chains
 alternating polymers.
 14. we can obtain a
 copolymer in equilibrium
 copolymer chain.



The alternative
 reported by Leclerc
 metallocene catalyst
 fluorenyl), they observe
 structures (M_1M_2)
 of the triad distribution
 bridged
 by
 $[\eta]_0^5\text{-C}_{10}\text{H}_8\text{S}$

are not block polymers since the blocks are too short for them to show their characteristic properties. However, some of these polymers have reactive side groups, to which can be grafted long side chains that will give the polymer block-like properties. These kinds of alternating polymers can be formed by copolymerization when $r_1 = r_2 = 0$. From equation 14, we can obtain $F_1 = 0.5$ for this case, which means the two monomers enter into the copolymer in equimolar amounts in a nonrandom, alternating arrangement along the copolymer chain.



The alternating copolymerization of ethene/propene using a metallocene catalyst reported by Leclerc and coworkers is one example of these reactions. With the zirconium metallocene catalyst **13** $\{[(3\text{-MeCp})(\text{Me}_2\text{C})(\text{Flu})]\text{ZrMe}_2\}$ (Cp = cyclopentadienyl, Flu = fluorenyl), they obtained a highly alternating copolymer. The percentage of alternating structures ($\text{M}_1\text{M}_2\text{M}_1$ and $\text{M}_2\text{M}_1\text{M}_2$) was estimated to be 81% based on ^{13}C NMR analysis of the triad distribution. Titanocene complexes based on an amido-fluorenyl ligand bridged by a dimethylsilylene group, catalyst **14** $[(\eta^1\text{:}\eta^5\text{-C}_{13}\text{H}_8\text{SiMe}_2\text{NCMe}_3)\text{TiMe}]^+[\text{B}(\text{C}_6\text{F}_5)_4]^-$, was used to catalyze the synthesis of a

perfectly alternating

polystyrene structure

The usual

charged by select

copolymer. Radia

minator was used

olefins and maleic

this copolymer were

and amines (Scheme

derivatives, they can

Alternating

maleimides were syn

The copolymers ha

allows modification

amphiphilic copolym

to the polymer back

alternating copolyme

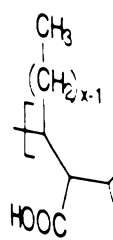
perfectly alternating ethylene/styrene copolymers with a well-defined isotactic polystyrene structure.⁴⁸

The usual homogeneous morphology of simple alternating copolymers can be changed by selectively grafting to functional groups purposely incorporated in the copolymer. Radical copolymerization with 2,2'-azobisisobutyronitrile (AIBN) as initiator was used to synthesize a series of alternating copolymers of straight-chain α -olefins and maleic anhydride with a molecular weight of 2,500-37,000. Derivatives of this copolymer were prepared by reaction of the anhydride residues with alcohols, water, and amines (**Scheme 2**).⁴⁹ Because of the amphiphilic characteristic of these copolymer derivatives, they can be used to prepare Langmuir-Blodgett (LB) multilayers.

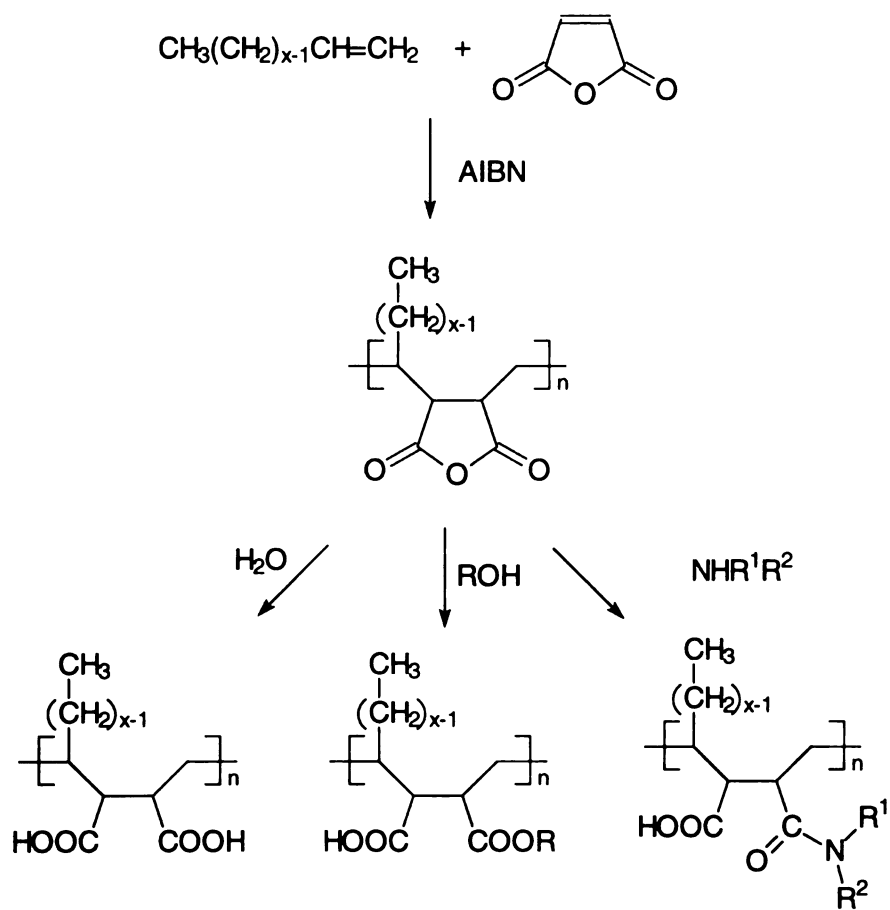
Alternating copolymers from isopropenyl isocyanate and N-substituted maleimides were synthesized by AIBN initiated radical copolymerization (**Scheme 3**).⁵⁰ The copolymers have an isocyanate group in the constitutional repeating unit which allows modification and functionalization in a polymer reaction. The preparation of amphiphilic copolymers having a hydrophobic backbone and a hydrophilic chain attached to the polymer backbone at every other repeat unit were demonstrated as well as an alternating copolymer with an NLO chromophore attached to the polymer.

Scheme 2. Synthesis of

polymers and derivatives



Scheme 2. Synthesis of derivatives of α -olefin maleic anhydride alternating copolymers and derivatives.



Scheme 3. F

styrenyl isocyanate

C

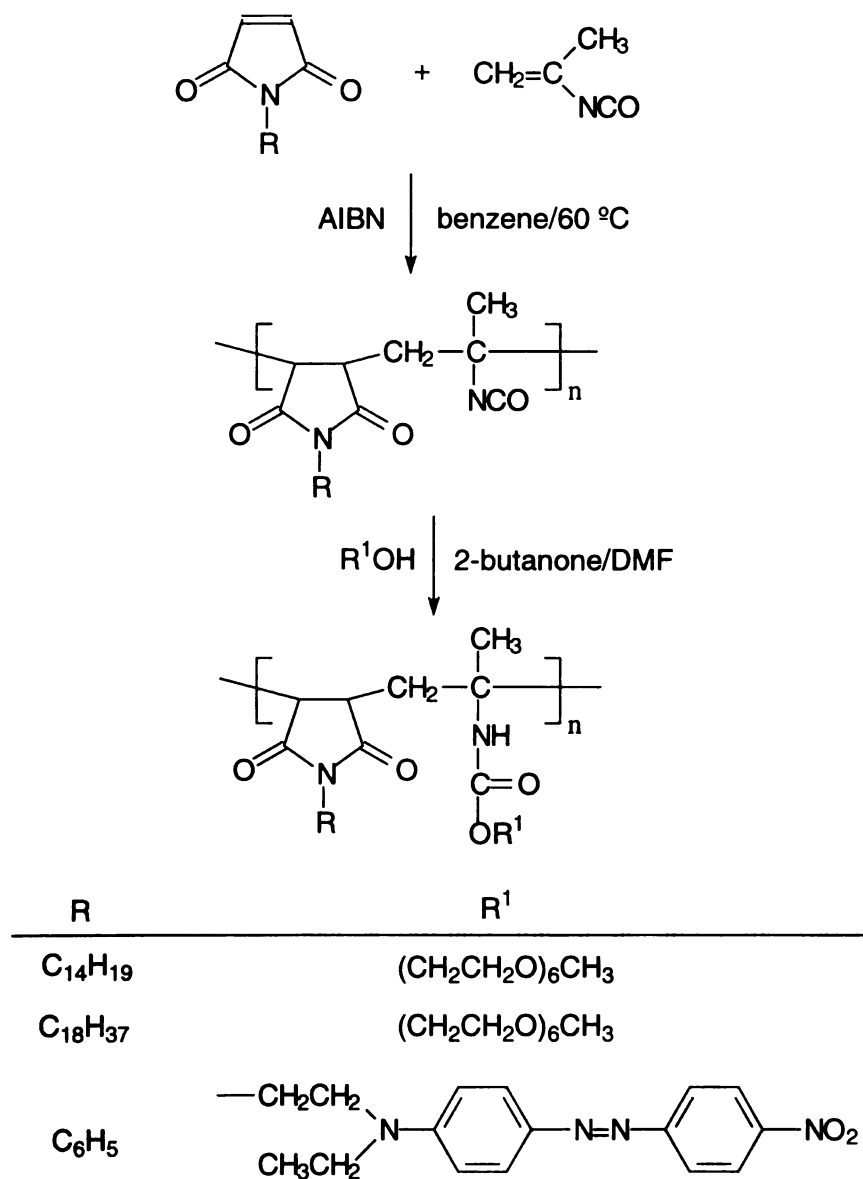
R

$C_{14}H_{19}$

$C_{18}H_{37}$

C_6H_5

Scheme 3. Functional polymers from N-substituted poly(maleimide-*alt*-isopropenyl isocyanate)s



2 Ionic living

(AB)_n archi
through sequential
of styrene-isoprene
of styrene with sec
styrene (**Scheme 4**)
to initiator. In this
specimens cast fro
structures.

Difunctional

This route has the a
with monofunctional
multiblock copolym
For example, a serie
styrene (S) and buta
living anionic poly
temperature with th
cyclohexane/diethyl
polymerization, dipl
reactivity, which is
MMA) carbonyl gr
MMA was polyme
morphologies such

2. Ionic living polymerization

$(AB)_n$ architectures are synthesized by ionic living polymerization techniques through sequential monomer addition. For example, well-defined multiblock copolymers of styrene-isoprene $(S_xI_y)_n$ (where $n = 1-4$) were synthesized by initiating polymerization of styrene with *sec*-butyl lithium followed by the sequential addition of isoprene and styrene (**Scheme 4**).¹⁹ Each block length is controlled by varying the ratio of monomer to initiator. In this example, the polystyrene fractions are kept at 0.5 and all the film specimens cast from toluene solutions were found to have an alternating lamellar structures.

Difunctional initiators can also be used to initiate sequential ionic polymerization. This route has the advantage of requiring half the sequential monomer additions needed with monofunctional initiators. With careful modification of the reaction conditions, multiblock copolymers with more than two kinds of segments also can be synthesized. For example, a series of, pentablock copolymers consisting of methyl methacrylate (M), styrene (S) and butadiene (B), (MSBSM) were successfully synthesized⁵¹ by sequential living anionic polymerization. Butadiene polymerization was initiated at room temperature with the di-adduct of *tert*-butyllithium and *m*-diisopropenylbenzene in a cyclohexane/diethyl ether mixture. Styrene was added, and on completion of the styrene polymerization, diphenyl ethene was added to terminal styrene anion to decrease the reactivity, which is necessary to prevent nucleophilic attack at the methyl methacrylate (MMA) carbonyl group. The solvent was changed to a cyclohexane/THF mixture and MMA was polymerized at -78 °C (**Scheme 5**). In addition to classical phase morphologies such as cylindrical and lamellar phases, these materials show two

nonclassical morph

by TEM.

Telechelic p

capacity to react w

of copolymers. Th

with a variety of ele

synthesized in q

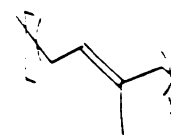
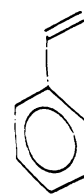
stoichiometric amo

of the amide pr

corresponding aron

in coupling reactio

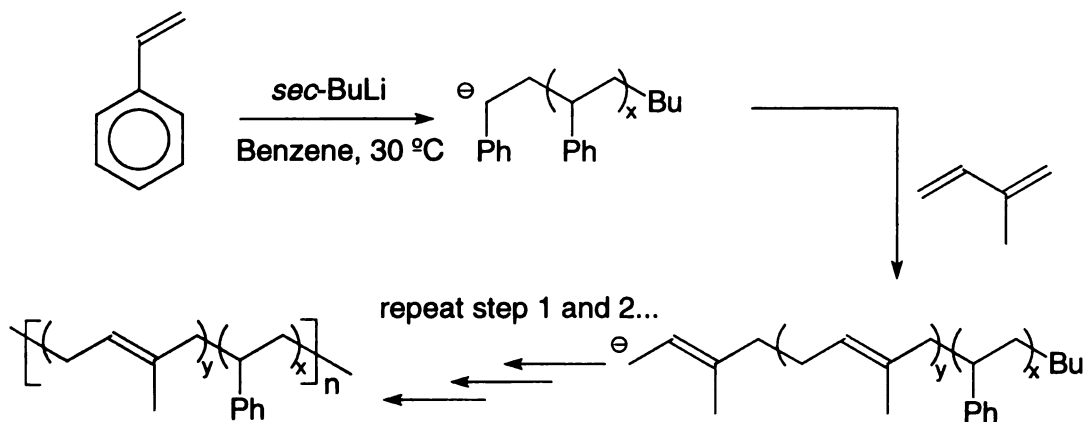
Scheme 4



nonclassical morphologies, i.e., catenoid-lamellar and strut phase structures as observed by TEM.

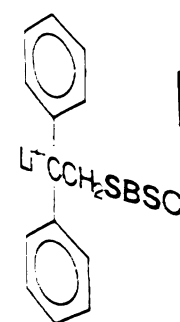
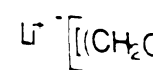
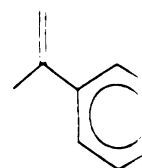
Telechelic polymers, polymers that containing one or more end groups with the capacity to react with other molecules, are useful for synthesizing block and other types of copolymers. These polymers can be prepared by terminating living anionic polymers with a variety of electrophilic reagents. As shown in **Scheme 6**, ω -amidopolystyrene was synthesized in quantitative yields by the reaction of poly(styryl)lithium with stoichiometric amounts of N,N-diisopropyl-4-(1-phenylethenyl)benzamide. Deblocking of the amide protecting group by acid hydrolysis quantitatively provides the corresponding aromatic carboxyl chain-end functionalized polystyrene which can be used in coupling reactions.⁵²

Scheme 4. Sequential anionic polymerization of styrene and isoprene

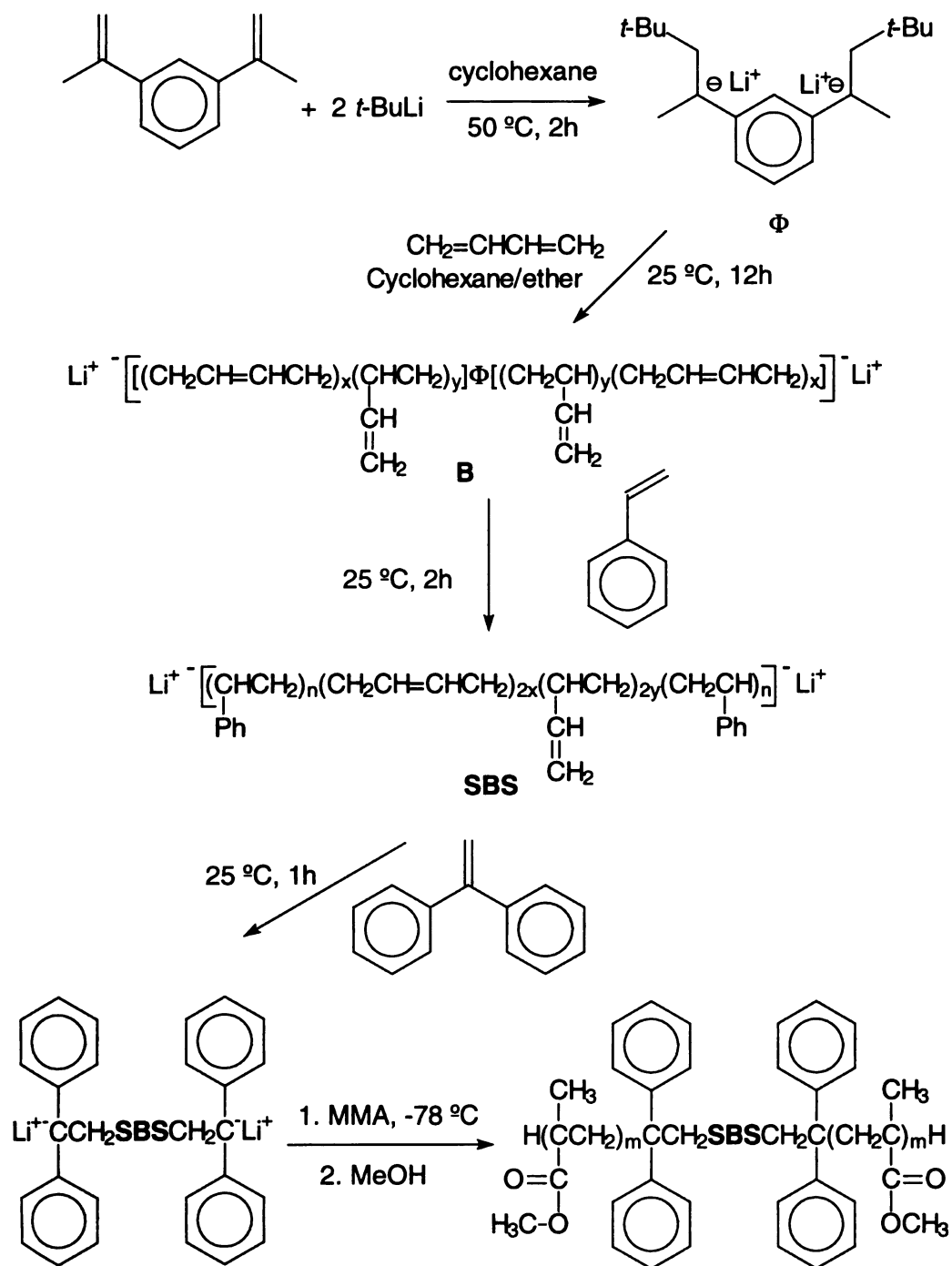


Scheme 5

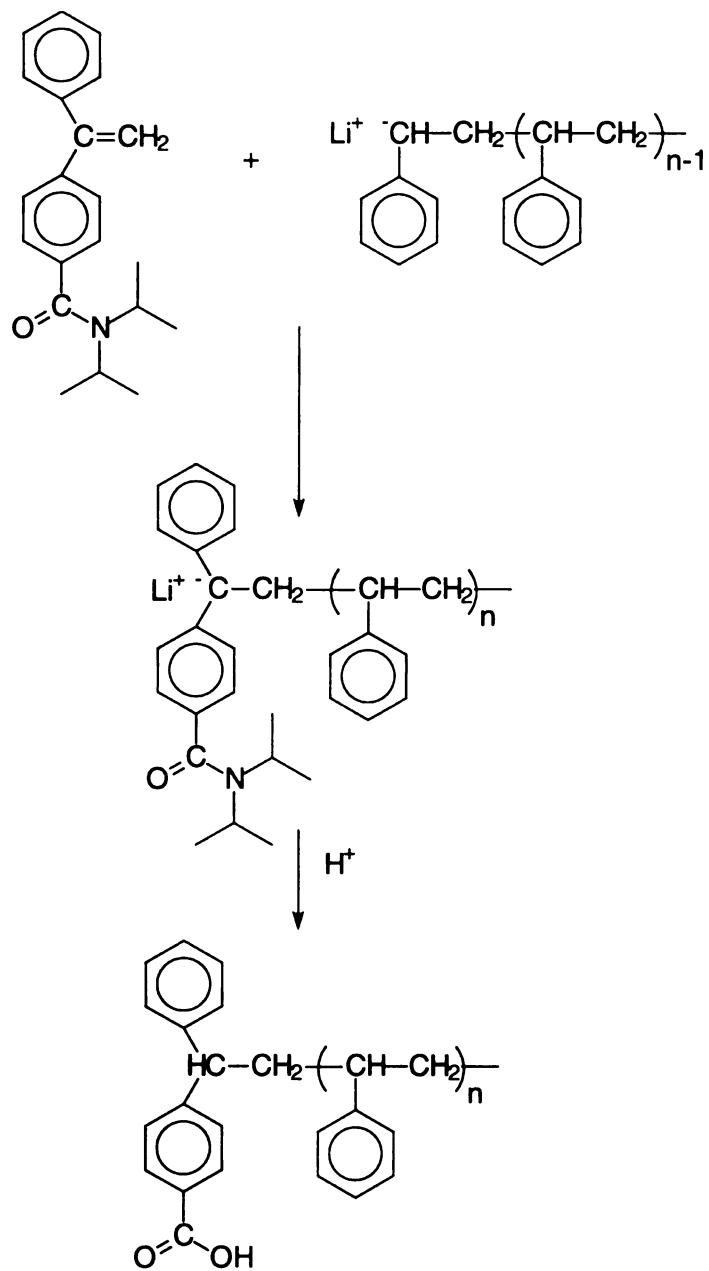
styrene-*b*-methyl m



Scheme 5. Synthesis of poly[methyl methacrylate-*b*-styrene-*b*-butadiene-*b*-styrene-*b*-methyl methacrylate] pentablock copolymer.



Scheme 6. Synthesis of a typical telechelic polymer



3. Step co

Typical
polymerization
diisocyanates.
of low molecu
oligomeric diis

Starting
from other po
ethylene oxide
polystyrene to
intermediate w

Step-gr
derivatives are
organolithiums
hydrocarbon an
of the use of th
was found that
the silylene blox

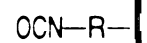
3. Step copolymerization

Typically, microblock copolymers are prepared by the step-growth polymerization of difunctional monomers derived from carboxylic acids, such as diisocyanates, anhydrides, diesters, and diacids with diols or diamines, often in the form of low molecular weight oligomers. In a typical example, as shown in **Scheme 7**, an oligomeric diisocyanate is reacted with a polyol to yield a polyamideurethane.⁵³

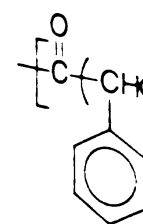
Starting materials for blocks used in step copolymerization can be synthesized from other polymerization methods. For example, Finaz *et al.*⁵⁴ prepared styrene-ethylene oxide (AB)_n copolymers by using phosgene to convert a dicarbanion-terminated polystyrene to a diacyl chloride-terminated oligomer, followed by condensation of this intermediate with polyethylene glycol (**Scheme 8**).

Step-growth polymerizations involving functional groups other than acid derivatives are also readily available and widely used. For instance, coupling of organolithiums and chlorosilanes is an effective way to make copolymers that contain hydrocarbon and silicon segments in their backbones. Shown in **Scheme 9** is an example of the use of this kind of reaction to make a σ - π conjugated alternating copolymer.⁵⁵ It was found that the σ - π conjugation was enhanced when the number of silicon atoms in the silylene block was increased.

Scheme 7. Synthesis of

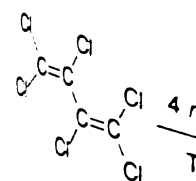


Scheme 8. Synthesis of

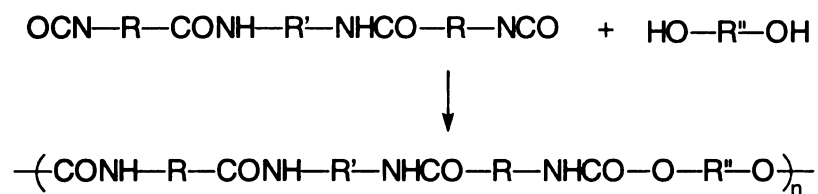


Scheme 9. Synthesis of

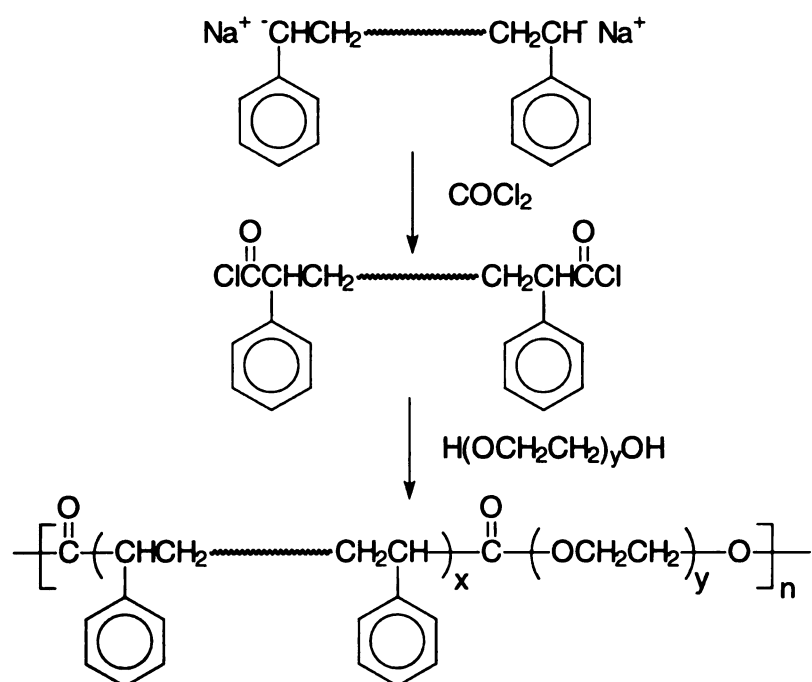
polymer



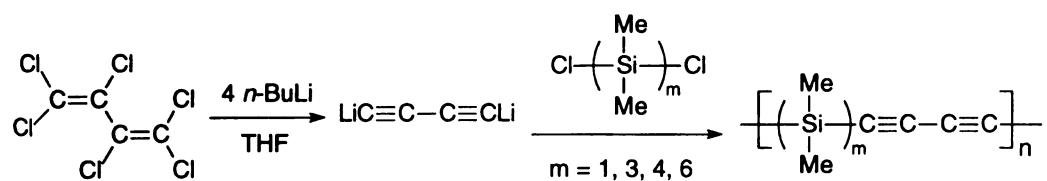
Scheme 7. Synthesis of polyamideurethanes



Scheme 8. Synthesis of styrene-ethylene oxide (AB)_n copolymers



Scheme 9. Synthesis of σ - π conjugated alternating silylene-diacetylene copolymer



4 Metathesis

In recent years, the impact in the area of polymerization processes, ROMP and ATRP, proceed via the same double bond to a metal. If the C=C double bond remains coordinated, forms the basis of irreversible, the inter and the rates of inter then.

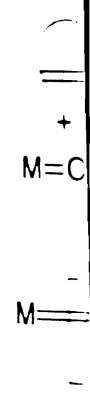
ADMET polymerization shown in Scheme 1. metallocyclobutane polymers. As noted, polymerizations, often volatile by-product drive the equilibrium

4. Metathesis Polymerization

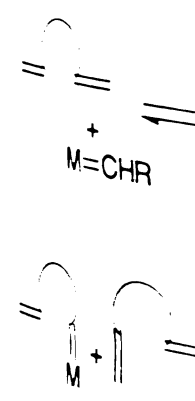
In recent years metathesis polymerization has made an increasingly significant impact in the advanced materials arena.⁵⁶ There are two kinds of metathesis polymerization processes involving alkenes, Ring Opening Metathesis Polymerization (ROMP) and Acyclic Diene Metathesis Polymerization (ADMET). Both polymerizations proceed via the same basic mechanism involving a 2 + 2 cycloaddition of an alkene double bond to a metal alkylidene (or carbene) to give a metallocyclobutane intermediate. If the C=C double bond is constrained within a ring, then the newly formed C=C double bond remains connected to the metal alkylidene. The mechanism shown in **Scheme 10** forms the basis of the ROMP reaction. ROMP can be living when the steps are irreversible, the intermediates are stable on the time scale of the polymerization reaction, and the rates of initiation and propagation reaction are of similar orders of magnitude, then.

ADMET polymerization involves step-growth polymerization of dienes. As shown in **Scheme 11**, the polymerization cycle involves the formation of metallocyclobutane intermediates that lead to dimer, trimer, and eventually to high polymers. As noted in the scheme, each step is reversible. Like many step-growth polymerizations, obtaining high molecular weight polymer relies on the generation of a volatile by-product, in this case ethylene, which is readily removed under vacuum to drive the equilibrium to favor the condensation process.

Scheme 10. R:

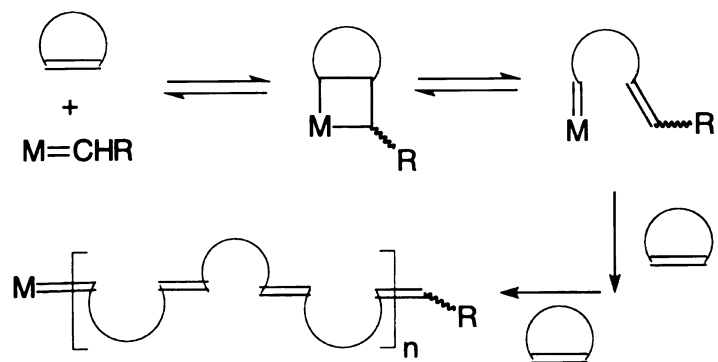


Scheme 11. Ac

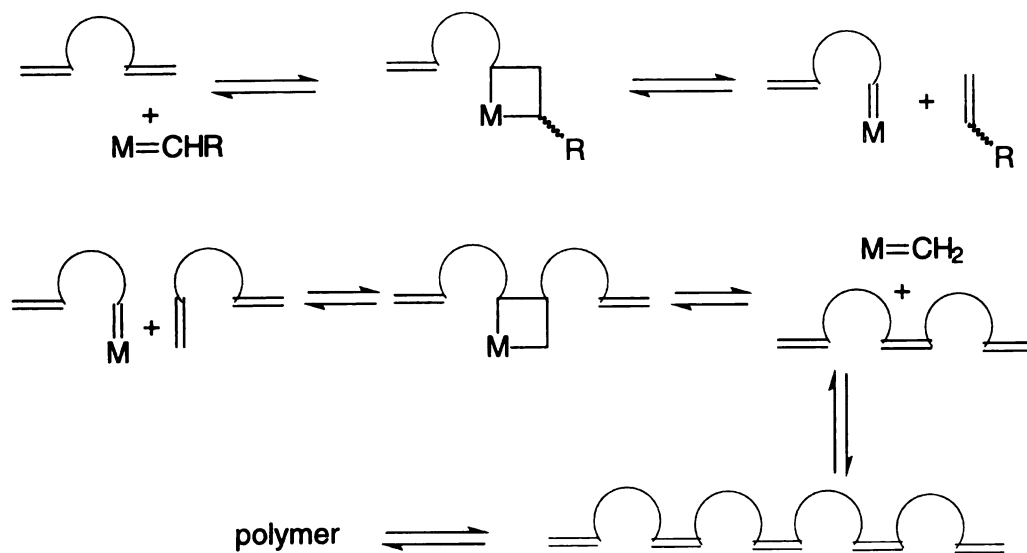


po

Scheme 10. Ring-opening metathesis polymerization (ROMP)



Scheme 11. Acyclic diene metathesis (ADMET) polymerization



The olefin

using it as a po

invented. This w

relatively stable

reactions have bee

of a transition m

examples. Wagne

polymerize 1,9-dec

$\text{WCl}_6/\text{EtAlCl}_2/\text{PrO}$

catalysts polymer

metathesis catalys

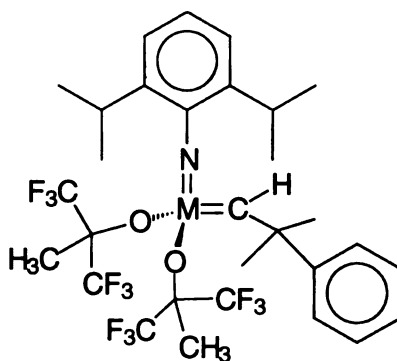
of organic functio

Well-def

developed in th

carrying out R

The olefin metathesis reaction has been known for many years,⁵⁷ but progress in using it as a polymerization technique was slow until well-defined catalysts were invented. This was especially true for ADMET since it requires highly active yet relatively stable and long lived catalysts. Traditionally, metathesis polymerization reactions have been carried out in solution using dual-component formulations consisting of a transition metal halide and a main group alkyl metal co-catalyst.⁵⁸ In early examples, Wagener and his colleagues⁵⁹ employed the $\text{WCl}_6/\text{EtAlCl}_2$ catalyst system to polymerize 1,9-decadiene and 1,5-hexadiene, and Nubel *et al.*⁶⁰ used a modified catalyst $\text{WCl}_6/\text{EtAlCl}_2/\text{PrOAc}$, to synthesize polypentenamer from 1,5-hexadiene. However, both catalysts polymerized hydrocarbon diene monomers with limited success. Since classical metathesis catalysts are generally strong Lewis acids, they do not tolerate a wide variety of organic functional groups in monomers.



15

Well-defined Lewis acid-free transition metal alkylidene complexes were developed in the late 80's and early 90's. These catalysts have been very successful in carrying out ROMP and ADMET polymerization of cyclic olefin and acyclic diene

monomers having

catalysts are m

coworkers⁶¹⁻⁶⁴

coworkers⁶⁵⁻⁶

Cl

C

The lig

olefin affinity

tolerate polar f

ROMP and A

oxygen, moist

synthesize.

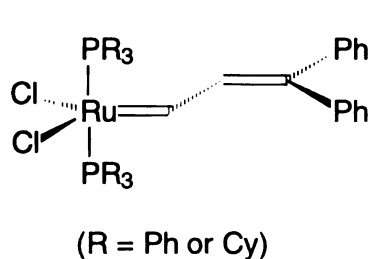
In cont

much less sens

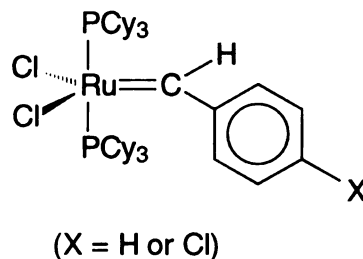
groups. In fac

aqueous medi

monomers having different organic functionalities. The most widely used metathesis catalysts are molybdenum and tungsten complexes **15** developed by Schrock and coworkers⁶¹⁻⁶⁴ and ruthenium complexes **16** and **17** developed by Grubbs and coworkers.⁶⁵⁻⁶⁸



16



17

The ligands in the Schrock's catalysts were carefully chosen to combine high olefin affinity and low Lewis acidity, so that they selectively react with olefins and tolerate polar functional groups. Schrock's catalysts are very effective in initiating both ROMP and ADMET polymerization. However, these catalysts are very sensitive to oxygen, moisture, and some reactive functional groups, and are inconvenient to synthesize.

In contrast, Grubbs' ruthenium carbene metathesis catalysts⁶⁵⁻⁶⁸ **16** and **17** are much less sensitive to oxygen and water, and they are more tolerant of organic functional groups. In fact, reactions using these complexes as catalysts can even be carried out in aqueous media.⁶⁹ Although they are effective for both ROMP⁷⁰ and ADMET

polymerization

Schrock's cata

Both A

well-designed

can be polymer

blocks and one

of 5,6-diphenyl

Konzelman⁷²

substituents also

Metathes

monomers. Wh

random copolym

monomer can ad

random copolym

norbornene macr

units (**Scheme 1**

triggered by the

polymerization w

measurements, the

index (RI) detecti

When the two ma

obtained because of

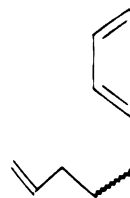
polymerization,⁷¹ their activity for ADMET polymerization is much less than for the Schrock's catalysts.

Both ADMET and ROMP have been used to prepare microblock copolymers. A well-designed monomer that contains different segments and polymerizable double bonds can be polymerized by metathesis methods to give a polymer with perfectly alternating blocks and one double bond in each repeating unit. For example, (**Scheme 12**) treatment of 5,6-diphenyl-1,5,9-decatriene, with Schrock's tungsten catalyst, allowed Wagener and Konzelman⁷² to selectively form an unsaturated polymer with perfectly alternating substituents along the backbone.

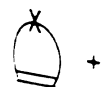
Metathesis polymerization can also be used to generate copolymers from two monomers. When the metathesis reactivity of the two monomers is similar, they form random copolymers (**Scheme 13**). The process can be easily explained since either monomer can add to the reactive species in the polymerization cycle, thus producing a random copolymer. Heroguez *et al.*⁷³ reported a ROMP copolymerization of two norbornene macromonomers containing either polystyrene⁷⁴ or polyethylene oxide⁷⁵ units (**Scheme 14**). Starting with a mixture of both macromonomers, ROMP was triggered by the addition of Schrock's molybdenum catalyst, and after 1 h, the polymerization was terminated with the addition of benzaldehyde. During GPC measurements, they found that the polymer was homogeneous to both UV and refractive index (RI) detection, which implies that the copolymer is not a block-like polymer. When the two macromonomers were added sequentially, a block copolymer can be obtained because of the living nature of ROMP.

Scheme 1

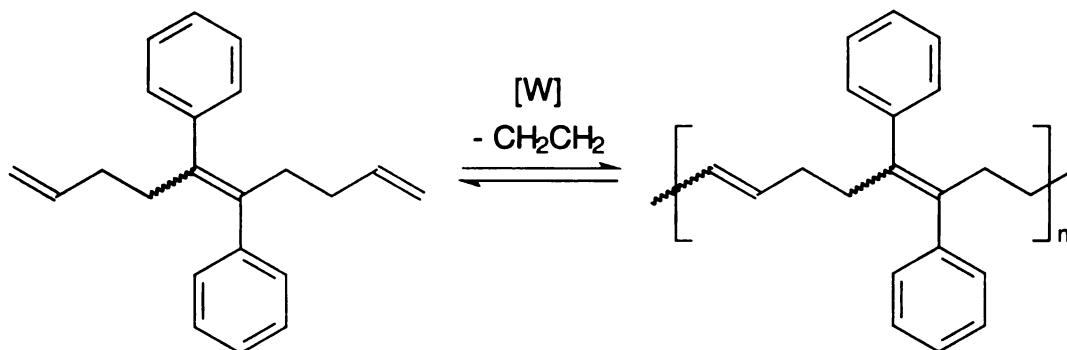
substituents along t



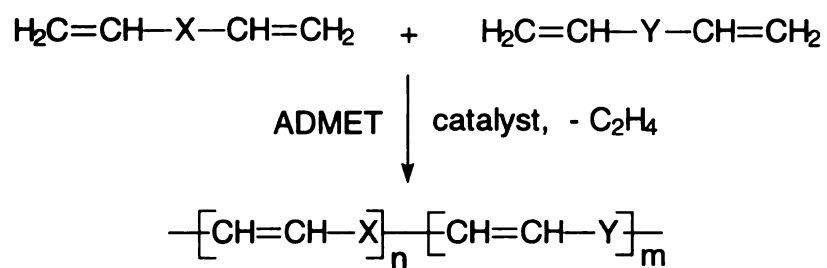
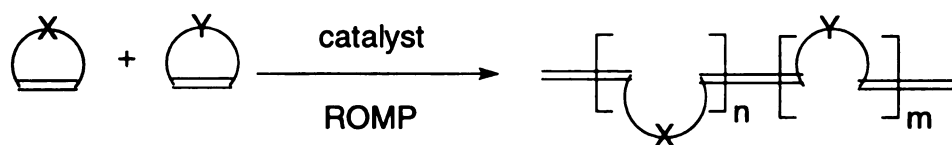
Scheme 13

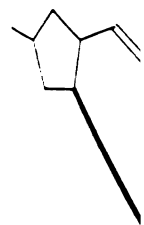


Scheme 12. Synthesis of unsaturated polymer with perfectly alternating substituents along the backbone

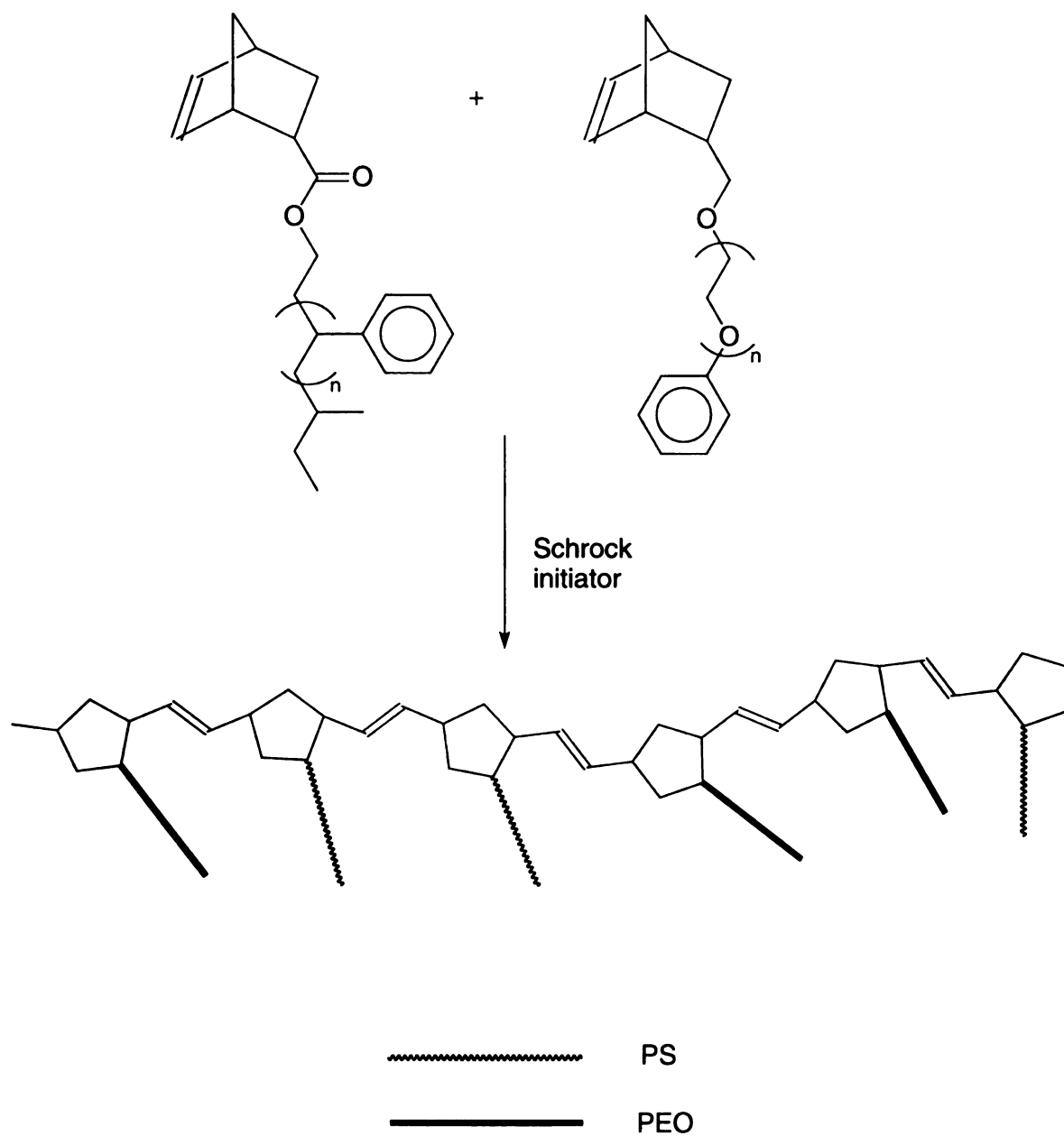


Scheme 13. Generalized metathesis copolymerization scheme





Scheme 14. Ring opening copolymerization of macromonomers



Block c

ADMET copoly

butenylene] **18**

copolymerization

weight⁷⁶ becau

insoluble oligo

(Scheme 15).⁷

tungsten cataly

solution of bip

concentration. I

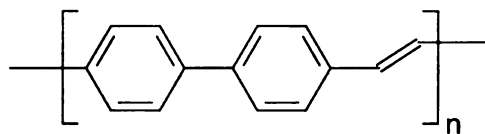
ethylene and p

biphenylene w

perfectly altern

studies.

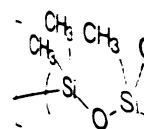
Block copolymers with an $(AB)_n$ structure can be synthesized by controlled ADMET copolymerization. For example, both poly[(hexamethyltrisiloxanediyl)-butenylen] **18** and polybiphenylene **19** can be obtained by ADMET polymerization, but copolymerization of the monomers does not yield a copolymer with high molecular weight⁷⁶ because of the dimerization and trimerization of the aromatic monomer to give insoluble oligomers. The cross metathesis was achieved with a controlled experiment (**Scheme 15**).⁷⁷ Diallylhexamethyltrisiloxane was first oligomerized with Schrock's tungsten catalyst and diluted in a toluene solution. To this system, a dilute toluene solution of biphenyldiene **20** was added over a period of 1 h. Because of its low concentration, homopolymerization of this monomer was limited. With the evolution of ethylene and propylene, the copolymer with alternating oligosiloxane butylene and biphenylene was obtained. However, the block lengths are not exact, so this is not a perfectly alternating system. The polymer structure was confirmed by NMR and TGA studies.



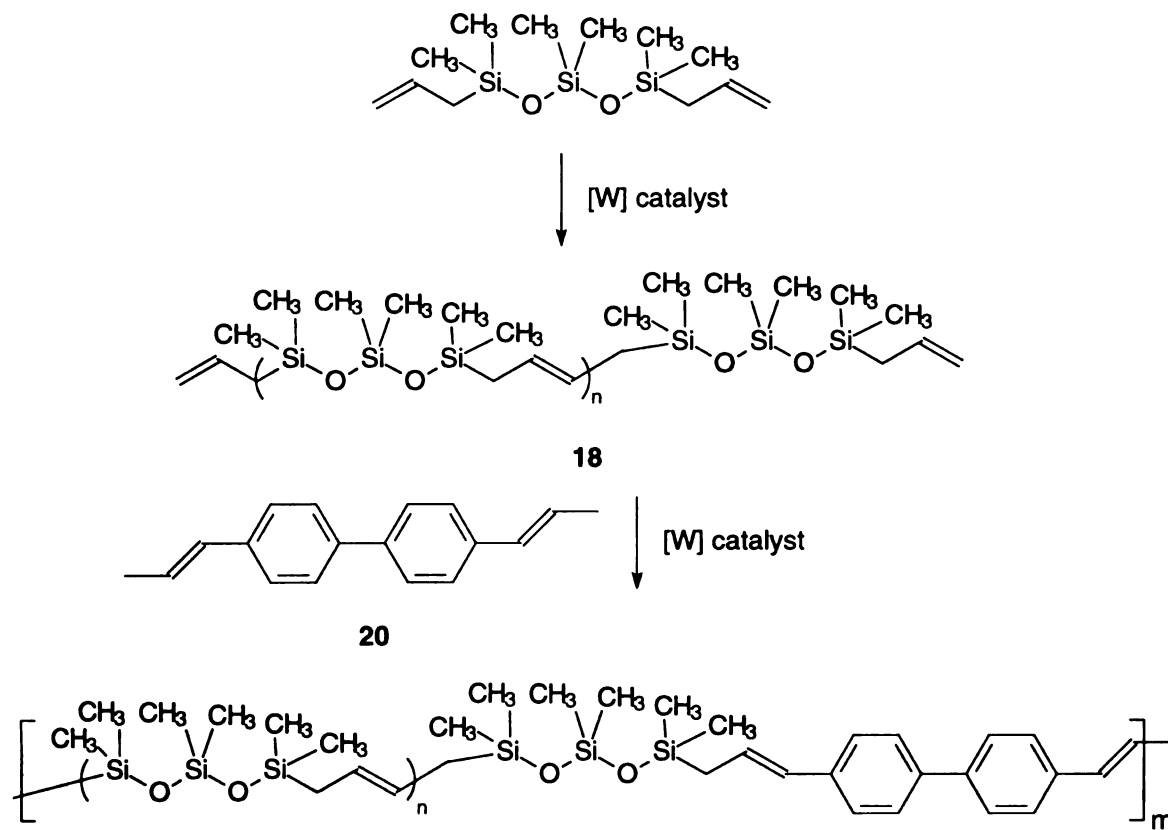
19

Scheme

nanylene]



Scheme 15. ADMET copolymerization to poly[(hexamethyltrisiloxanediyl)-butenylene]



5. Comparison of copolymers

Although
has advantages
this project
copolymerization
uniform block
zero is very low
control, but the
In addition, the
portion of mo
can not be very

ROMP

blocks, it can
all reactions,
polymerization
limits the sec
to prepare, an

Step-

copolymers
monomers, t
growth poly
molecular w

5. Comparison of different polymerization methods for obtaining $(AB)_n$ copolymers

Although $(AB)_n$ block copolymers can be synthesized in many ways, each method has advantages and disadvantages. Uniformity of segment length is a major concern in this project since it greatly affects the crystallinity. Most conventional chain copolymerization methods, such as radical and ionic polymerization, do not generate uniform block lengths. Also, the number of monomer pairs with both r_1 and r_2 equal to zero is very limited. Living polymerization can generate monodisperse blocks with good control, but the blocks are not of exact length and are described by a Poisson distribution. In addition, termination and chain transfer reactions occur with the addition of each new portion of monomers. Therefore, n , the number of repeating unit in an $(AB)_n$ copolymer can not be very large.

ROMP is also a chain polymerization. If the monomer is designed to contain both blocks, it can give exactly alternating microblock copolymers. However, as required by all reactions, polymerization must result in a decrease of free energy, and in ring opening polymerization, the ring strain determines the polymerizability of cyclic monomers. This limits the scope of ROMP polymerizations. In addition, large cyclic olefins are difficult to prepare, and thus most ROMP examples involve the opening of small rings.

Step-growth polymerizations are usually used to prepare most microblock copolymers because of easy access to the needed monomers. By carefully selecting monomers, the resulting copolymers normally have exact block lengths. However, step-growth polymerizations require exact stoichiometry for the polymerizations to reach high molecular weight. Many step growth polymerizations are condensation reactions that

yield a small
removal of the
high molecular
condensation a

The A
polymerization
the α,ω diene
needed for RC
enables system
polymers with

Comp
more sensitive
There have be
dependent on

V. Target

We ar
where the AB
Scheme 16. th
block is an e
bond, while I
hydrophobic,

yield a small molecule by-product such as water. Because of its equilibrium nature, removal of the byproduct is crucial for driving the equilibrium to high conversions and high molecular weights. Compared to chain-growth polymerizations, reaction times for condensation schemes are usually long.

The ADMET scheme is a step growth process and compared to ROMP, ADMET polymerization rates are much slower for the synthesis of the same polymer. However, the α,ω dienes needed for ADMET generally are easier to prepare than the cyclic olefins needed for ROMP, allowing easy access to a wide variety of monomer structures. This enables systematic studies of the evolution of the structures and properties of the polymers with variations in the lengths of the individual microblocks.

Compared to traditional polymerization methods, metathesis polymerization is more sensitive to impurities and functional groups due to the sensitivity of the catalysts. There have been reports showing that the success of this kind of polymerization is largely dependent on the purity of the monomer.^{59,78,79}

V. Target molecules in this research

We are interested in a set of block copolymers, $(AB)_n$ microblock copolymers, where the AB pattern is repeated n times and both blocks can crystallize. As shown in **Scheme 16**, the polymers contain two blocks with distinctly different properties. The A block is an exact length oligoethylene or oligoethylene that contains a single double bond, while B block is an exact length oligoethylene oxide. Thus the A block is hydrophobic, and the B block is hydrophilic. The amphiphilic character of these

microblocks of

surfactants, p

ionic conduct

Scher

Base

strongly pha

studied to d

connectivity

of the block

block length

morphologic

PEPEO mi

different cr

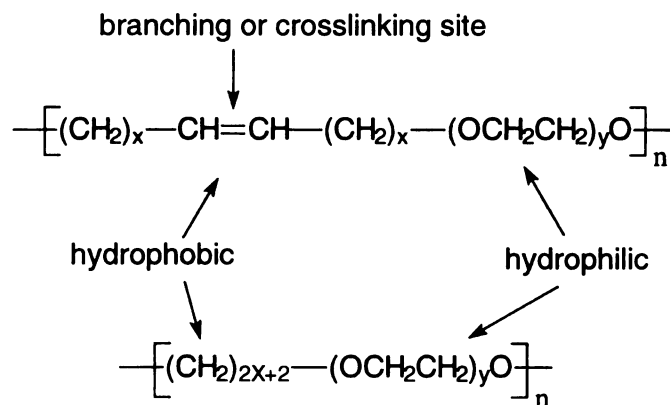
crystallizes

These featu

and give ris

microblocks could lead to surfactant behavior and therefore have practical applications as surfactants, polymer blend compatibilizers, and because of the polyether segments, as ionic conductors.

Scheme 16. Target $(AB)_n$ microblock copolymers



Based on the properties of the homopolymers, these copolymers are expected to strongly phase separate and be highly crystalline. The crystalline systems that have been studied to date have often been poorly defined in terms of the block lengths and their connectivity. Being able to incorporate exact length segments can increase the regularity of the block copolymer and therefore increase the crystallinity. Because of the shorter block lengths in $(AB)_n$ copolymers, these polymers may exhibit more complicated morphologies than simple AB block copolymers. One particularly interesting feature of PE/PEO microblock polymers is that the PE and PEO blocks normally adopt strikingly different crystal structures. PE crystallizes in a planar zigzag conformation, and PEO crystallizes in a 7_2 helix with 7 ethylene oxide units completing two turns (**Figure 5**). These features of the copolymer component can lead to competition between structures and give rise to interesting copolymer properties.

The r
are of signifi
or for crossli

The
copolymers
crystal size
chain entang
the behavior
with the gen
16. and $y =$
chemical con
weight mole
systems. Th
microblock c

VI. Sever

1. Polye

Polye
polyethylene
Linear alkane
marked pref
where L is th

The regularly spaced double bonds in the unsaturated version of these copolymers are of significance. They can be used as a site for branching to make grafted polymers, or for crosslinking to form three dimensional network materials.

The characterization of copolymers is often complicated, and crystalline copolymers are even more challenging. Molecular weight distributions, variations in crystal size and perfection, the presence of interlamellar polymer chains and polymer chain entanglements all add complexity to block copolymers. To aid in understanding the behavior of these polymers, we synthesized a series of exact length triblock oligomers with the generic structure $\text{H}(\text{CH}_2)_x(\text{OCH}_2\text{CH}_2)_y\text{O}(\text{CH}_2)_x\text{H}$, where $x = 6, 8, 10, 12, 14$ and 16 , and $y = 2-8, 10$, and 14 . The blocks in these model compounds have the same chemical components as the target polymers, but because they are simple low molecular weight molecules, it is easier to test the origin of a specific property in the model systems. These model compounds may provide simple rules for the study of $(\text{AB})_n$ microblock copolymers.

VI. Several polymers directly related to this project

1. Polyethylene and polyethylene oxide

Polyethylene is one of the most widely used commercial polymers. Unbranched polyethylenes, or long chain normal alkanes, are of specific relevance to this project. Linear alkanes with about 150 carbon atoms can form chain-folded crystals. There is a marked preference for integral folding, whereby the fold length l adopts values $\approx L/n$, where L is the extended chain length and n an integer.⁸⁰ As described earlier, crystals

with different

many long c

temperature.

crystallization

crystallization

This effect is

obstruction

overgrowth.

Polym

crystals obtained

of the alkane

orthorhombic

form was obtained

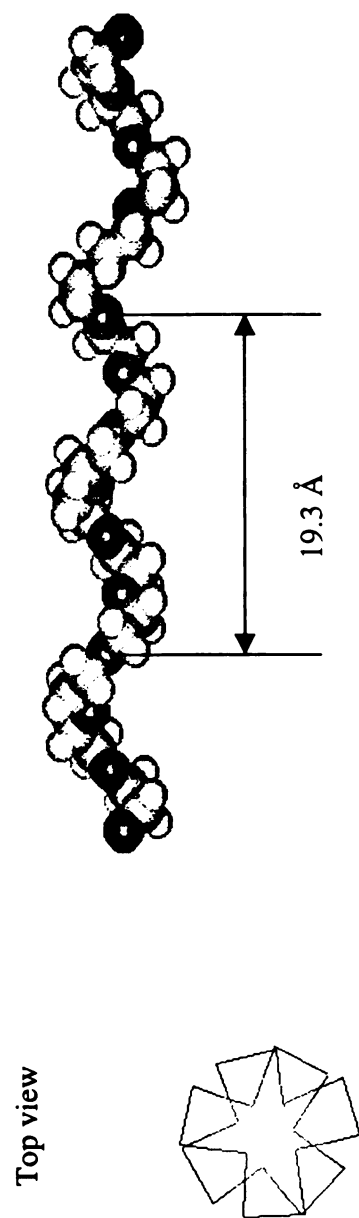
inclined with

were also obtained

conditions, d

with different thickness can be obtained by using different crystallization conditions. For many long chain normal alkanes, the crystallization rates depend on the crystallization temperature, i.e. at a certain temperature below the melting temperature, the crystallization rate reaches a maximum. Interestingly, by further lowering the crystallization temperature a few degrees, the crystallization rates reach their minimum. This effect is interpreted in terms of “self poisoning” of the crystal growth surface, i.e. obstruction to chain extension by frequent deposition of the nearly-stable chain-folded overgrowth.⁸¹

Polymorphism also exists for *n*-alkanes. There are four polymorphic forms for crystals obtained under different conditions. Under all circumstances, the conformations of the alkanes are trans planar zigzag (See **Figure 5**). The most stable form adopts an orthorhombic unit cell with four chains parallel to the *c* axis.⁸² A different orthorhombic form was observed by Khoury *et al.*⁸³ and Kobayashi *et al.*,⁸⁴ in which the chains are inclined with respect to the plane defined by the chain-ends. Two monoclinic structures were also observed for *n*-alkanes.^{85,86} With different solvent and crystallization conditions, different structures or mixtures of different structures were obtained.⁸⁷



Structure of polyethylene oxide



Structure of linear polyethylene

Figure 5. Structures of polyethylene oxide and linear polyethylene.

Another

chain normal al

approximately 1

DSC curve star

powder X-ray

intensively stud

angle X-ray sca

The nature of t

close to the PE

chain ends de

isomerization.

gauche conform

move in the lo

now changes to

completely diso

in properties su

transformation.

Polyethy

applications. P

for ion conducti

additives. Ther

known as oxya

Lewis acid or b

Another commonly observed phenomenon for unbranched polyethylenes and long chain normal alkanes is their premelting behavior seen in DSC scans. Starting from approximately 10 °C below the melting point of the polyethylene extended crystal, the DSC curve starts to deviate from its baseline, and the longest d spacings shown in the powder X-ray diffraction pattern continually decrease. This phenomenon has been intensively studied by Raman and IR spectroscopy,⁸⁸⁻⁹⁰ DSC,^{90,91} ¹³C NMR,⁹¹ small angle X-ray scattering,⁹² and electron diffraction⁹³ both individually and concurrently. The nature of the transformation is summarized as follows. When the temperature is close to the PE melting point, the regular packing of the end-groups is disrupted and the chain ends develop a disordered state that allows trans-gauche conformational isomerization. The inner methylenes still hold their all-trans conformation. As the gauche conformations increase to a certain percentage, the whole chain can rotate and move in the longitudinal direction. The original orthorhombic or monoclinic packing now changes to hexagonal packing to allow the movements. Final melting is achieved by completely disordering the trans conformation and disrupting the packing order. Changes in properties such as d-spacings, and chain conformations can be observed during this transformation.

Polyethylene oxide is a hydrophilic polymer with a broad range of commercial applications. PEO has a very high salt affinity and therefore, can act as electrolyte host for ion conducting polymers.⁹⁴ It is also an important component in surfactants and food additives. There are two major synthetic pathways for polyethylene oxides. The first, known as oxyalkylation, is the polymerization of ethylene oxides in the presence of Lewis acid or base catalysts. The products are viscous liquids to waxy solids with a

maximum mo
polymerization
system. The
alkaline earth
reach as high

Pure 1

8.05 Å, b = 1

helical struct

fiber period c

$\pm \text{OCCO} \pm$

trans, gauche

been confirm

studies 97-10

concluded to

neighboring

et al. 106-108

same structur

by X-ray di

through a tric

monoclinic p

tension. Whe

maximum molecular weight of approximately 10,000. Another method involves the polymerization of ethylene oxide on a catalytic surface in a heterogeneous reaction system. The catalysts effective for the second reactions are alkaline earth oxides⁹⁵ or alkaline earth carbonates.⁹⁶ The molecular weight by this polymerization method can reach as high as 5,000,000.

Pure PEO readily crystallizes. The crystal has a monoclinic unit cell with $a = 8.05 \text{ \AA}$, $b = 13.04 \text{ \AA}$ and $\beta = 125.4^\circ$. The PEO molecule in the crystalline state has a 7_2 helical structure, which contains seven ethylene oxide repeat units with two turns in the fiber period of 19.3 \AA (See **Figure 5**). The internal rotation angles of this molecule are $\tau(\text{OCCO}) = 65^\circ$ and $\tau(\text{CCOC}) = 188^\circ$, which correspond to the succession of a nearly trans, gauche, trans conformation along O-C-C-O bonds. These structural features have been confirmed by X-ray structure analyses as well as through extensive spectroscopic studies.⁹⁷⁻¹⁰⁴ The origin of this conformation has been carefully studied and is concluded to be due to the presence of a polarizable environment created by a neighboring PEO chain, and not to some intrinsic conformational preference.¹⁰⁵ Booth *et al.*¹⁰⁶⁻¹⁰⁸ studied macrocyclic polyethylene oxides and found that they also adopt the same structure. PEO takes a planar zigzag conformation under tension.¹⁰⁹ As indicated by X-ray diffraction and Raman spectroscopy,¹¹⁰ the planar zigzag molecule passes through a triclinic unit cell, where the packing of the PEO chains is very similar to that of monoclinic polyethylene. However, the planar zigzag conformation is stable only under tension. When stress is removed, the planar zigzag modification disappears rapidly. PEO

also assumes

resorcinol¹¹²

The T_g

°C. The melt

then levels off

perfect crystal

crystallizes. It

formation of

points depend

annealing at

and the non-

Crystals form

2 C_4E_7

Since

homopolymers

to obtain the

resulting mo-

molecule li-

crystalline P

the same

surfactants.

$(OCH_2CH_2)_$

also assumes various conformations in crystalline complexes with urea, thiourea,¹¹¹ resorcinol¹¹² and HgCl₂,^{113,114}.

The T_g determined for high molecular weight PEOs are between $-65\text{ }^{\circ}\text{C}$ and $-60\text{ }^{\circ}\text{C}$. The melting point of unfolded PEO increases with molecular weight up to 6,000 and then levels off at a value of about $65\text{ }^{\circ}\text{C}$.¹¹⁵ The thermodynamic melting point of a perfect crystal of infinite dimension has been calculated to be $76\text{ }^{\circ}\text{C}$.¹¹⁶ When PEO crystallizes, both integer and non-integer chain folding are widely observed. The formation of crystals with different lamellar thickness and therefore different melting points depends greatly on the molecular weight, solvent and thermal history. With annealing at different temperatures, isothermal lamellar thickening and thinning occur, and the non-integer folded crystallites are converted to integer folded forms.¹¹⁷⁻¹²³ Crystals formed from complexes of PEO and nitrophenol also show similar behavior.¹²⁴

2. C_xE_y nonionic surfactants and $C_xEO_yC_x$ amphiphilic triblock oligomers

Since *n*-alkyl chains and PEO adopt strikingly different structures in their homopolymers, when they are connected to form a block copolymer they must compete to obtain the conformation that best meets their energy and kinetic requirements. The resulting molecular structures can have a planar zigzag conformation throughout the molecule like crystalline PE, a helical conformation for the whole molecule like crystalline PEO, or a planar zigzag PE segment and a helical PEO segment can coexist in the same molecule. Such structures are most commonly seen in nonionic surfactants.^{125,126} The simplest such surfactants have the general formula $\text{CH}_3(\text{CH}_2)_x\text{-(OCH}_2\text{CH}_2)_y\text{OH}$ (simplified as C_xEO_y). Their solid state structures have been studied

by Raman spe

nonionic surf

segment conf

alkyl chain le

compounds w

molecular co

oxyethylene

a trans conf

conformation

point, C.E.s.

depending o

experiments

aliphatic an

with the al

axis, 131.13

A

triblock o

Raman s

$H-CH_2-CH_2-O$

claimed th

example,

be amorp

samples.

by Raman spectroscopy¹²⁷⁻¹³⁰ and X-ray crystallography.¹³¹ In a study of a series of nonionic surfactants where $x = 1-16$ and $y = 1-8$, Matsuura *et al.* found that the PEO segment conformation depends not only on the oxyethylene chain length but also on the alkyl chain length, and that there exists at least six distinctive conformational forms. For compounds where $x \leq 4$, the conformation of the PEO segment is helical. For $x \geq 5$, the molecular conformation depends on the oxyethylene chain length; as the number of oxyethylene units increases, the conformation changes from an all trans conformation to a trans conformation for the alkyl and a helical conformation for the PEO segment. This conformational transition takes place at $m = 3-4$. Being coincident with this transition point, C_8E_3 , $C_{12}E_3$, and $C_{16}E_3$ crystallize into either the extended form or the diblock form depending on the crystallization conditions. Combined electron and X-ray diffraction experiments show that for relatively long polyethylene oxide segments, (**Figure 6**) the aliphatic and polyether segments segregate in bilayers stacked parallel to the chain axis, with the alkyl chains tilted about $25-30^\circ$ with respect to the polyethylene oxide helix axis.^{131,132}

A related set of surfactants is a series of methylene-oxyethylene-methylene triblock oligomers.^{100,133-139} Booth *et al.*^{100,133-138} used X-ray, DSC, IR and Raman spectroscopy to study triblock oligomers with the general formula $H(CH_2)_x(OCH_2CH_2)_yO(CH_2)_xH$, where $y \approx 15$, $x = 1-18$ and $y \approx 9$, $x = 1-26$. Booth claimed that the crystallinity of each segment greatly depends on the segment length. For example, in compounds with long alkyl chains, the center oxyethylene segment tends to be amorphous while the alkyl chains are crystalline, and vice versa. For all crystalline samples, the oxyethylene segment takes a 7_2 helical conformation as in polyethylene

oxide, and t

alkyl group

ethylene ox

not of exact

In a

block is a fi

2-7, the mol

coordinate c

trans/helical

chain length

was sugges

oxyethylene

than that of

conformatio

oxide, and the crystalline alkyl groups take their usual planar zigzag conformation. The alkyl groups are tilted about 24° from oxyethylene helical axis. No planar zigzag ethylene oxide conformations were observed. Note that the ethylene oxide oligomers are not of exact length which can affect the results.

In a solid state study¹⁴⁰⁻¹⁴³ of a series of triblock ABA' oligomers where the A block is a fixed length alkyl the length of the A' group was varied, i.e. $C_8E_4C_x$, where $x = 2-7$, the molecular conformations were determined by spectral analysis based on normal coordinate calculations. The conformations of these ABA' compounds change from the trans/helical/trans form to the fully extended form (trans/trans/trans) with increasing alkyl chain length (x). The extended structure of the oxyethylene chain is stabilized for $x \geq 3$. It was suggested that the end alkyl blocks stabilize the extended structure of the oxyethylene block in the triblock compounds when the length is comparable to or longer than that of the oxyethylene block. The results of these studies demonstrate that the conformation of the oxyethylene chain is affected strongly by the adjoining alkyl chains.



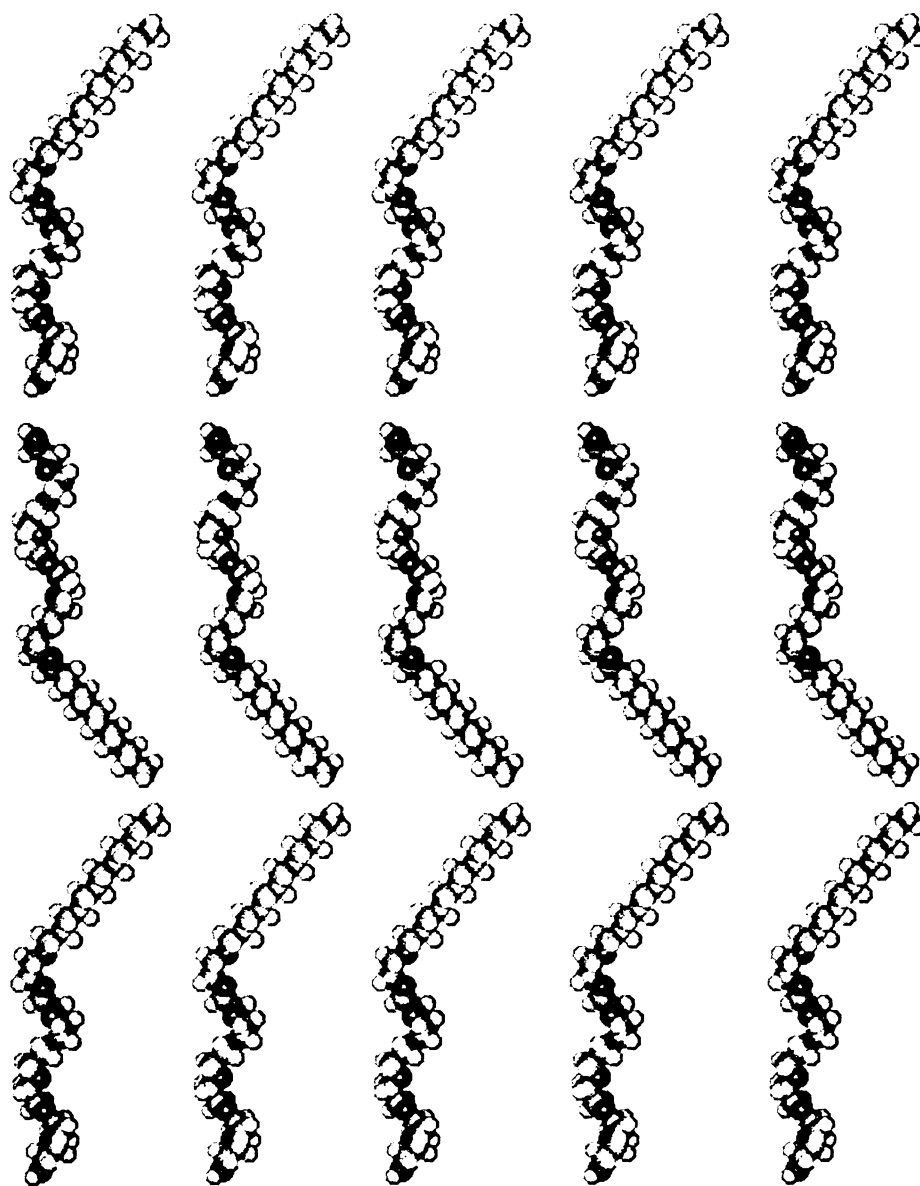


Figure 6. Solid state structure of surfactants C_xEO_y

3. Mic

olig

One

been stud

oxyethylene

α,ω -dibrom

thioethylene

triblock oli

were also

thioethylene

particularly

depend on

Like

helix. The

tendency to

ascribed to

Because of

and melts

observed

indicated t

Vibrational

segment, c

core. How

3. Microblock copolymers containing oligothioethylene, oligoethylene and oligooxyethylene

One structural analog of the exact length $(AB)_n$ microblock copolymers that have been studied here are the copolymers of ethylene/thioethylene, **21**, and oxyethylene/thioethylene, **22**. Mathias *et al.* used nucleophilic displacement of α,ω -dibromides by α,ω -dithiolates to prepare these hydrocarbon-thioethylene and thioethylene-oxyethylene microblocks (shown in **Scheme 17**).^{144,145} A group of triblock oligomers with formula $\text{CH}_3(\text{CH}_2)_9(\text{SCH}_2\text{CH}_2)_y\text{S}(\text{CH}_2)_9\text{CH}_3$, where $y = 1-5$, were also synthesized (**Scheme 18**). Litt *et al.* reported an interfacial route to thioethylene-oxyethylene microblocks.¹⁴⁶ The DSC scans of these materials are particularly interesting and complicated, and often contain multiple transitions that depend on the thermal history of the samples.

Like polyethylene oxide, polythioethylene also adopts a helical conformation, a 2_1 helix. The conformations along one repeat unit S-C-C-S are gauche-trans-gauche. The tendency to form helical conformations in the thioethylene system is strong and has been ascribed to strong dipolar interactions between C-S-C groups in adjacent chains.¹⁴⁷ Because of the strong interaction, polythioethylene is insoluble in virtually all solvents and melts at over 200 °C.¹⁴⁸ For these polymers, a single exothermic transition was observed between two endothermic transitions, and polarized optical microscopy indicated that at least some order was maintained up to the highest melting transition. Vibrational spectroscopy studies of the model compound with the shortest thioethylene segment, $\text{C}_{10}\text{ES}_1\text{C}_{10}$, showed that it adopted a trans conformation for the thioethylene core. However, the remaining compounds all have helical thioethylene cores. The x-ray

diffraction

be attribut

the C₁ES

planar stru

two meltin

vibrational

increasingl

C₁ES;C₁ES

atoms adop

gauche con

gauche to t

similar to t

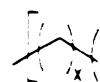
conformatio

since the PE

diffraction patterns of the $C_{10}ES_yC_{10}$ series show no distinct low angle reflections that can be attributed to a lamellar structure. In addition, two melting transitions are observed for the $C_{10}ES_3C_{10}$ and $C_{10}ES_4C_{10}$ model compounds. Based on solid state NMR experiments, planar structures were assigned for these models in the temperature range between the two melting transitions. At room temperature, (below the lowest melting transition), vibrational spectroscopy and NMR data indicate that the thioethylene segments are increasingly dominated by gauche conformations as the length of segments increase. In $C_{10}ES_2C_{10}$, the conformation around the center S atom is gauche while the two external S atoms adopt trans conformations as shown in **Figure 7**. Similar to the model compounds, gauche conformations dominate in the $(C_xES_2)_n$ copolymers. A significant amount of gauche to trans isomerization was observed close to the melting temperature, which is similar to the PE premelting behavior. For the series of $(EO_xES_y)_n$ copolymers, the conformations of the ES segments are similar to those in polythioethylene homopolymers since the PEO chains are more flexible.

Scher

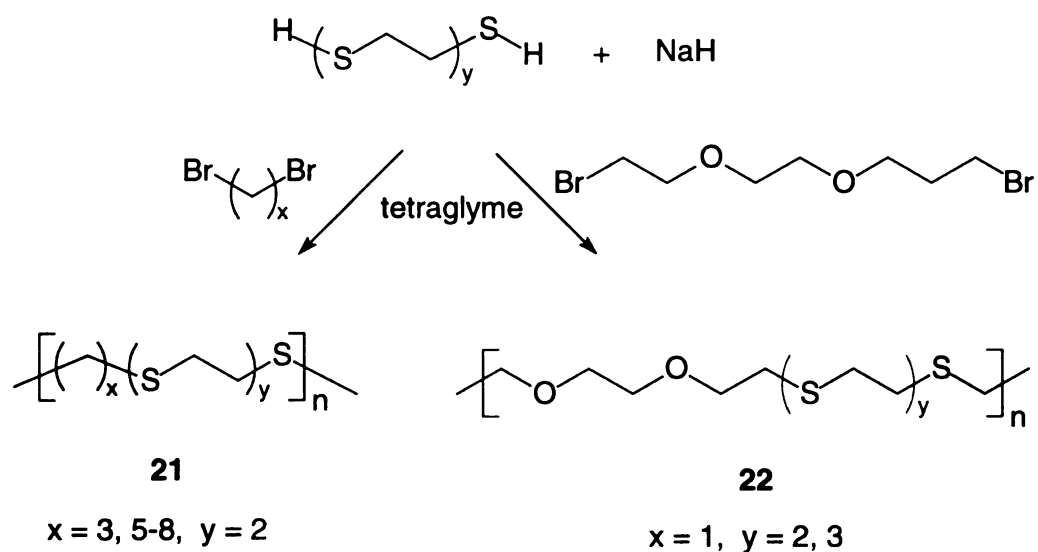
segments



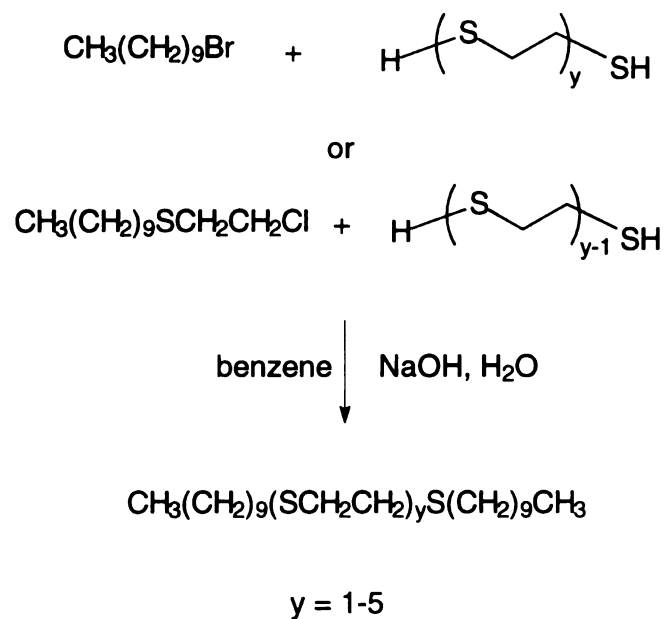
$x = 3, 5$

Schem

Scheme 17. Synthesis of microblock copolymers containing thioethylene segments



Scheme 18. Synthesis of triblock oligomers $\text{CH}_3(\text{CH}_2)_9(\text{SCH}_2\text{CH}_2)_y\text{S}(\text{CH}_2)_9\text{CH}_3$



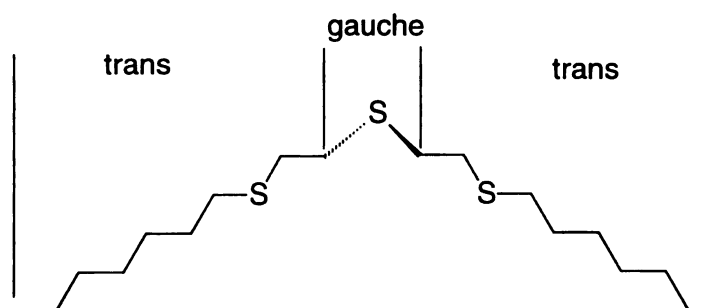


Figure 7. Conformation of triblock oligomer $C_{10}ES_2C_{10}$

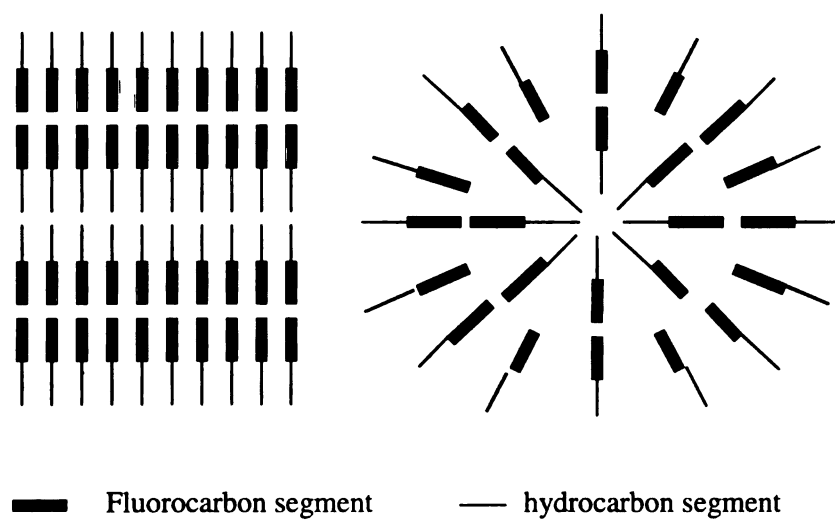


Figure 8. Structures of diblock oligomers F_nH_m

4. Flu

Like
alkanes are
been severa
backbones.

Dib
their melt
studies den
solid-solid
oligomers
lamella sur
lamella sur
reported fo
incompatib
F₁₂H₂₂ Me
of solution

Figure 8
transition a
in the fluor
concentric
These mod
NMR expe

4. Fluorocarbon-hydrocarbon microblock copolymers

Like normal hydrocarbons and polyethylene oxides, perfluoroalkanes and normal alkanes are two very different species both in terms of structure and property. There have been several kinds of copolymers and oligomers that combine these two segments in their backbones.

Diblock oligomers $F(CF_2)_n(CH_2)_mH$ (F_nH_m for short) have been studied both in their melt and crystalline phases by Raman and X-ray scattering experiments. DSC studies demonstrated that the materials undergo at least one, and in some cases even two, solid-solid phase transitions before melting. For relatively short alkyl chains, the diblock oligomers form monolayer crystals in which the molecules are tilted with respect to the lamella surface below the solid-solid transition and become arranged perpendicular to the lamella surface above the solid-solid transition.^{149,150} Bilayer lamellar crystals were reported for molecules with longer hydrocarbon segments and can be explained by the incompatibility of fluorocarbon and hydrocarbon segments.¹⁴⁹⁻¹⁵³ Based on studies of $F_{12}H_{20}$, Moller and Hopken¹⁵⁴ suggested a model for the crystal and transition behavior of solution and melt crystallized samples. A highly ordered bilayer lamellar crystal (**Figure 8** left) forms when crystallized from solution, which can have a reversible transition at 250 K that corresponds to the disordering of the alkyl chains with no change in the fluorocarbon segment. At 308 K, the lamellar crystal is irreversibly changed to a concentric cylinder crystal (**Figure 8** right), which is the same as crystallized from melt. These models can be used to explain the behaviors observed in DSC and solid state ^{13}C NMR experiments, and are also supported by SEM observations.

A se

Rabolt *et al*

perfluoronal

conformati

chain in pla

Raman-act

characteris

occurs at t

the whole

very close

hydrocarbo

chains tilt

melt state

effectively

segments

through th

the link

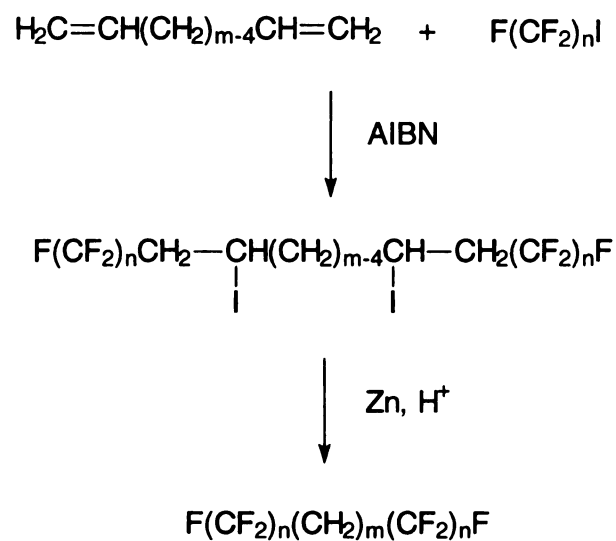
oligomers

temperatu

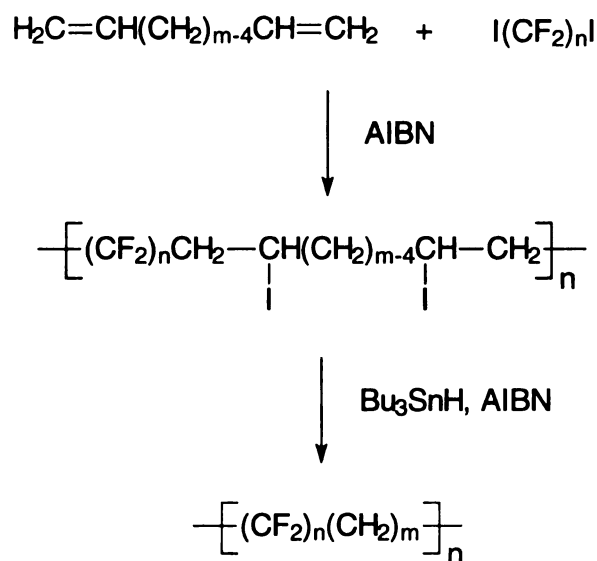
-0.4°C

A series of symmetric triblock oligomers $F_nH_mF_n$ have been studied intensively by Rabolt *et al.*¹⁵⁵⁻¹⁵⁷ These materials are prepared by coupling an α,ω -diene with a perfluoroalkyl iodide followed by dehalogenation (**Scheme 19**).^{156,158} The molecular conformation is presumably the fluorocarbon in a helical conformation and the alkyl chain in planar zigzag conformation. It was concluded¹⁵⁶ from solid state studies of the Raman-active longitudinal acoustical mode (LAM) that the vibrational frequency is characteristic of the entire extended molecule and no decoupling of the chain vibration occurs at the juncture between the helical and planar zigzag segments. This means that the whole molecular chain is crystalline, the alkyl chain and the fluorocarbon chains are very close to colinear, and the segments have similar vibrational modulus. For PEO-hydrocarbon oligomers, the modulus of PEO is only 1/10 of the alkanes,¹³⁴ the alkyl chains tilt $> 20^\circ$ from the PEO helix axis, and the vibrations are more perturbed. In the melt state, however, disordering of the hydrocarbon segment at the melting point effectively decouples the longitudinal oscillations. With the two rigid fluorocarbon segments still in their crystalline conformation, their frequency is perturbed by each other through the hydrocarbon linkage when the link is short, but the perturbation is lost when the link is long. Liquid crystalline behavior is also observed for these triblock oligomers.¹⁵⁷ While lacking the rigid mesogenic groups typical of liquid crystals, the temperature range for them to form a stable smectic B liquid crystal phase is very small — 0.4°C below their melting points.

Scheme 19. Synthesis of triblock oligomer $F_nH_mF_n$



Scheme 20. Synthesis of microblock copolymers containing fluorocarbon and hydrocarbon segments



copo

only

descri

altern

copo

by a

origi

and

tetra

para

that

fluor

fluor

Stad

crys

mes

the

Thur

soft

Copolymers of tetrafluoroethylene and ethylene can be synthesized by bulk copolymerization initiated by azo compounds.¹⁵⁹ However, the structure obtained can only be statistically controlled and the segments are short. Griffin *et al.*^{160,161} described the preparation of a highly regular microblock copolymer containing alternating fluorocarbon and hydrocarbon segments with precise block lengths. These copolymers are similar in structure to our target molecules. The polymer was synthesized by a modification of the routes used to prepare the di- and triblock semifluorinated oligomers. The iodo compounds used were difunctional — α,ω -diiodoperfluorocarbons and the reduction step was completed with $\text{HSn}(\text{Bu})_3$ (**Scheme 20**). The ethylene tetrafluoroethylene alternating copolymer crystallizes in an orthorhombic cell with four parallel planar zigzag chains^{162,163} although calculations of the isolated chain indicate that the most stable form is a 3_2 helix.¹⁶⁴ As shown in **Figure 9**, having the fluorocarbon next to the hydrocarbon in adjacent chains (rather than fluorocarbon on fluorocarbon) is required to accommodate the cross sectional difference in this polymer. Studies of the polymers synthesized by Griffin *et al.* show the formation of liquid crystalline domains analogous to those seen in low molecular weight analogs. This mesophase, caused by the rigidity of the fluorocarbon, extends from the melting point of the alkyl segments to the eventual melting (disordering) of the fluorocarbon segments. Thus, fluorinated $(\text{AB})_n$ microblock copolymers correspond to a combination of hard and soft blocks analogous to thermoplastic polyurethanes.

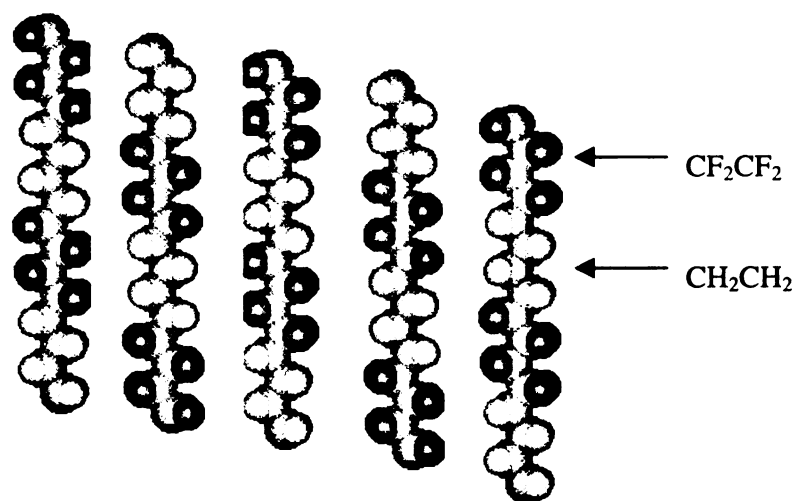


Figure 9. Solid state packing of polymer $(\text{CH}_2\text{CH}_2\text{CF}_2\text{CF}_2)_n$

1.

1.

oxid

stmp

com

com

unm

exa:

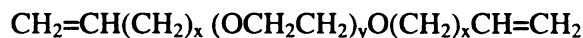
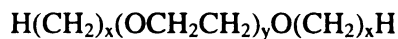
RESULTS

I. Synthesis and Purification

1. Acronyms for the compounds in this research

All compounds synthesized in this research contain two segments — an ethylene oxide chain and either an *n*-alkyl or an *n*-alkyl chain with one double bond. For simplicity in referring to these compounds, a nomenclature system similar to that commonly used for PEO/PE surfactants is used in place of the full names of the compounds. Thus, a methylene unit is abbreviated as C and the ethylene oxide repeat unit as EO. The two methine carbons of the double bond are abbreviated as π . An example of the naming protocol is shown in **Scheme 21**.

Scheme 21. Examples of acronyms for compounds

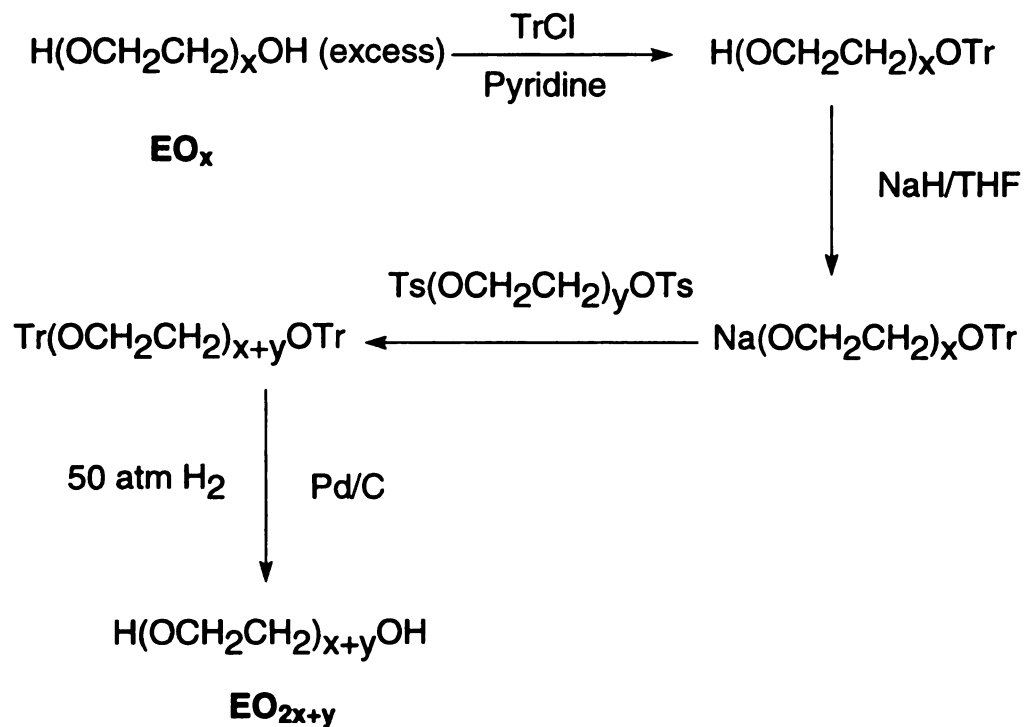


2. Exact length oligoethylene glycols

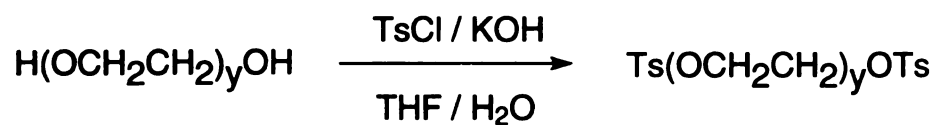
Having sufficient amounts of exact length ethylene glycol oligomers is critical for this research. Exact length oligoethylene glycols are commercially available up to 6 repeat units and we adopted a modified version of the approach of Keegstra *et al.*¹⁶⁵ to prepare glycols where y is 6-10 and 14. The route to these PEGs is outlined in **Scheme 22**. Monotritylation of selected glycols was achieved in bulk by treating a large excess of the glycol with trityl chloride in the presence of pyridine. The monotritylate of the glycols were then coupled with ditosylates of another glycol by treatment with NaH to yield an extended ethylene oxide chain with both ends protected by trityl groups. The glycols were de-protected through high-pressure hydrogenolysis with a Pd/C catalyst. The overall yield for this five-step synthesis was > 90%.

The starting ethylene glycols for the syntheses were the commercially available di-, tri- and tetraethylene glycols, while the resulting glycols were exact length glycols as long as tetradecaethylene glycol. The selected glycol combinations used in this project are listed in **Table 1**. The main reason for these combinations is the commercial availability of the starting materials, and considerations such as minimizing side reactions were also applied. The tosylation reactions were carried out in a THF/water mixed solvent system as shown in **Scheme 23** to give exclusively the desired ditosylate products.

Scheme 22. Synthesis of exact length oligoethylene glycols



Scheme 23. Synthesis of oligoethylene glycol ditosylates



3.

prop

libra

was

equi

of d

com

temp

moie

shor

pur:

char

Table 1. Combinations of $\text{TrEO}_x\text{H} + \text{TsEO}_y\text{Ts}$ used in the synthesis of EO_{2x+y}

	y			
x	2	3	4	6
2	EO_6	EO_7	EO_8	
3		EO_9	EO_{10}	
4	EO_{10}			EO_{14}

3. Triblock amphiphilic oligomers—model compounds

The ABA triblock amphiphilic oligomers are a set of compounds with interesting properties and serve as model compounds for understanding the polymer behavior. A library of these oligomers $\text{C}_x\text{EO}_y\text{C}_x$ where $x = 6, 8, 10, 12, 14, 16$, and $y = 2-8, 10, 14$, was synthesized. They were prepared by treating the appropriate glycol with NaH and 2 equivalents of the desired alkyl bromide (**Scheme 24**). The reactivity of the sodium salts of di and triethylene glycols was low, probably because of the ease of forming a chelate complex by the terminal oxygen atoms. The reaction mixtures were heated to the reflux temperature of the solvent to facilitate the reaction for these two cases. Depending on the molecular weight, the products ranged from viscous oils to waxy solids. Products with short chain lengths were initially purified by distillation, and all samples were also purified by low temperature crystallization. Because the solubility of the amphiphiles changes with chain length, the short chain compounds ($y = 2,3$) were crystallized from

S. 1

dis

dec

ob

pre

se

dis

dis

cr

sol

ser

wh

eth

the

of

chro

acetone while the longer chain compounds ($y = 4-8, 10, 14$) were crystallized from methanol.

4. Monomers

The monomers, α,ω -alkenyloligoethylene oxides where $x = 2-4, 8, 10$ and $y = 6-8, 10, 14$, were prepared by coupling the sodium salts of alkenols and oligoethylene oxide ditosylates (**Scheme 25**). The alkenols, 3-buten-1-ol, 4-penten-1-ol, 5-hexen-1-ol, 9-decen-1-ol and 10-undecen-1-ol were purchased from commercial sources. The oligoethylene oxide ditosylates and the corresponding oligoethylene glycols were prepared as described earlier.

The monomers previously prepared by Qiao¹⁶⁶ have shorter ethylene oxide segments ($y \leq 5$), therefore they have lower boiling points and were purified by distillation. The boiling points for the monomers prepared in this study are too high for distillation, and new purification methods were used for purifying these monomers. The crude monomer was first isolated by column chromatography to give yellow oils or solids. All of the monomers were isolated as pure compounds except for the $\pi C_2EO_y C_2\pi$ series of monomers. These monomers were contaminated by structurally similar isomers where the terminal double bonds were isomerized into internal double bonds allylic to the ethylene oxides ($C\pi CEO_y C\pi C$). Further study is needed to find a better way to separate the isomers or to restrict the isomerization reactions.

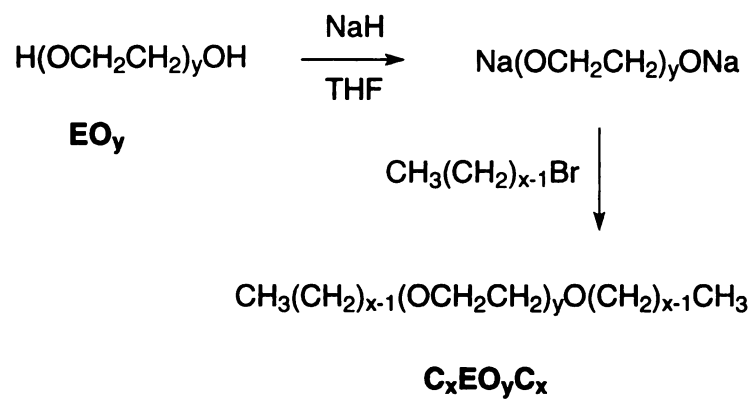
Because of the amphiphilic nature of the segments in the monomers, the polarities of the monomers change with composition. The polarities of the eluents for chromatography were adjusted accordingly and **Table 2** shows the eluents used for the

corresponding monomers. The monomers were further purified under argon by stirring them as hexane solutions (except for tetradecaethylene oxide series $\pi\text{C}_x\text{EO}_{14}\text{C}_x\pi$, where the solvent is toluene,) over a fresh sodium mirror followed by filtration through a funnel packed with Celite[®] and acidic alumina. The purification set-up is shown in **Figure 10**. All the purified monomers were stored in a drybox for future polymerization.

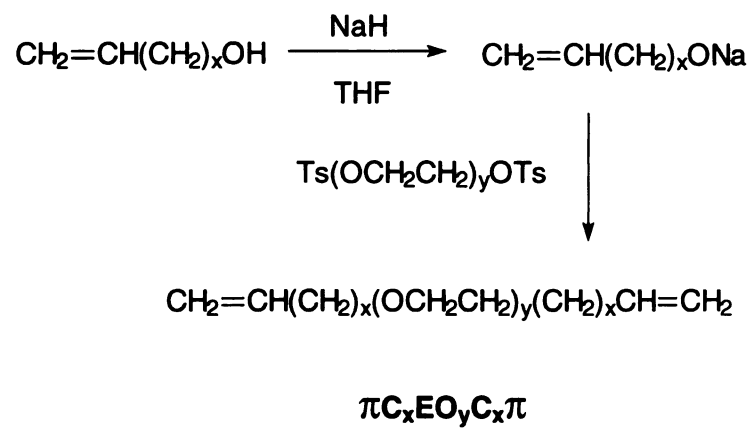
Table 2. Eluents for purification of monomers ($\pi\text{C}_x\text{EO}_y\text{C}_x\pi$) by column chromatography

	y				
x	6	7	8	10	14
2	75/25 EtOAc / hexanes	EtOAc	90/10 EtOAc / MeOH	90/10 EtOAc / MeOH	90/10 EtOAc / MeOH
3	EtOAc	90/10 EtOAc / hexanes	90/10 EtOAc / MeOH	90/10 EtOAc / MeOH	90/10 EtOAc / MeOH
4	75/25 EtOAc / hexanes	90/10 EtOAc / hexanes	90/10 EtOAc / MeOH	90/10 EtOAc / MeOH	90/10 EtOAc / MeOH
8	50/50 EtOAc / hexanes	75/25 EtOAc / hexanes	90/10 EtOAc / hexanes	90/10 EtOAc / hexanes	95/5 EtOAc / MeOH
9	50/50 EtOAc / hexanes	75/25 EtOAc / hexanes	75/25 EtOAc / hexanes	90/10 EtOAc / hexanes	95/5 EtOAc / MeOH

Scheme 24. Synthesis of triblock oligomers $\text{C}_x\text{EO}_y\text{C}_x$



Scheme 25. Synthesis of monomers $\pi\text{C}_x\text{EO}_y\text{C}_x\pi$



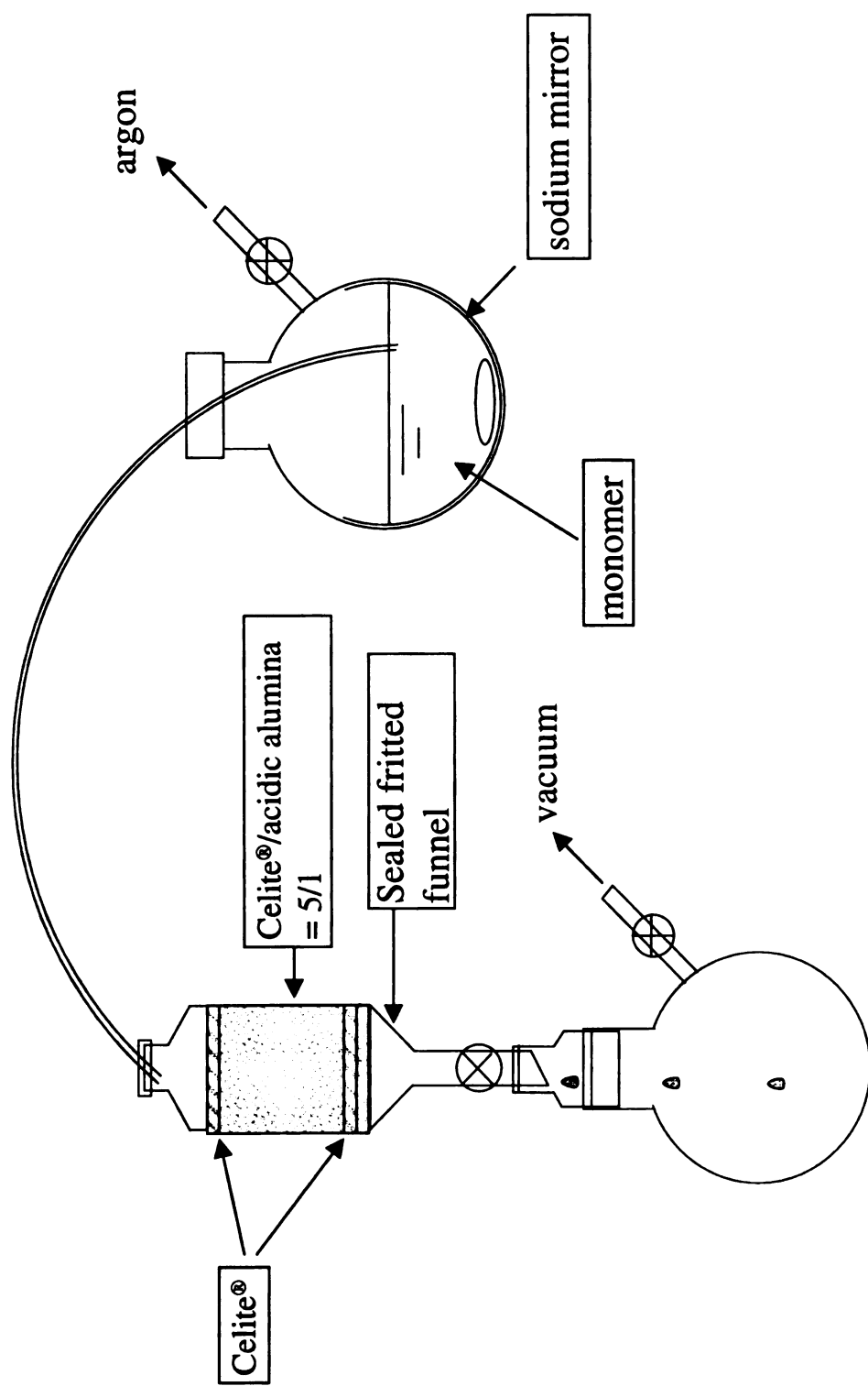


Figure 10. Monomer purification set-up

poly

mol

were

me.

As

ethy

bo

poi

was

sol

due

by

by

terr

all

(8)

Ta

5. Polymers

Unsaturated polymers $(C_x\pi C_xEO_y)_n$

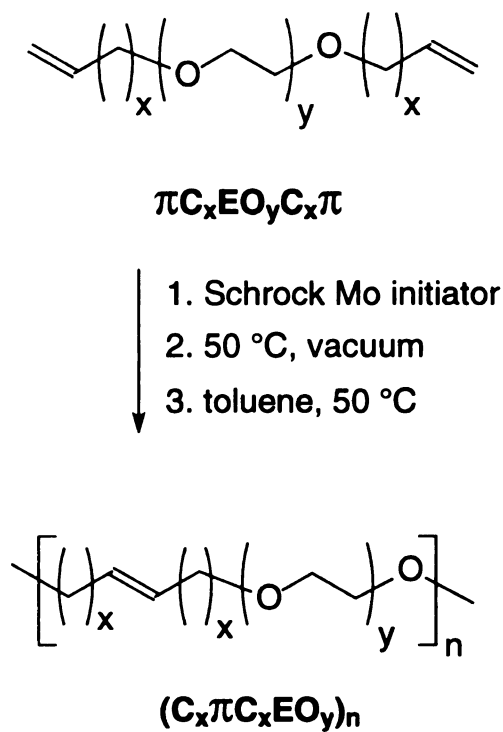
The unsaturated polymers $(C_x\pi C_xEO_y)_n$ were synthesized by ADMET polymerization of oligoethylene oxide α, ω -dialkenyl ethers using Schrock's molybdenum alkylidene catalyst **15**. The polymerizations, generalized in **Scheme 26**, were carried out on a 5 g scale for most polymers.

The catalysts were added as a solid to the liquid monomers; for monomers with melting points higher than room temperature, they were melted and kept at about 50 °C. As the catalyst dissolved in the monomers to give a yellow homogeneous solution, ethylene gas was released vigorously. Since the monomers and polymers have high boiling points, high vacuum was applied to the reaction system throughout this bulk polymerization stage. When the polymerization became too viscous to stir, dry toluene was added to lower the viscosity and vacuum was occasionally applied. The reaction solution color changed from yellow to dark brown during the polymerization, presumably due to partial decomposition of the catalyst. The polymerization progress was monitored by periodically taking samples from the reaction and measuring their molecular weight by GPC. Once the desired molecular weight was reached, the polymerization was terminated by adding 1 mL of methanol.

Except for monomer $\pi C_2EO_7C_2\pi$, whose purification needs further investigation, all monomers were polymerized to give high molecular weight polymers in good yield (88% and above). The polymerizable monomers for this research to date are listed in **Table 3**.

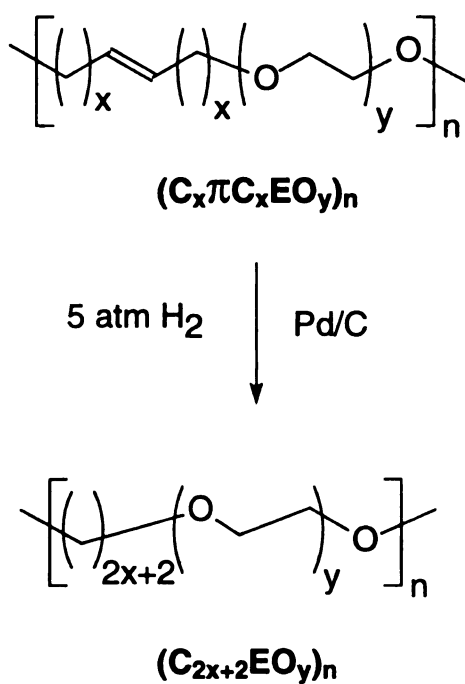
Sch
(C₁₇C₁EO)_n

Scheme 26. Synthesis of unsaturated polymers $(C_x\pi C_xEO_y)_n$



Scheme 27. Synthesis of saturated polymers from unsaturated polymers

$(C_x\pi C_xEO_y)_n$



The polymer work-up procedure included precipitating the toluene solutions of the polymer into hexanes and drying the isolated polymer under high vacuum until constant weight was obtained. In order to obtain high molecular weight samples, some polymers were fractionated by precipitation from THF solutions into methanol or isopropanol. Since the polymer polarity changes with respect to the two segment fractions, solvents for precipitation were adjusted accordingly. They are listed in **Table 4**.

Table 3. Monomers $\pi C_xEO_yC_x\pi$ polymerizable by ADMET polymerization.

	y								
x	2	3	4	5	6	7	8	10	14
2	^a +				±	±	±	±	±
3	^a +	^a +	^a +	^b +	+	+	+	+	+
4	^a +	^a +	^a +	^a +	+	+	+	+	+
6	^a +		^a +						
8		^b +			+	+	+	+	+
9		^b +			+	+	+	+	+

(+) monomer has been polymerized into polymer

(±) further purification investigation is necessary

a: polymers obtained by Jun Qiao

b: monomers available, small scale polymerizations were tested successfully

Table 4. Solvents used for precipitating polymers $(C_x\pi C_xEO_y)_n$.

	y				
x	6	7	8	10	14
3	Hexanes	Hexanes	Hexanes	Hexanes / <i>iso</i> -propanol	Hexanes / <i>iso</i> -propanol
4	Hexanes	Hexanes / <i>iso</i> -propanol	Hexanes	Hexanes / <i>iso</i> -propanol	Hexanes / <i>iso</i> -propanol
8	Hexanes / Methanol	Hexanes / Methanol	Hexanes / <i>iso</i> -propanol	Hexanes / <i>iso</i> -propanol	Hexanes / <i>iso</i> -propanol
9	Hexanes / Methanol	Hexanes / Methanol	Hexanes / <i>iso</i> -propanol	Hexanes / <i>iso</i> -propanol	Hexanes / <i>iso</i> -propanol

Saturated polymers

Several saturated polymers $(C_xEO_y)_n$, where $x = 10$, $y = 6-8, 10, 14$ and $x = 20$, $y = 7$, were synthesized by reducing their unsaturated analogs as outlined in **Scheme 27**. The reduction reaction involved the hydrogenation of the unsaturated polymer with H_2 under catalytic conditions.

The hydrogenation reactions were carried out at room temperature at 5 atm H_2 pressure with a 5 mol% catalyst loading. Complete reduction took approximately 5 hours. The molecular weights of the hydrogenated polymers are lower than their unsaturated analogs. The cause of the decrease in molecular weight will be discussed in the Discussion.

II

1.

an

th

co

an

A

on

at

ot

x

pl

se

sa

re

16

re

dis

en

ea

II. Properties of triblock oligomers $C_xEO_yC_x$

1. Thermal behavior

The thermal properties of triblock amphiphilic oligomers were analyzed by DSC and optical microscopy. In DSC studies, most samples were heated to 100 °C to erase thermal history, quenched to –100 °C at 200 °C/min, heated at 10 °C/min to 100 °C, cooled to –100 °C at 10 °C/min, and finally heated to 100 °C at 10 °C/min.

Figure 11 shows a typical thermogram for sample $C_{14}EO_3C_{14}$. The runs shown are the heating and cooling scans taken after quenching the melted sample to –100 °C. As shown in the figure, the sample showed a sharp endothermic melting peak with an onset at 42.7 °C, and upon cooling, a sharp exothermic crystallization peak with an onset at 38 °C, several degrees lower than its melting point. No other thermal transitions were observed for this sample. Since the $C_{14}EO_3C_{14}$ molecule is small and simple, the heating scan after quenching is the same as that obtained after slow cooling.

The rest of the DSC thermograms are shown as a series of stacked plots with each plot containing ABA oligomers with the same alkyl length, but different ethylene oxide segment lengths. For better comparison, the DSC responses are normalized to the same sample weight. The temperature ranges of the plots are narrowed to include only those regions where transitions were observed. The DSC scans shown in **Figure 12, 13, 14, 15, 16 and 17** are heating scans of oligomers $C_xEO_yC_x$ where $x = 6, 8, 10, 12, 14$ and 16 respectively, taken after the samples were quenched to –100 °C. All samples showed distinct melting endotherms. Some samples also showed exotherms before their melting endotherms, which is an indication of crystallization during the DSC heating scan. The endothermic peaks can be categorized in three types as shown in **Figure 18**. Type **I** is a

well-defi

such as

Type III

types of

endothe

oligome

y

2

3

4

5

6

7

8

1

1

well-defined symmetric peak like that of $C_{14}EO_3C_{14}$. Type **II** is a relatively broad peak such as in $C_{14}EO_{10}C_{14}$, where the lower temperature side of the peak rises gradually. Type **III** is multiple melting endotherm such as in $C_{14}EO_7C_{14}$. **Table 5** summarizes the types of peaks for each ABA triblock sample. Exotherms that appear before the endotherm are also noted in the table.

Table 5. Summary of the types of DSC endotherms observed for ABA triblock oligomers $C_xEO_yC_x$.

	x					
y	6	8	10	12	14	16
2	II	II	I	I	II	II
3	I	II	I	I	I	I
4	III ^a	II	II	I	II	II
5	III	I	II	I	II	II
6	II	II ^a	I ^a	II ^a	II ^a	II ^a
7	II	II	III	III	III	III
8	II	II	I	II	II	II ^a
10	I	II	II	II	II	II
14	I	II	II	II	II	II

a: exotherm observed before endotherm(s).

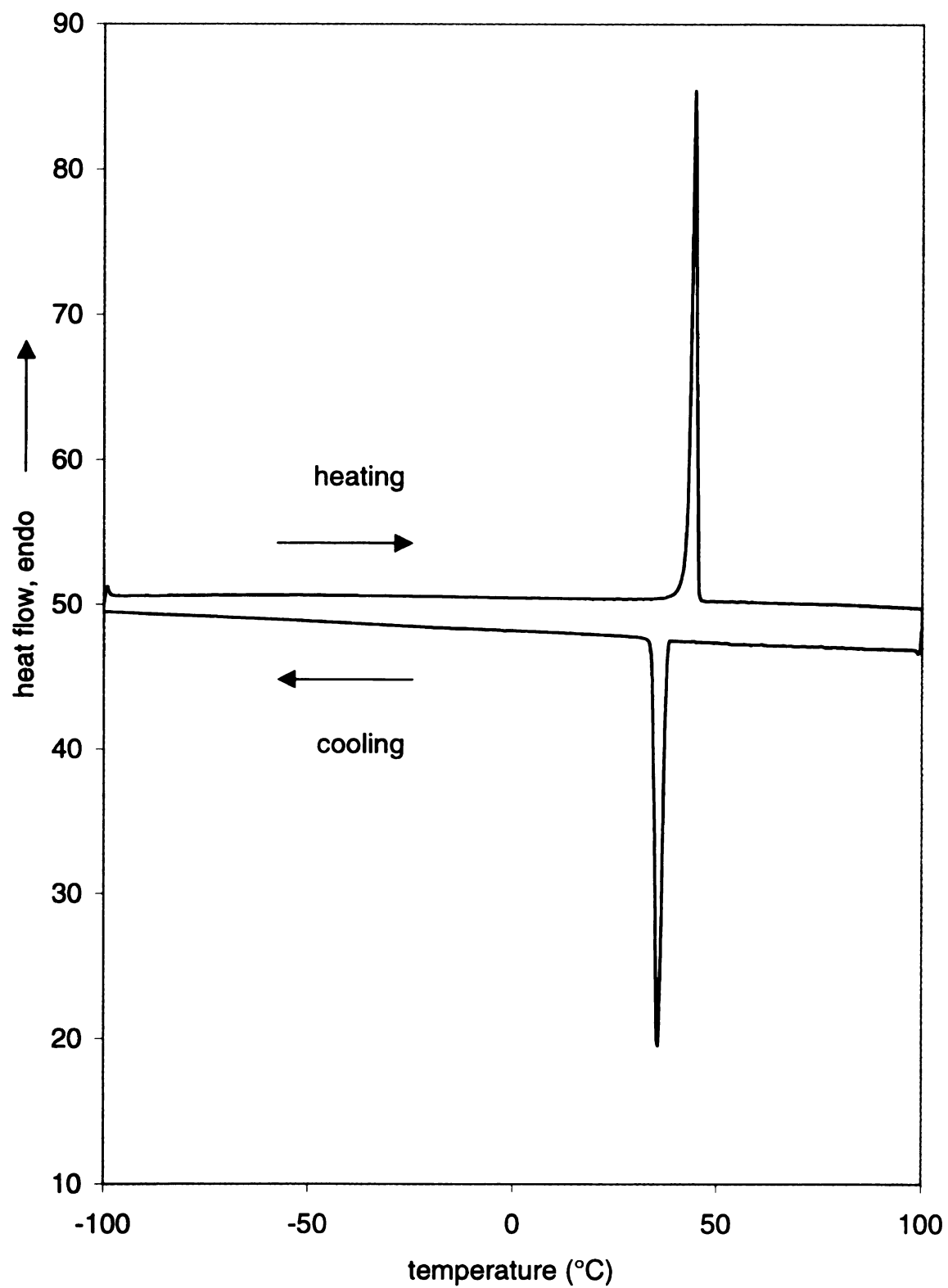


Figure 11. DSC heating and cooling scans of triblock oligomer $C_{14}EO_3C_{14}$

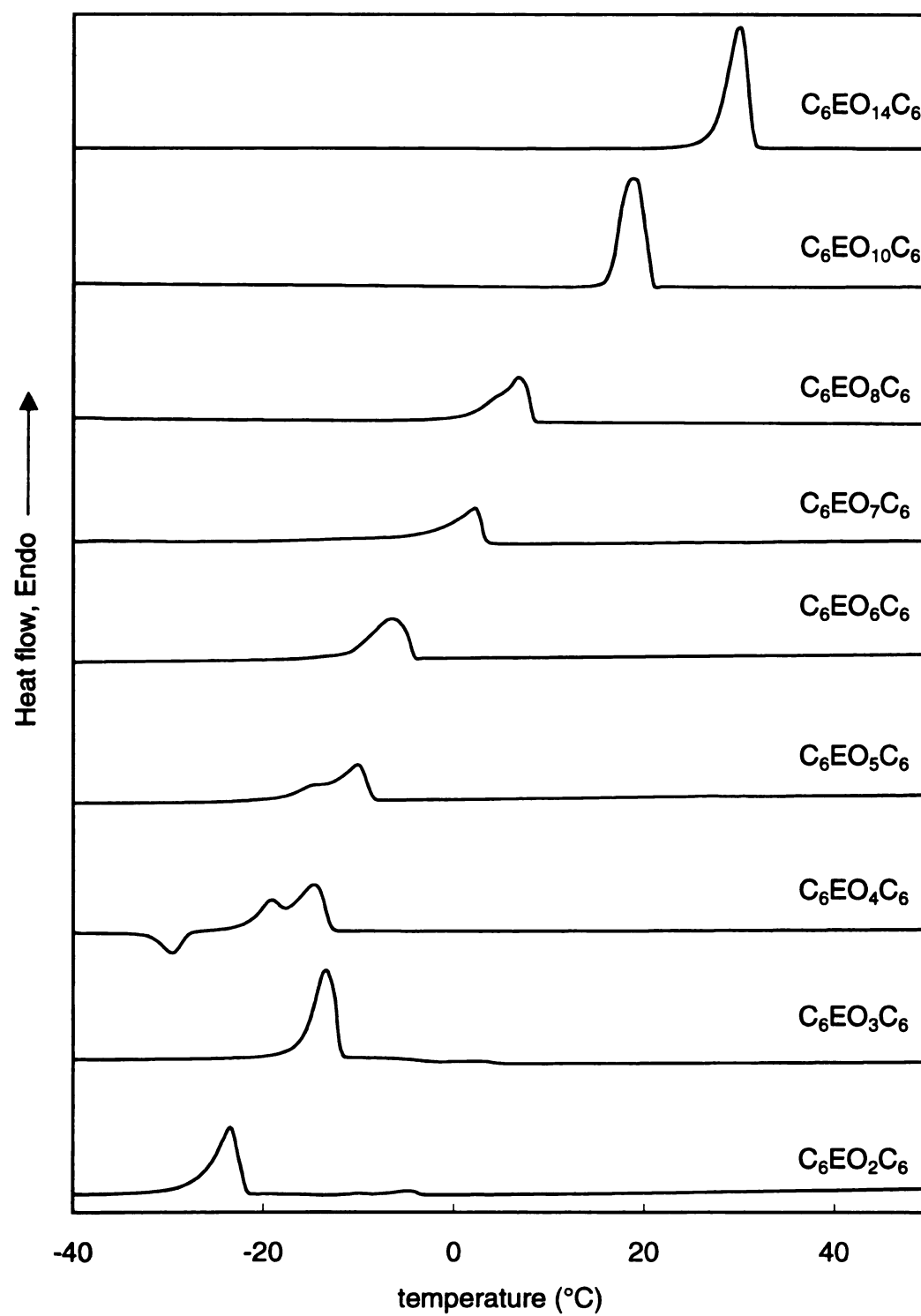


Figure 12. DSC heating scans of triblock oligomers $C_6EO_yC_6$

Heat flow, Endo 

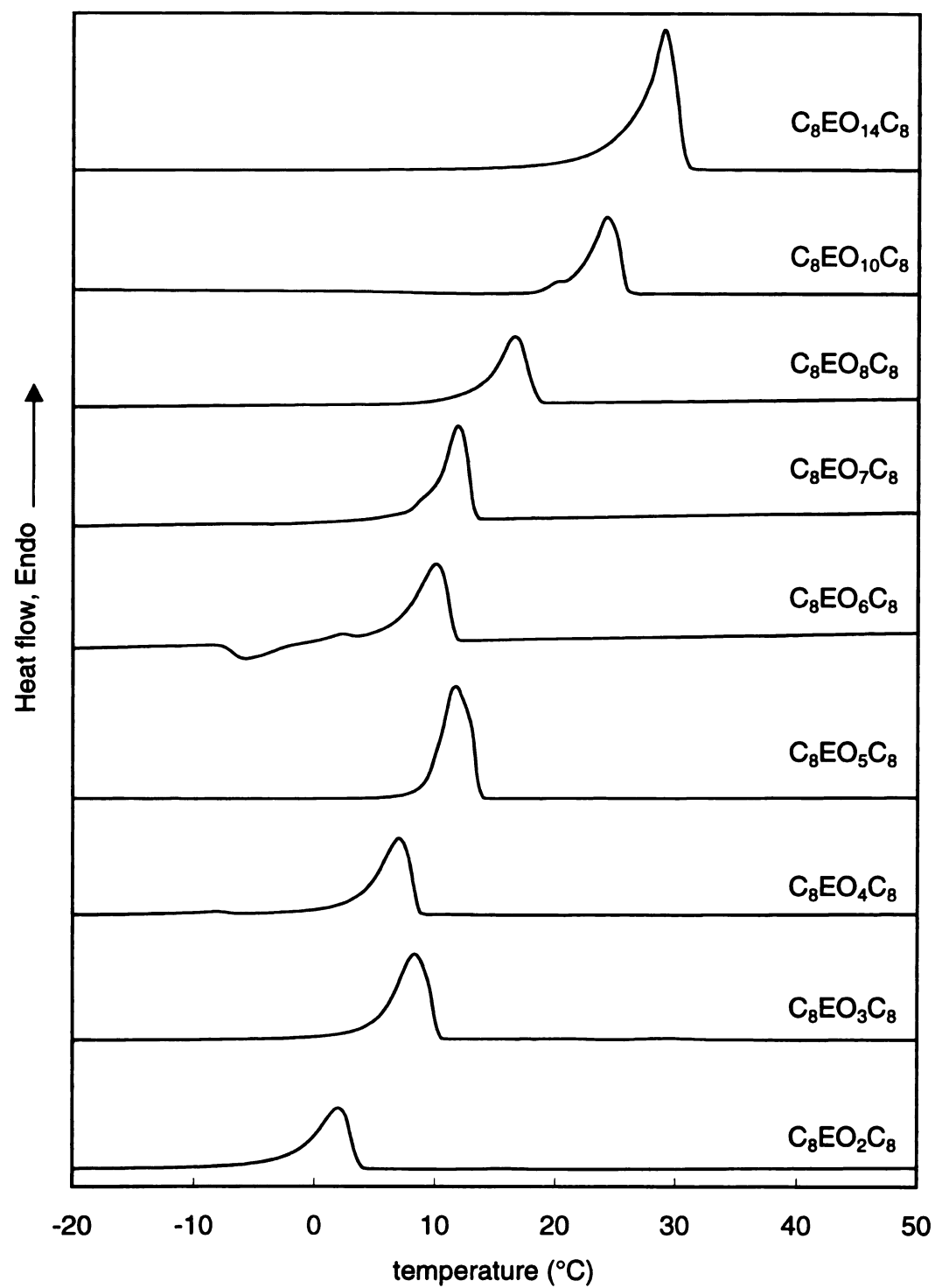


Figure 13. DSC heating scans of triblock oligomers $C_8EO_yC_8$

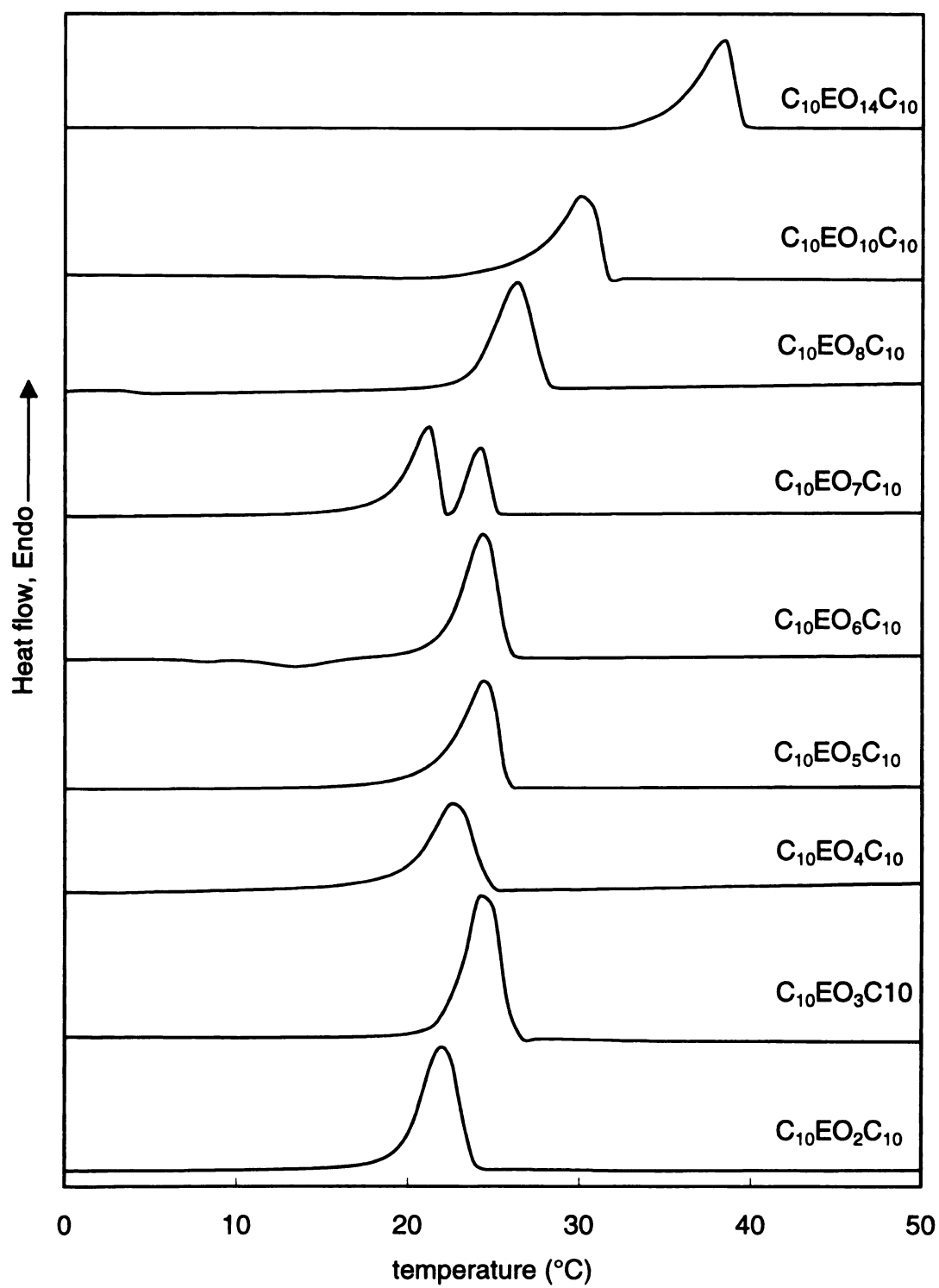


Figure 14. DSC heating scans of triblock oligomers $C_{10}EO_yC_{10}$

Heat flow, Endo 

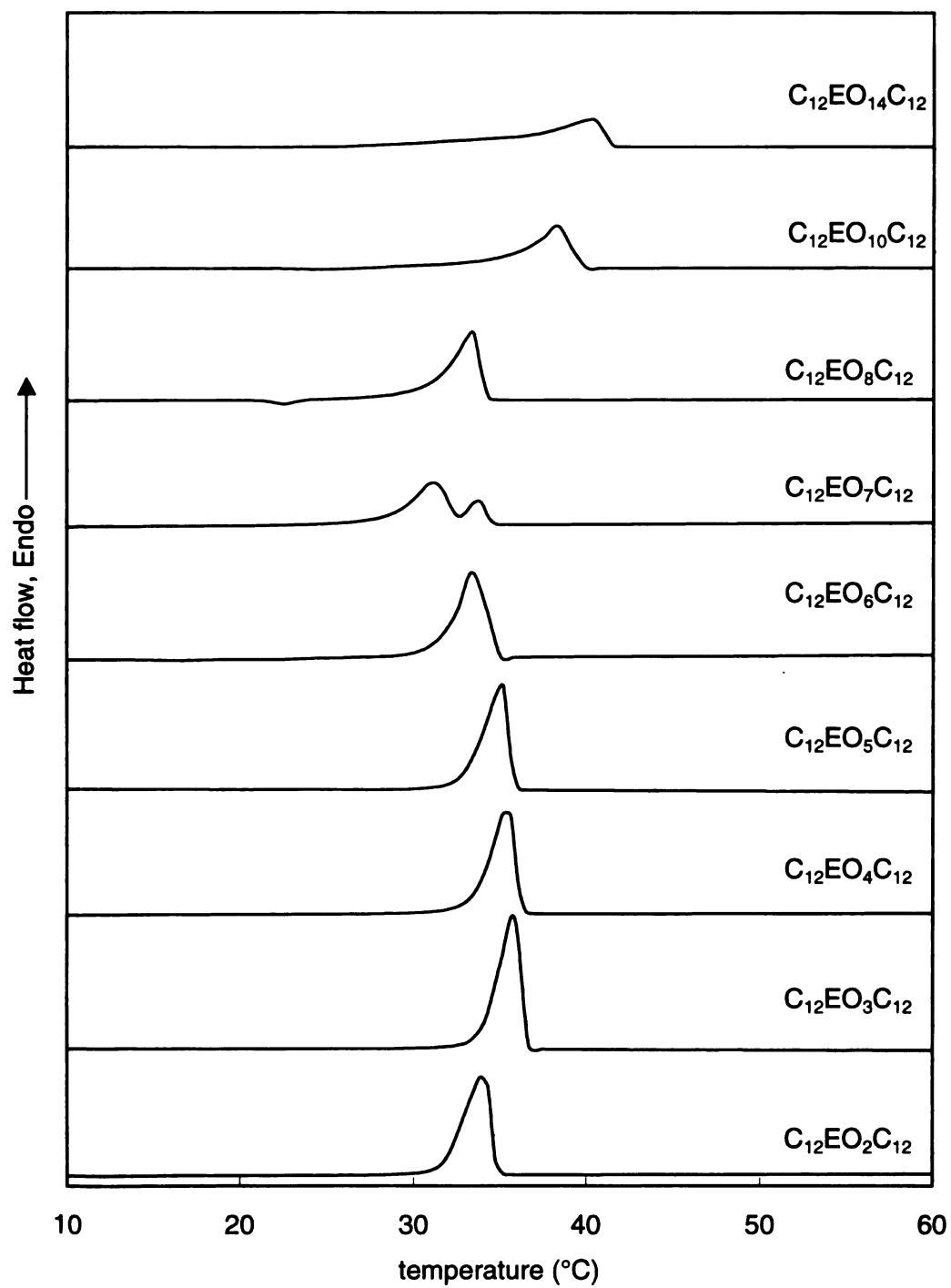


Figure 15. DSC heating scans of triblock oligomers $C_{12}EO_yC_{12}$

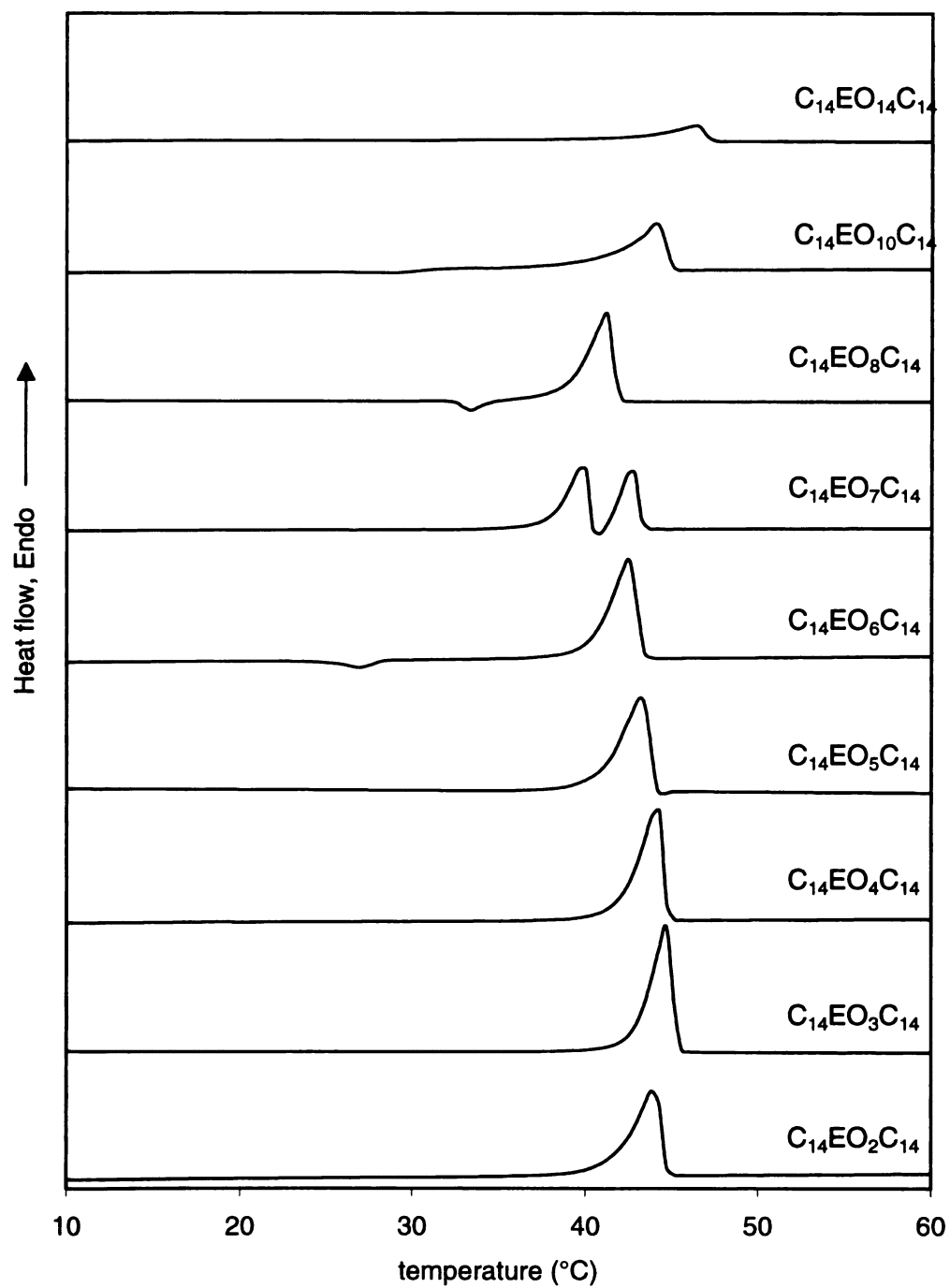


Figure 16. DSC heating scans of triblock oligomers $C_{14}EO_yC_{14}$

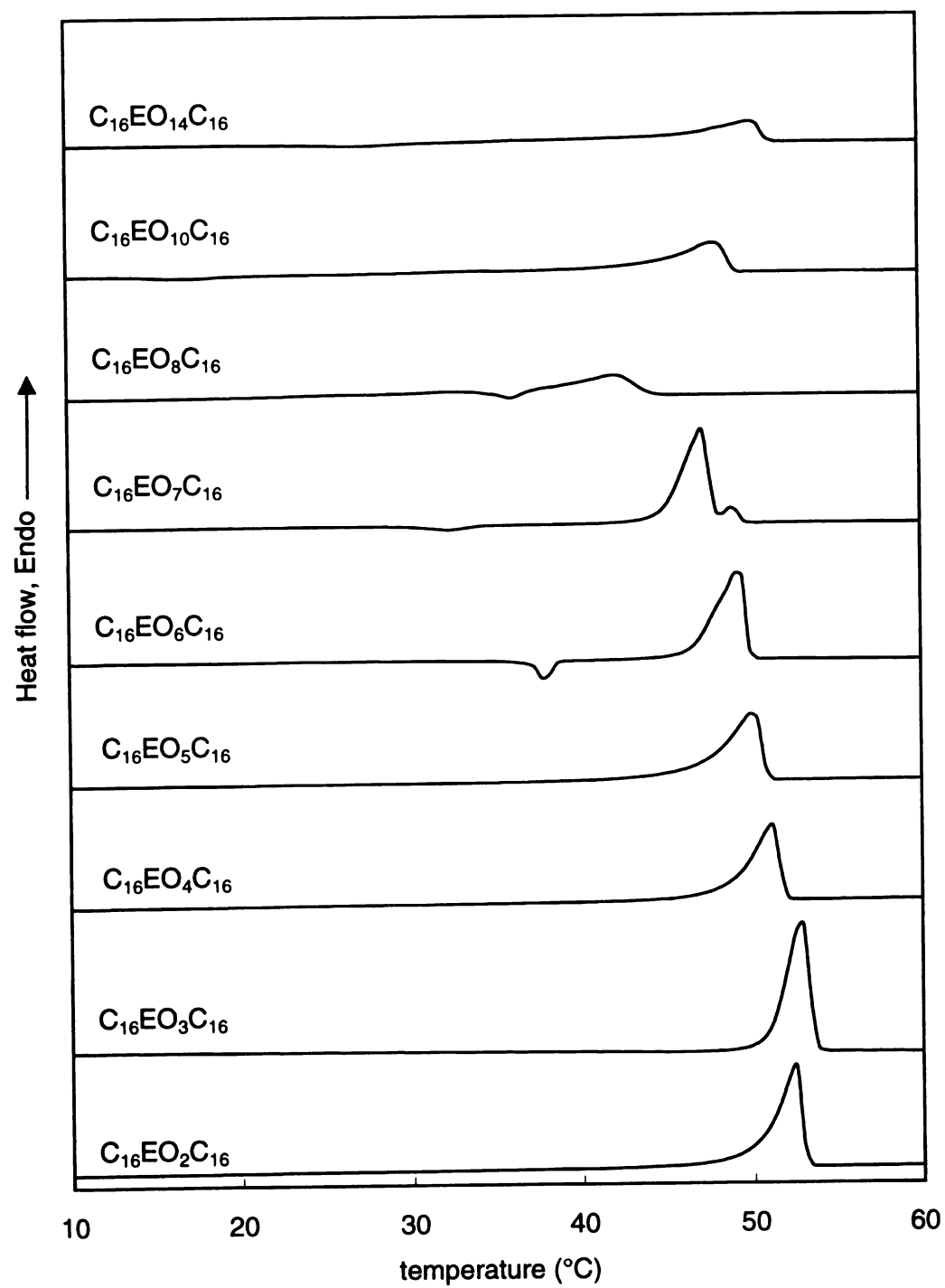


Figure 17. DSC heating scans of triblock oligomers $C_{16}EO_yC_{16}$

Fig

F

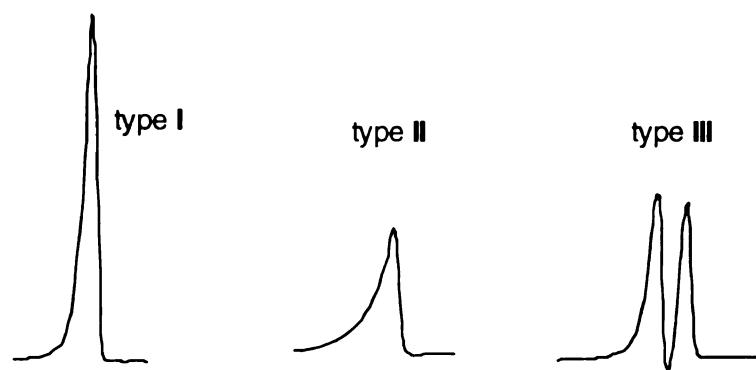


Figure 18. Types of DSC endotherm peaks seen for triblock oligomers

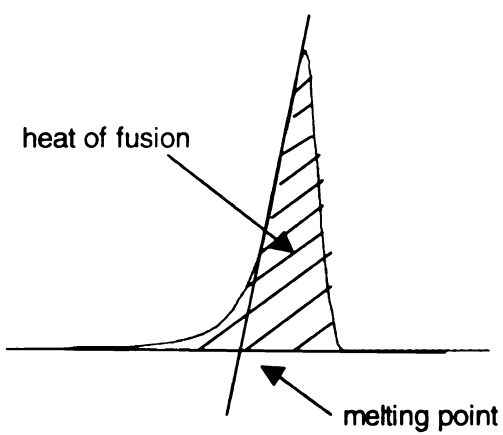


Figure 19. Melting point and heat of fusion measured by DSC

also ob

on-set

linear p

consist

endoth

corre-

as the

54 unit

area u

will be

The melting points T_m and heats of fusion ΔH_{fus} for these triblock oligomers were also obtained from DSC measurements. As shown in **Figure 19**, the T_m was taken as the on-set of the melting endotherm, which can be obtained by finding the intersection of the linear portion of the low temperature side of the peak and the baseline. This method is in consistent with the calibration of the DSC equipment. Except for samples with type **III** endotherms, which show solid-solid transformations, T_m s measured in this way also correspond well with the results from polarized optical microscopy, where T_m is defined as the point of total loss of sample birefringence under polarized light. The T_m s of these 54 triblock oligomers are shown in **Table 6**. The heats of fusion, indicated as the shaded area under the endotherm in **Figure 19**, are reported in Table 7. The T_m and ΔH_{fus} trends will be discussed in the Discussion section.

Table 6. Melting points (°C) of ABA triblock oligomers $C_xEO_yC_x$.

	x					
y	6	8	10	12	14	16
2	-25.9	-1.9	19.5	31.6	41.5	50.1
3	-16.1	5.0	22.0	33.6	42.7	50.9
4	-21.7, -19.3	3.6	19.4	33.4	42.0	48.6
5	-18.1, -13.8	9.3	21.4	32.8	41.1	46.9
6	-11.5	0, 6.4	21.8	31.2	40.2	46.4
7	-2.6	9.4	18.5, 22.8	28.6, 31.9	38.1, 40.9	44.6, 48.1
8	2.2	13.6	23.7	30.9	38.8	41.4
10	15.7	21.1	26.7	35.0	40.5	43.6
14	26.5	26.0	35.5	38.5	43.5	47.5



Table 7. Heats of fusion (J/g) of ABA triblock oligomers $C_xEO_yC_x$.

	x					
y	6	8	10	12	14	16
2	100	107	160	178	178	190
3	147	152	156	194	194	207
4	104	129	138	175	190	164
5	112	151	151	179	186	185
6	82	112	144	167	180	169
7	97	123	144	143	165	184
8	81	110	140	151	153	107
10	138	118	136	133	150	118
14	127	114	129	124	129	134

It was noted that many samples showed double melting behavior in the DSC heating scans, especially for the series of triblocks with 7 ethylene oxide units. These multiple transitions indicate that multiple crystal forms exist in these samples. The DSC heating scans of this series after flash quenching were re-plotted in **Figure 20**. We can see that for $x \geq 10$, all of the DSC scans showed double melting transitions. For $x = 6$ and 8, no double melting observed, but the peaks were significantly broadened. Because

of

gou

ex

w

pe

(4

m

D

le

b

n

c

n

u

c

of its interesting behavior, this series was studied in more detail. Sample $C_{14}EO_7C_{14}$ is a good representative of this series and thus was chosen for most of the detailed experiments.

A series of controlled experiments were carried out on $C_{14}EO_7C_{14}$. One study was the convertibility of those two peaks in DSC. It was observed that the higher melting peak diminished with increased holding times at 50 °C, above the sample's melting point (41 °C). The melt-quenched sample was held at 35 °C, a few degrees below the lower melting point of the sample for different periods. The sample was then heated and its DSC heating scans was recorded as shown in **Figure 21**. As shown in the figure, the lower melting peak gradually converted to the higher melting peak as the annealing time became longer. This set of experiments showed that the two crystal forms obtained from melt crystallization can be interconverted. Details will be discussed later.

The $C_{14}EO_7C_{14}$ sample was also tested to see if solvent will affect the structure of crystal formed from solution. Samples was crystallized from methanol and hexanes respectively and the DSC heating scans were recorded on samples from room temperature and are shown in **Figure 22**. The DSC traces for these two samples are different, with the sample crystallized from hexanes melting at 39 °C, (ΔH_{fus} 164 J/g,) and the sample crystallized from methanol melting at 41°C, (ΔH_{fus} 169 J/g).

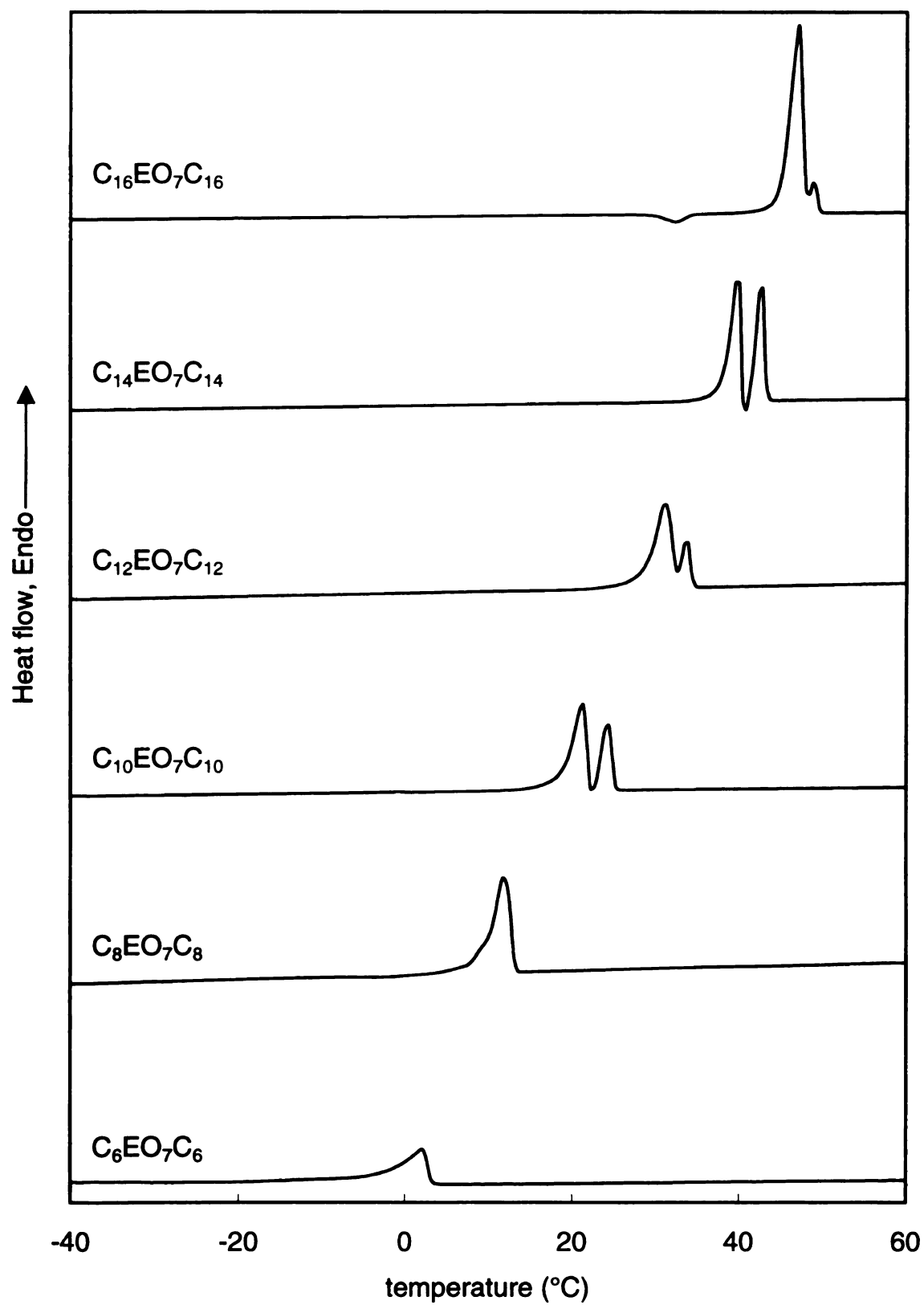


Figure 20. DSC heating scans of triblock oligomers $C_xEO_7C_x$

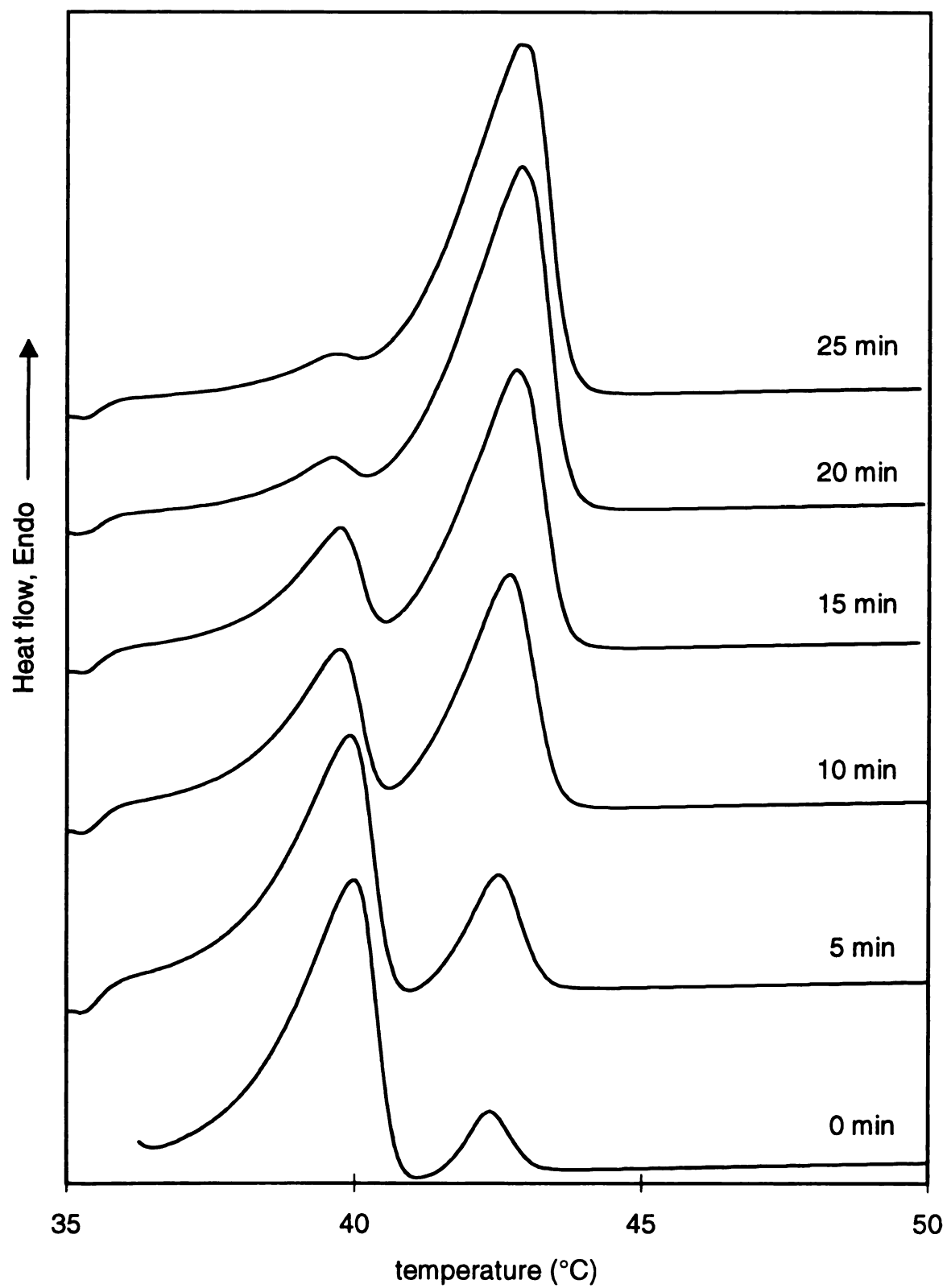


Figure 21. DSC heating scans of triblock oligomers $C_{14}EO_7C_{14}$ annealed at 35 °C for indicated time

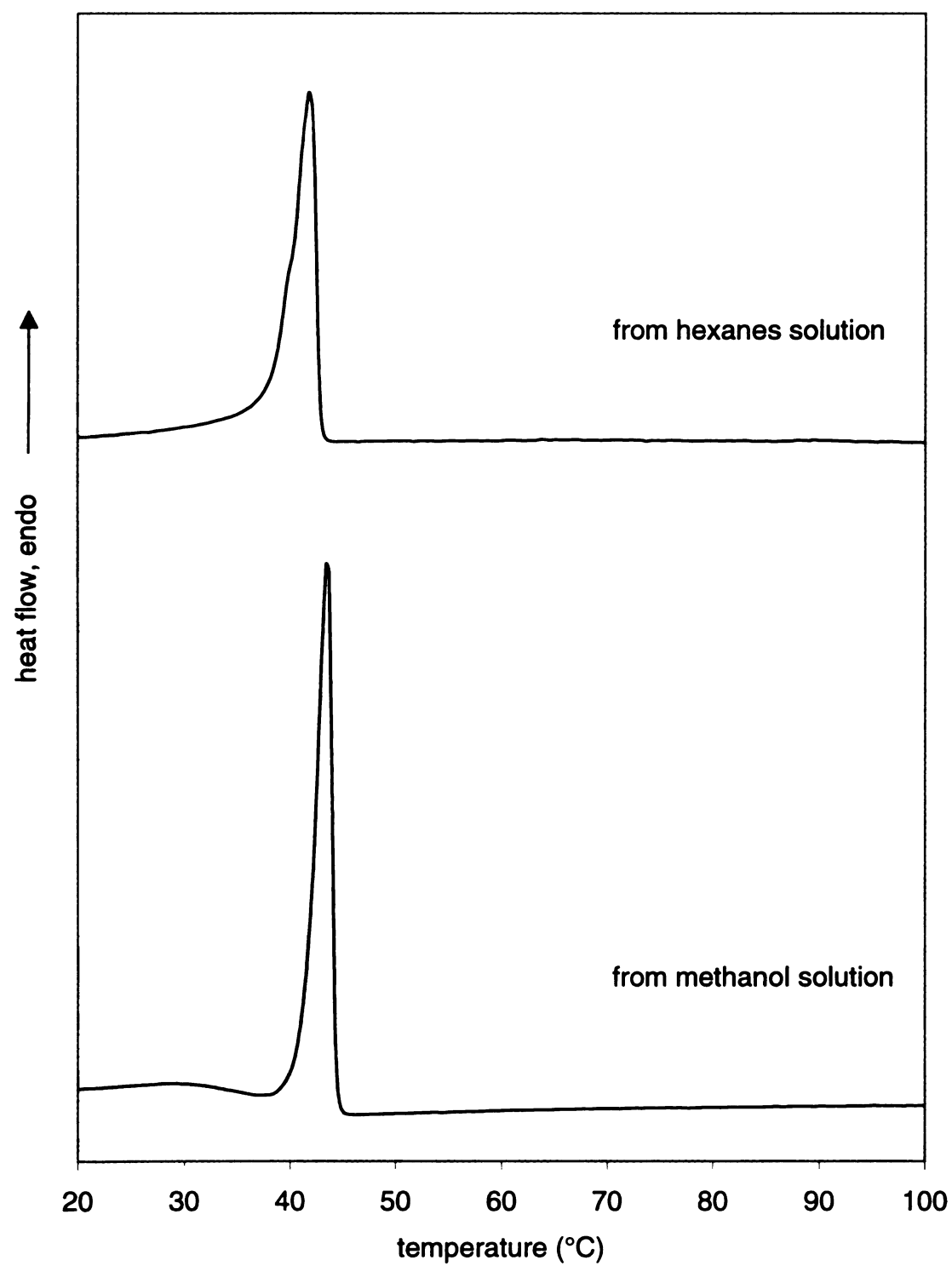


Figure 22. DSC heating scans of triblock oligomers $C_{14}EO_7C_{14}$ crystallized from different solutions.

2. Powder X-ray diffraction

Characterization by powder X-ray diffraction (XRD) was performed for most of the triblock oligomers. The low angle powder XRD pattern of oligomer $C_{16}EO_3C_{16}$, a typical sample of an oligomer with a short ethylene oxide segment, is shown in **Figure 23** and the higher angle data in **Figure 24**. In **Figure 23**, the well-defined series of $00l$ lines indicates a layered structure was formed. The layer spacing was calculated using the Bragg equation (equation 14) to be 51.3 Å based on the $00l$ d-spacing.

$$d = \lambda / 2 \sin \theta \quad \text{eq. 14}$$

In **Figure 24**, in addition to the $00l$ peaks that extend to higher angles, several peaks shown between 19° and 30° are very important in determining the crystal unit cell and detailed packing. An analysis and comparisons based on these peaks will be made in the Discussion.

For comparison, the XRD profiles of the series of triblock oligomers $C_{14}EO_yC_{14}$ ($y = 2-8, 10, 14$), obtained by solution crystallization are displayed in **Figure 25** for lower angles and in **Figure 26** for wider angles. All of these samples have well-defined $00l$ series peaks at lower angles (**Figure 25**), which confirms that all of the triblock oligomers have lamellar structures in their crystalline phase. One can also see that the d-spacing (best indicated by the first peak) became longer as the length of the ethylene oxide segments increased, except for $y = 7$ and 8. The calculated d-spacing values are listed in **Table 8**. In wide angle XRD profiles (**Figure 26**), the diffraction patterns are similar for samples with $y = 2-7$ and also for $y = 8, 10, 14$. This suggests that the crystals mainly exist in two kinds of packing formats.

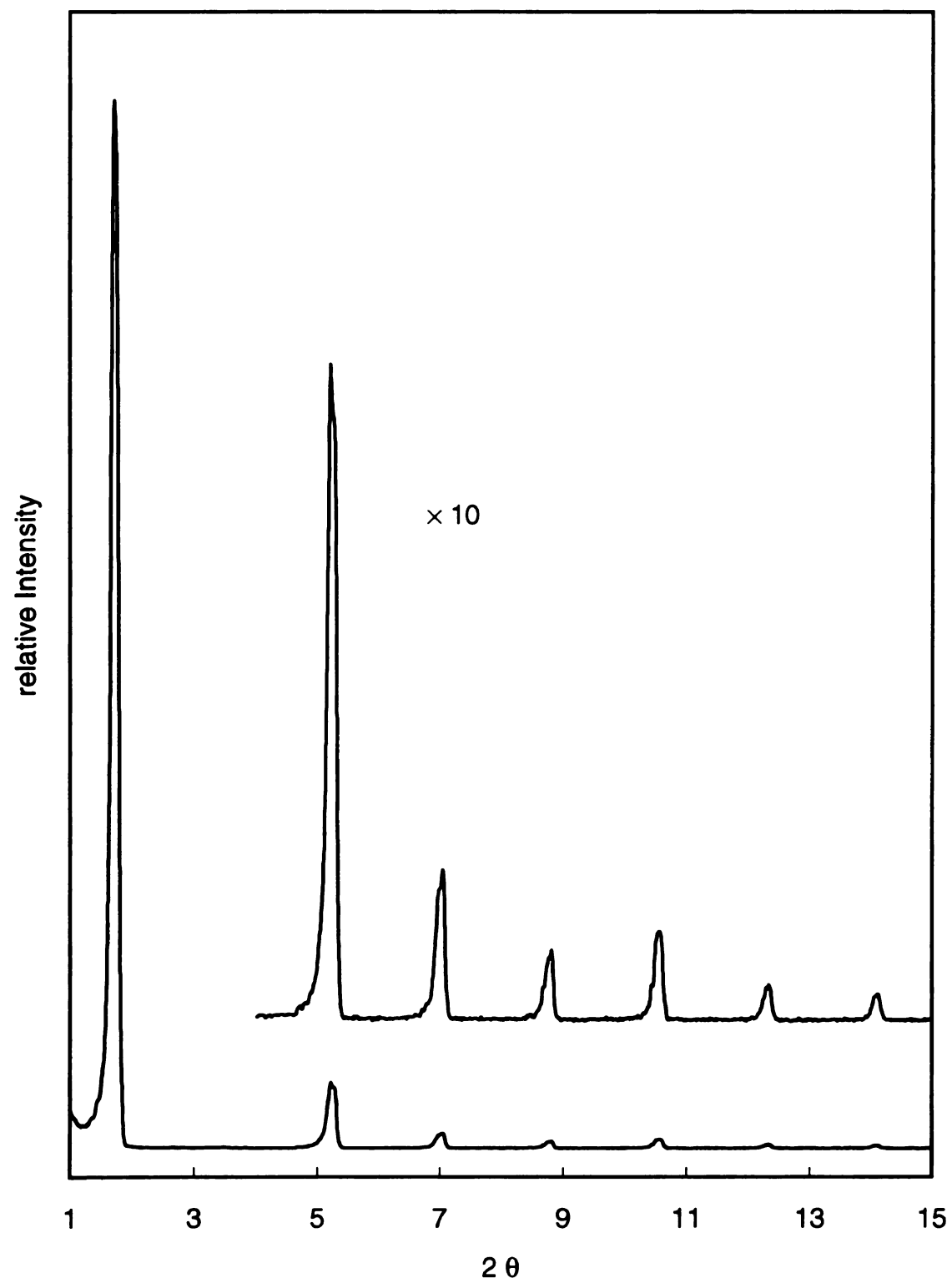


Figure 23. Low angle XRD for $\text{C}_{16}\text{EO}_3\text{C}_{16}$.

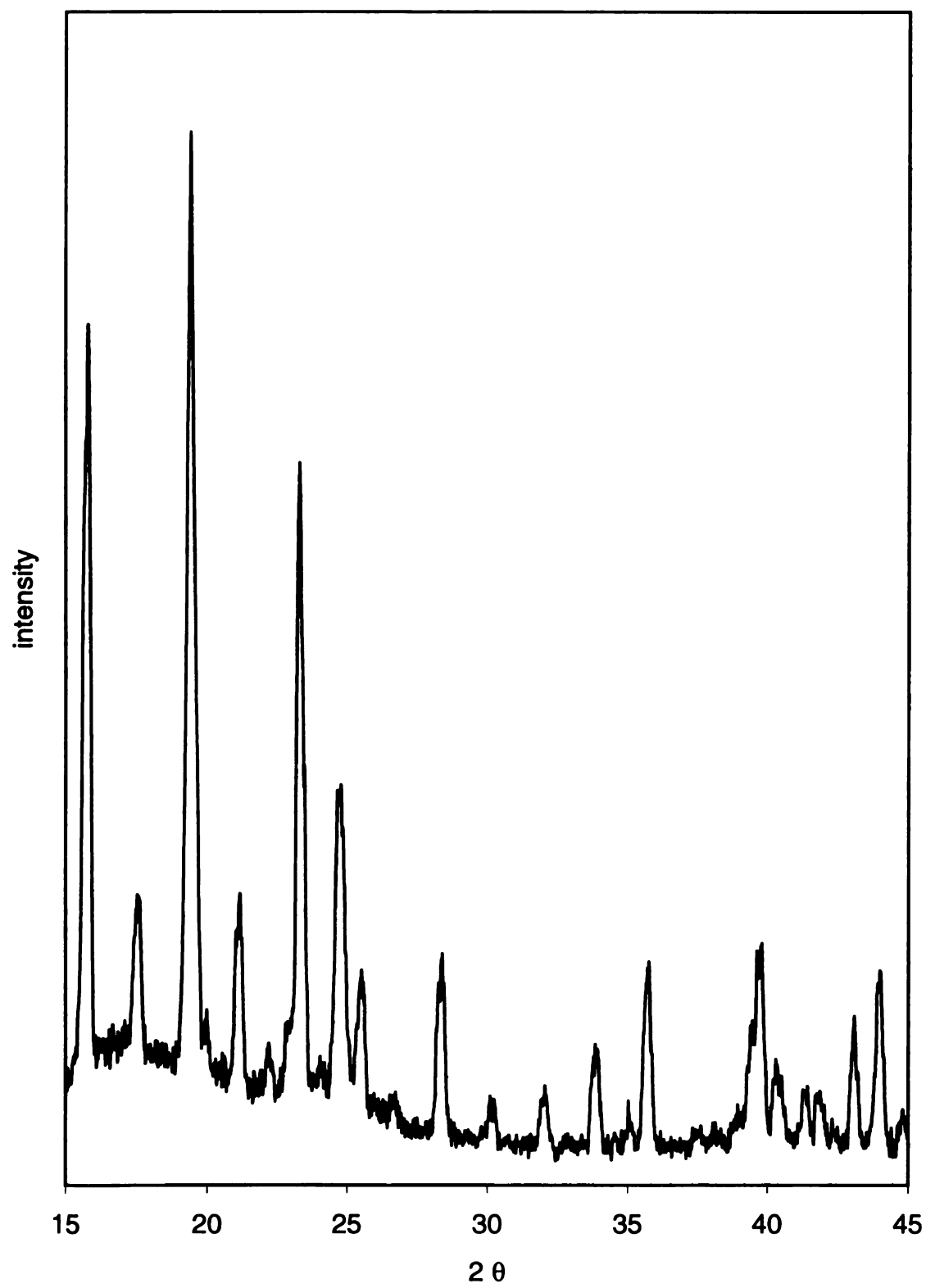


Figure 24. Wide angle XRD for $\text{C}_{16}\text{EO}_3\text{C}_{16}$.

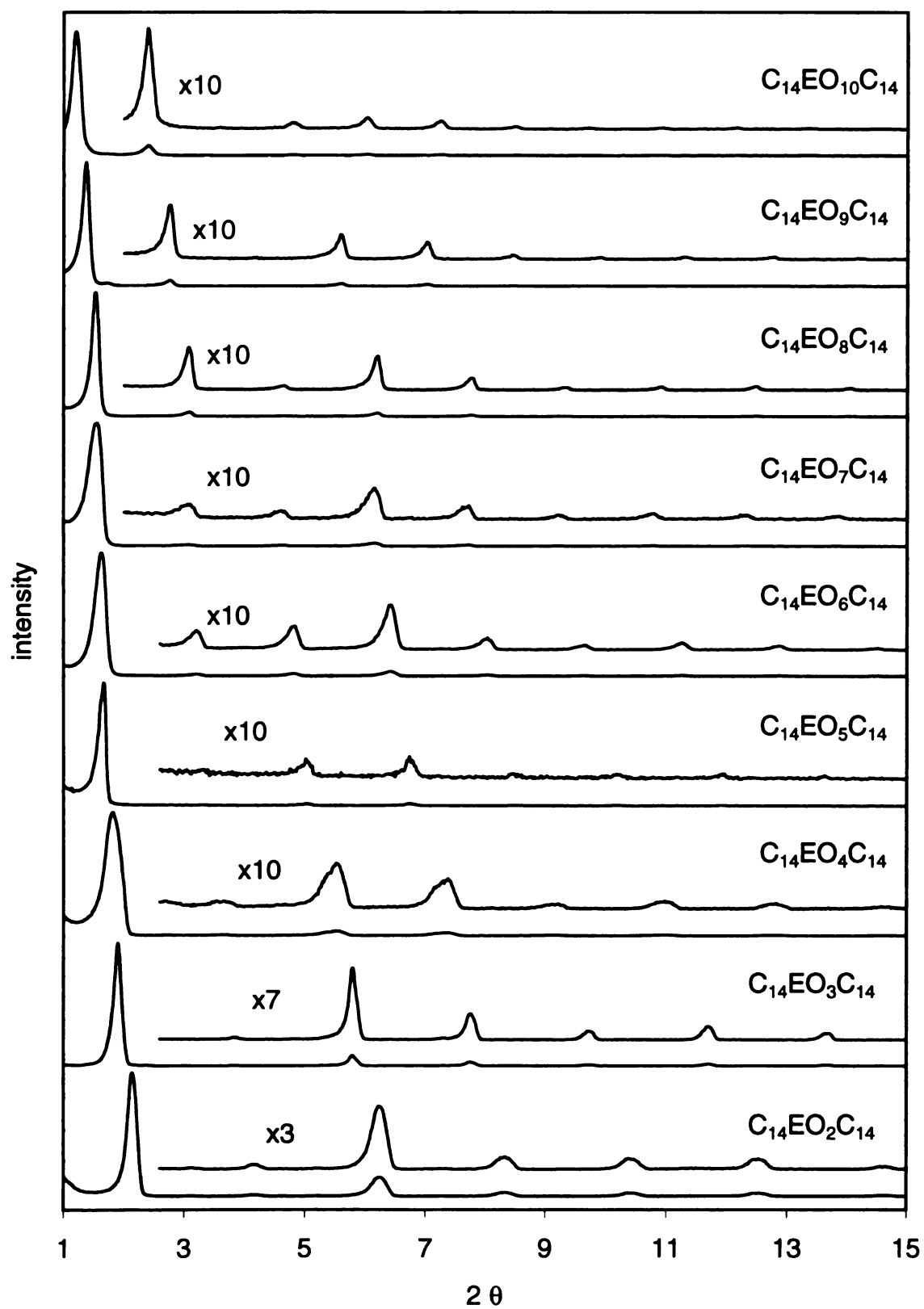


Figure 25. Low angle powder XRD of triblock oligomers $C_{14}EO_yC_{14}$.

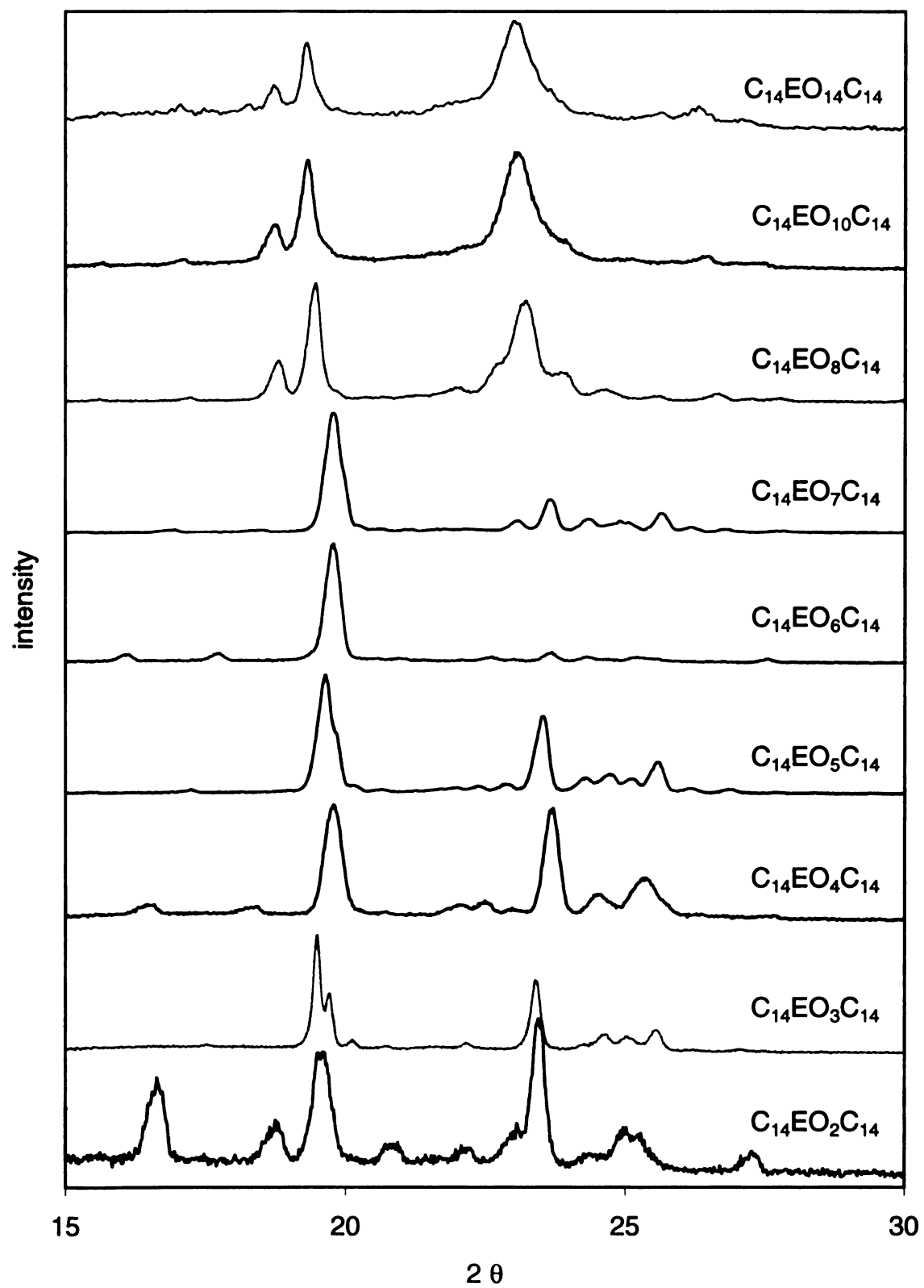


Figure 26. Wide angle powder XRD of triblock oligomers $C_{14}EO_yC_{14}$.

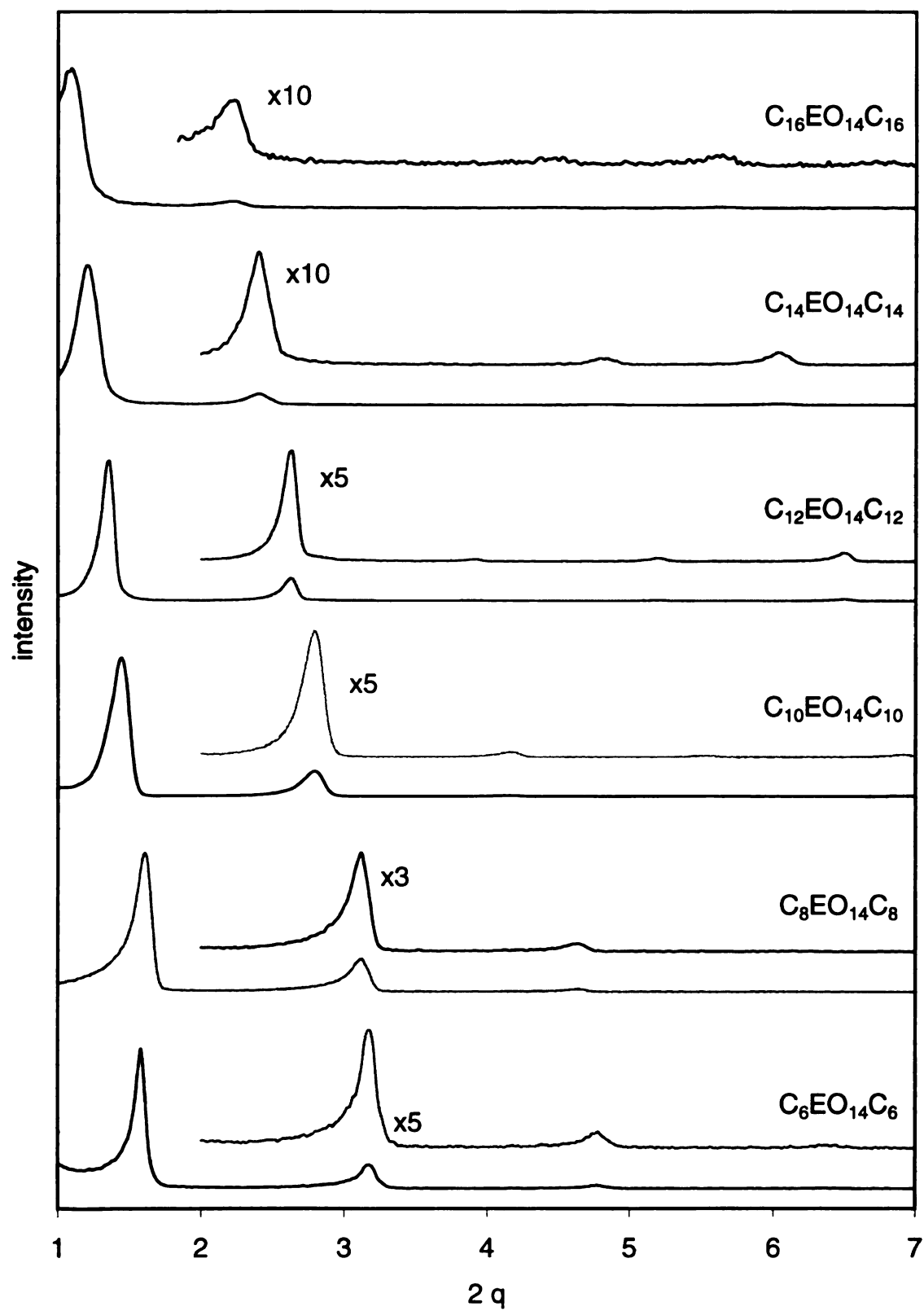


Figure 27. Low angle powder XRD of triblock oligomers $C_xEO_{14}C_x$.

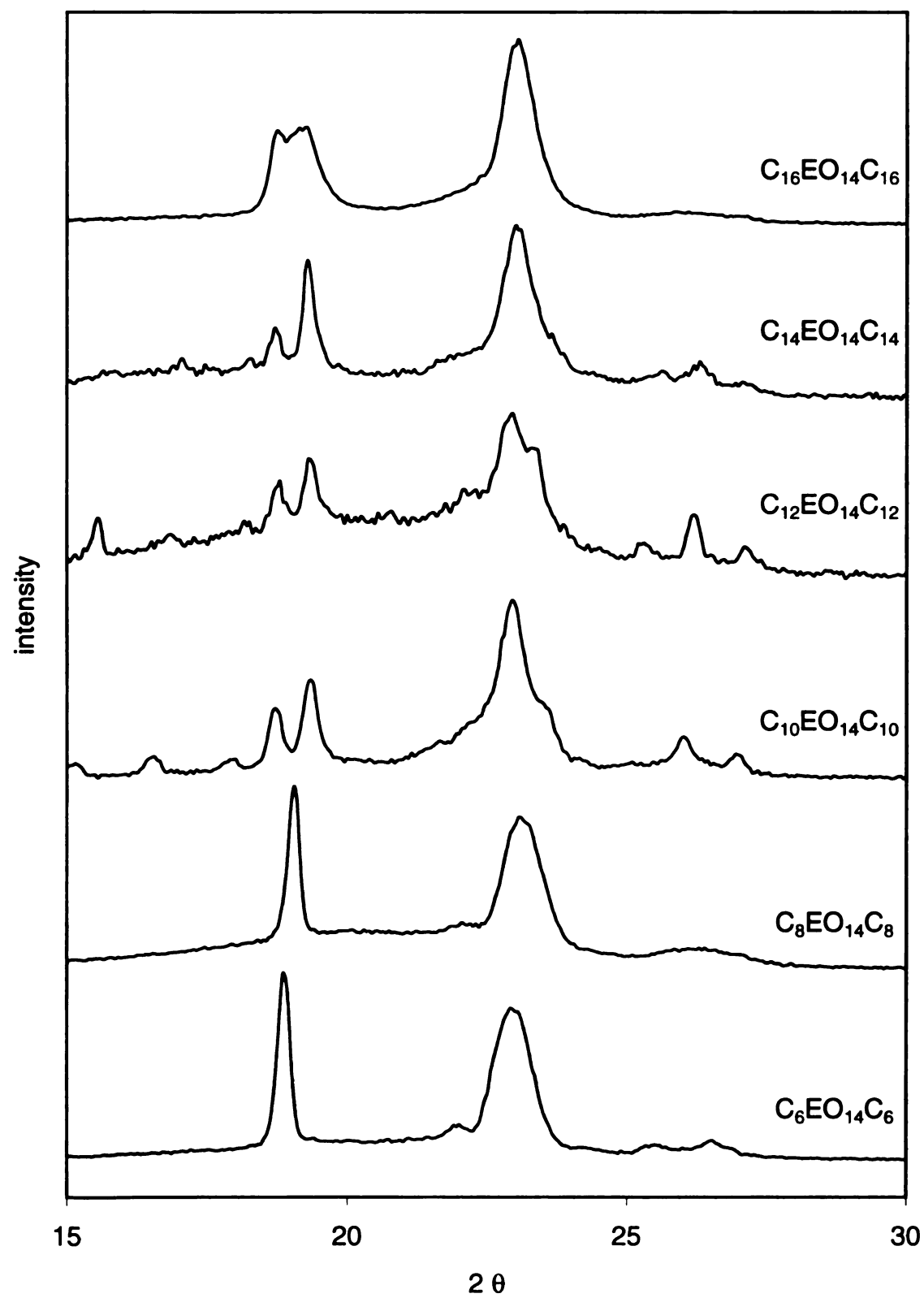


Figure 28. Wide angle powder XRD of triblock oligomers $C_xEO_{14}C_x$.

Table 8. d-spacings (Å) for triblock oligomers ($C_{14}EO_yC_{14}$) with tetradecyl alkyl segments.

y	2	3	4	5	6	7	8	10	14
d (Å)	41.3	46.4	48.7	53.1	54.4	60.1	57.7	64.5	75.1
Δd (Å)	-	5.1	2.3	4.4	1.3	5.7	-2.4	-	

The XRD scans for a series of triblock oligomers $C_xEO_{14}C_x$, with a constant ethylene oxide block length of $y = 14$ and $x = 6, 8, 10, 12, 14$ and 16 are shown in **Figure 27** (lower angles) and **28** (higher angles). The XRD pattern for all the samples in this series are similar from 20 to 30° 2θ values, while in the lower angle portion, the d-spacing increases as the alkyl segments become longer. However, the increase in the increments Δd , defined by the d-spacing differences between the samples with values of x and $x+2$, are not linear. Their values are tabulated in **Table 9**.

Table 9. d-spacings (Å) for triblock oligomers ($C_xEO_{14}C_x$) with tetradecaethylene oxide segments.

x	6	8	10	12	14	16
d (Å)	56.2	55.1	61.9	65.5	75.1	84.0
Δd (Å)	-	-1.1	5.7	9.3	18.9	28.2

C₁₄EO₇C₁₄

As we already seen from DSC studies, triblock oligomers with 7 ethylene oxide units show the most interesting behavior. As in the DSC studies, we chose **C₁₄EO₇C₁₄** as a representative oligomer for most of the XRD studies. Other samples in this series were also tested and were found to behave similarly to this compound. This compound was subjected to a series of experiments to identify the structures and their transformations.

The first issue we focused on was the different structures that form when **C₁₄EO₇C₁₄** is crystallized under different conditions. Powder XRD experiments were performed on samples obtained by crystallization from methanol, from hexane, from the melt with a slow cooling rate to room temperature, from the melt after fast quenching to subambient temperature, and by self-seeded isothermal crystallization from the melt close to the equilibrium melting temperature. **Figures 29** (low angles) and **30** (wide angles) show the XRD data from samples obtained by crystallization from solutions, and by slow and fast cooling from the melt. All of the samples show characteristic lamellar behavior as evidenced by the well-defined 00l peaks. Their d-spacings were clearly different, with crystallization from methanol solution resulting in the longest, 60.1 Å, crystallization from hexanes solution the shortest, 52.7 Å, and the two melt crystallization results in between, 54.6 Å from slow cooling and 56.3 Å from fast quenching. Their high angle diffraction patterns were also quite different. The flash quenched sample has a pattern at $2\theta = 19.7^\circ$ and between 22.5° to 27° that is similar to that obtained from methanol. However, small peaks at 18.6° and a shoulder at 19.3° seen in the flash quenched sample also match peaks in the slow cooled sample. Crystals obtained from hexane bear the least

resemblance to the other samples. These results indicate that the samples crystallized under different conditions do give very different crystals.

To further test the melt crystallized sample structure change with sample history, we carried out another set of experiments. The sample was melted and held at 100 °C for one hour to totally randomize any ordering in the melt sample, quenched to liquid nitrogen temperature, and then was allowed to warm up to room temperature in a desiccator to prevent moisture build up. The XRD pattern of the sample was taken immediately, after 3 hours and after 15 hours. Their profiles are given in **Figures 31 and 32**. From **Figure 31**, we can see that the lowest diffraction angle, initially at 1.58° and corresponding to a d-spacing of 56 Å, shifted to lower angles after 3 h at room temperature, and finally shifted to an angle that corresponds to the d-spacing given by sample crystallized from methanol, 60.1 Å. From their higher angle diffraction profiles, we observed the change of their XRD pattern from one that is quite similar to that of samples slowly crystallized from melt, to one like that obtained from methanol. It seems that the crystal form obtained from methanol is the most thermodynamically stable form.

To further test this hypothesis, we used self-seeded isothermal crystallization to obtain the most stable crystal from the melt. Self-seeding was achieved by carefully melting a crystalline sample until only a few tiny crystalline needles were seen under a polarized microscope. The system was then held at less than 1 °C below the crystal melting point for crystals grow. By doing this, only the most thermodynamically stable crystal seeds exist, and the only crystal that forms during crystallization are these with the structure of the seed. The crystal thus obtained was characterized by XRD over a period of 2 months to test its stability. The XRD results taken immediately after the crystal was

obtained, after being stored at room temperature for 2 days, and after 2 months are shown in **Figures 33** and **34**. As can be seen from both figures, there was no change during this storage period. This phenomenon was also confirmed by Raman and IR spectroscopy.

We also performed an experiment to test the isothermal conversion of one crystal form to another above room temperature, which is similar to the DSC experiment described earlier. The sample was flash quenched from the melt to liquid nitrogen temperature, and then quickly heated to 35 °C. Diffraction patterns were taken at low angles as a function of time. As can be seen in **Figure 35**, the sample's highest peak, originally at approximately 1.64°, shifted to a lower angle. At 14 min, this peak had diminished while a new peak at 1.54° emerged. Eventually, all of the sample was converted into the stable high temperature form.

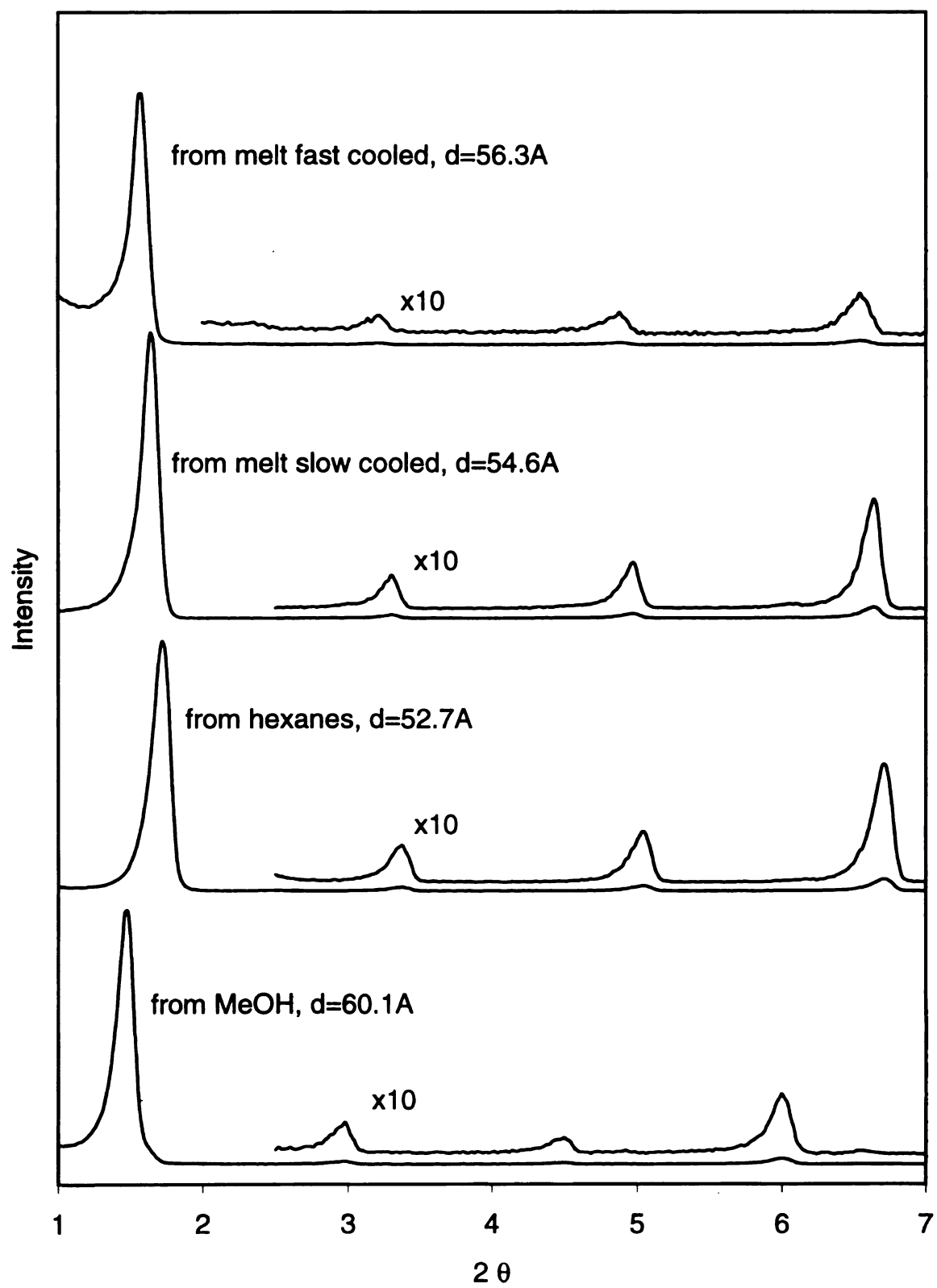


Figure 29. Low angle powder XRD of $C_{14}EO_7C_{14}$ crystallized by different methods.

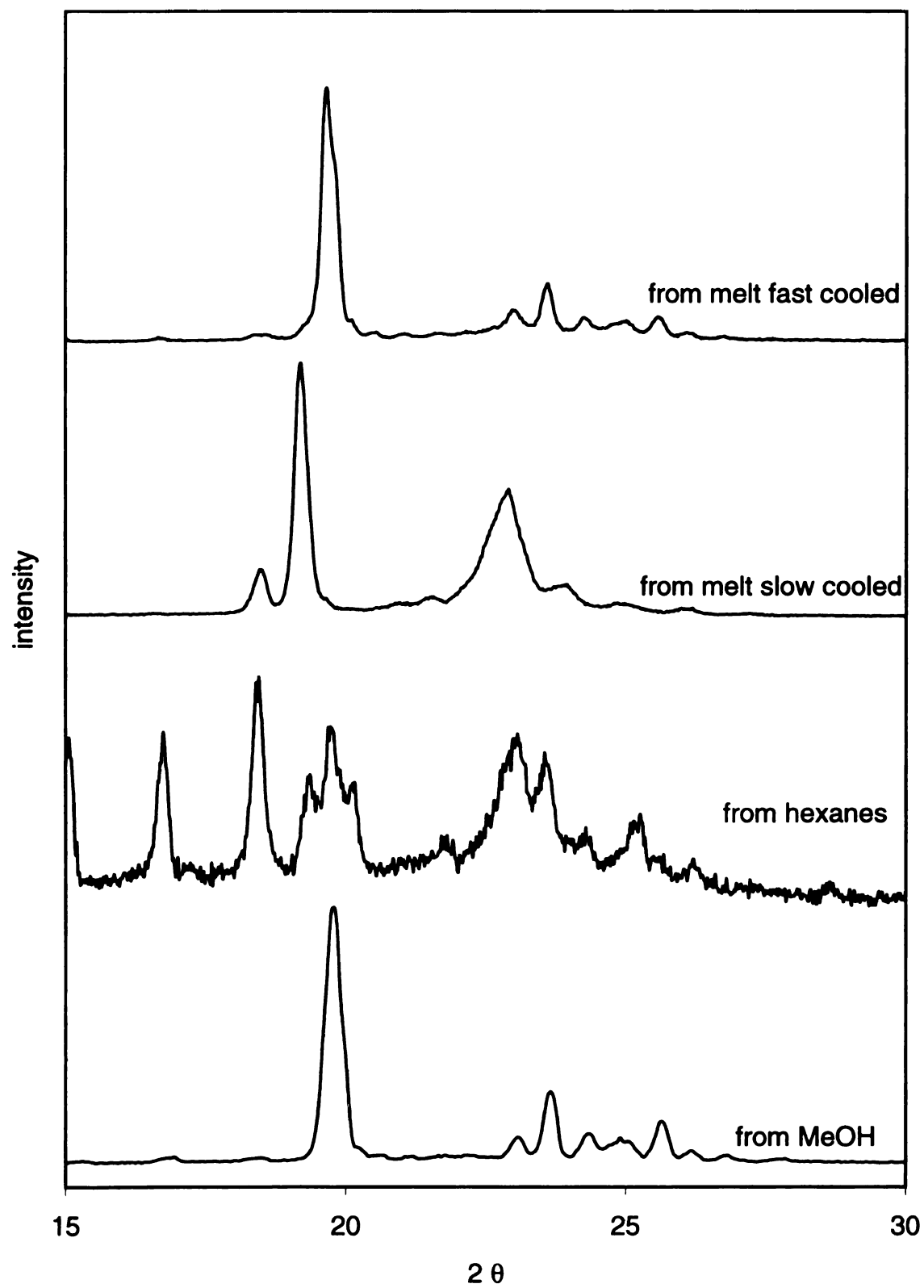


Figure 30. Wide angle powder XRD of $C_{14}EO_7C_{14}$ crystallized by different methods.

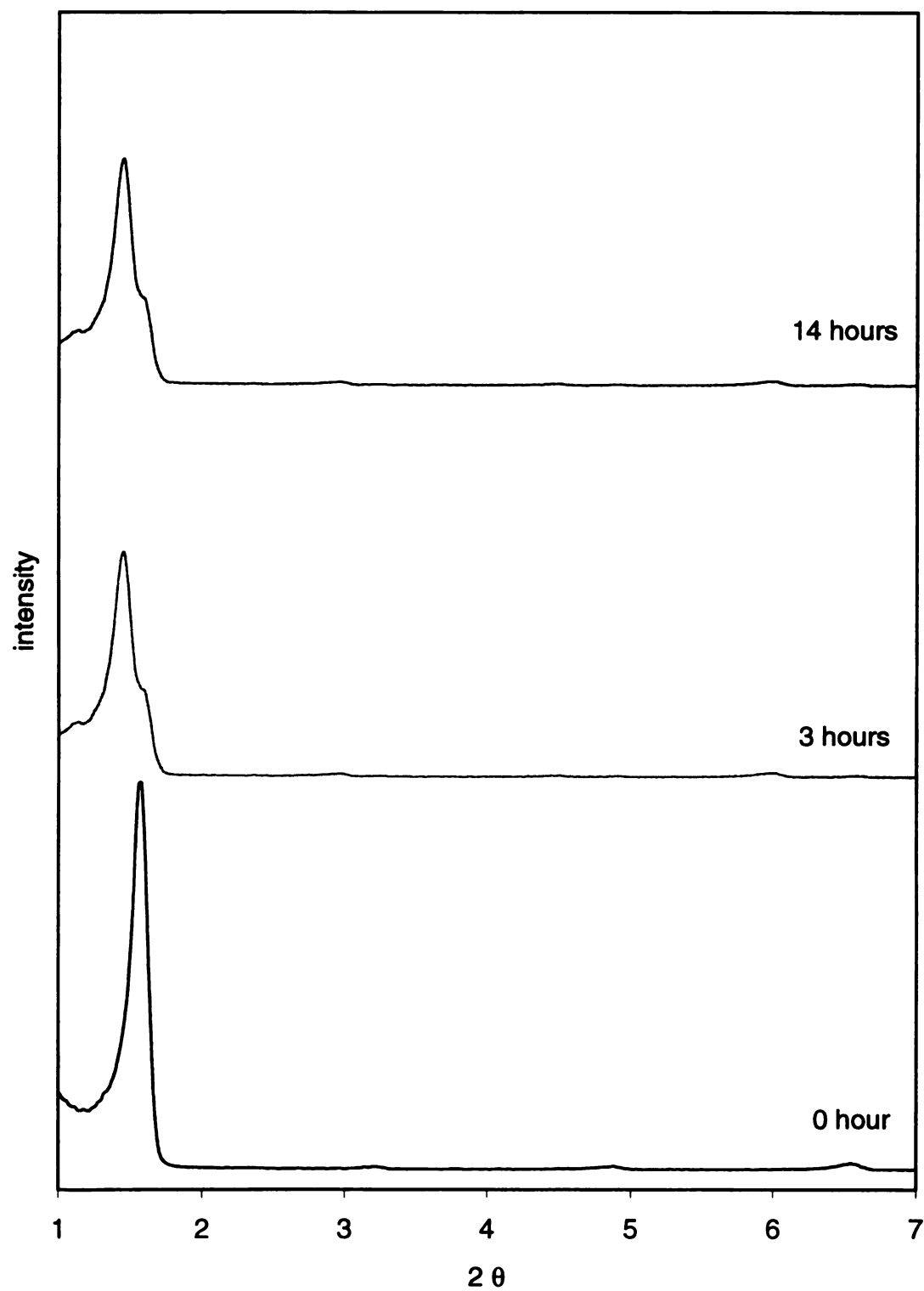


Figure 31. Low angle powder XRD of $C_{14}EO_7C_{14}$. Crystal obtained by flash quenching from the melt, then holding at room temperature for the periods of time as indicated.

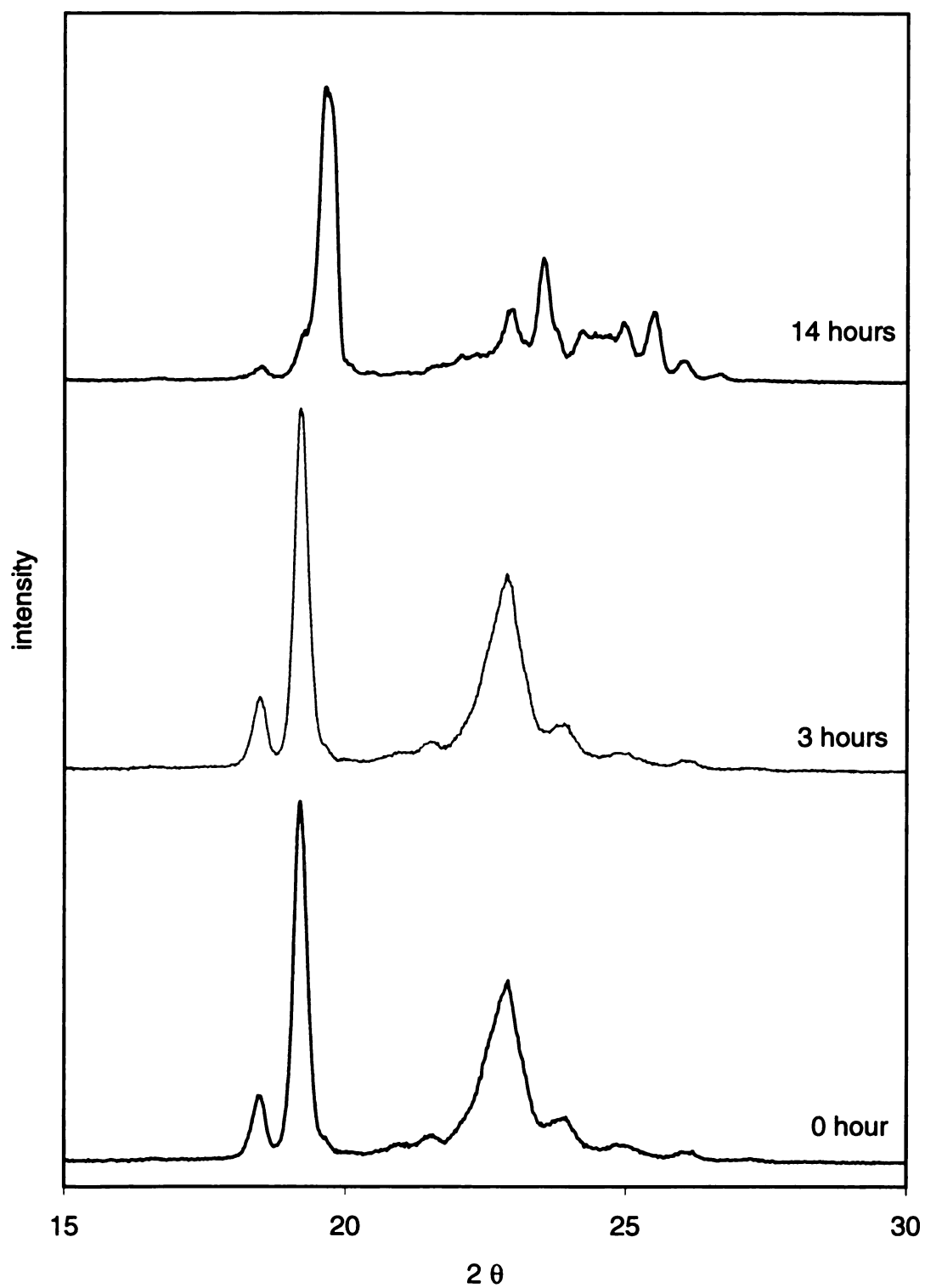


Figure 32. Wide angle powder XRD of $C_{14}EO_7C_{14}$. Crystal obtained by flash quenching from the melt, then holding at room temperature for the periods of time as indicated.

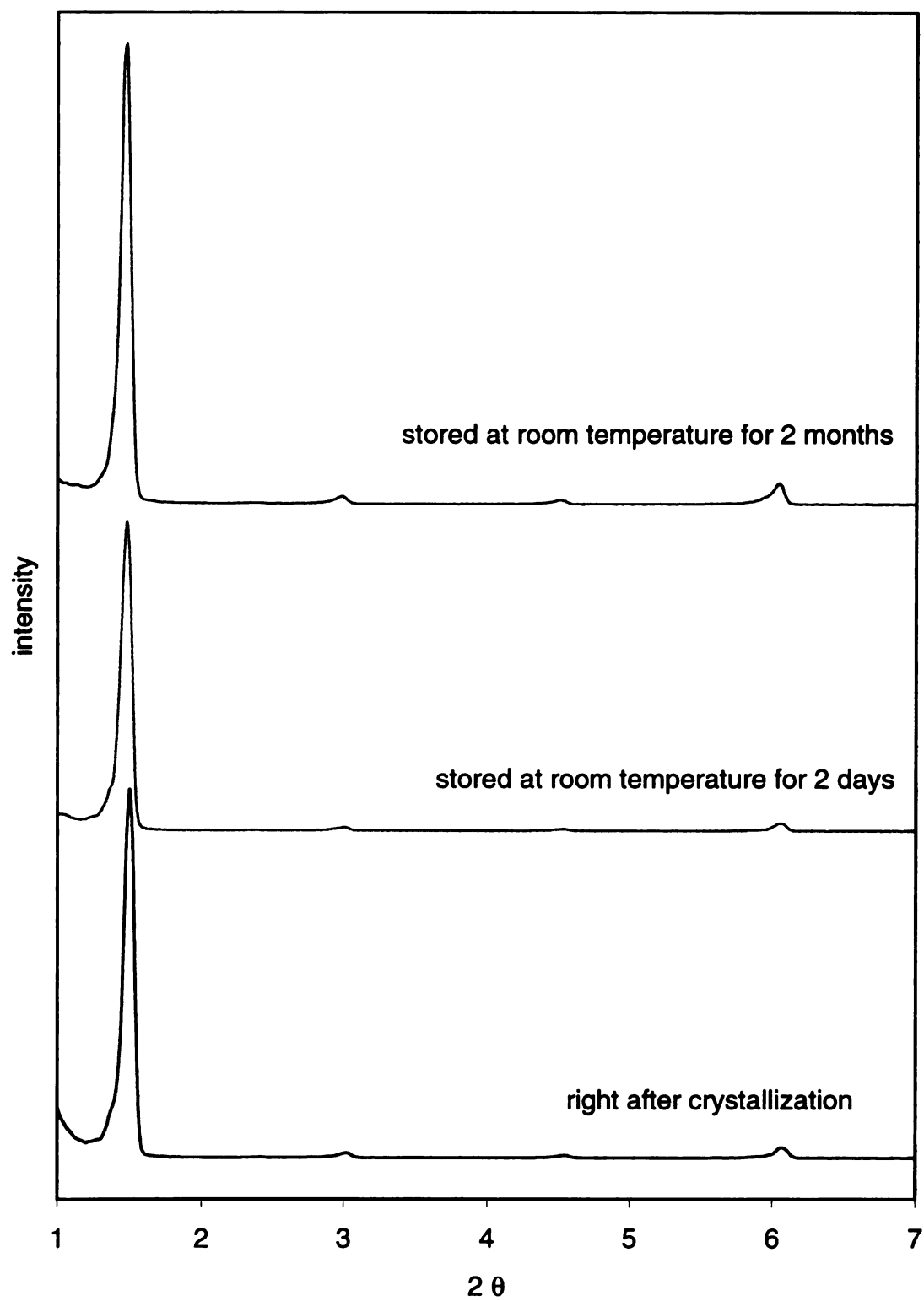


Figure 33. Low angle powder XRD of $C_{14}EO_7C_{14}$ crystals obtained by isothermal crystallization at 41.5 °C.

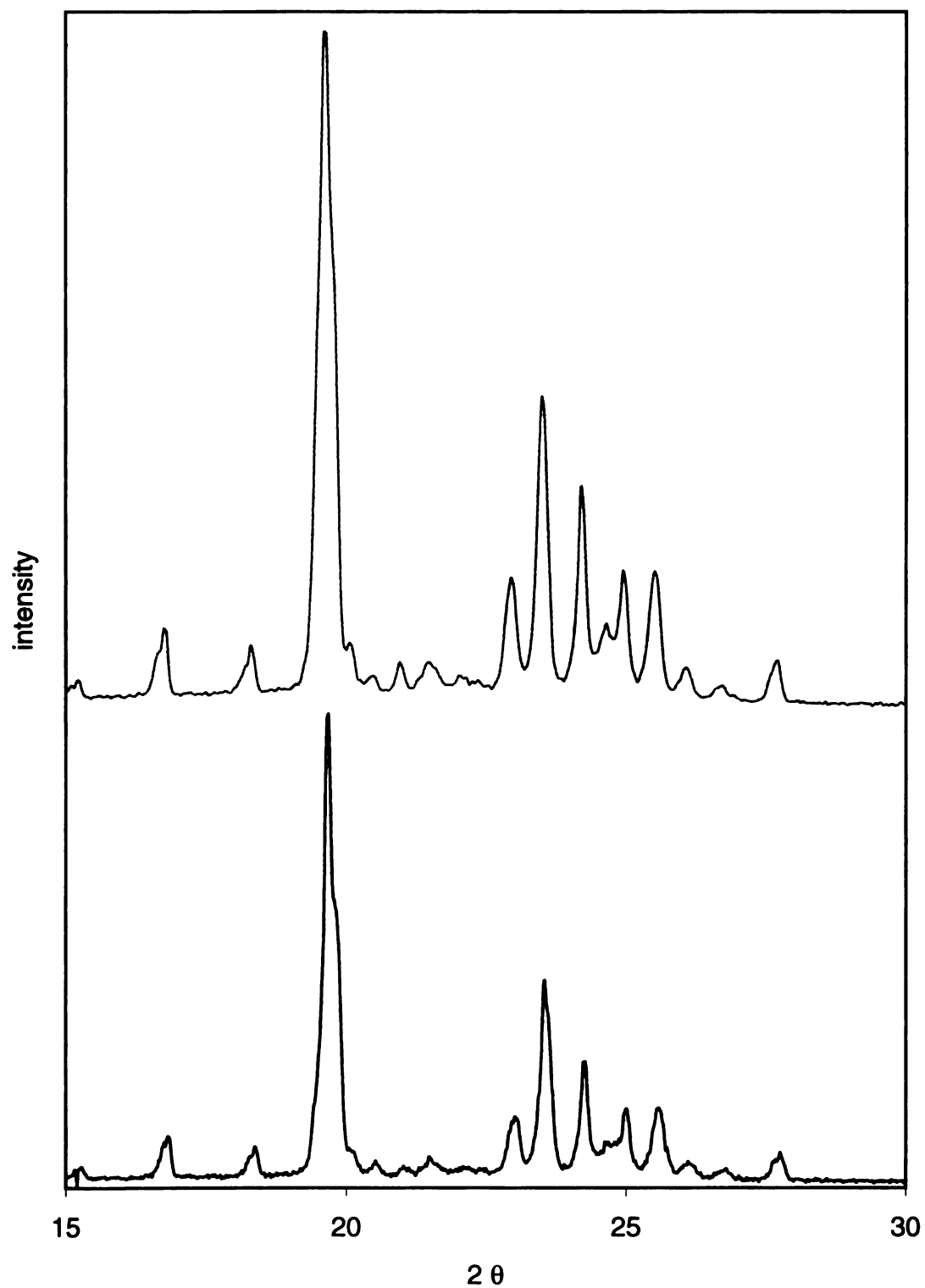


Figure 34. Wide angle powder XRD of $C_{14}EO_7C_{14}$ crystals obtained by isothermal crystallization at 41.5°C . Bottom: crystal tested right after obtained. Top: crystal stored at room temperature for two months.

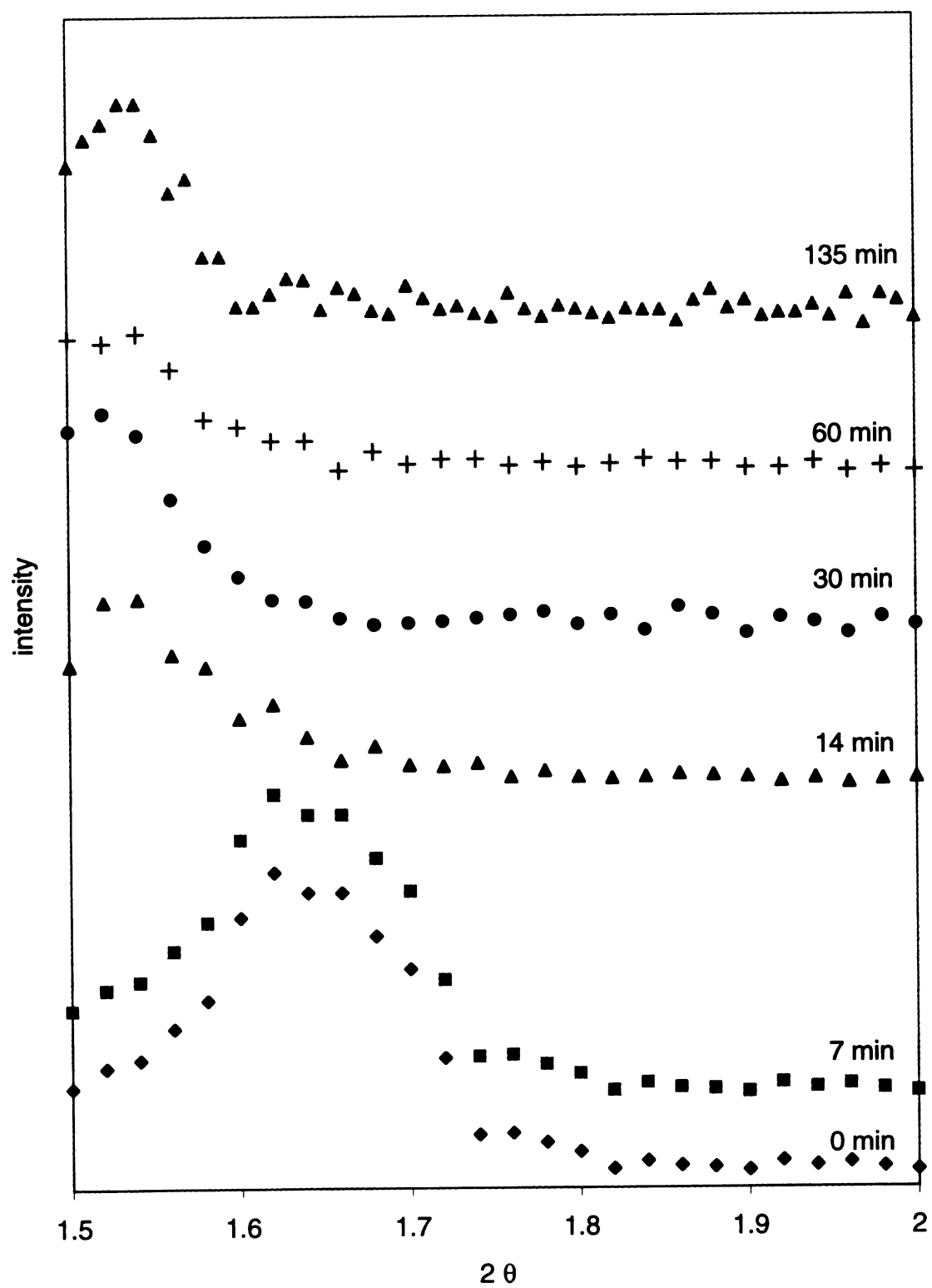


Figure 35. Powder XRD evolution of $C_{14}EO_7C_{14}$ annealed at 35°C .

3. Spectroscopic characterizations

Spectroscopic tools including ^1H NMR, ^{13}C NMR, FTIR and Raman spectroscopy were used to characterize the triblock oligomers. Detailed spectroscopic data such as the NMR spectra appear in the Experimental section, and are not repeated here.

IR and Raman experiments which can show the details of molecular structures such as packing information and molecule chain conformations, were used to elucidate the triblock oligomer structures, especially that of $\text{C}_{14}\text{EO}_7\text{C}_{14}$, which showed interesting multiple crystalline phases. Samples for IR and Raman experiments were prepared either by melt crystallization on a substrate, or by depositing the desired oligomer as a solution onto a polished silicon slide, and evaporating the solvent to dryness in a moisture free environment.

The IR spectra for $\text{C}_x\text{EO}_y\text{C}_x$ where $y \leq 6$ are similar. A typical spectrum of $\text{C}_{14}\text{EO}_3\text{C}_{14}$ is shown in **Figure 36**. Specific attention was paid to the low frequency region since it contains useful information about crystal packing and molecular conformation. For example, the band at 718 cm^{-1} in **Figure 36** can be assigned to planar zigzag alkyl chains packed in a triclinic unit cell.

Samples with 7 ethylene oxide units, $\text{C}_x\text{EO}_7\text{C}_x$, crystallized under different conditions had different spectra. **Figure 37** shows the IR spectra of $\text{C}_{14}\text{EO}_7\text{C}_{14}$ crystallized from hexanes and methanol. It can be seen that the two spectra are quite different in the low frequency region. Samples crystallized from hexanes showed bands at 1147 , 1111 and 851 cm^{-1} which are characteristic for low frequency PEO in a helical

conformation.^{100,101} The bands for samples obtained from methanol are very similar to that of $C_{14}EO_3C_{14}$.

Raman spectra were also taken of the two $C_{14}EO_7C_{14}$ samples. Again, their spectra were very different (**Figure 38**). Bands at 1042, 1150, 1275 and 1497 cm^{-1} , which are known to be characteristic of planar zigzag PEO, were observed in spectra of samples crystallized from methanol, while bands at 854, 864, 1002 and 1484 cm^{-1} for helical PEO were observed in spectra of hexane crystallized samples.

Crystals of melt quenched $C_{14}EO_7C_{14}$ were monitored while stored at room temperature for several days (**Figure 39**). From the Raman data, it can be concluded that the melt-quenched sample first adopted a helical conformation for the PEO segment and then changed to a planar zigzag conformation. This is indicated by the obvious change in the Raman spectra between days 2 and 4. Crystals obtained from melt quenched $C_{14}EO_{14}C_{14}$ sample, however, did not show such a change. As shown in **Figure 40**, the spectra for this sample were virtually the same through out the test period—indicating that the PEO segment maintained a helical conformation.

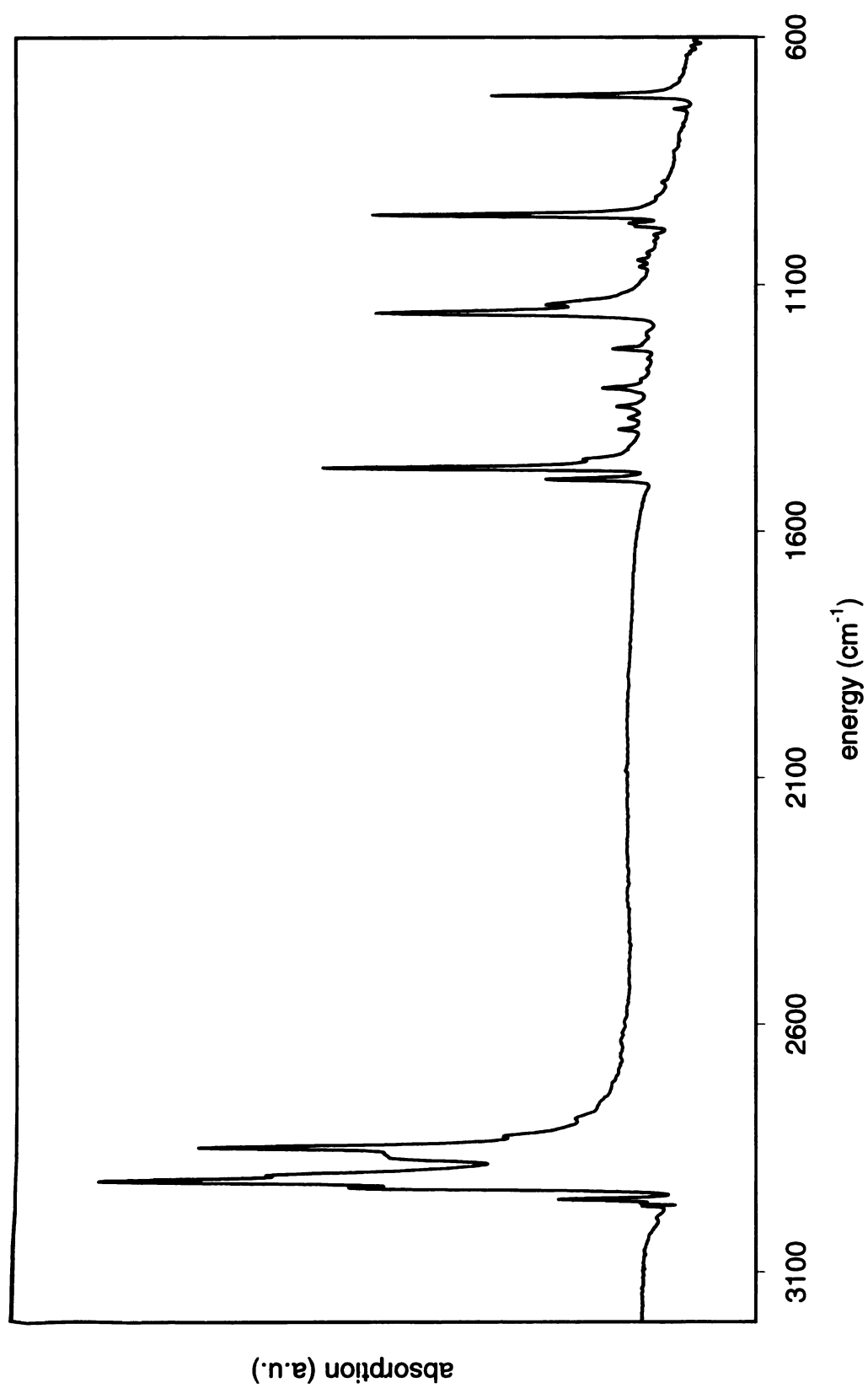


Figure 36. IR spectrum of $C_{14}EO_3C_{14}$.

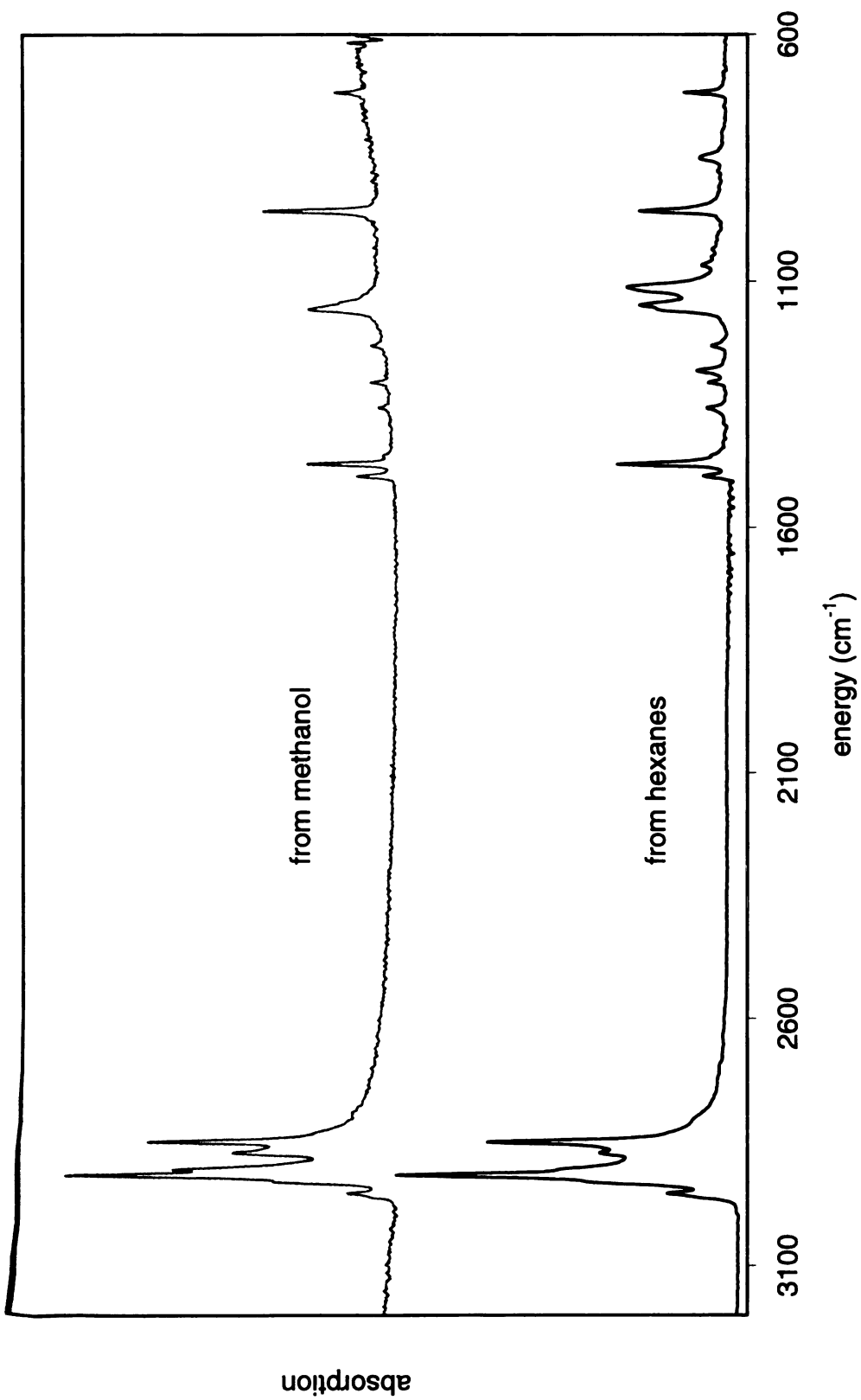


Figure 37. IR spectra of $\text{C}_{14}\text{EO}_7\text{C}_{14}$ crystallized from hexanes (bottom) and methanol (top) solutions.

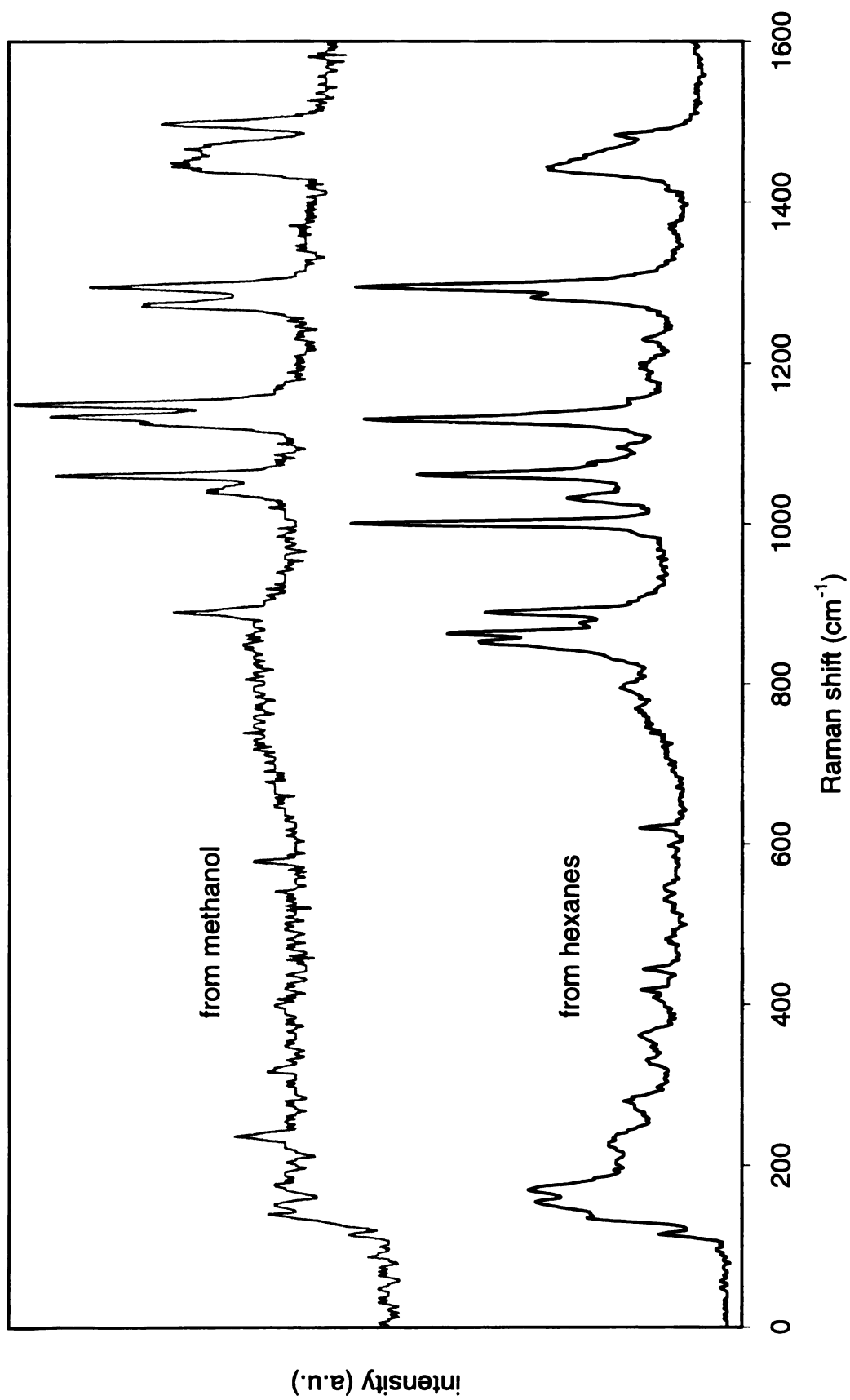


Figure 38. Raman spectra of $\text{C}_{14}\text{EO}_7\text{C}_{14}$ crystallized from hexanes (bottom) and methanol (top).

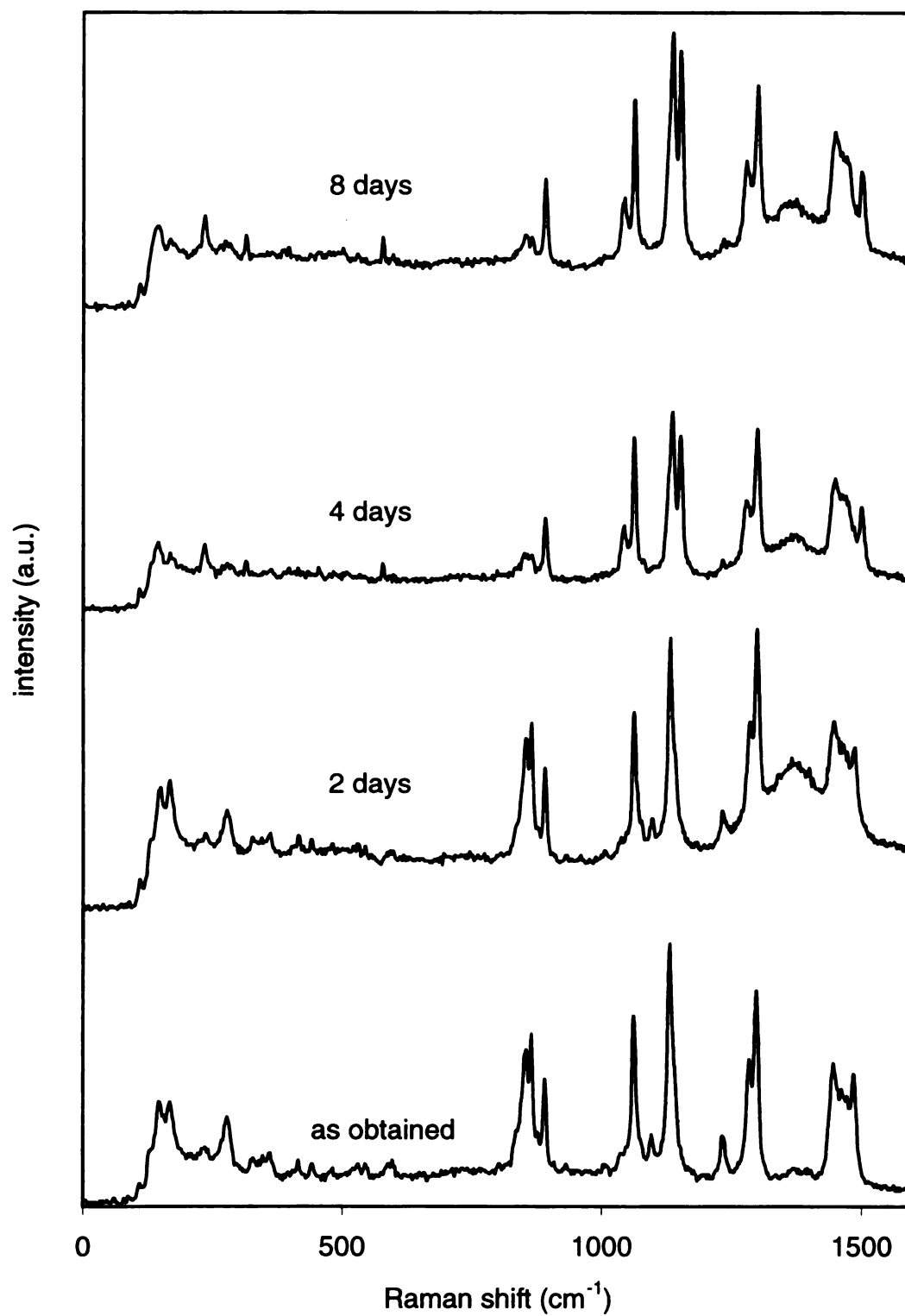


Figure 39. Raman spectra of $C_{14}EO_7C_{14}$. Samples were obtained by quenching from the melt, and stored at room temperature. Spectra were taken at the time intervals indicated in the figure.

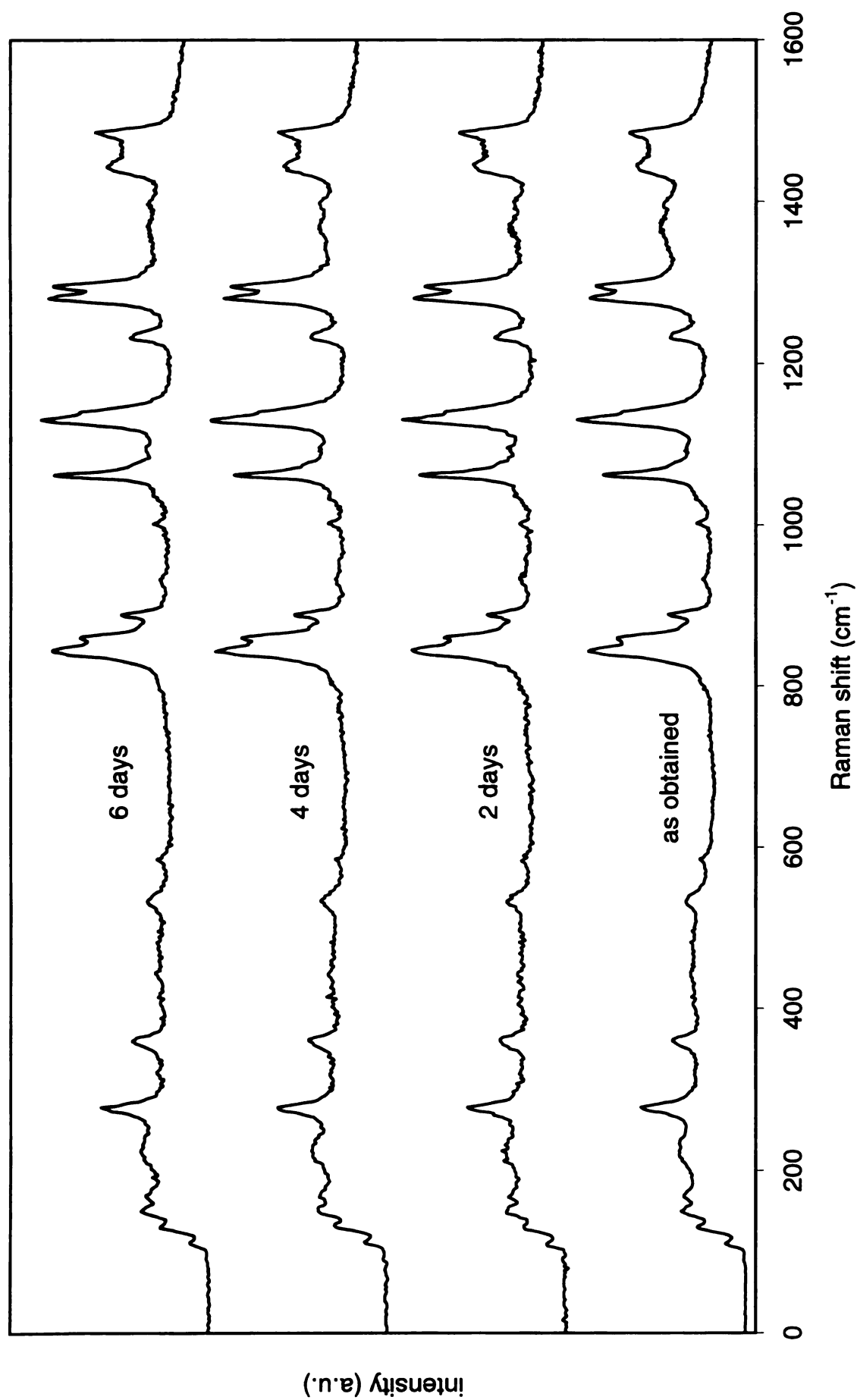


Figure 40. Raman spectra of $C_{14}EO_{14}C_{14}$. Samples were obtained by quenching from the melt, and stored at room temperature. Spectra were taken at time intervals indicated in the figure.

III. Properties of unsaturated (AB)_n microblock copolymers (C_xπC_xEO_y)_n

1. Physical properties

The molecular weights and polydispersity indexes (PDI) of the unsaturated polymers are collected in **Table 10**. Our target molecular weight for the polymers was 50,000 g/mol and most polymerizations met that target. PDI values for polymers obtained after precipitation in hexanes were near 2, typical for step-growth polymerizations. Despite attempts to remove all catalyst residues, the purified polymers had a slight yellow to green tinge, which is believed to be due to catalyst residues.

Because of the amphiphilic nature of the two segments, the polymers are soluble in an unusually broad range of organic solvents, including polar and non-polar solvents. The solubility depends on the segment lengths. Polymers with long alkenyl segments and relatively short ethylene oxide segments are more soluble in non-polar solvents such as toluene and carbon tetrachloride and are even slightly soluble in normal alkanes. In contrast, polymers with an opposite ratio of components (short alkenyl segment, long ethylene oxide segment) are more soluble in polar solvents such as chloroform, ethyl acetate, acetone, acetonitrile and methanol. Polymers (C₃πC₃EO₁₄)_n and (C₄πC₄EO₁₄)_n are even soluble in water because of their long ethylene oxide segments. Solvents like THF and dialkyl ethers that contain both polar and non-polar groups, can dissolve all of the polymers.

Table 10. Molecular weights and PDI values of unsaturated polymers
(C_xπC_xEO_y)_n.^a

Polymer	M _n	PDI	Total yield (%)
(C ₃ πC ₃ EO ₆) _n	25,500	1.71	85
(C ₄ πC ₄ EO ₆) _n	48,800	1.84	97
(C ₈ πC ₈ EO ₆) _n	58,500	1.41	84
(C ₉ πC ₉ EO ₆) _n	67,800	1.56	89
(C ₃ πC ₃ EO ₇) _n	26,400	1.89	98
(C ₄ πC ₄ EO ₇) _n	55,500	1.79	98
(C ₈ πC ₈ EO ₇) _n	58,300	1.40	81
(C ₉ πC ₉ EO ₇) _n	40,600	1.41	85
(C ₃ πC ₃ EO ₈) _n	47,200	1.73	95
(C ₄ πC ₄ EO ₈) _n	19,400	1.61	85
(C ₈ πC ₈ EO ₈) _n	65,700	1.46	94
(C ₉ πC ₉ EO ₈) _n	60,100	1.51	91
(C ₃ πC ₃ EO ₁₀) _n	54,500	1.57	97
(C ₄ πC ₄ EO ₁₀) _n	98,500	1.38	95
(C ₈ πC ₈ EO ₁₀) _n	41,300	1.74	99
(C ₉ πC ₉ EO ₁₀) _n	52,700	1.46	99
(C ₃ πC ₃ EO ₁₄) _n	17,400	2.00	97
(C ₄ πC ₄ EO ₁₄) _n	41,700	1.52	98
(C ₈ πC ₈ EO ₁₄) _n	21,100	1.87	98
(C ₉ πC ₉ EO ₁₄) _n	63,200	1.64	97

a. The molecular weights refer to the highest molecular weight portion if the sample was fractionated. Yields are the total yield after precipitation from hexane.

2. Morphologies of unsaturated polymers

All of the polymers are crystallizable, but some polymers have melting points below room temperature. Thus at room temperature, polymers $(C_x\pi C_xEO_y)_n$ where $x = 3$ and 4 , $y = 6-8$ are amorphous, while all of the other polymers are crystalline. Micrographs of the crystalline polymers under cross-polarized light are shown in **Figures 41 to 45**. All of the crystallized polymers form spherulites as indicated by the characteristic Maltese cross pattern, however, many of the samples differ in the details of their morphologies. Both polymers $(C_8\pi C_8EO_6)_n$ and $(C_9\pi C_9EO_6)_n$ crystallized as banded spherulites as shown in **Figure 41** with similar small band widths. Polymers $(C_8\pi C_8EO_7)_n$ and $(C_9\pi C_9EO_7)_n$ also crystallize as banded spherulites (**Figure 42**), however, the band widths were quite different, with the bands of $(C_8\pi C_8EO_7)_n$ about 30 times that of $(C_9\pi C_9EO_7)_n$. Polymers crystals from $(C_8\pi C_8EO_8)_n$ and $(C_9\pi C_9EO_8)_n$ also were banded spherulites (**Figure 43**) with the band width larger for $(C_8\pi C_8EO_8)_n$.

Polymers in the $(C_x\pi C_xEO_{10})_n$ series crystallized differently. As shown in **Figure 44**, $(C_3\pi C_3EO_{10})_n$ formed banded spherulites while $(C_x\pi C_xEO_{10})_n$ polymers where $x = 4, 8$ and 9 crystallized sluggishly. Polymer $(C_4\pi C_4EO_{10})_n$ needed to be sheared to induce crystallization into ill-defined spherulites while polymers $(C_8\pi C_8EO_{10})_n$ and $(C_9\pi C_9EO_{10})_n$ crystallized into tiny banded spherulites after an extended time at room temperature. For polymers with 14 ethylene oxide units, none showed banding and the spherulite sizes were relatively large (**Figure 45**). Normally, the bands of the banded spherulites are visible under cross-polarized light, but not under normal light. For most of the banded spherulites in this study, the bands can be clearly seen without cross-

polarized light. Shown in **Figure 46** is a micrograph of a banded spherulite sample of $(C_8\pi C_8EO_7)_n$ taken without cross-polarized light. The bands are clearly seen and can be compared to the same sample in **Figure 42**. Similar observations were reported for PEO samples and were ascribed to the step-growing or spiral-growth of spherulites rather than from lamellae twisting.²⁸ Further studies need to be carried out to clarify the cause of banding in $(C_x\pi C_xEO_y)_n$ spherulites.

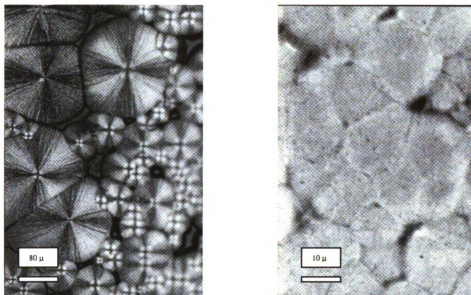


Figure 41. Micrographs of polymers $(C_8\pi C_8EO_6)_n$ (left) and $(C_9\pi C_9EO_6)_n$ (right) under cross-polarized light

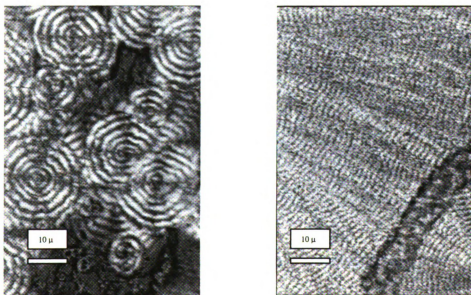


Figure 42. Micrographs of polymers $(C_8\pi C_8EO_7)_n$ (left) and $(C_9\pi C_9EO_7)_n$ (right) under cross-polarized light

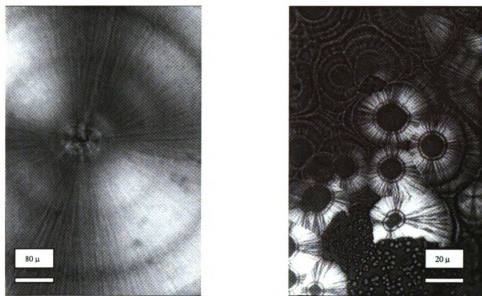


Figure 43. Micrographs of polymers $(C_8\pi C_8EO_8)_n$ (left) and $(C_9\pi C_9EO_8)_n$ (right) under cross-polarized light



Figure 46. Micrograph of polymer $(C_8\pi C_8EO_7)_n$ under non-crosspolarized light

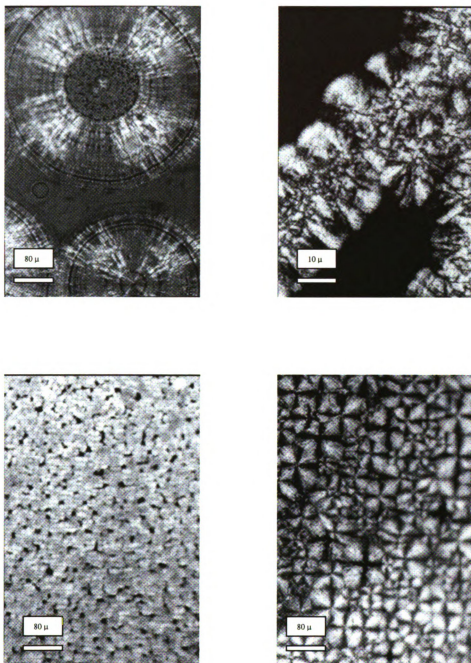


Figure 44. Micrographs of polymers $(C_3\pi C_3EO_{10})_n$ (upper left), $(C_4\pi C_4EO_{10})_n$ (upper right), $(C_8\pi C_8EO_{10})_n$ (lower left), and $(C_9\pi C_9EO_{10})_n$ (lower right) under cross-polarized light.

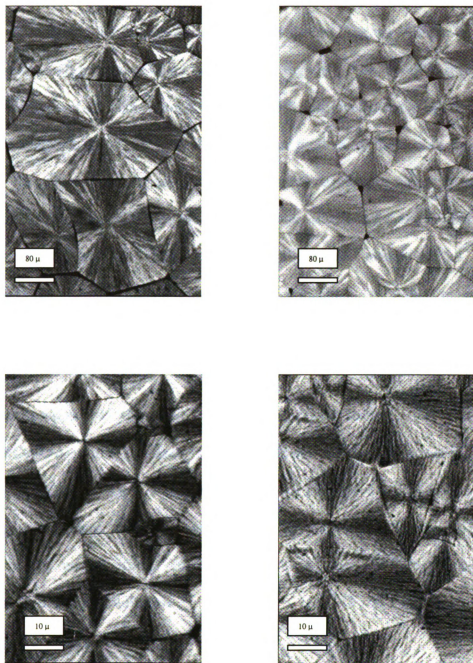


Figure 45. Micrographs of polymers $(C_3\pi C_3EO_{14})_n$ (upper left), $(C_4\pi C_4EO_{14})_n$ (upper right), $(C_8\pi C_8EO_{14})_n$ (lower left), and $(C_9\pi C_9EO_{14})_n$ (lower right) under cross-polarized light.

3. Spectroscopic characterizations

Since the polymers are homologous, their NMR spectra look very similar to each other. For example, all have resonances in three main regions of the ^1H NMR spectrum — methylene protons of the alkenyl segments at 1.4–3.5 ppm, methylene protons of the ethylene oxide segments at 3.5–3.7 ppm and the methine protons for the double bonds at 5.3–5.5 ppm. The methine protons can be used as quantitative indicator for the degree of polymerization. As the polymerization proceeds, the peaks shown at 5.8 and 4.9 ppm for the terminal double bonds gradually disappear, while peaks emerge at 5.4 ppm corresponding to the internal double bonds. This change means the α,ω -diene monomer was converted into oligomers and then to polymers. Similar transformations were also observed in ^{13}C NMR and FTIR spectroscopy.

IR spectroscopy was also used to study the polymer conformation changes. Polymer $(\text{C}_9\pi\text{C}_9\text{EO}_7)_n$ was crystallized from the melt, hexanes and methanol, as was done for the $\text{C}_{14}\text{EO}_7\text{C}_{14}$ sample. However, as shown in **Figure 47** (only the low frequency region is shown), the spectra are basically the same for each sample. This indicates there are no significant conformational differences for polymer chains crystallized under different conditions.

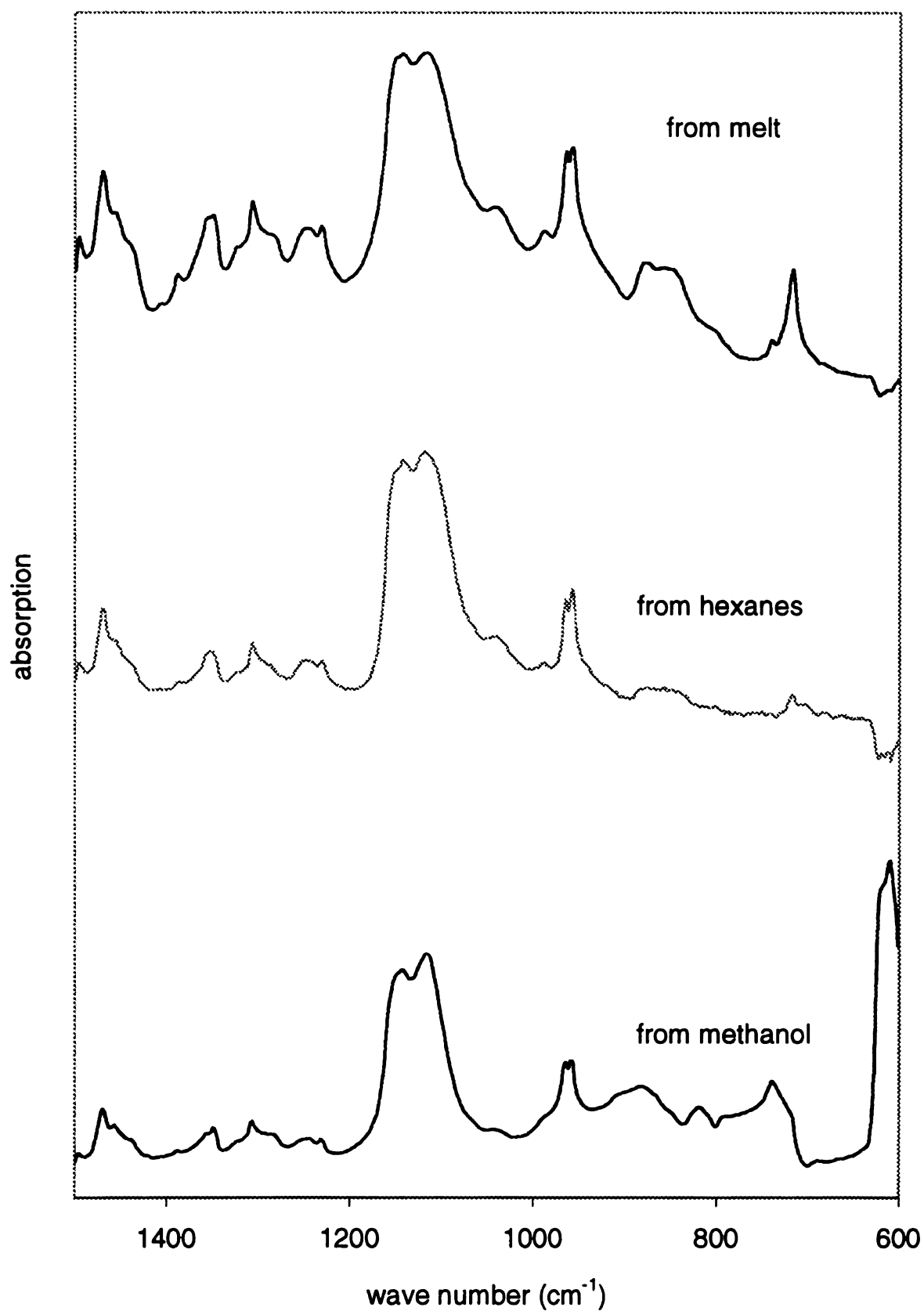


Figure 47. Low frequency region IR for polymer $(C_9\pi C_9EO_7)_n$ crystallized using different methods.

4. Thermal behavior of the unsaturated polymers

The unsaturated polymers were analyzed by DSC to characterize their thermal properties. Each sample was originally crystallized from the melt at room temperature for at least one month to allow full crystallization. All samples were first heated at 10 °C/min from 20 °C to 105 °C and then held at that temperature for 5 minutes to allow complete randomization of the polymer sample. The sample was then quenched to –100 °C at 200 °C/min, heated at 10 °C/min to 100 °C, cooled to –100 °C at 10 °C/min, and finally heated at 10 °C/min to 100 °C.

Shown in **Figure 48** to **51** are the heating scans taken after flash quenching the polymers to –100 °C. The data presented are for polymers with the same alkenyl segment length, i.e. polymers $(C_x\pi C_xEO_y)_n$ where $x = 3, 4, 8, 9$ respectively. All of the polymers show T_g s at low temperatures. Their values are shown in **Table 11**. As shown in **Figure 48** for polymer $(C_3\pi C_3EO_6)_n$, the scans are complicated. A T_g at –58 °C, is followed by an exothermic crystallization at –49 °C and three overlapping melting and crystallization peaks. One crystalline phase melts, which is then followed by two alternating crystallization and melting processes as the temperature increases. Polymer $(C_3\pi C_3EO_7)_n$ showed similar multiple melting and crystallization behavior except there was no low temperature crystallization exotherm. Polymer $(C_3\pi C_3EO_8)_n$ showed one major melting endotherm followed by a small endotherm. Polymer $(C_3\pi C_3EO_{10})_n$ only showed one broad endothermic peak, and polymer $(C_3\pi C_3EO_{14})_n$ showed a narrow endothermic peak. Polymers in the $(C_4\pi C_4EO_y)_n$ series with $y = 6-8$ showed melting transitions on both sides of a crystallization transition, while polymers with $y = 10$ and 14 only showed single endotherms (**Figure 49**). Polymers in the $(C_8\pi C_8EO_y)_n$ series

followed the same trend as that of the previous series, except the second endotherm for polymer $(C_8\pi C_8EO_8)_n$ was very small (**Figure 50**). Polymer $(C_9\pi C_9EO_6)_n$ showed three endotherms with exotherms between each endotherm (**Figure 51**), like that of its analog in $(C_3\pi C_3EO_y)_n$ series. Other than this sample, the rest of the samples had DSC transitions that resembled their homologs of the previous series.

Table 11. Glass transition temperatures ($^{\circ}\text{C}$) of the unsaturated polymers $(C_x\pi C_xEO_y)_n$

	y				
x	6	7	8	10	14
3	-57.5	-53.3	-57.7	-65.4	-58.5
4	-55.8	-67.2	-56.6	-65.1	-55.5
8	-48.6	-52.5	-52.4	-66.0	-64.7
9	-45.8	-52.8	-53.9	-63.3	-62.8

In order to study the effects of melt crystallization conditions on crystal formation, all of the polymers were subjected to a heating scan after the samples were annealed at a selected temperature for 30 minutes. The annealing temperatures were chosen to be either just below or just after an endotherm detected in the DSC heating scans taken after quenching. These results were compared with scans of samples stored at room temperature, samples that had been flash quenched from the melt, and samples that had been slowly cooled from the melt. **Figures 52 to 56** are the data for polymers

$(C_3\pi C_3EO_y)_n$ where $y = 6, 7, 8, 10$ and 14 respectively. For polymer $(C_3\pi C_3EO_6)_n$ (**Figure 52**), we can see that it is amorphous at room temperature. As shown by the shape and area under the endotherms, slow cooling resulted in better low melting crystals (sharper endotherms) than did fast quenching. The highest temperature endotherm showed no change due to annealing. Polymer $(C_3\pi C_3EO_7)_n$ (**Figure 53**) also is amorphous at room temperature. The multiple peaks at 15-25 °C were barely visible in the slow cooled sample, which is opposite to the previous sample. However, annealing at 0 °C enhanced these higher melting peaks. Annealing at higher temperatures further increased the areas of the higher melting peaks. Polymer $(C_3\pi C_3EO_8)_n$ (**Figure 54**) and polymer $(C_3\pi C_3EO_7)_n$ have similar behavior. No endotherms were seen for polymer $(C_3\pi C_3EO_{10})_n$ (**Figure 55**) for the room temperature sample, even though the sample appears to be somewhat crystalline. Recalling the morphology results in the previous section that showed that this polymer is hard to crystallize, this result is not surprising. That annealing the sample at 18 °C for 30 minutes did not yield any crystalline phase also confirmed the difficulty in crystallization for this sample. Annealing also gave rise to higher melting peaks for other DSC traces. DSC scans of polymer $(C_3\pi C_3EO_8)_n$ (**Figure 56**) annealed at room temperature showed two endotherms at about 27 and 30 °C respectively. Melt crystallized samples annealed under different conditions only yielded the lower peak. However, increasing the annealing time at 20 °C did shift the endotherm to higher temperature. The remaining polymers behaved similar to the already described $(C_3\pi C_3EO_y)_n$ series, and are not described here. Their DSC plots are included in the appendix for reference.

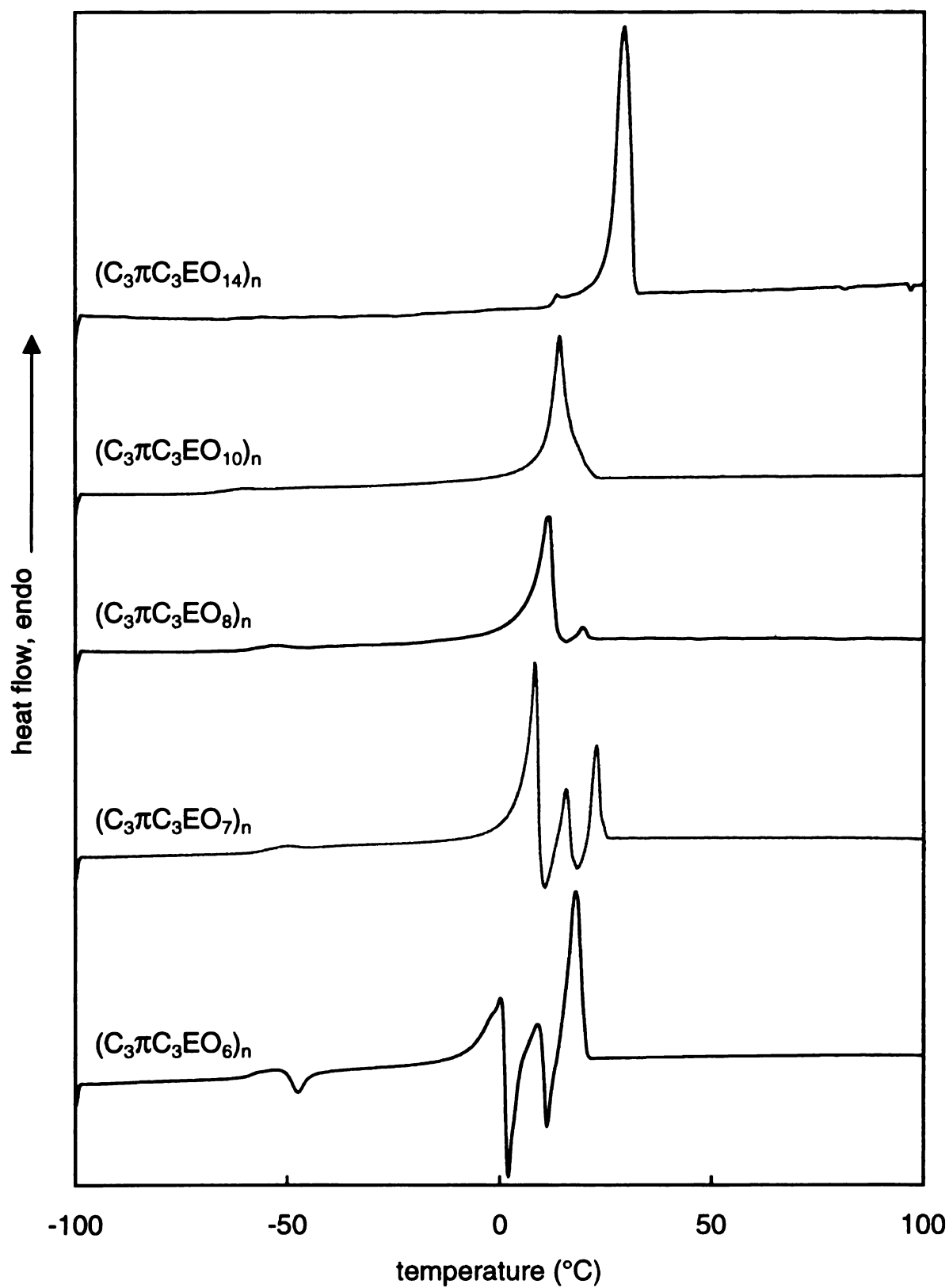


Figure 48. DSC heating scans of polymer $(C_3\pi C_3EO_y)_n$ after flash quenched from the melt.

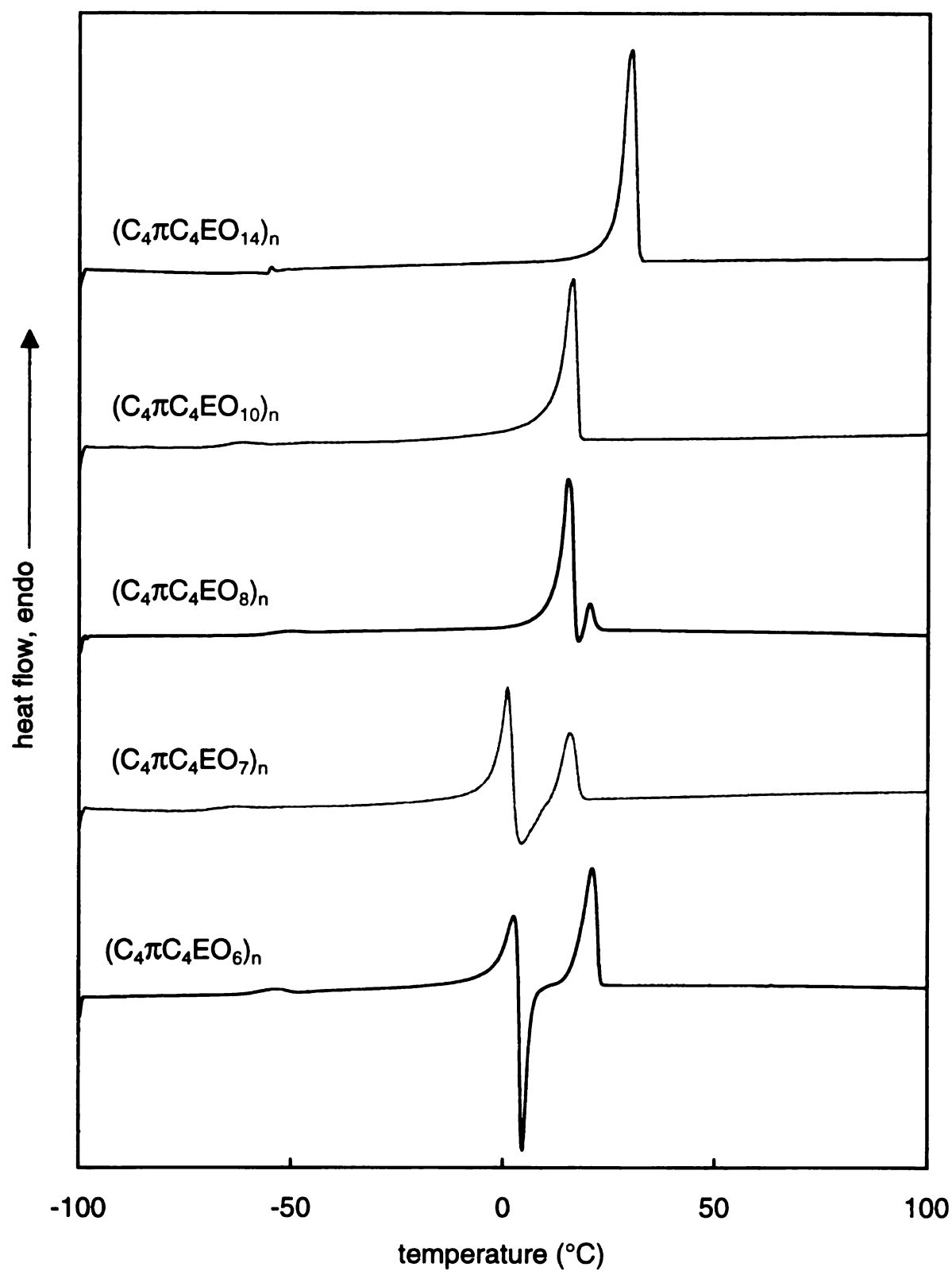


Figure 49. DSC heating scans of polymer $(C_4\pi C_4EO_y)_n$ after flash quenched from the melt.

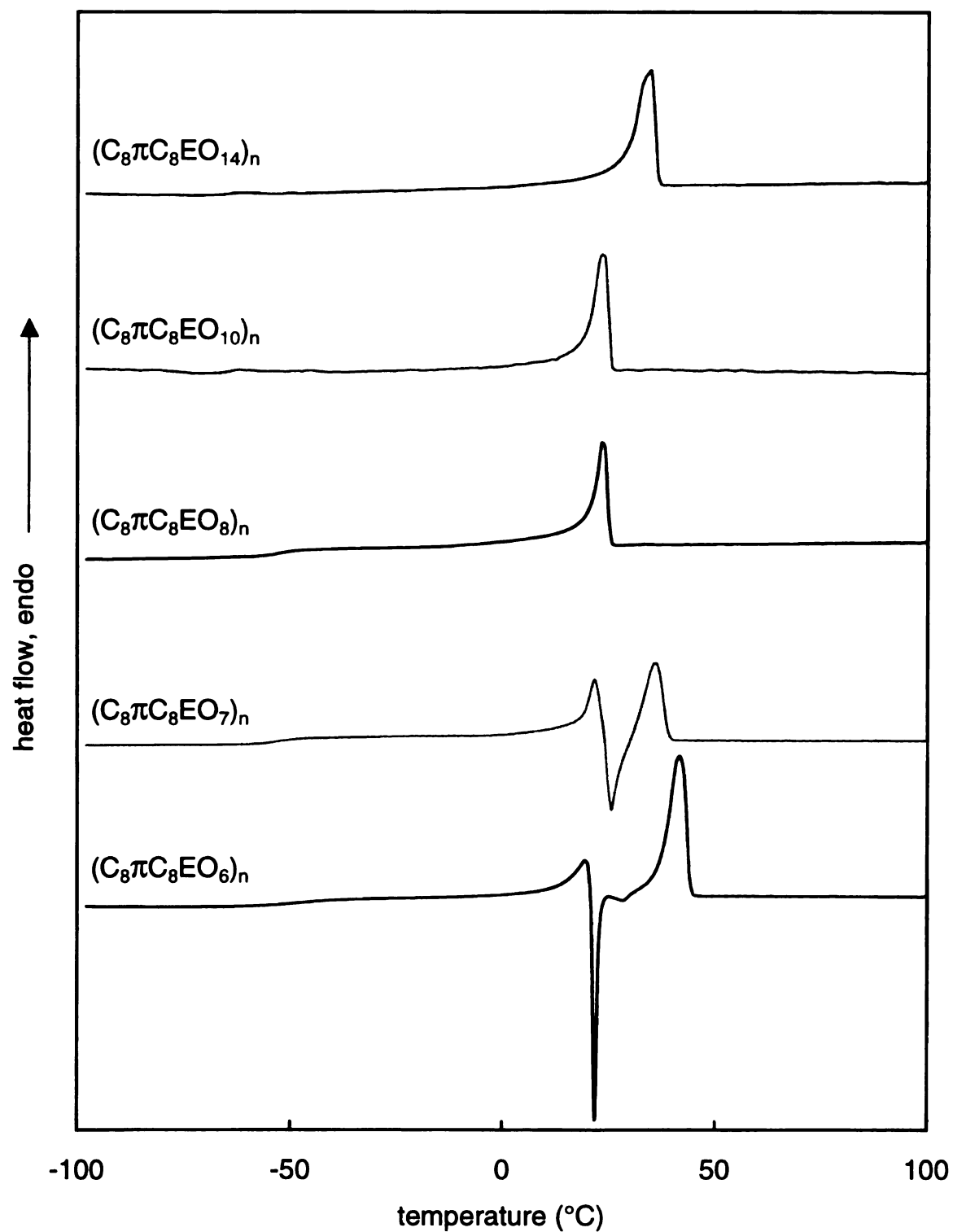


Figure 50. DSC heating scans of polymer $(C_8\pi C_8EO_y)_n$ after flash quenched from the melt.

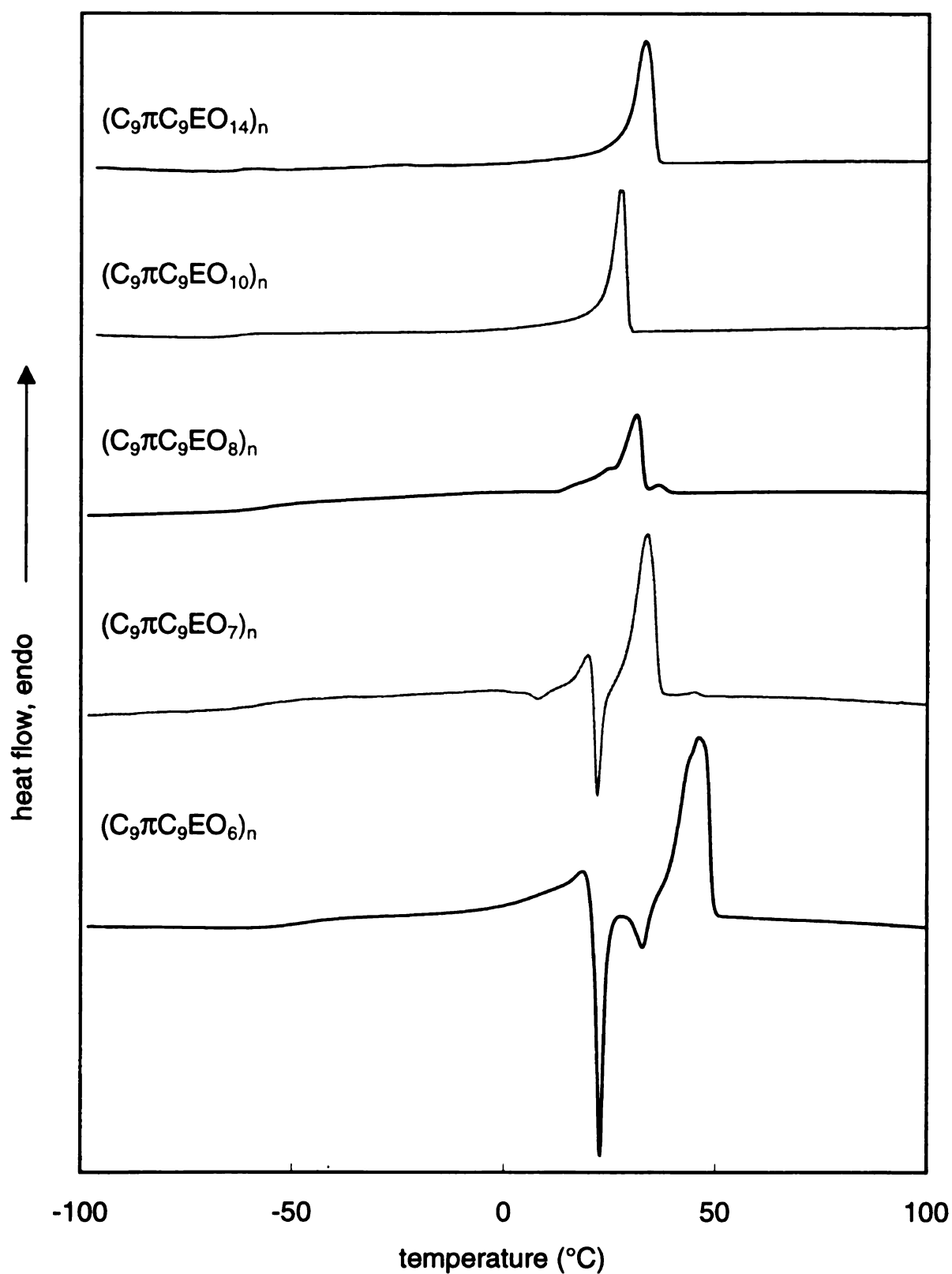


Figure 51. DSC heating scans of polymer $(C_9\pi C_9EO_y)_n$ after flash quenched from the melt.

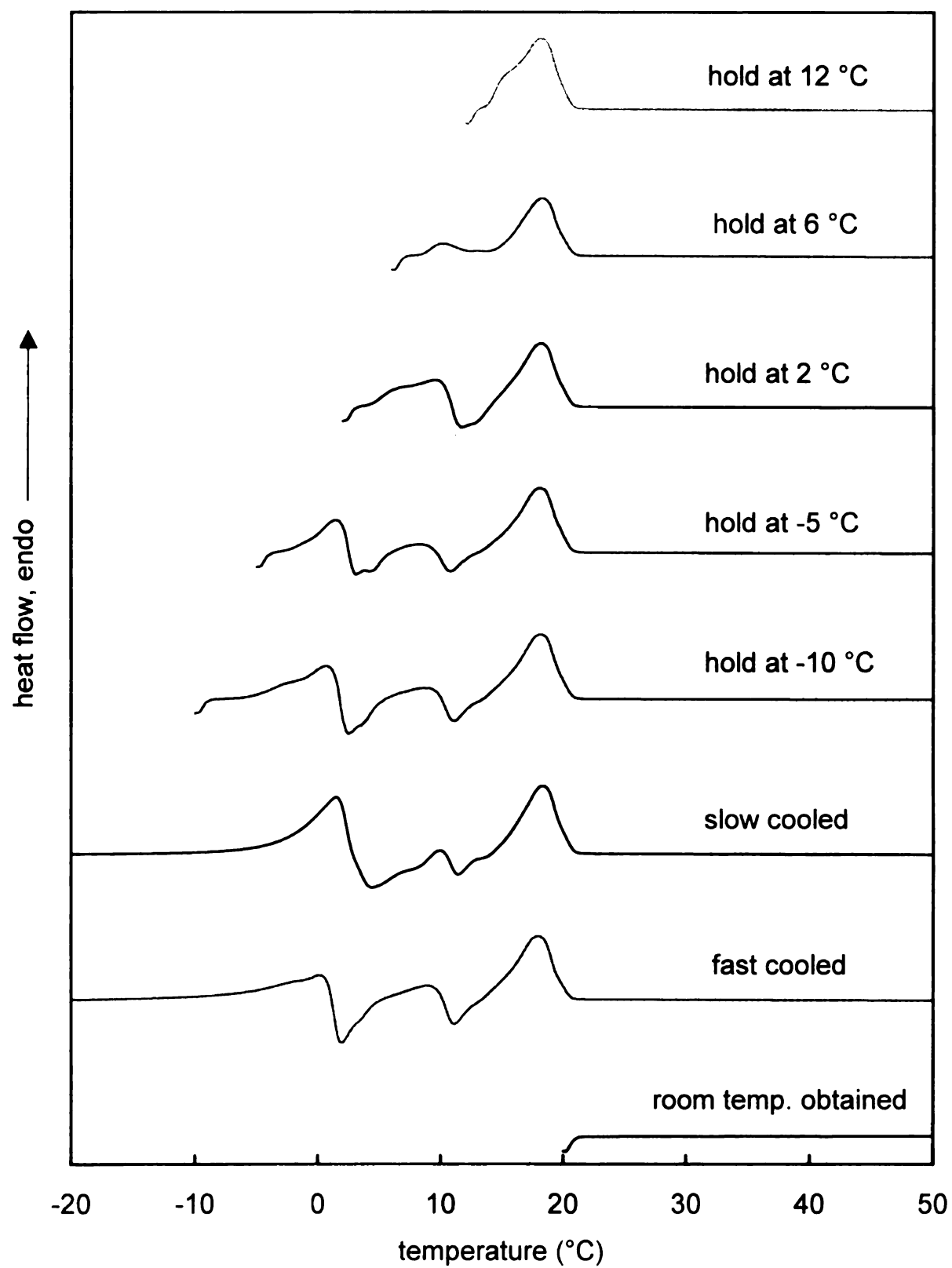


Figure 52. DSC heating scans of polymer $(C_3\pi C_3EO_6)_n$ with different crystallization histories.

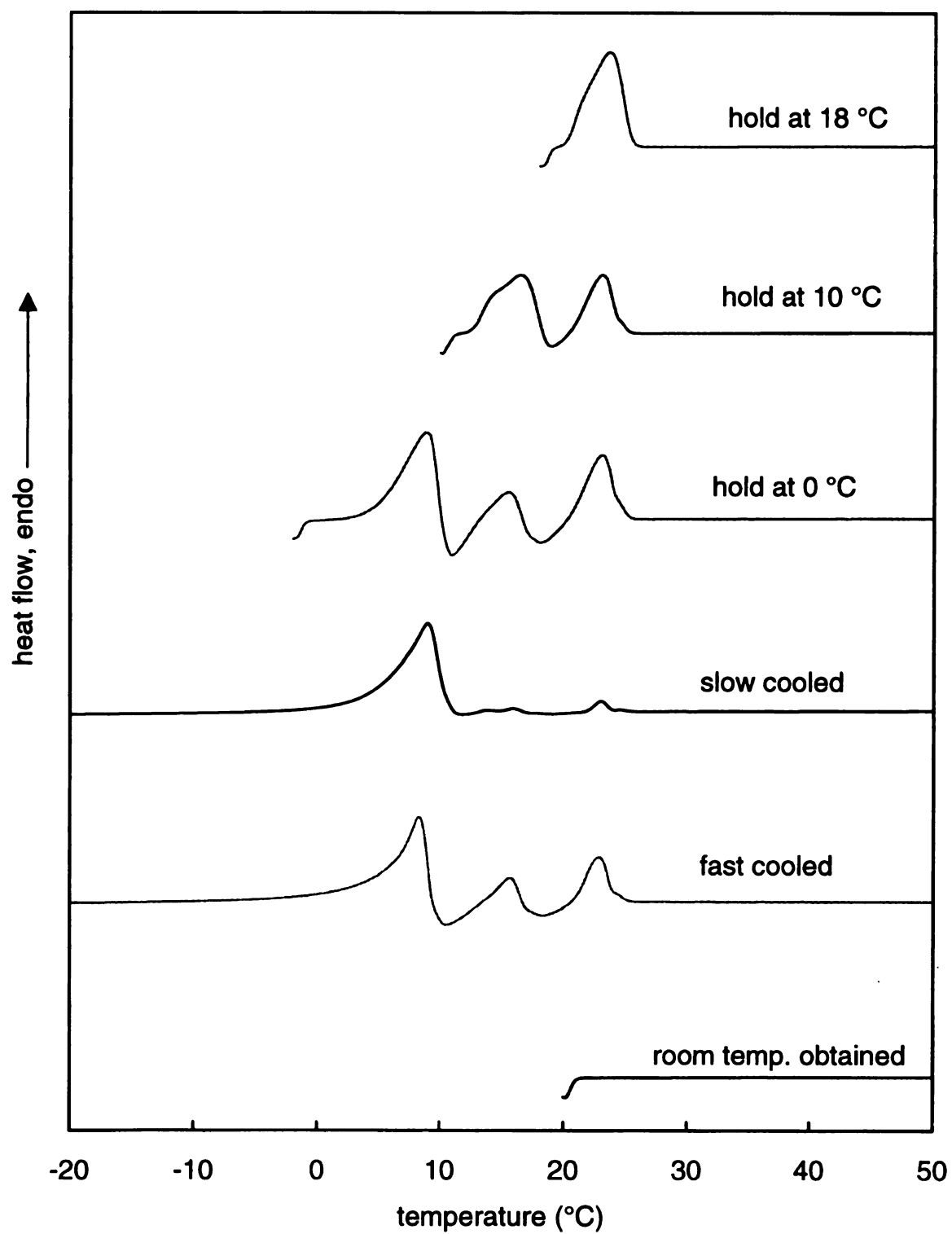


Figure 53. DSC heating scans of polymer $(C_3\pi C_3EO_7)_n$ with different crystallization histories.

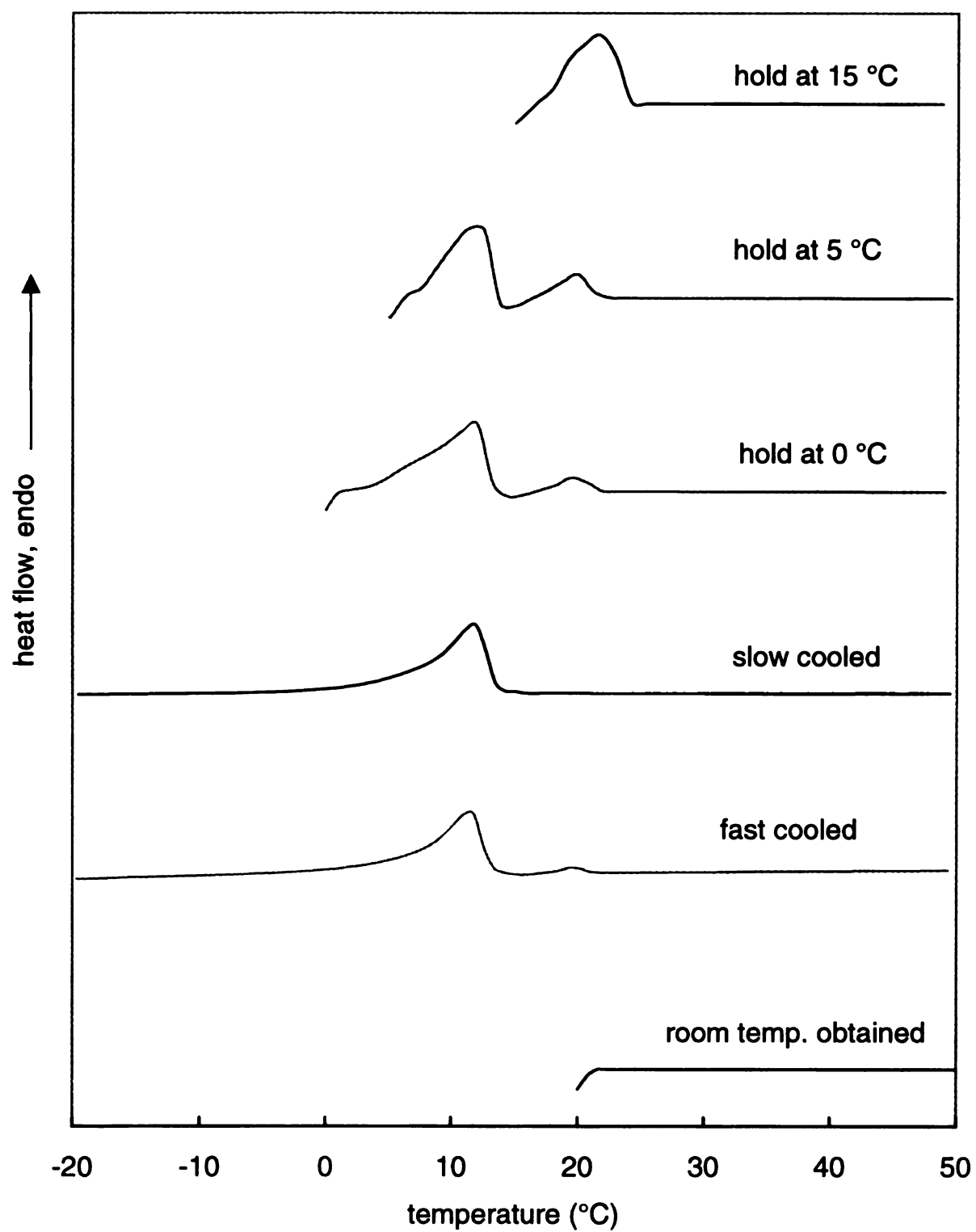


Figure 54. DSC heating scans of polymer $(C_3\pi C_3EO_8)_n$ with different crystallization histories.

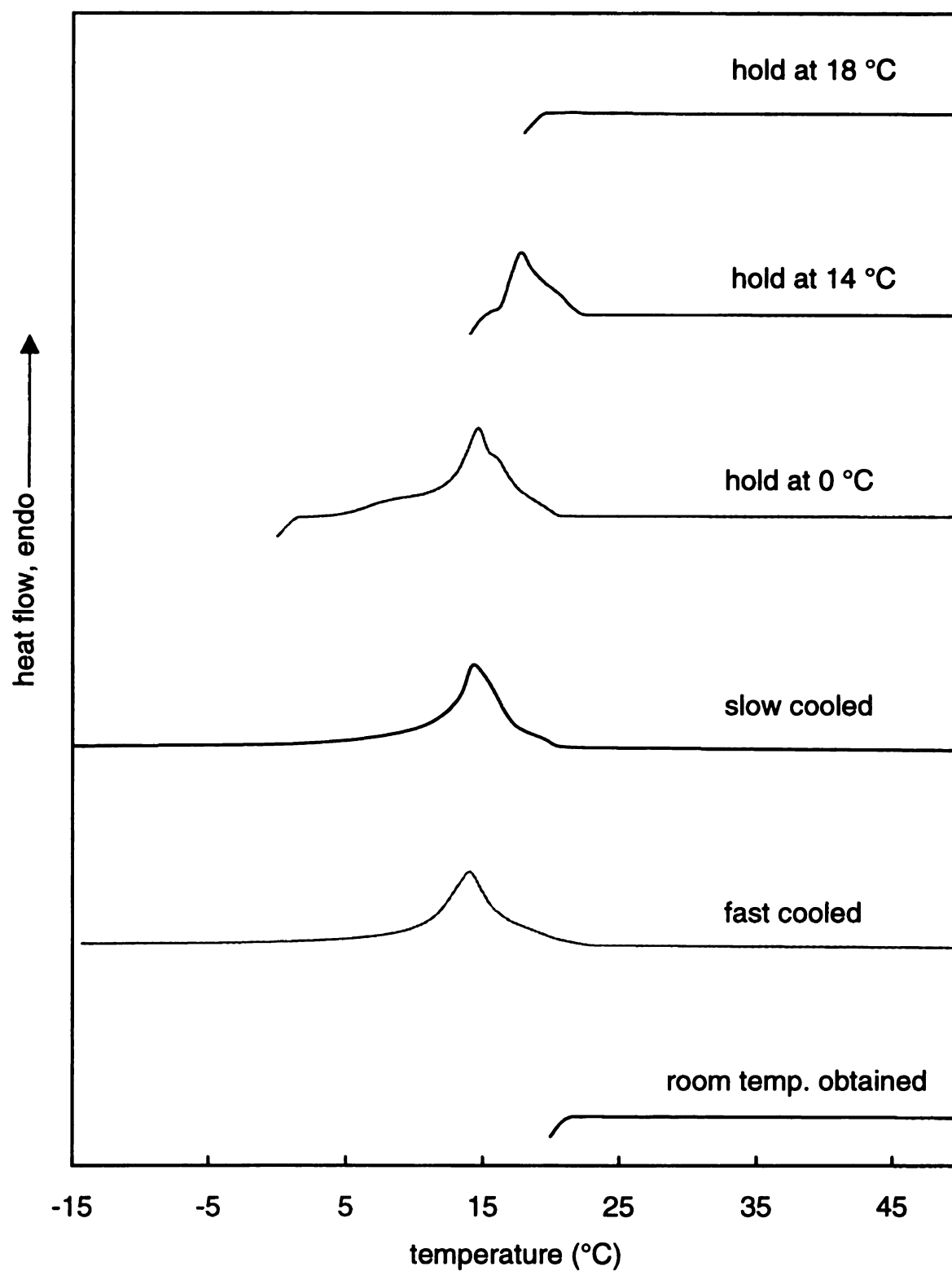


Figure 55. DSC heating scans of polymer $(C_3\pi C_3EO_{10})_n$ with different crystallization histories.

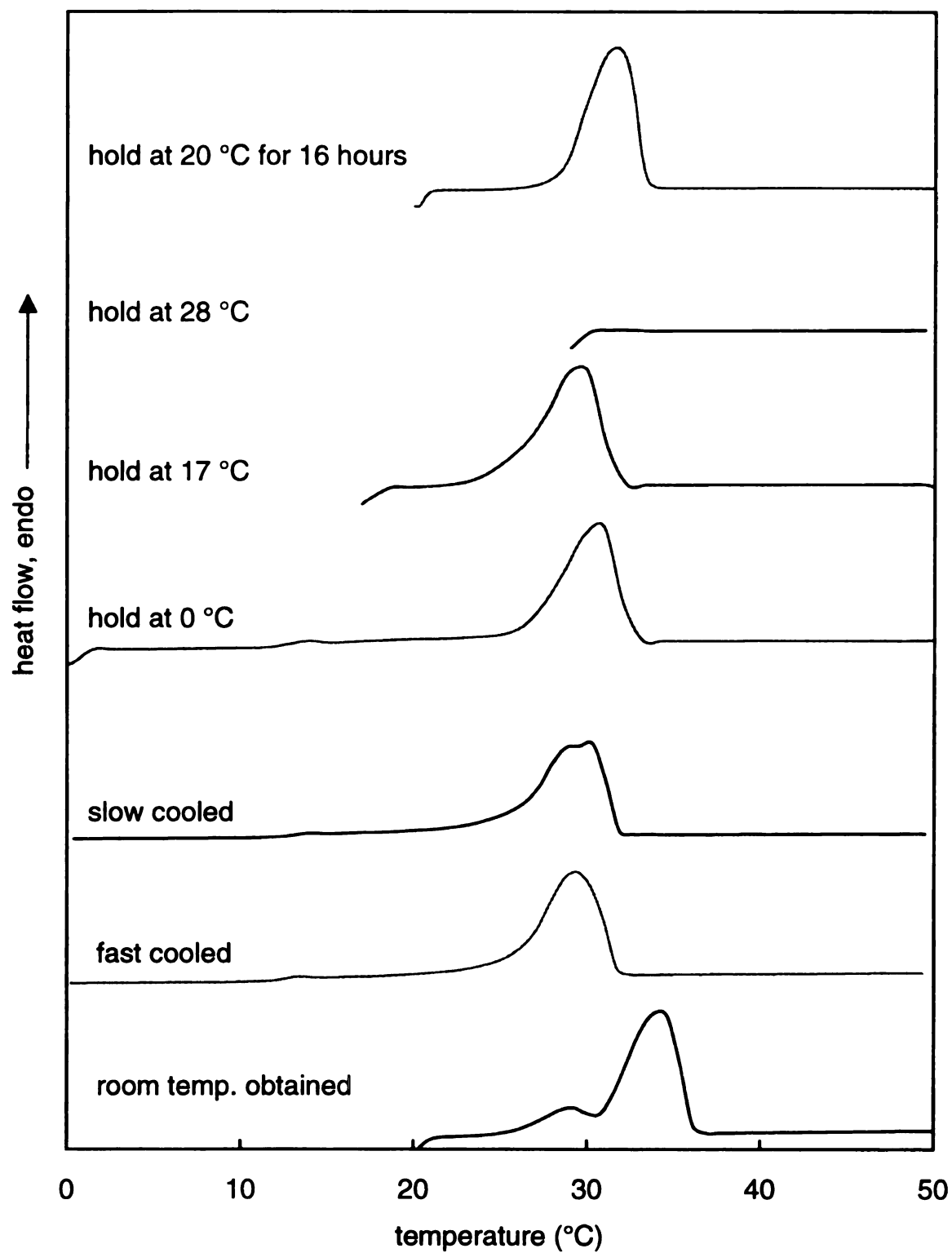


Figure 56. DSC heating scans of polymer $(C_3\pi C_3EO_{14})_n$ with different crystallization histories.

The temperatures of the polymer melting transitions are summarized in **Table 12**. If a sample gives a different T_m transition under different annealing conditions, the highest transition temperature is also listed with a note of the crystallization conditions.

Table 12. Melting transition temperatures (°C) of polymers $(C_x\pi C_xEO_y)_n$.

	y				
x	6	7	8	10	14
3	-3.8, 5.4, 13.7	4.6, 13.4, 20.7	6.6, 18.8	10.0, 16.5 ^a	25.9, 30.7 ^b
4	-2.0, 16.0, 17.3 ^c	-7.5, 8.0, 13.0 ^c	12.9, 18.7, 20.0 ^d	12.7	24.5, 30.6 ^e , 31.9 ^b
8	14.7, 36.7, 40.0 ^b , 42.1 ^f	18.7, 30.8, 31.1 ^b	20.7, 23.2 ^b , 31	19.3, 30.0 ^b	30.7, 31.3 ^b
9	7.3, 33.3, 37.3, 43.4 ^b	14.0, 28.3, 28.7 ^b	20.0, 24.1, 34.4, 36.3 ^b	23.1, 31.1 ^b	28.0, 30.6 ^b , 34.4 ^g

a. annealed at 14 °C for 30 minutes. b. annealed at room temperature for long time. c. annealed at 10 °C for 30 minutes. d. annealed at 17 °C for 30 minutes. e. annealed at 28 °C for 30 minutes. f. annealed at 40 °C for 30 minutes. g. annealed at 20 °C for 30 minutes.

In addition to DSC experiments, we used DMA to further establish the nature of the thermal transitions seen in the DSC scans. Temperature sweep DMA can be used to detect glass transitions, crystallization and melting transitions. It is more sensitive than DSC for observing subtle transitions. The combined information of probe position, storage (E') and loss modulus (E''), and $\tan \delta$ (δ is the phase angle) can give a more complete description of the nature of the transformation. However, the amount of sample

required for DMA is much larger than for DSC and the operation is more complicated. Therefore, DMA experiments were performed only on a few samples. One example is shown in **Figure 57** together with the DSC heating scan for polymer $(C_{40}PEO_3)_n$. The DMA sample was prepared by the same protocol used to obtain the DSC results, flash quenching from 105 °C using liquid nitrogen. The initially amorphous sample was run in a parallel plate geometry at a frequency of 1 Hz. Decreases in the probe position were found at -50 °C and near -5 °C. The first transition correlates to an exothermic transition in the DSC data and an increase in E' , and thus corresponds to the densification of the sample during crystallization. The second transition, near -5 °C, is related to a decrease in E' , an increase in $\tan \delta$, and an endothermic transition in the DSC data. During this transition, the sample softens and the probe eventually penetrates through the sample, an obvious indication of melting.

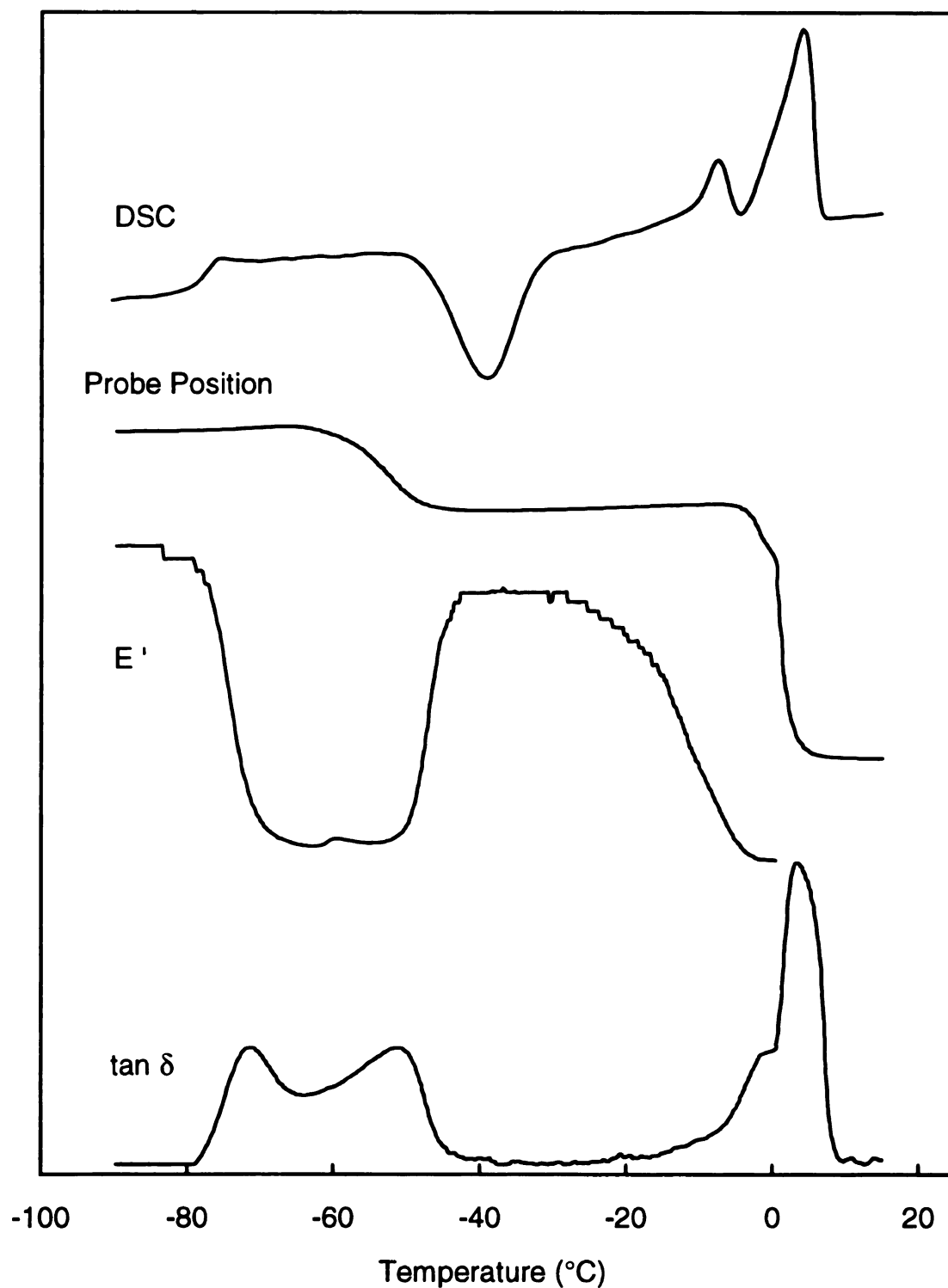


Figure 57. DMA and DSC of polymer $(C_4\pi C_4EO_3)_n$ heating scans. The bottom 3 traces are DMA results for a sample in a parallel plate geometry.

5. XRD of unsaturated polymers

The polymer $(C_9\pi C_9EO_7)_n$ was characterized by XRD experiments. Data for samples crystallized from hexane, methanol and the melt respectively are shown in **Figures 58** (low angles) and **59** (high angles). Since it is hard to obtain well crystallized polymer samples, the XRD scans do not have an ideal signal/noise ratio. However, from low angle XRD one can see that the highest ordered peaks appear almost at the same position, corresponding to a d-spacing approximately 42.4 Å. In the higher angle region, samples crystallized from hexane showed a slight difference from the other two. The peak at 19.5° is absent in the other two samples and the intensity ratios at 22-27° are also different.

An attempt was made to correlate the multiple transitions in DSC heating scans to polymer structure. XRD data were taken for polymer $(C_x\pi C_xEO_y)_n$ at different temperatures. The polymer sample was first melt-quenched to liquid nitrogen temperature, and then heated to temperatures just below or past the transition point indicated in the DSC scan (**Figure 60**). XRD were taken at those temperatures and their profiles are shown in **Figure 61**. At -80 °C, below the polymer's T_g , the sample appeared to be amorphous and only a halo at around 20° was visible. As the temperature increased to above T_g , where chain segments were able to move and rearrange into a more ordered structure, diffraction peaks start to emerge. Peaks at low angles were barely seen until -15 °C. At that temperature, after the second crystallization exotherm, a broad diffraction at around 3.7° was seen that persisted until the sample was melted. Presumably an ordered structure with a long spacing formed. In the high angle region, a major peak at 22.8° first emerged with another smaller peak at 19.4° at just above T_g . As

the peak at 19.4° became sharper and better defined, it also shifted slightly to a lower angle. The sample crystallinity was finally lost as the temperature increased to above the melting points. All peaks disappeared except for the halo around 20° . Interestingly, its peak position was shifted to a lower angle than the original halo position. Partial analysis of the results appears in the Discussion section.

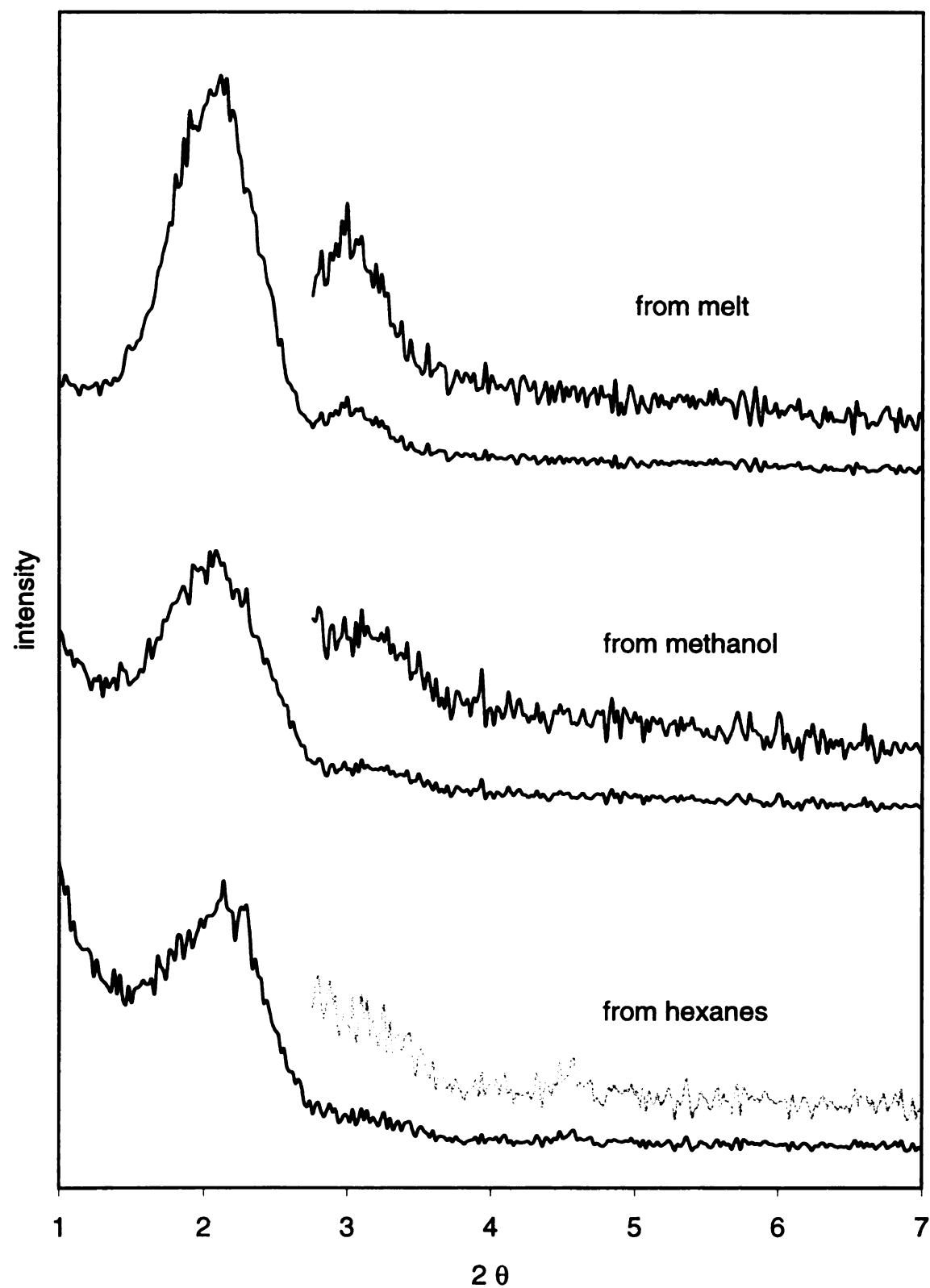


Figure 58. Low angle XRD of polymer $(C_9\pi C_9EO_7)_n$ sample prepared using different crystallization conditions

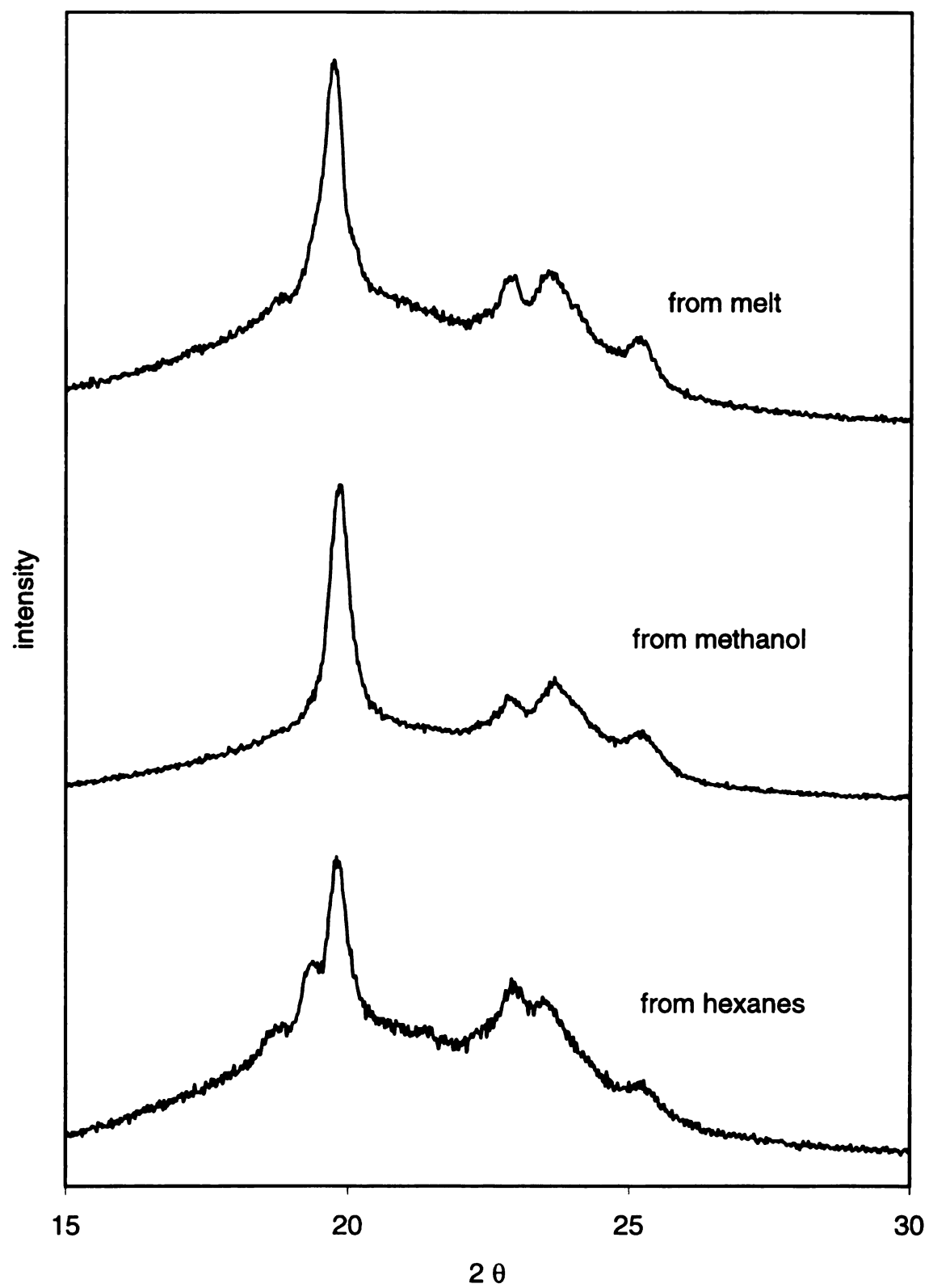


Figure 59. Wide angle XRD of polymer $(C_9\pi C_9EO_7)_n$ samples prepared using different crystallization conditions

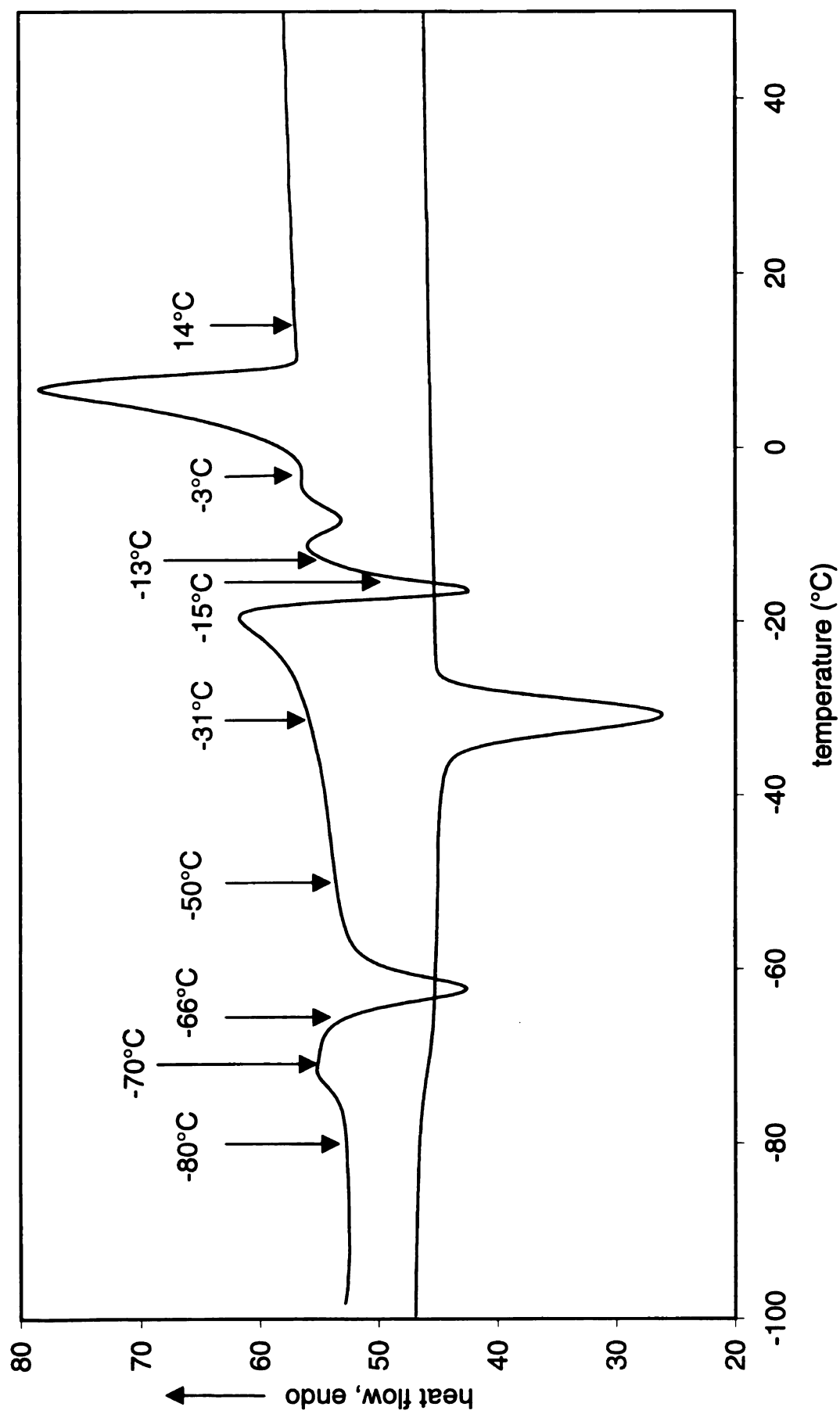


Figure 60. DSC of polymer $(C_4\pi C_4EO_5)_n$ heating and cooling at 10 °C/min after flash quenched from the melt. Arrows indicate the temperatures where XRD experiments were performed.

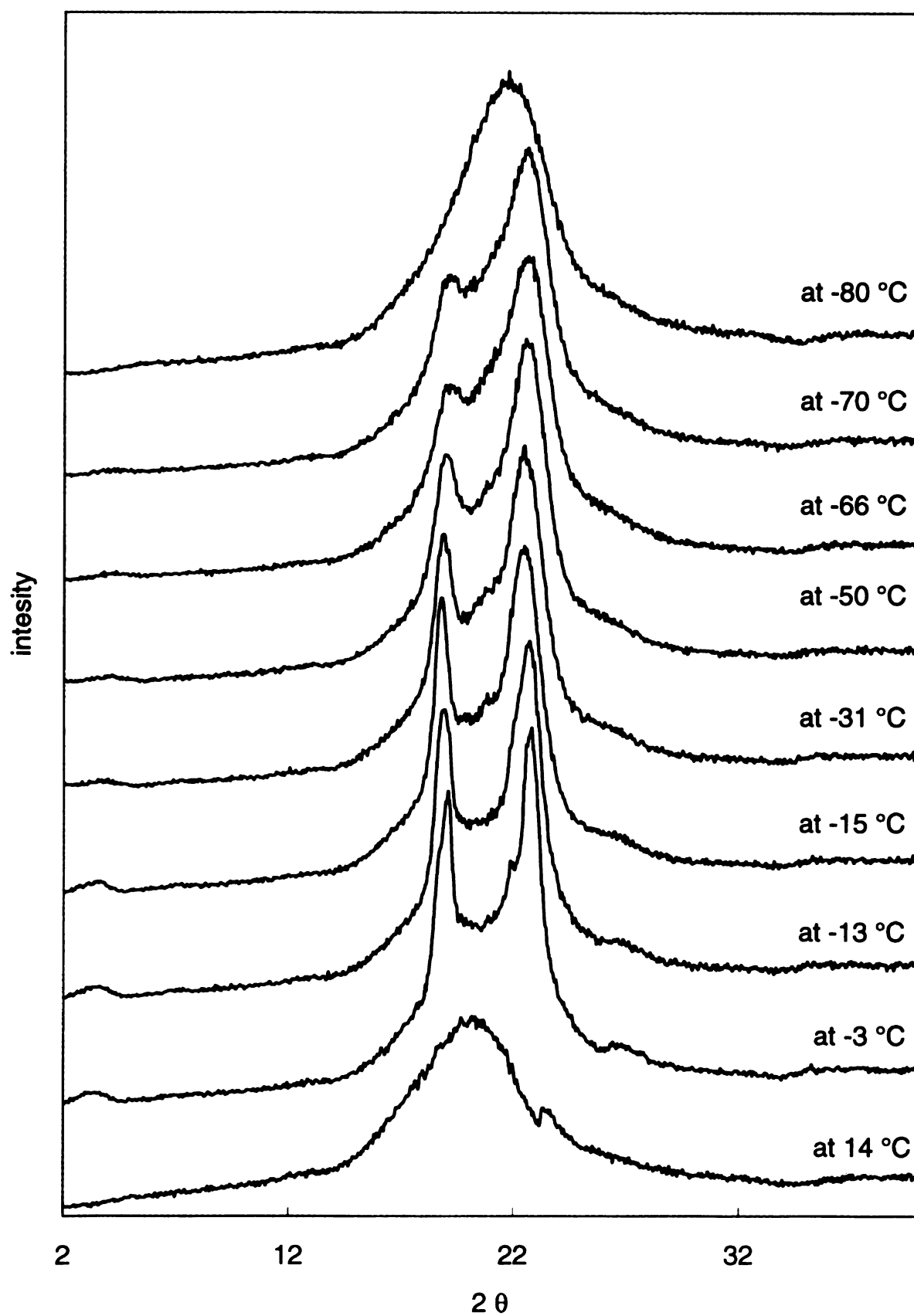


Figure 61. XRD of polymer $(C_4\pi C_4EO_5)_n$ as a function of temperature

IV. Properties of saturated (AB)_n polymers (C_xEO_y)_n

1. Physical properties

The molecular weights and polydispersities of the hydrogenated polymers are given in **Table 13** together with their corresponding unsaturated precursors. As can be observed in the table, their molecular weights all dropped after hydrogenation. The saturated polymers are white, presumably because most of the residue catalyst was removed during the reaction and the work-up procedure. Since the polarity of the saturated polymers is not significantly altered by hydrogenation, they exhibit the same solubility trends seen for the unsaturated polymers. Both saturated and unsaturated polymer can absorb moisture, therefore they must be kept in a desiccator.

Table 13. Comparison of the molecular weights and polydispersities of the hydrogenated polymers $(C_{2x+2}EO_y)_n$ and their unsaturated precursors $(C_x\pi C_xEO_y)_n$.

Unsaturated polymer			Saturated polymer			
polymer	M_n	PDI	polymer	M_n	PDI	Yield
$(C_4\pi C_4EO_6)_n$	48,800	1.84	$(C_{10}EO_6)_n$	11,800	1.64	97%
$(C_4\pi C_4EO_7)_n$	25,100	2.27	$(C_{10}EO_7)_n$	15,800	1.85	98%
$(C_4\pi C_4EO_8)_n$	19,400	1.41	$(C_{10}EO_8)_n$	13,200	1.98	98%
$(C_4\pi C_4EO_{10})_n$	28,300	2.01	$(C_{10}EO_{10})_n$	24,100	2.41	99%
$(C_4\pi C_4EO_{14})_n$	13,200	1.81	$(C_{10}EO_{14})_n$	8,500	1.58	99%
$(C_9\pi C_9EO_7)_n$	11,800	1.44	$(C_{20}EO_7)_n$	9,500	1.45	99%

2. Morphology of saturated polymers

All of the saturated polymers are crystalline at room temperature. Crystals obtained by crystallization at room temperature for at least 3 weeks were viewed using cross-polarized optical microscopy.

Shown in **Figure 62** are crystals of $(C_{10}EO_6)_n$ and $(C_{10}EO_7)_n$ viewed under polarized light. Crystals from these two samples are banded spherulites, but unlike the unsaturated polymers, the bandwidths are not uniform for all spherulites. In addition, the bands were not always concentric. For example, in the $(C_{10}EO_6)_n$ sample, the bandwidth

on the front spherulite is about half of that of the background spherulite. Furthermore, spherulite bandwidths can increase with annealing time (at room temperature). This can be clearly seen in **Figure 63**, for a crystalline sample of polymer $(C_{10}EO_7)_n$. Crystals originally formed at room temperature have mainly small bands like that in the lower middle section of the picture. After being stored for a while, they gradually grew into large spherulites with larger bandwidths. The reasons behind this phenomenon needs further study. One possibility could be unfolding of polymer chains to form more extended chains, which results in lamellar thickening.

The remaining micrographs shown in **Figure 64** are for polymers $(C_{10}EO_8)_n$, $(C_{10}EO_{10})_n$, $(C_{10}EO_{14})_n$ and $(C_{20}EO_7)_n$. These crystals were ordinary spherulites except for $(C_{10}EO_{10})_n$, whose spherulites show obvious light extinction at the center. The crystals that constructing the spherulites were also more sheaf-like comparing to the other crystalline samples.

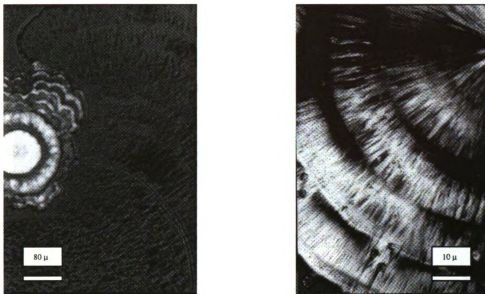


Figure 62. Micrographs of polymers $(C_{10}EO_6)_n$ (left) and $(C_{10}EO_7)_n$ (right) under cross-polarized light

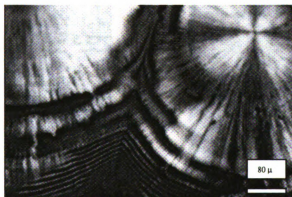


Figure 63. Micrograph of polymer $(C_{10}EO_7)_n$ under cross-polarized light showing different band widths.

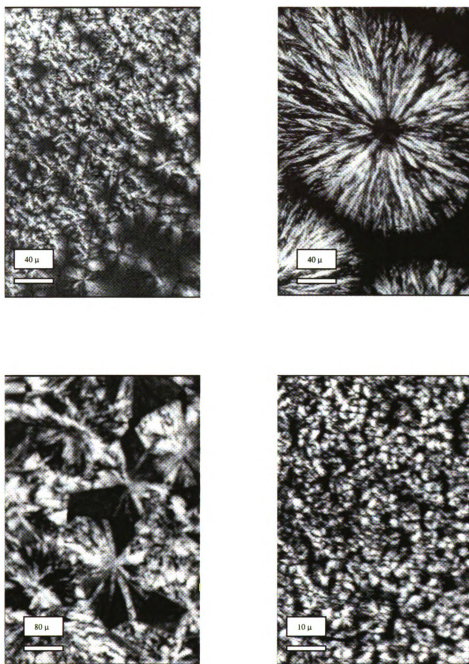


Figure 64. Micrographs of polymers $(C_{10}EO_8)_n$ (upper left), $(C_{10}EO_{10})_n$ (upper right), $(C_{10}EO_{14})_n$ (lower left), and $(C_{20}EO_7)_n$ (lower right) under cross-polarized light.

3. Thermal behavior of the saturated polymers

The saturated polymers were also analyzed by DSC. The sample preparation and experiment methods were the same as for the unsaturated polymers. Shown in **Figure 65** are the DSC heating scans taken after flash quenching polymers $(C_{10}EO_y)_n$ where $y = 6, 7, 8, 10$ and 14 respectively. All of the polymers show T_g s at low temperature. Except for polymer $(C_{10}EO_{14})_n$, which showed only one endotherm, all of the polymers show a melting-crystallization-melting sequence. When the ethylene oxide segments become longer, the low temperature melting transition becomes more prominent for polymers with $y = 7, 8$ and 10 , indicating that the low melting structures favor long ethylene oxide segments. The T_g s and melting transition temperatures for samples crystallized after quenching and for samples annealed at room temperature are shown in **Table 14**.

In order to study the effects of melt crystallization conditions on crystal formation, all of the saturated polymers were annealed and their DSC scans were taken in the same way as for the unsaturated polymers. **Figures 66 to 70** show the DSC heating scans for polymers $(C_{10}EO_y)_n$ where $y = 6, 7, 8, 10$ and 14 respectively. For all saturated polymers, samples stored at room temperature have the highest melting points among all the crystallization histories. For polymer $(C_{10}EO_6)_n$ (**Figure 66**), the DSC traces looks similar for both quenched and slow cooled samples. However, annealing the quenched sample at 3°C shifted the lower melting peak to an even lower temperature, which appears abnormal at first glance. Moreover, similar phenomena were observed for polymer $(C_{10}EO_7)_n$ (**Figure 67**). The DSC heating trace taken after slow cooling shows 3 endotherms but only 2 after quenching. After annealing at 0°C , the second endotherm seen in the DSC scan of the slow cooled sample disappeared while the first endotherm

grew. This phenomenon will be discussed later. When crystallized and annealed at room temperature, polymer $(C_{10}EO_{14})_n$ (**Figure 70**) showed two overlapping endotherms indicating that two kinds of structures exist at room temperature. Flash quenching and slow cooling both gave a lower melting crystal than the two crystals formed after long term room temperature annealing. Annealing at 20 °C for 30 minutes increased the melting point, and annealing at 30 °C for 30 minutes gave a mixture of crystals, those obtained from short time annealing at 20 °C and one of the low melting crystalline forms seen for long term room temperature annealing. Finally, annealing at 33 °C gave mainly the highest melting crystal. The thermal behavior of polymers $(C_{10}EO_8)_n$ and $(C_{10}EO_{10})_n$ was not surprising.

Table 14. T_g and T_m s of saturated polymers. (°C)

Polymer	T_g	T_m
$(C_{10}EO_6)_n$	-78.7	11.2, 21.8, 22.6 ^a
$(C_{10}EO_7)_n$	-63.1	6.8, 22.2, 25.0 ^a
$(C_{10}EO_8)_n$	-64.9	2.5, 19.6, 23.1 ^a
$(C_{10}EO_{10})_n$	-65.9	14.6, 25.3, 28.4 ^a
$(C_{10}EO_{14})_n$	-63.7	24.3, 26.6, 37.4 ^a
$(C_{20}EO_7)_n$	-52.9	11.1, 28.9, 44.7, 45.7 ^a

a. annealed at room temperature for more than 2 weeks

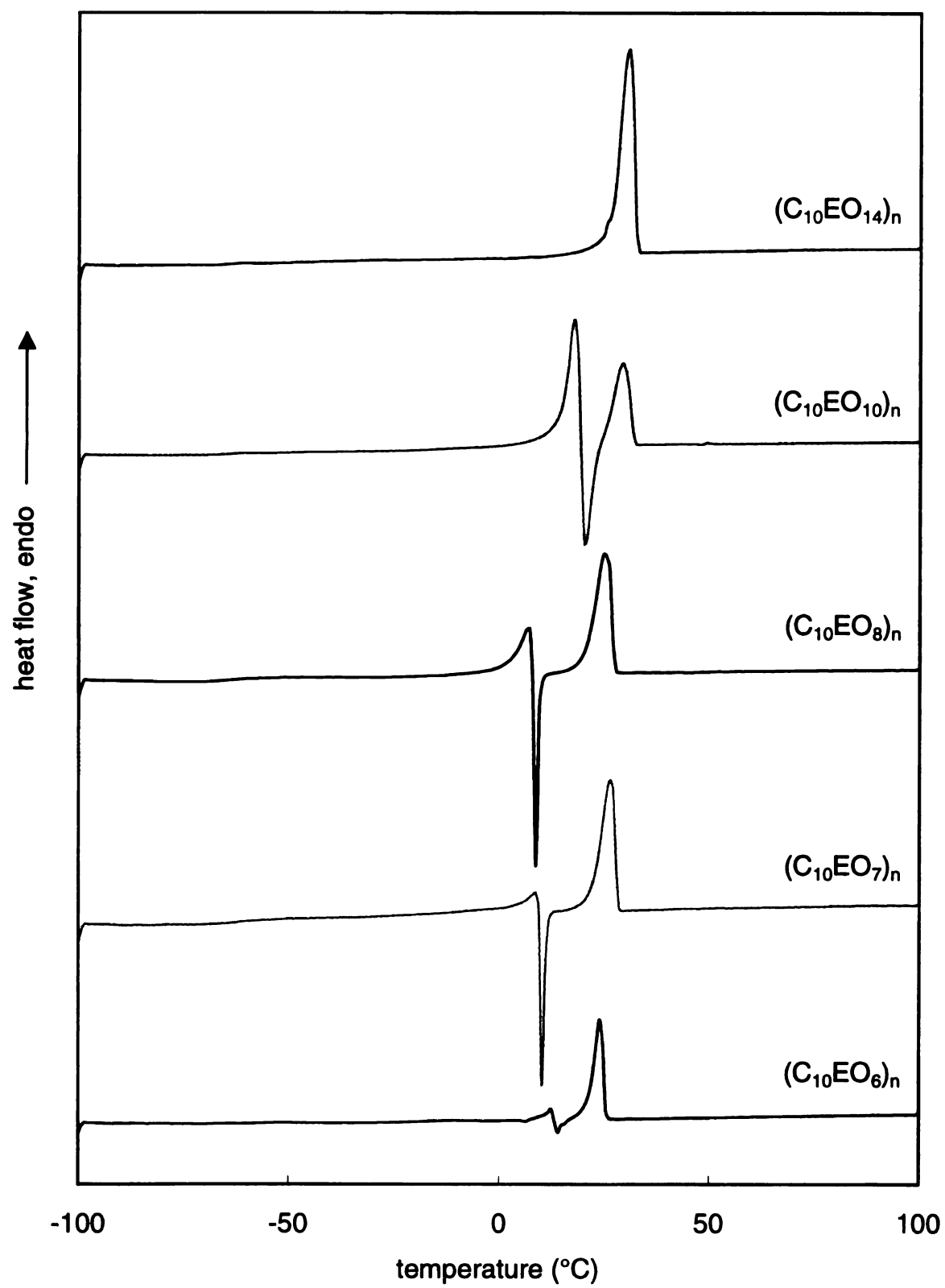


Figure 65. DSC heating scans of polymers $(C_{10}EO_y)_n$ after flash quenching.

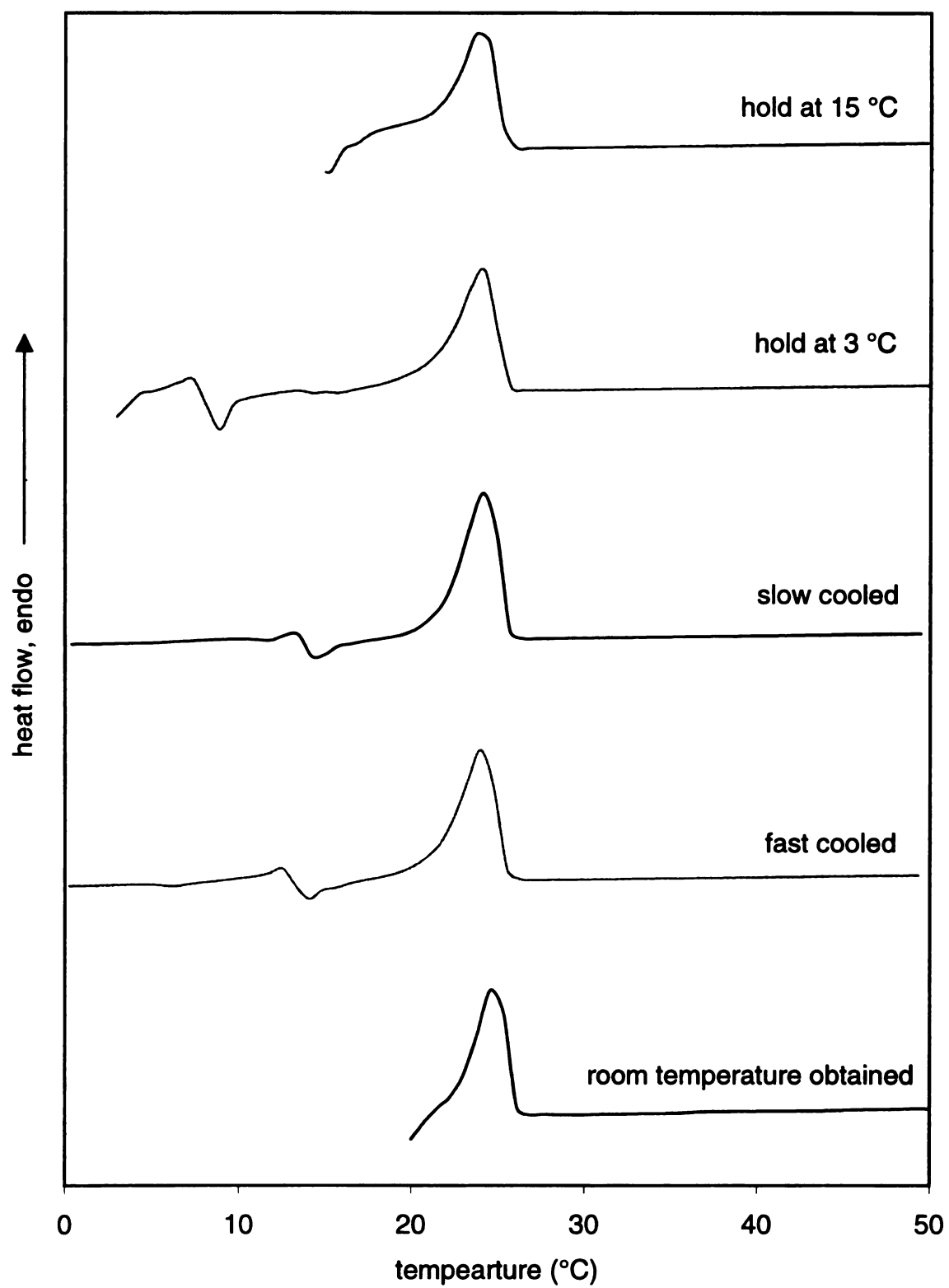


Figure 66. DSC heating scans of polymer $(C_{10}EO_6)_n$ with different crystallization histories.

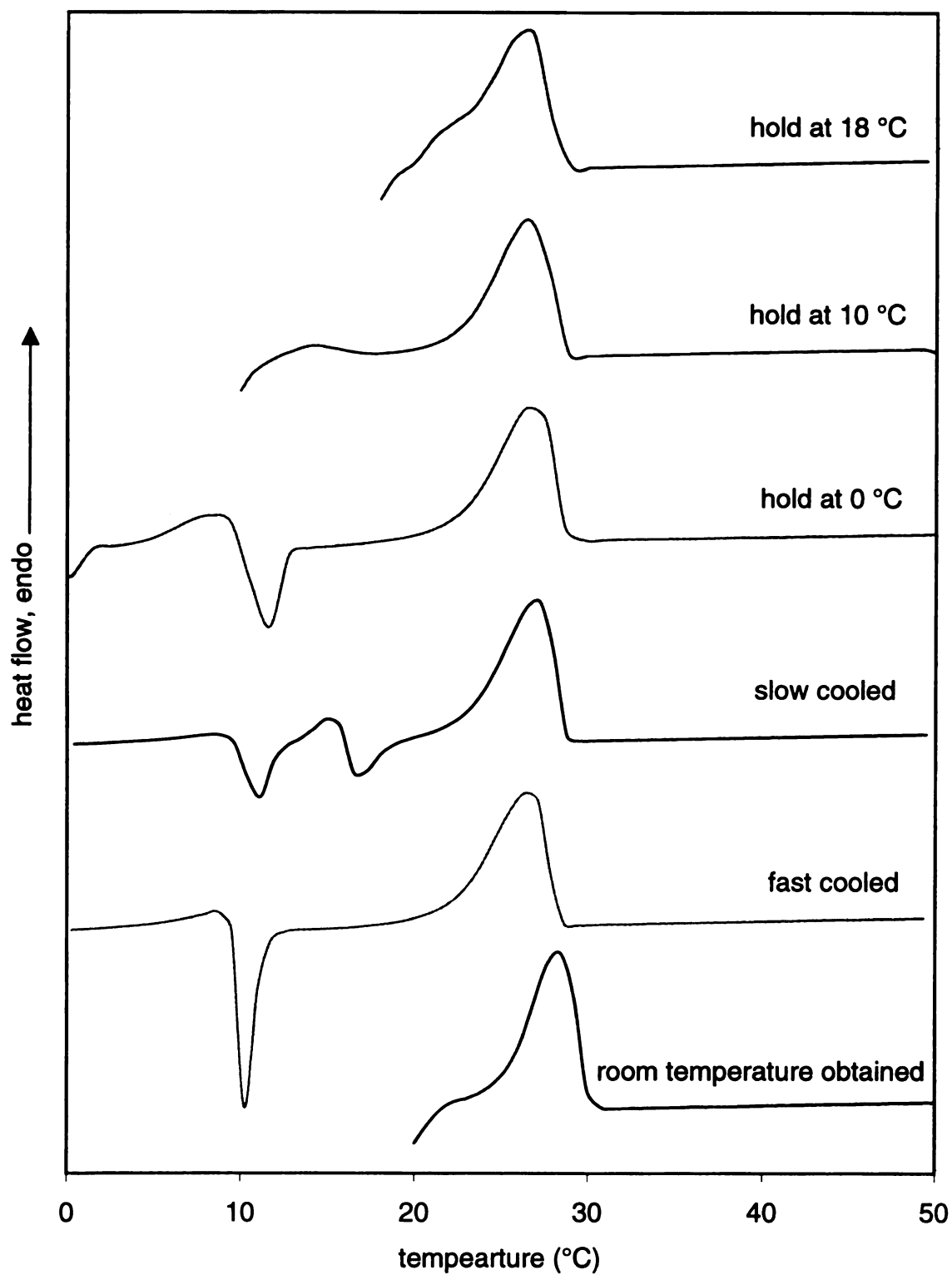


Figure 67. DSC heating scans of polymer $(C_{10}EO_7)_n$ with different crystallization histories.

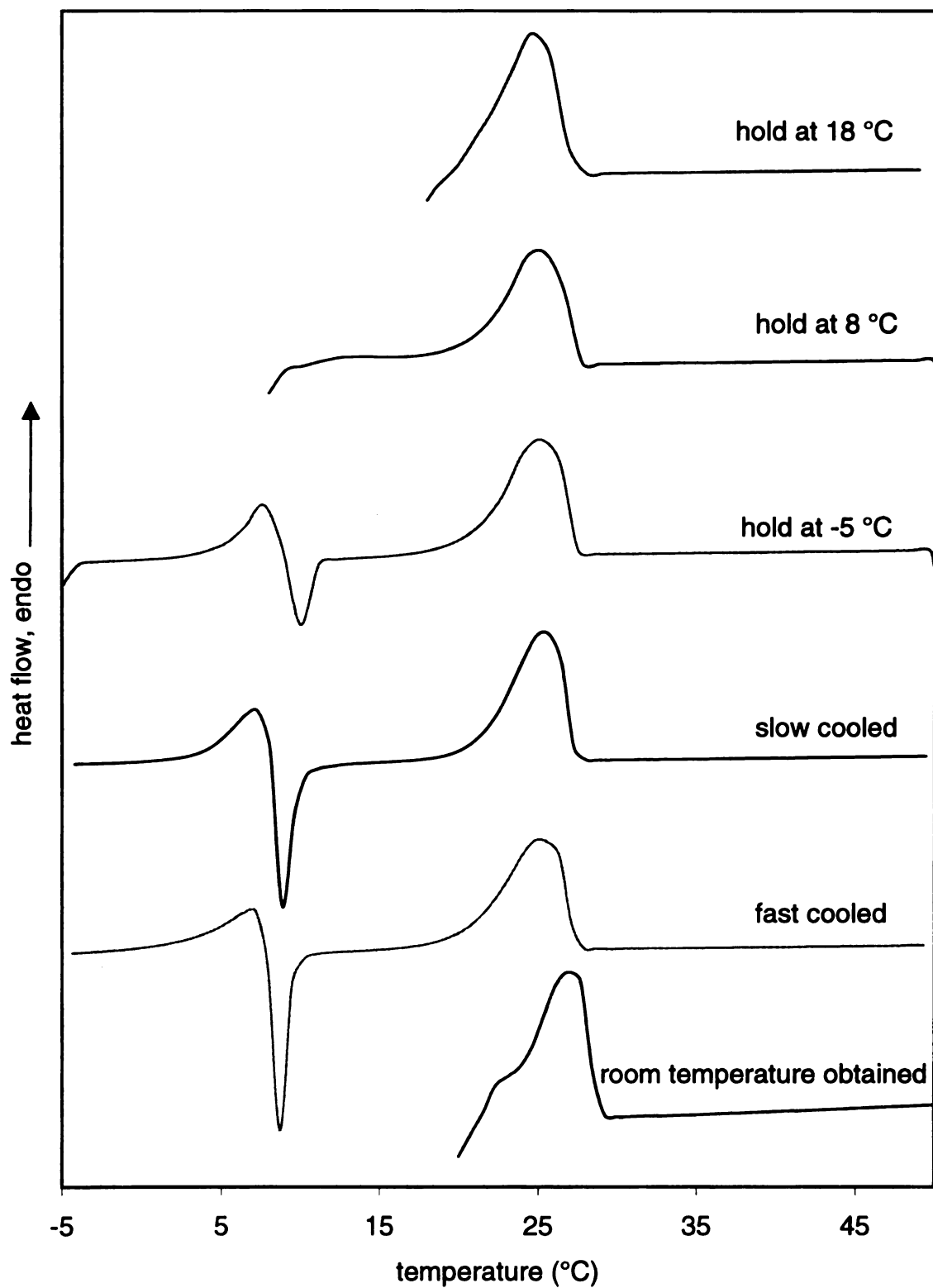


Figure 68. DSC heating scans of polymer $(C_{10}EO_8)_n$ with different crystallization histories.

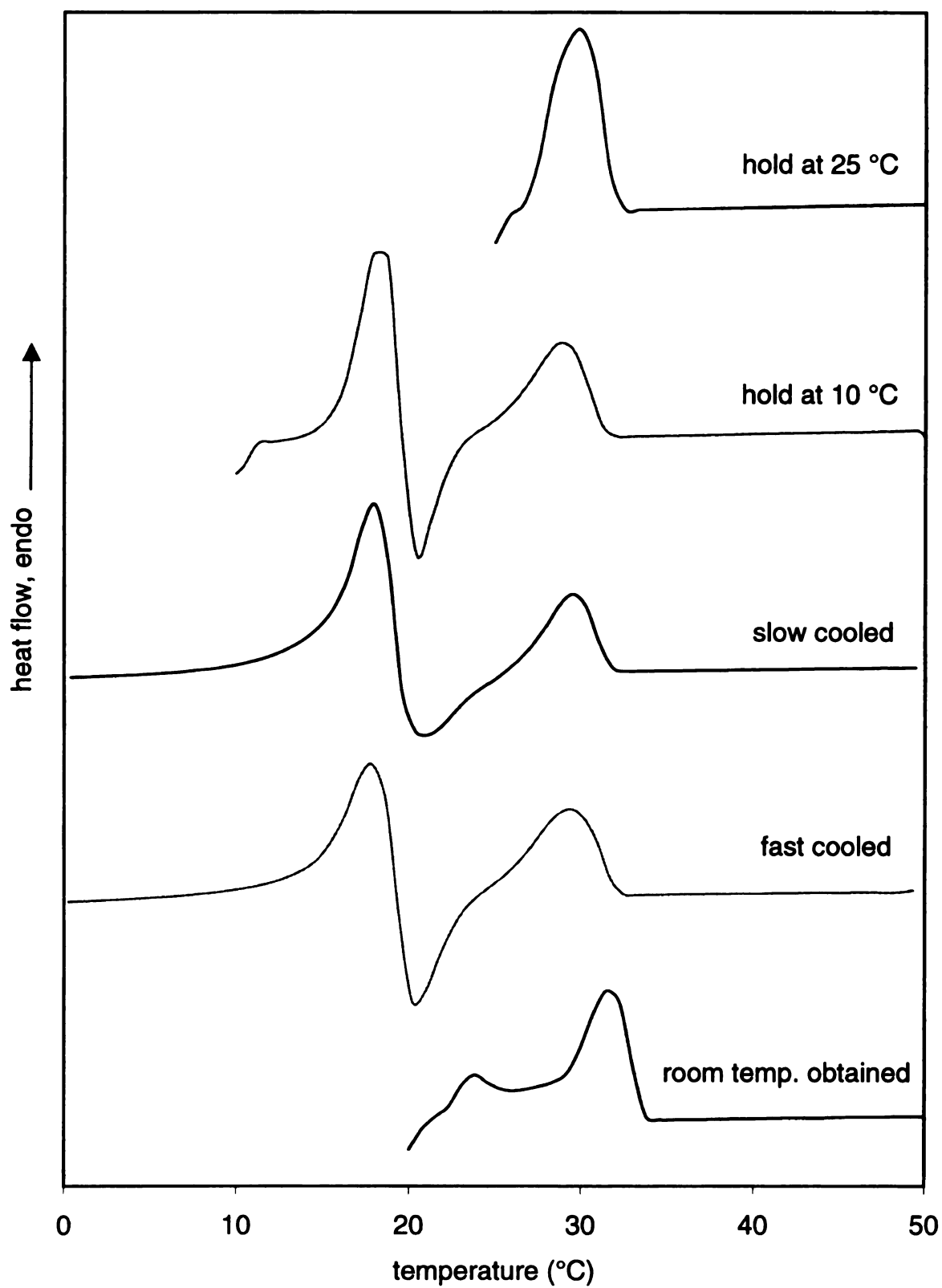


Figure 69. DSC heating scans of polymer $(C_{10}EO_{10})_n$ with different crystallization histories.

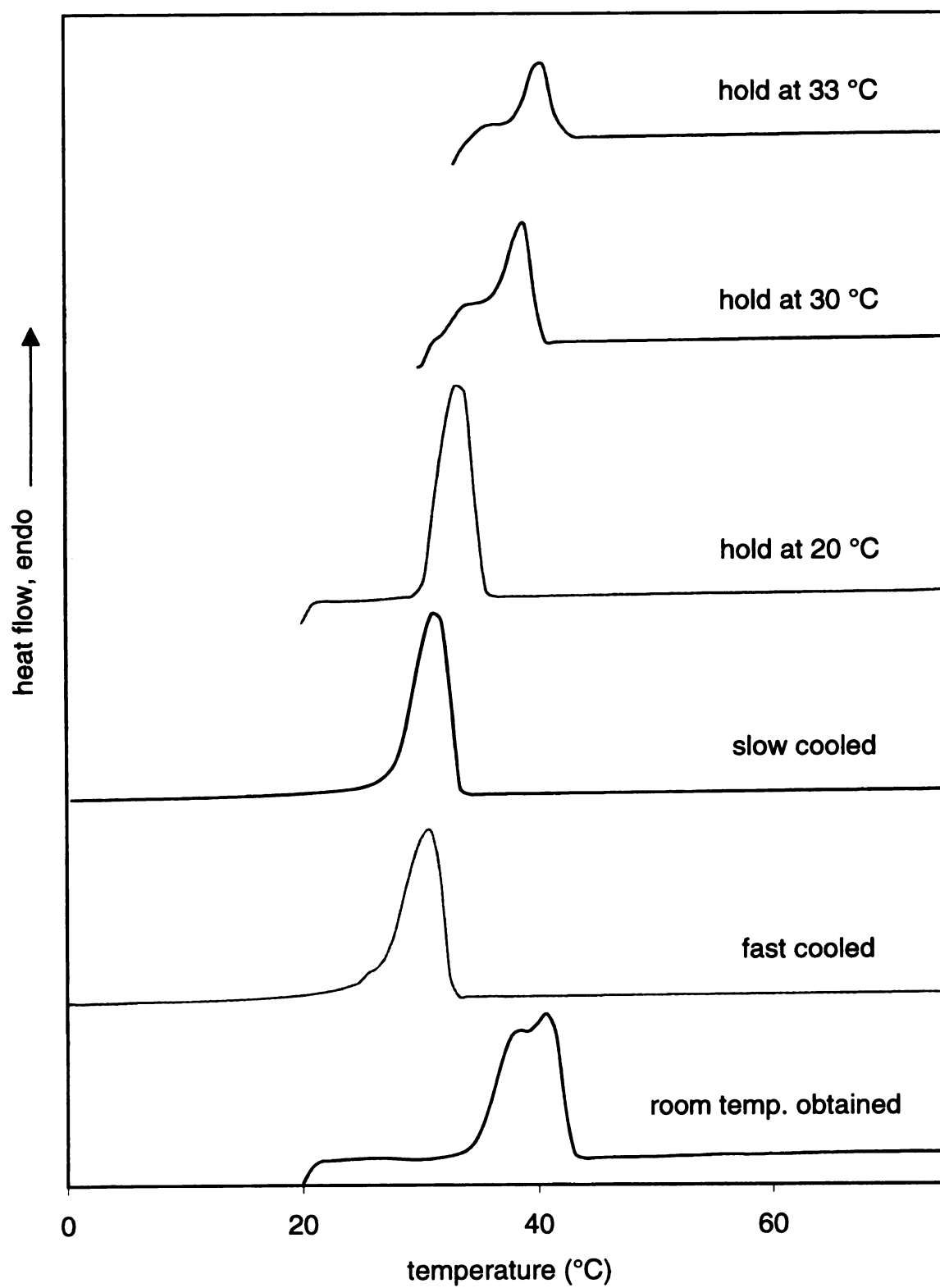


Figure 70. DSC heating scans of polymer $(C_{10}EO_{14})_n$ with different crystallization histories.

4. Spectroscopic characterization

The most prominent change for a saturated polymer compared to its precursor is the removal of the double bonds. This was clearly seen from spectroscopic characterization. For example, in ^1H NMR, the peaks at 5.4 ppm, which correspond to the internal double bonds, gradually diminish during the hydrogenation process. Other than this change and some minor shifts of the protons on the carbons adjacent to the original sp^2 carbons, the spectrum looks similar to that of the unsaturated polymer. Disappearance of bands that correspond to double bond vibrations were also sighted in IR and Raman spectra.

IR spectroscopy was again used to study the polymer conformations. Polymer $(\text{C}_{20}\text{EO}_7)_n$ was crystallized from hexanes and methanol, as previously done for the $\text{C}_{14}\text{EO}_7\text{C}_{14}$ sample. As shown in **Figure 71** (only the low frequency region is shown), the spectra are quite different which indicates that different conformations or crystal packing exist in the polymer chains as crystallized from different solutions. The details will be discussed later.

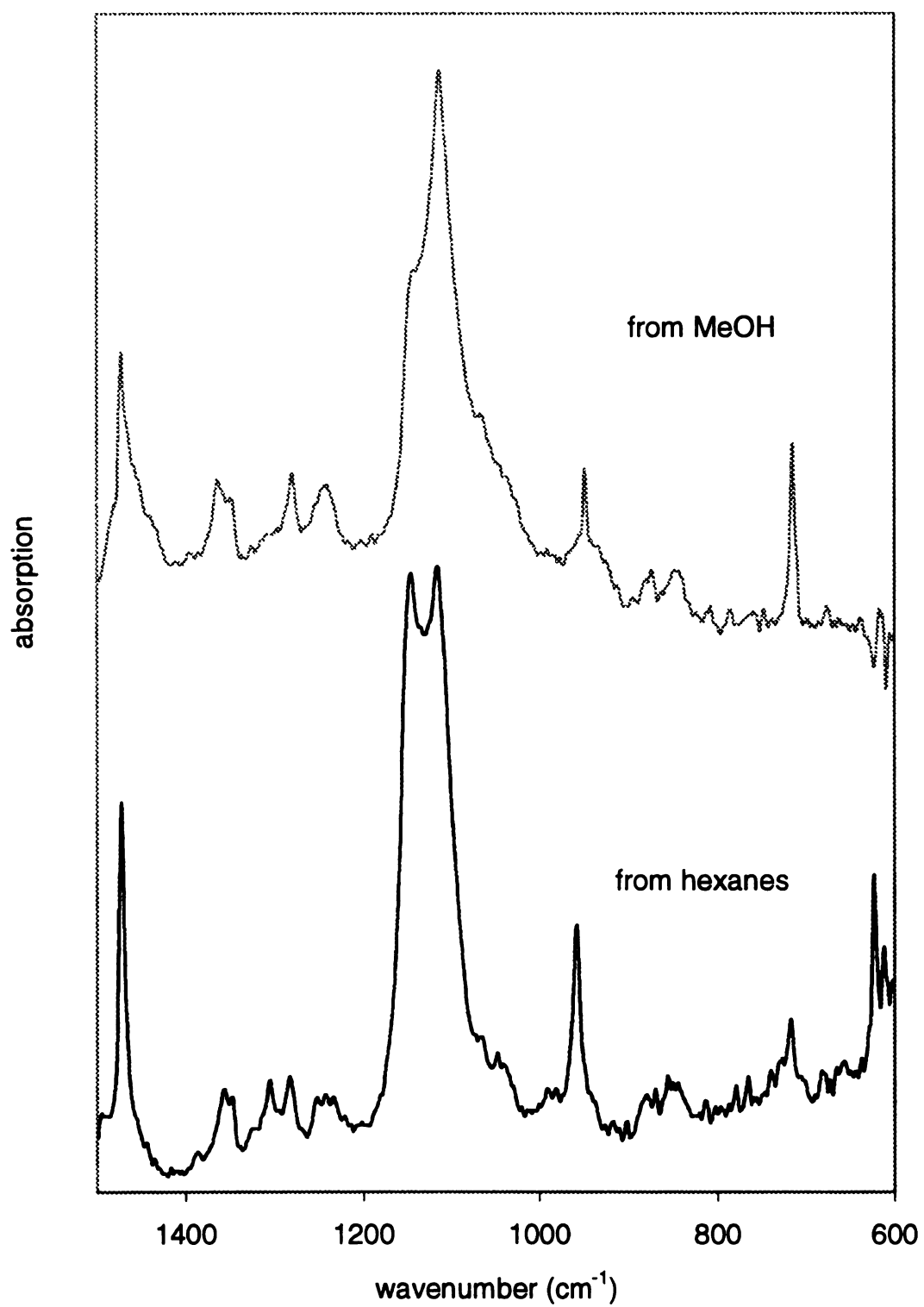


Figure 71. IR spectra of polymer (C_{20}EO_7)_n crystallized with different solvents

5. XRD results for saturated polymers

We attempted to obtain XRD results for saturated polymers $(C_xEO_y)_n$, however, due to the limited amount of saturated polymer samples available with $y \geq 6$, we were unable to obtain spectra for these polymers with reasonable signal/noise ratios. These samples will be tested once larger quantity of sample are available.

As was attempted for the unsaturated polymers, we tried to correlate the DSC transitions of the saturated polymer $(C_{10}EO_5)_n$ with the polymer structure. The sample was treated in the same way as described for the unsaturated polymer. The temperatures where XRD data were taken are shown in the DSC curves of this sample in **Figure 72**. The XRD profiles are shown in **Figure 73**. It is seen that even for fast quenching in liquid nitrogen, some crystalline material formed as indicated by a sharp peak at about 20° and several small peaks on top of the amorphous halo. This implies that the saturated polymers are very easy to crystallize. Heating the polymer to -25°C , which is above the polymer T_g , initiated additional crystallization. A new peak emerged at 24°C and became better defined as the sample was heated to 12°C . After passing the first endotherm, peaks appeared at 21.7° and 22.1° 2θ values. These peaks disappeared after the polymer was heated past the second DSC endotherm. All of the diffraction disappeared once the polymer was melted. When the polymer was cooled to below its crystallization temperature, the sample diffracted again. However, although the pattern persisted, all of the peaks were shifted to higher angles. Further discussion is included in Discussion section.

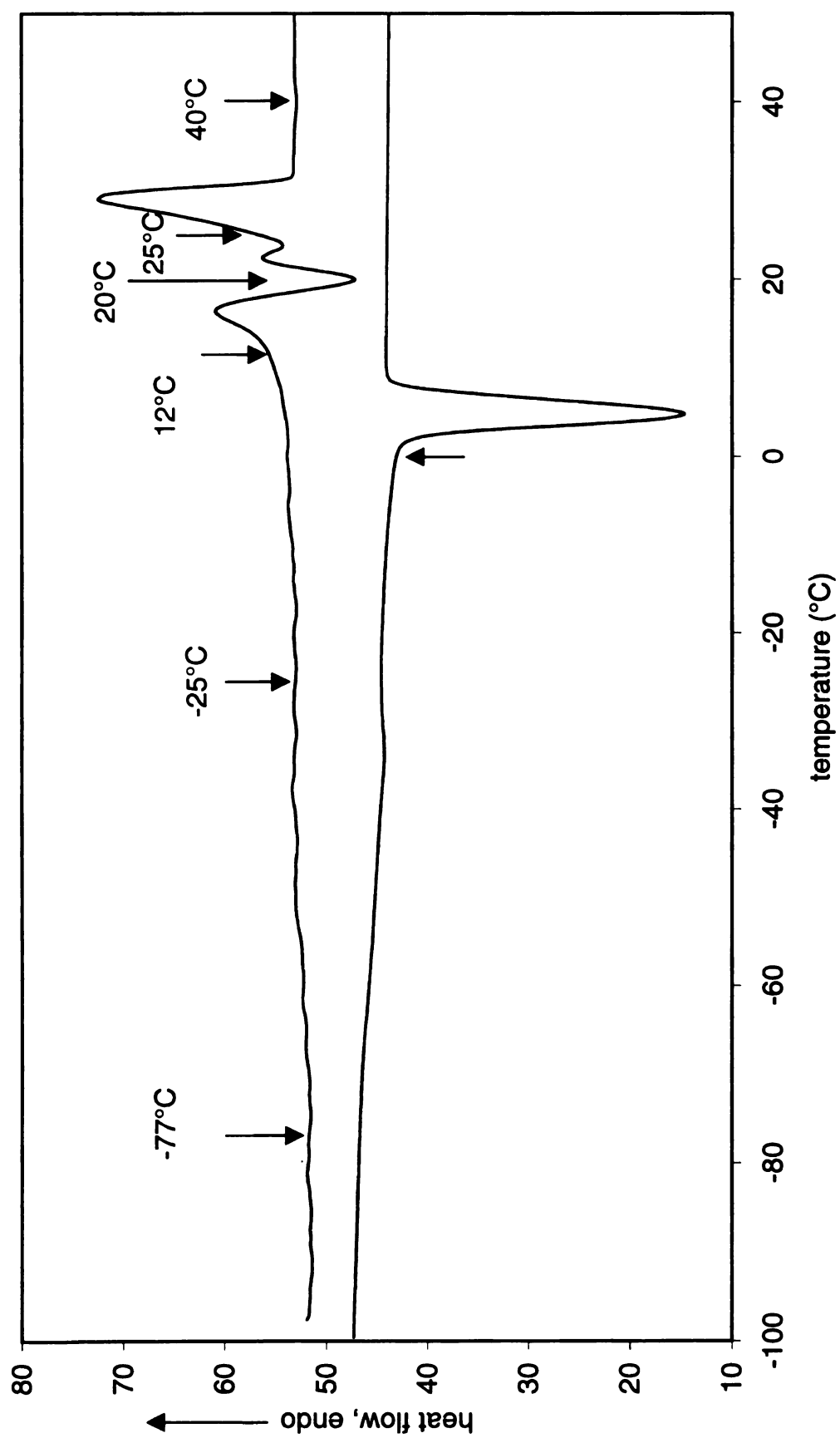


Figure 72. DSC of polymer $(C_{10}EO_5)_n$ heating and cooling at 10 °C/min after flash quenched from the melt. Arrows indicate the temperatures where XRD experiments were performed in addition to -178 and -130 °C.

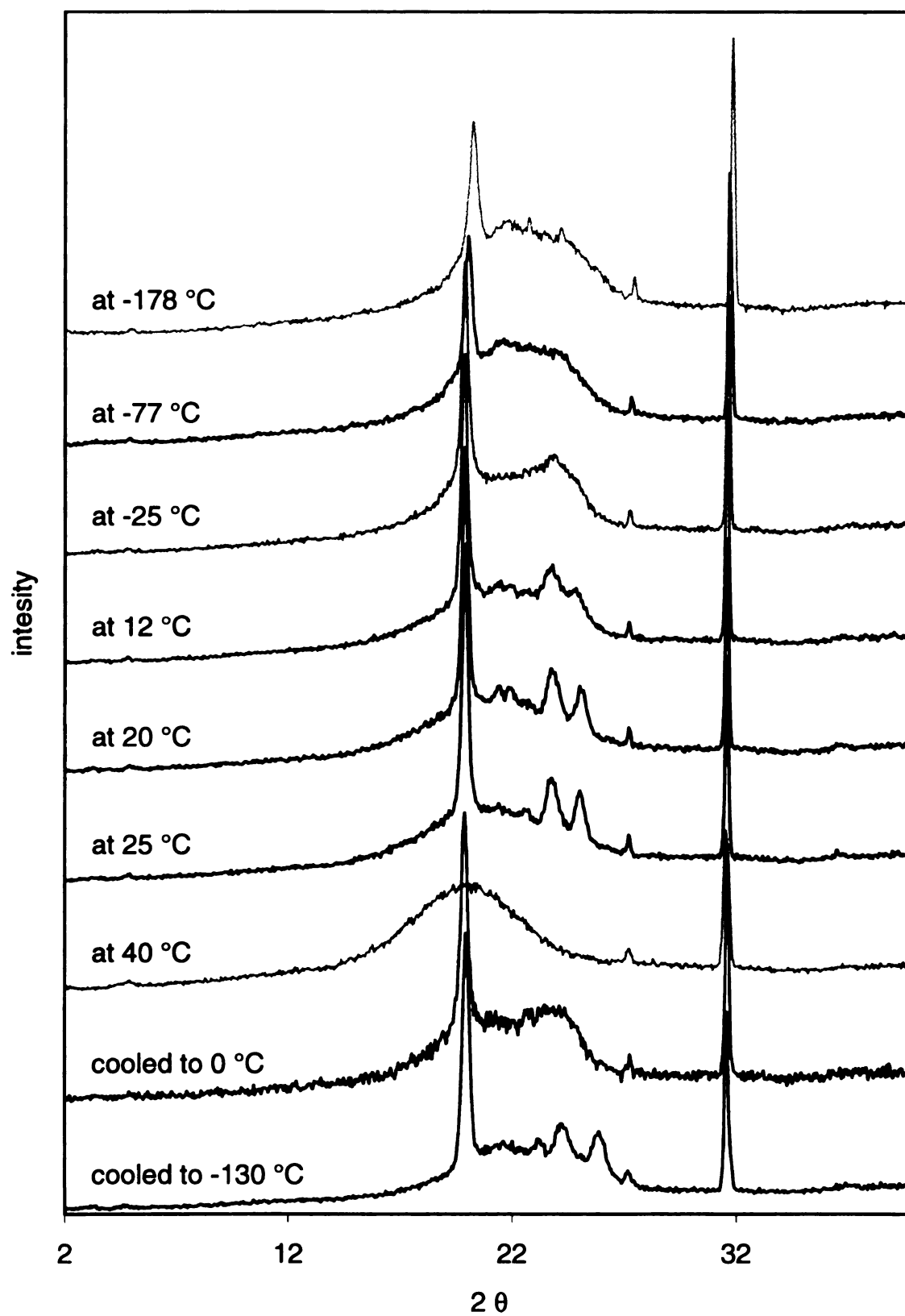


Figure 73. XRD of polymer $(C_{10}EO_5)_n$ as a function of temperature. Note: peaks at 31.7° 2θ are diffraction from NaCl impurity.

DISCUSSION

I. Synthesis and Purification

1. Synthesis of exact length ethylene glycols

Because the physical properties of the block copolymers are sensitive to distributions in the lengths of the blocks, compounds where the length of each block was exact needed to be prepared. Exact length alkyl or alkenyl segments are readily available, and thus the main synthetic challenge is obtaining the exact-length PEGs needed for the desired ABA structures. PEGs are commercially available in a variety of molecular weights, but only a limited number of exact-length glycols are available in high purity. Chromatographic separation of glycols from commercially available PEG mixtures was considered, but to ensure the purity of the glycols in the amounts needed (tens of grams), we opted for an iterative synthetic approach that allowed us to access a broad range of PEG lengths on large scales. With the increased interest in using PEGs in polymer-supported solid phase synthesis, cyclic ethers, and as elements of new materials, there have been several reports describing the synthesis of exact length PEGs. We adopted a modified version of the approach of Keegstra *et al.*¹⁶⁵ to prepare glycols where *y* is 6-10 and 14. The route to these PEGs is outlined in **Scheme 22**.

Success in any iterative synthesis demands that each step proceeds in high yield and that each intermediate be readily purified. Our work incorporated modified work-up protocols designed to simplify product isolation and minimize the need for chlorinated

solvents. For the preparation of the ditosylates, we used aqueous KOH instead of the powdered KOH/CH₂Cl₂ mixture used by Keegstra. KOH and TsCl have limited solubility in CH₂Cl₂ and therefore the KOH needed to be powdered and the reaction concentration can not be very high. By switching to a THF/water solvent system, the solubility of all the reactants was greatly enhanced. In addition, ditosylate products are insoluble or poorly soluble in water, and therefore were excluded from aqueous phase and helped drive the equilibrium toward the products. In our hands we found that the aqueous system gave purer products in higher yield. Furthermore, we noted that the conditions used by Keegstra (dry CH₂Cl₂/KOH) are very similar to those used for preparing chain extended polyethylene oxide polymers.¹⁶⁷ By switching to an aqueous system, we also eliminated chain extension as a potential side reaction.

The work-up procedure for the monotritylates was also simplified, enabling us to obtain pure products in high yield. Both the monotritylate and ditritylate syntheses were modified to eliminate the need for CH₂Cl₂. Water played an important role in the modification. Previously, because it was thought that water might reduce the reaction yield, water was strictly excluded from the reaction and during the work-up. We, on the other hand, found that the monotritylates are almost insoluble in water, and the excess reactant (ethylene glycol) and pyridinium hydrochloride, are very soluble in water. Therefore, water was used to precipitate the monotritylates from the glycol solution and then was used in the washing procedures.

In the deprotection reaction, the H₂ pressure was increased to 50 atm from 5 atm¹⁶⁵ to drive the reaction to completion in a shorter time. Washing the methanol solution of oligoethylene glycol with hexanes also facilitated the removal of trace

amounts of the triphenyl methane byproduct. With these modifications, the overall yield of most of the five step syntheses can be $\geq 90\%$, enabling us to obtain sufficient amounts of exact length PEGs.

2. Monomer purification

Since Schrock's molybdenum catalyst is very sensitive to impurities such as water, oxidants and chelating functional groups, the monomers for ADMET need to be very pure. Both the polymerizability and polymer molecular weight depend greatly on monomer purity.^{78,79}

Of the $\pi C_xEO_yC_x\pi$ monomers we synthesized, only the low molecular weight monomers can be purified by vacuum distillation. When $y \geq 6$, the boiling points of the monomers are too high for distillation. We developed a new method to purify monomers in this category. First, we used column chromatography to separate the monomer to $> 95\%$ purity. The remaining impurities were believed to be trace amounts of water, alcohol and a side product that seems to contain an aldehyde. All of these can react with sodium metal to give salts. However, only freshly exposed sodium metal can react with them. We borrowed the purification method used to purify solvents for anionic polymerization—the use of sodium mirrors. The fresh sodium surface was formed by vacuum sublimation of a small chunk of the metal to form a mirror-like coating on inner surface of the flask. The impurities react with the fresh sodium surface and eventually are converted to a salt. In the conventional purification scheme, the sodium mirror purification is followed by distillation, which is not applicable for $y \geq 6$. We considered an alternative—filtration. Since the salt particles formed are small and the ethylene oxide

segments of the monomer can solublize salts well, a competitive substrate needs to be provided to absorb them. Because the impurities after the purification reactions exist as anions, an acid is required, preferably a weak acid that can be easily separated from the monomer. A solid phase weak acid would be an ideal candidate, and acidic alumina satisfied all the requirements. In order to reduce excess absorption of the monomers and the passage of small particles passing through the filter pad, the alumina was mixed with Celite® in a 1:5 ratio. This material was packed in the middle of a small column flanked by pure Celite® on both ends to further prevent leakage of small salt particles through the filter, and the packing materials from being stirred by the solution stream (**Figure 10**).

This method was a key step in obtaining high purity monomers for this project, and greatly expanded the scope of pure monomers available for ADMET polymerization.

3. Polarity changes of the compounds in this research

The building blocks of the copolymers in this research can be viewed as analogs of polyethylene and polyethylene oxide. These two building blocks have opposite polarities. Polyethylene is hydrophobic and soluble in non-polar organic solvents, while polyethylene oxide is hydrophilic and soluble in most polar solvents including water. By connecting these two kinds of blocks in one molecule, it is expected their polarities should show systematic changes based on the volume fractions of the two blocks in the copolymer.

The solubility parameter is defined as in equation 15⁴

$$\delta = (\Delta E/V)^{1/2} \quad \text{eq. 15}$$

where ΔE is the energy of vaporization to a gas at zero pressure (i.e., at infinite separation of the molecules), and V is the molar volume of the material. The quantity $\Delta E/V$ is the energy of vaporization per cm^3 . This term is sometimes called the cohesive energy density. Based on the simplest notion about solubility “like dissolves like”, polymers or oligomers will dissolve in solvents that have similar δ values.

The solubility parameter for a polymer structure may be calculated using empirical group attraction constants, G ($\text{cal}^{1/2}\text{cm}^{3/2}\text{mol}^{-1}$), for each group.

$$\delta = \frac{\rho \Sigma G}{M} \quad \text{eq. 16}$$

where ρ (g/cm^3) represents the density and M (g/mol) is the repeat unit molecular weight.

We made a simple estimate of the solubility parameters of the unsaturated polymers synthesized for this project based on the known values for polyethylene and polyethylene oxide. For a specific polymer, the formula $(\text{C}_x\pi\text{C}_x\text{EO}_y)_n$ indicates it consists of a $(\text{CH}_2\text{CH}_2)_x$ segment, a $(\text{CH}=\text{CH})$ segment, a $(\text{OCH}_2\text{CH}_2)_y$ segment and one O atom. The G values of $(\text{CH}=\text{CH})$ and the O atom are 222 and 70 respectively (units omitted).¹⁶⁸ Giving the solubility parameter and density values of polyethylene (7.9 and 0.85 respectively¹⁶⁹) and polyethylene oxide (9.9 and 1.20 respectively¹⁶⁹), the G values of $(\text{CH}_2\text{CH}_2)_x$ and $(\text{OCH}_2\text{CH}_2)_y$ were calculated to be 260 and 363 respectively. Therefore,

$$\Sigma G = 260x + 363y + 222 + 70 \quad \text{eq. 17}$$

Meanwhile, the repeat unit molecular weight can be calculated from the polymer formula and the polymer density can be estimated based on the density of PE and PEO

and the component weight fractions. As a rough estimate the density of the alkenyl segment was taken the same as that of PE. The polymer density estimation is now written as:

$$\rho_{polymer} = \rho_{PEO}W_{PEO} + \rho_{PE}(1-W_{PEO}) \quad \text{eq. 18}$$

where W_{PEO} is the weight fraction of PEO segment in the polymer.

Using the known values, the solubility parameters δ were calculated and are shown in **Table 15** and plotted in **Figure 74**. From the figure, we can see that the solubility parameter increases as the ethylene oxide fraction increases. Also when the alkenyl fraction increases, the solubility parameter drops. Solubility parameters of some common solvents are given in the figure for comparison.

This systematic change in solubility parameters explains the requirement for a series of solvent adjustments needed for monomer and polymer purification. For example, all of the polymers have solubility parameters between 8.3 and 9.5 (cal/cm³)^{1/2}, explaining why toluene ($\delta = 8.9$) can be used to dissolve all of the polymers. Hexanes, with δ close to 6.6 (cal/cm³)^{1/2}, can be used to precipitate all the polymers. Meanwhile, only polymers with long alkenyl and short ethylene oxide segments can be precipitated in alcohols. The values of the calculated solubility parameters can be used as a guideline for choosing the solvent for purification and further manipulations of the polymers. However, when each segment is long enough, this δ model, based on the averaging the effects of the two types of blocks, breaks down. At some block length, phase separation is strong enough so that the blocks will act independently. This prediction was proved by the solubility of polymer (C₃ π C₃EO₁₄)_n in water, whose calculated δ value, 9.52, is 13.9

smaller than the δ of water (23.4). The solubility is presumably due to the formation of micelle-like structures in water, which is also observed in a preliminary result in some triblock oligomers.

Table 15. Solubility parameters δ [(cal/cm³)^{1/2}] of unsaturated polymers (C_xπC_xEO_y)_n.

	y								
x	2	3	4	5	6	7	8	10	14
3	8.57	8.80	8.96	9.08	9.18	9.25	9.31	9.40	9.52
4	8.51	8.73	8.89	9.01	9.11	9.18	9.25	9.34	9.47
8	8.34	8.52	8.67	8.79	8.88	8.96	9.04	9.15	9.30
9	8.31	8.49	8.63	8.74	8.84	8.92	8.99	9.11	9.27

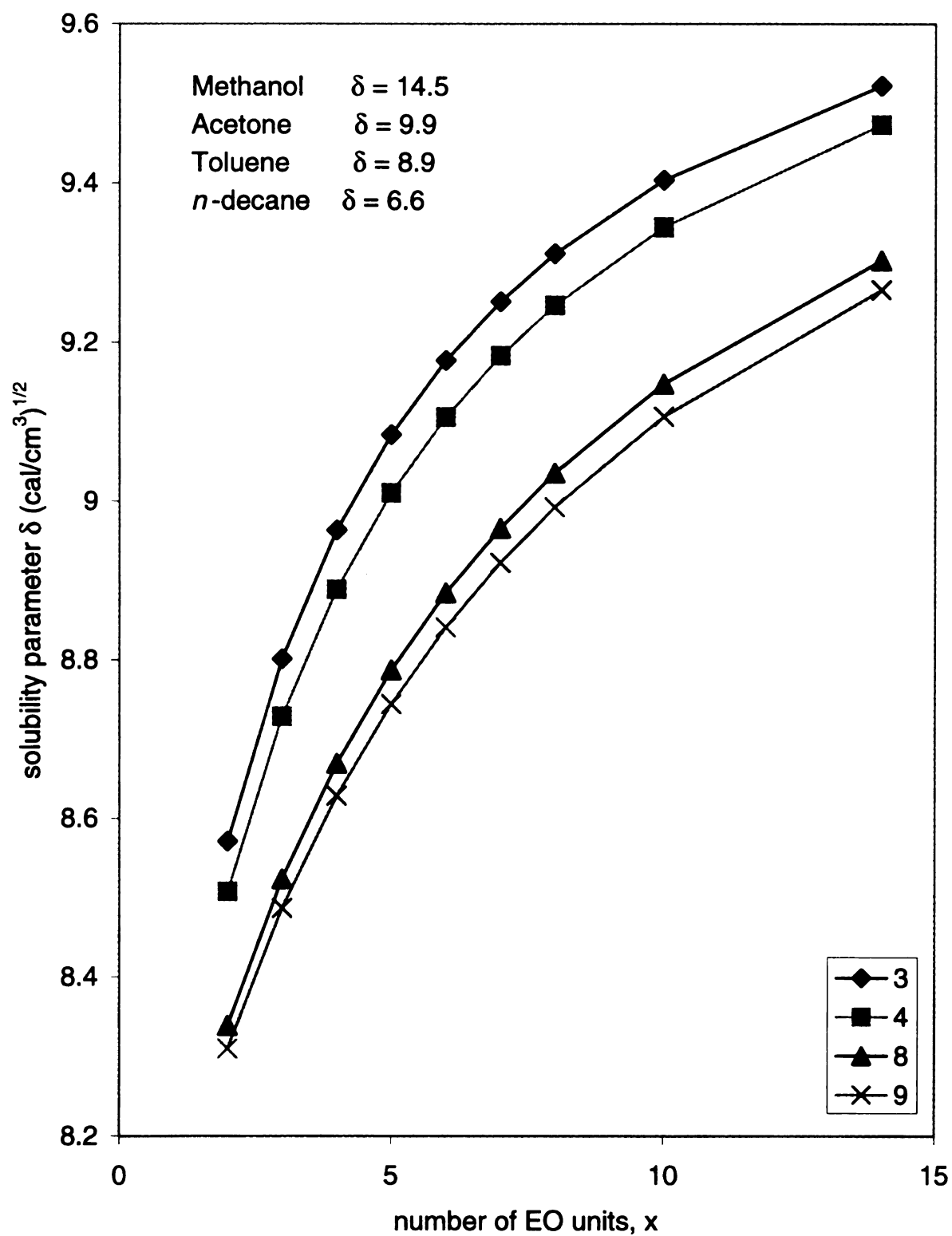


Figure 74. Estimated solubility parameters of unsaturated polymers $(C_x\pi C_xEO_y)_n$. Numbers in the inset are x values.

4. Polymerization details

Polymerizability of monomers

Polymers were successfully synthesized from all the monomers made in this research except for the $\pi\text{C}_2\text{EO}_y\text{C}_2\pi$ series of monomers. The monomers in this series were contaminated by the allylic isomerization of the terminal double bonds as shown in **Scheme 28**. Since the properties of these compounds are so similar, isolation of pure $\pi\text{C}_2\text{EO}_y\text{C}_2\pi$ monomers was almost impossible. Double bonds allylic to the oxygen atoms are thought to form a stable adduct during polymerization as shown in structure **23**.^{170,171} The oxygen atom chelates to the Mo atom and blocks the site for further reaction, thus leading to poisoning of the catalyst. The possibility of forming a cyclic product via ring closing metathesis was also proposed for some numbers of the $\pi\text{C}_2\text{EO}_y\text{C}_2\pi$ series.¹⁶⁶ However, since the problems persist for all of the monomers in the series, this hypothesis seems unlikely to be correct. We believe the chelating effect of the oxygen is the main reason for the failure of the polymerization in this series.

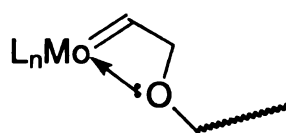
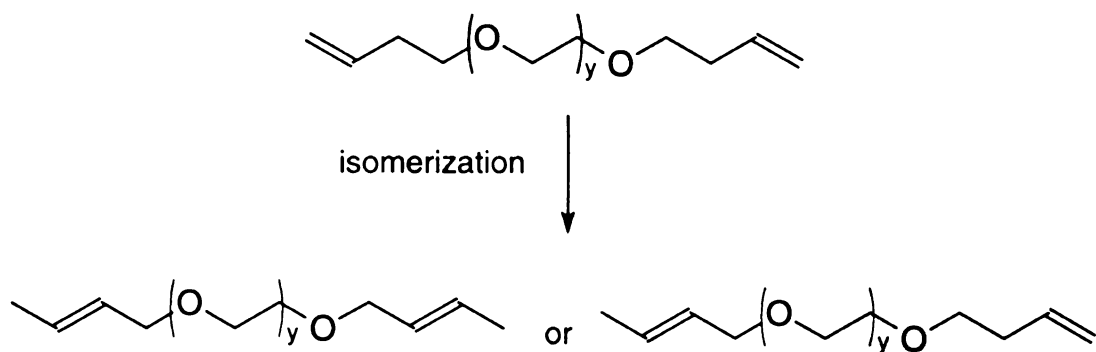
Molecular weight related factors

ADMET polymerization is a step growth polymerization. It has been shown¹⁶⁶ for the polymerization of this family of ethylene oxide segmented polymers, that the molecular weights increase with their degree of polymerization, X_n as

$$X_n = 1/(1-p) \quad \text{eq. 19}$$

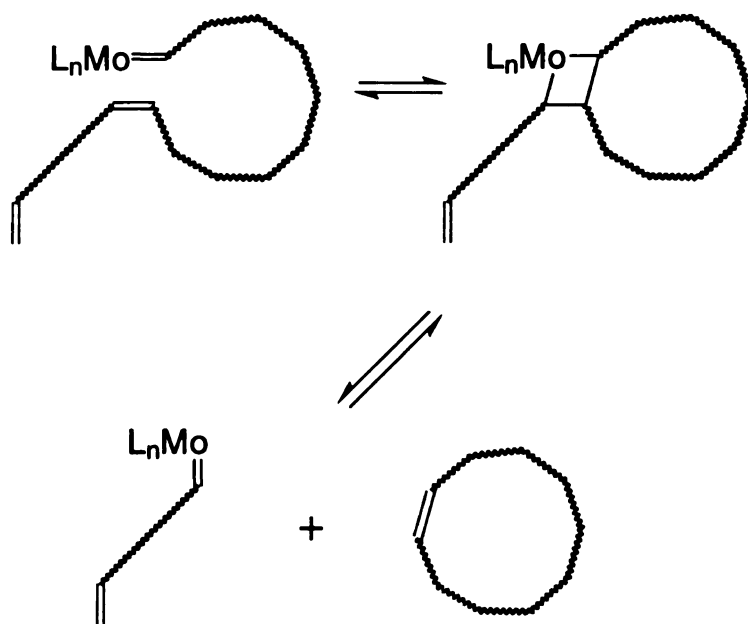
where p is the fractional conversion of the terminal vinyl groups to internal double bonds.

Scheme 28. Isomerization of $\pi\text{C}_2\text{EO}_y\text{C}_2\pi$ double bonds



23

Scheme 29. Back-biting for polymer degradation



The polymerization reaction competes with side reactions that can either terminate the reaction, such as catalyst degradation, or lower the molecular weight, such as “back biting”. Schrock’s molybdenum catalyst is unstable above 60 °C.⁶⁴ When polymerizing monomers in the bulk state, the reaction has to be run at 50 °C to melt the monomers, but at this temperature, the catalyst slowly decomposes which leads to a decrease in polymerization rate in addition to that caused by the reduction in the concentration of the terminal double bonds. Occasional additions of small amounts of catalyst were used to solve this problem for long reaction times.

The back biting reaction is shown in **Scheme 29**, where the propagating intermediate attacks a double bond in its own chain instead of reacting with the terminal double bond of another molecule to extend the polymer chain. The result of this reaction is a new linear reactive intermediate and a macrocyclic ring. This side reaction is more favored when the reaction system is dilute, since the chance of a reactive site meeting another molecule to extend the chain is less than that of finding another double bond in its own molecule. This phenomenon was best observed for high molecular weight polymers. Diluting the polymerization with solvent always resulted in reduction of the molecular weight. On the other hand, when the polymerization system is too viscous, the reaction rate is low since it is diffusion controlled. To increase the diffusion rate, the viscosity was decreased by both increasing the temperature (which can only be raised to 50 °C) and addition of solvent. According to our experience, adding one 15 mL portion of toluene to a 5 g scale reaction after the bulk polymerization stage always gave good results.

Saturated polymer molecular weight

When the unsaturated polymers were reduced to saturated polymers, their molecular weight dropped substantially (see **Table 13**). This phenomenon was observed for both catalytic hydrogenation and reactions using tosylhydrazine (TsNHNH_2). Previously, the molecular weight decline was suspected to be an artifact of the GPC measurement. It was proposed that the hydrodynamic radii of the saturated polymers might be smaller than for the unsaturated polymers.¹⁶⁶ Since GPC is a relative method that measures the molecular weight by measuring the particle size, it is possible to obtain higher than expected molecular weight values if the polymer is highly swollen. However, when we used membrane osmometry, which gives absolute molecular weights, we found a similar molecular weight drop. This confirmed that degradation occurred during the reduction of the unsaturated polymer.

Given the high salt affinity of the PEO segments, trace amounts of catalyst residues were always present in the purified polymers, and the polymers appeared to be colored as a result. However, the saturated polymers were always white solids immediately after hydrogenation. If stored in air for more than several days, the white color reverted to almost the same color as their unsaturated precursors. We terminated the catalytic hydrogenation before the unsaturated polymers were completely reduced. These samples were colorless after work-up. We believe that the residual catalyst was reduced during hydrogenation to give a colorless oxidative state for molybdenum. If molybdenum is in a lower oxidative state, it probably played a role in degrading the polymers to lower molecular weight. Further experiments are needed to fully elucidate the problem.

II. Structure and properties of triblock oligomers

In our triblock oligomers, which also serve as model compounds for our $(AB)_n$ microblock copolymers, we incorporate exact length segments of polyethylene (A) and polyethylene oxide (B) into the oligomers in a ABA pattern. The PEO and PE segments strongly phase separate and unlike most block copolymers, both segments crystallize to form a rich variety of crystalline phases. One particularly interesting feature of PE/PEO microblock polymers is that the PE and PEO blocks normally adopt strikingly different crystal structures. PE typically crystallizes in an orthorhombic unit cell with the chains aligned along the c-axis in a planar zigzag conformation while PEO crystallizes as a 7_2 helix,⁹⁷ although a stress-induced metastable phase which contains planar zig-zag chains has been reported.^{109,110} By chemically connecting these blocks into one molecule, we observed a variety of structures in the ABA oligomers.

1. ABA oligomers $C_xEO_yC_x$ with $y \leq 6$

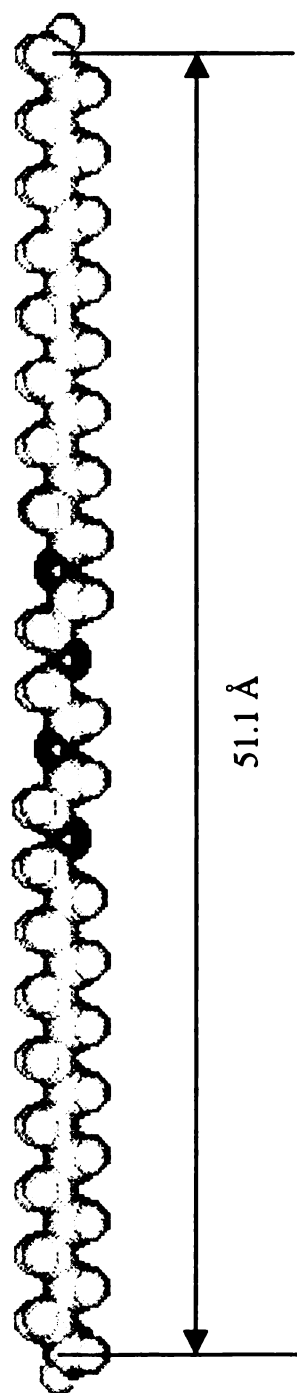
Since the A and B segments adopt different structures in their homopolymers, they will have to compete to get the best structure in the same molecule. The PE segments have a single link to the PEO segment, and their conformation should be the ordinary planar zigzag conformation. This can be inferred from the 718 cm^{-1} band in IR spectra, a CH_2 rocking vibration with a planar zigzag packing. The PEO segment is flanked by two PE segments, and thus it is not easy for it to adopt its preferred helical conformation. All triblocks show similar behavior in the IR (**Figure 37**), XRD (**Figure 29, 30**) and DSC (**Figure 22**) and therefore we believe they have similar solid state structures. We chose a representative oligomer, $C_{16}EO_3C_{16}$, to further investigate the molecular structure. Powder XRD showed that this compound crystallized to form a

lamellar structure as evidenced by the well-defined series of *00l* peaks. We calculated the molecule's end to end distance using a molecular mechanics routine considering two different PEO conformations. As shown in **Figure 75**, the oligomer with PEO in a helical conformation gives an end to end distance of 47.2 Å, compared to 51.1 Å for a planar zigzag conformation. Comparing the calculated results with the 51.3 Å layer d-spacing from powder XRD indicates that the structure of triblock $C_{16}EO_3C_{16}$ has fully extended chains oriented normal to the layers with the ethylene oxide core in a planar zigzag conformation as illustrated in **Figure 76**.

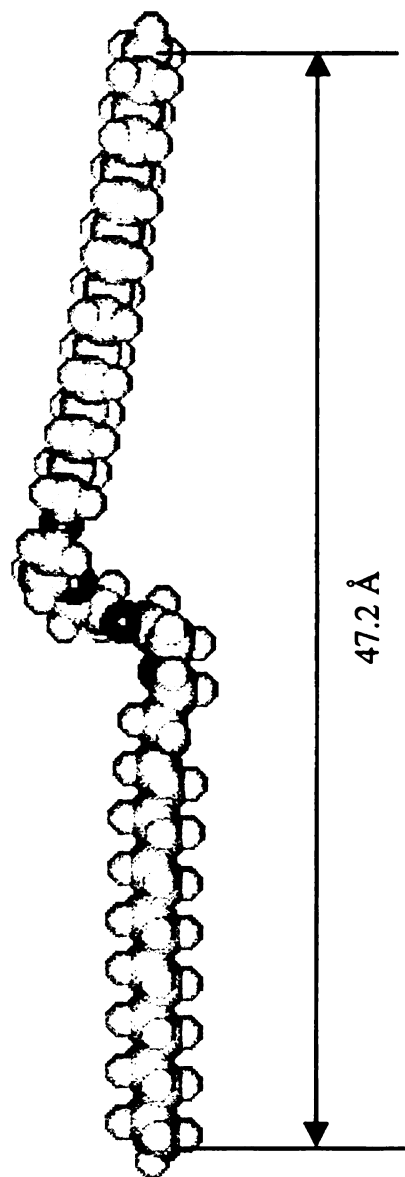
2. ABA oligomers $C_xEO_yC_x$ with $y = 7$

Crystallization of oligomers from solvent

Samples with 7 ethylene oxide units were the most interesting since XRD (**Figure 29 and 30**) and DSC data (**Figure 22**) depend on sample history. We first focus on the structures of solvent crystallized $C_{14}EO_7C_{14}$. This sample has a melting point of 41 °C when crystallized from methanol, but melts at 39 °C when crystallized from hexane (**Figure 22**). The XRD results however, show that these two samples have distinctly different packing arrangements in the solid state. For the sample crystallized from methanol, the XRD results give a layer spacing of 60.1 Å, while the corresponding value for samples crystallized from hexanes is 52.7 Å. Thus, layered crystals of comparable stability are formed but the individual molecules in the layers have different conformations.



Triblock oligomer $C_{16}EO_3C_{16}$ in linear conformation



Triblock oligomer $C_{16}EO_3C_{16}$ with helical ethylene oxide unit

Figure 75. Triblock oligomer $C_{16}EO_3C_{16}$ calculated end to end distance with different PEO conformations.

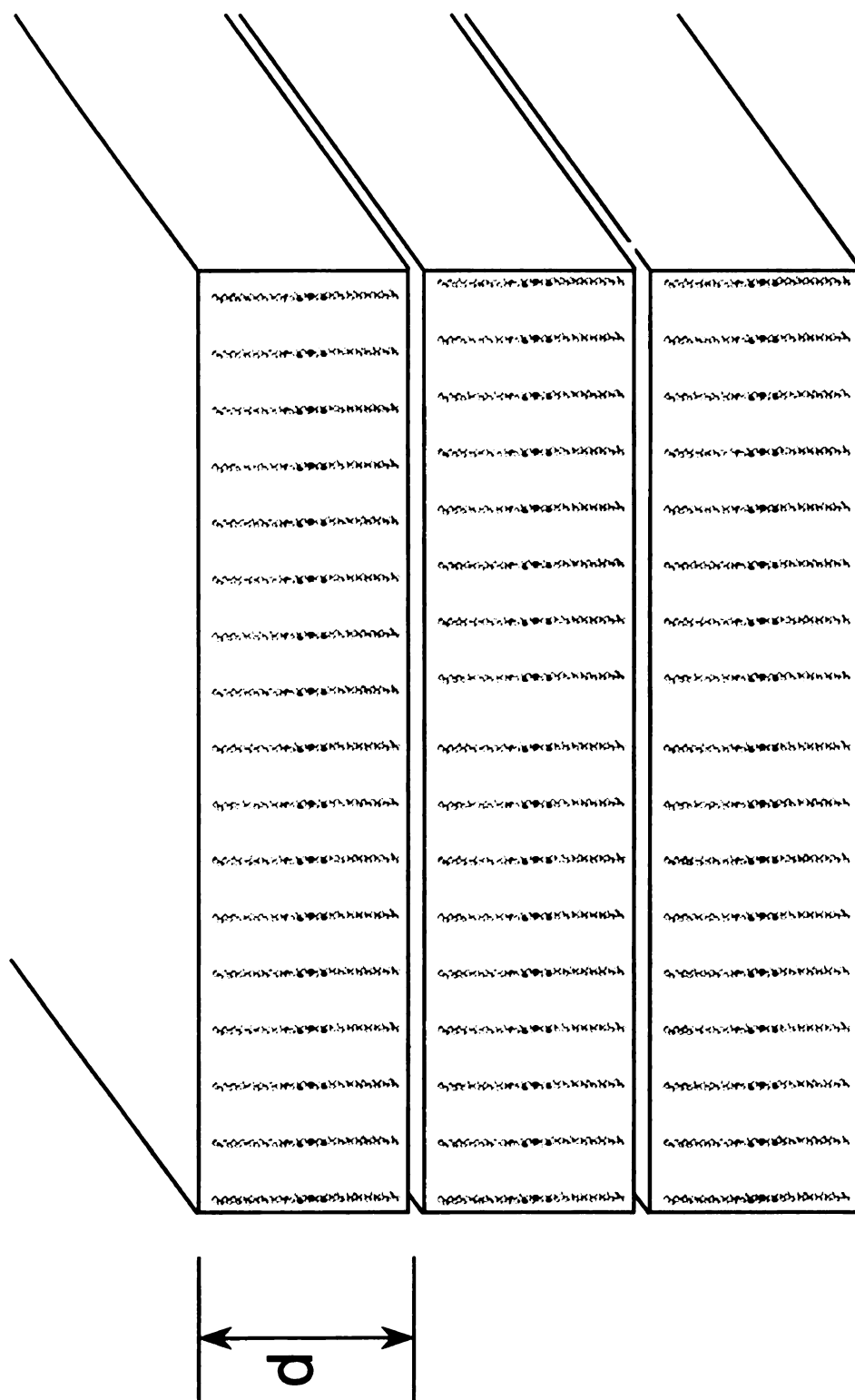


Figure 76. Triblock oligomer $C_{16}EO_3C_{16}$ with lamellar structure.

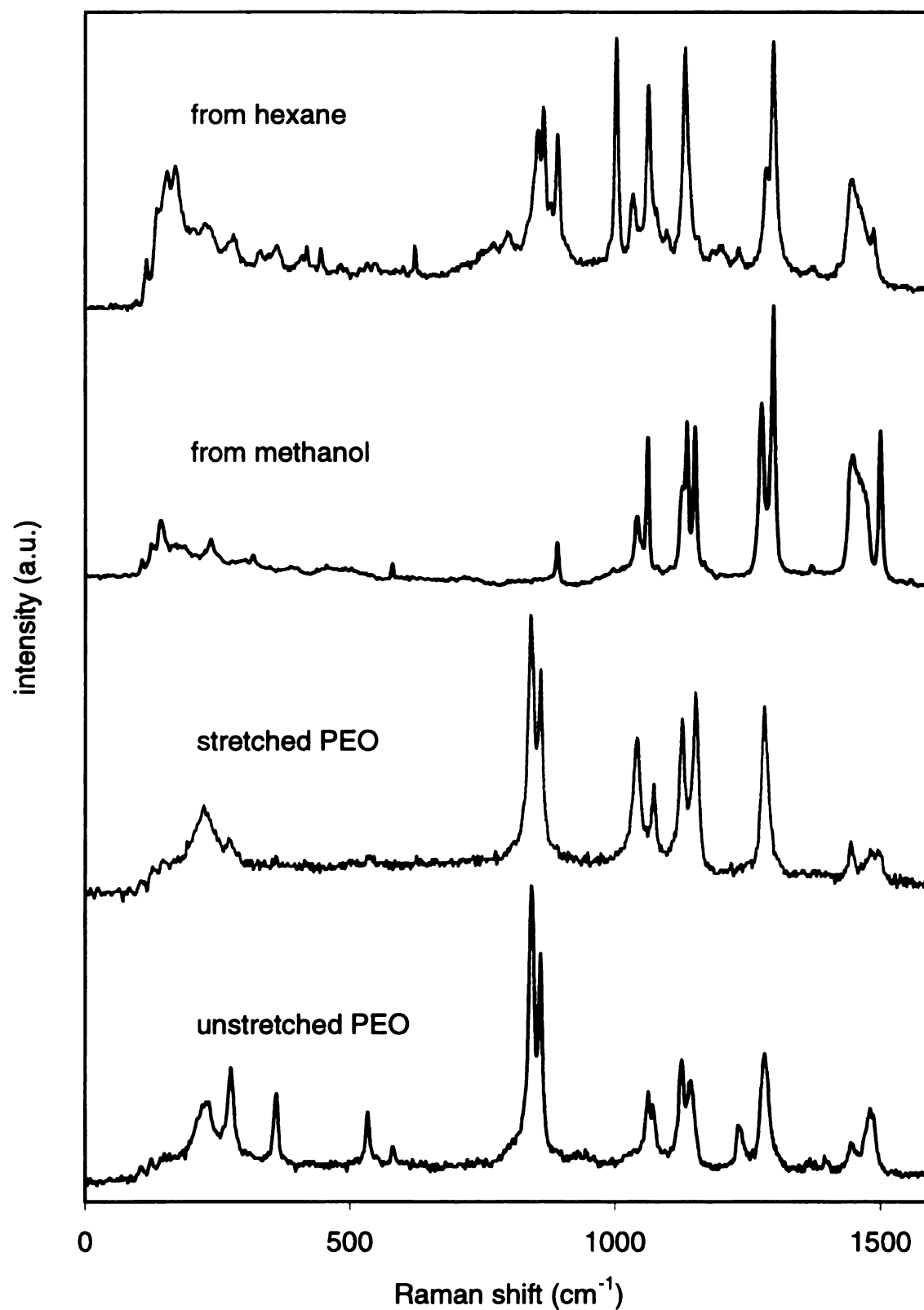


Figure 77. Raman spectra comparison between $C_{14}EO_7C_{14}$ and PEO.

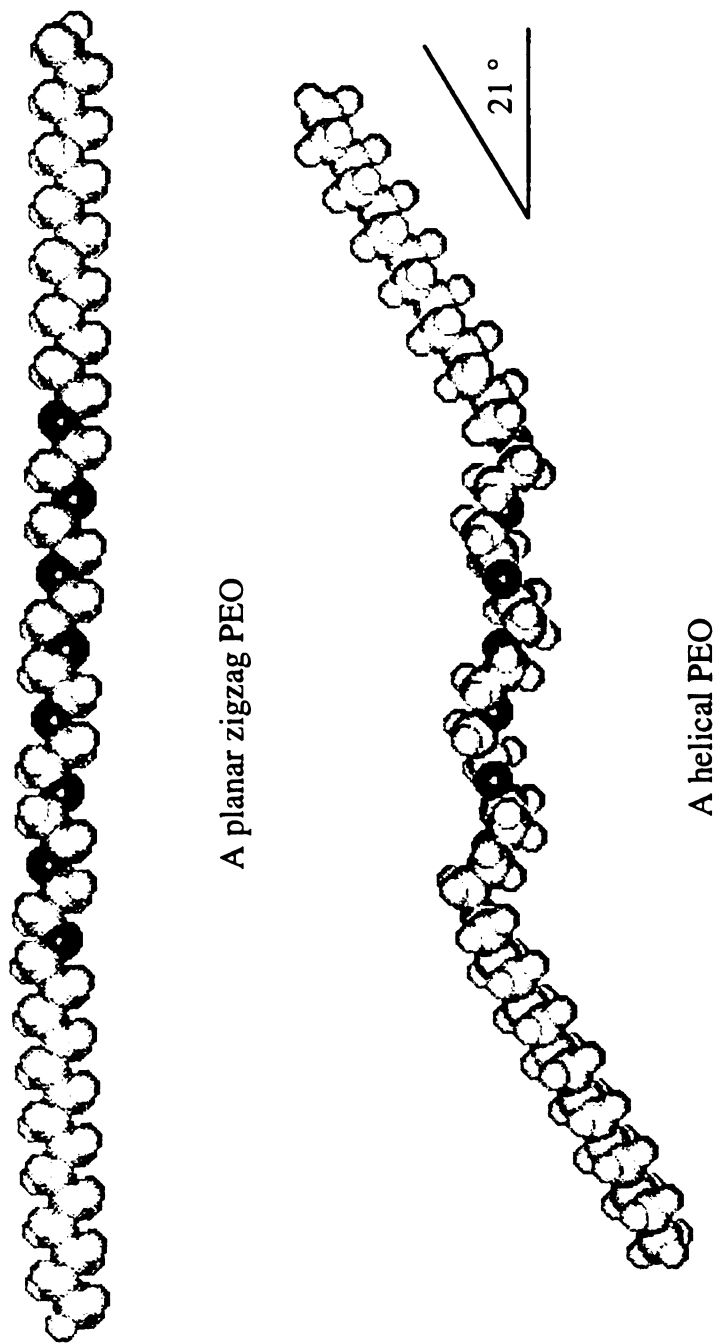


Figure 78. Triblock oligomer $C_{14}EO_7C_{14}$ structures obtained from solvent crystallization. Top: from methanol. Bottom: from hexane.

The nature of the difference between the two structures can be seen in **Figure 77**. Shown are the Raman spectra for samples crystallized from hexanes and methanol compared with a regular PEO sample and a PEO sample under tension. The sample crystallized from methanol has bands at 1498 (CH₂ bending), 1150 (CH₂ rocking) and 1041 cm⁻¹ (CC stretching), a pattern that is identical to that of highly oriented PEO held under tension. Such samples have been shown by x-ray diffraction to have a planar zigzag backbone conformation.^{109,110} The spectra also match the data from a C₁₄EO₃C₁₄ oligomer that has a planar zigzag conformation. Thus the chain conformation for samples crystallized from methanol must be the fully extended trans conformation shown in at the top of **Figure 78**. The same conclusion is reached from an analysis of the IR data (**Figure 37**). Meanwhile, the d-spacing measured for this sample (60.1 Å) agrees well with the calculated molecular end to end distance (60.4 Å) in a fully extended conformation.

To assign the chain conformation of samples crystallized from hexanes, we again focused on the Raman and IR data. The spectra show the bands characteristic of helical PEO (**Figure 77**), and the structure that best fits the data has a PEO core axis with the conformation of a 7₂ helix flanked by alkyl groups in their usual planar zigzag conformation (evidenced by the 718 cm⁻¹ IR band). The calculated length of the linear structure is larger than the layer spacing observed by XRD, but by tilting the alkyl chains 21° relative to the PEO core (see bottom structure in **Figure 78**), the overall length fits the layer spacing, and provides more efficient packing for the alkyl groups. Similar conformations also have been proposed for AB nonionic surfactants^{128,131,132} and for a series of ABA oligomers where m = 9.^{136,138}

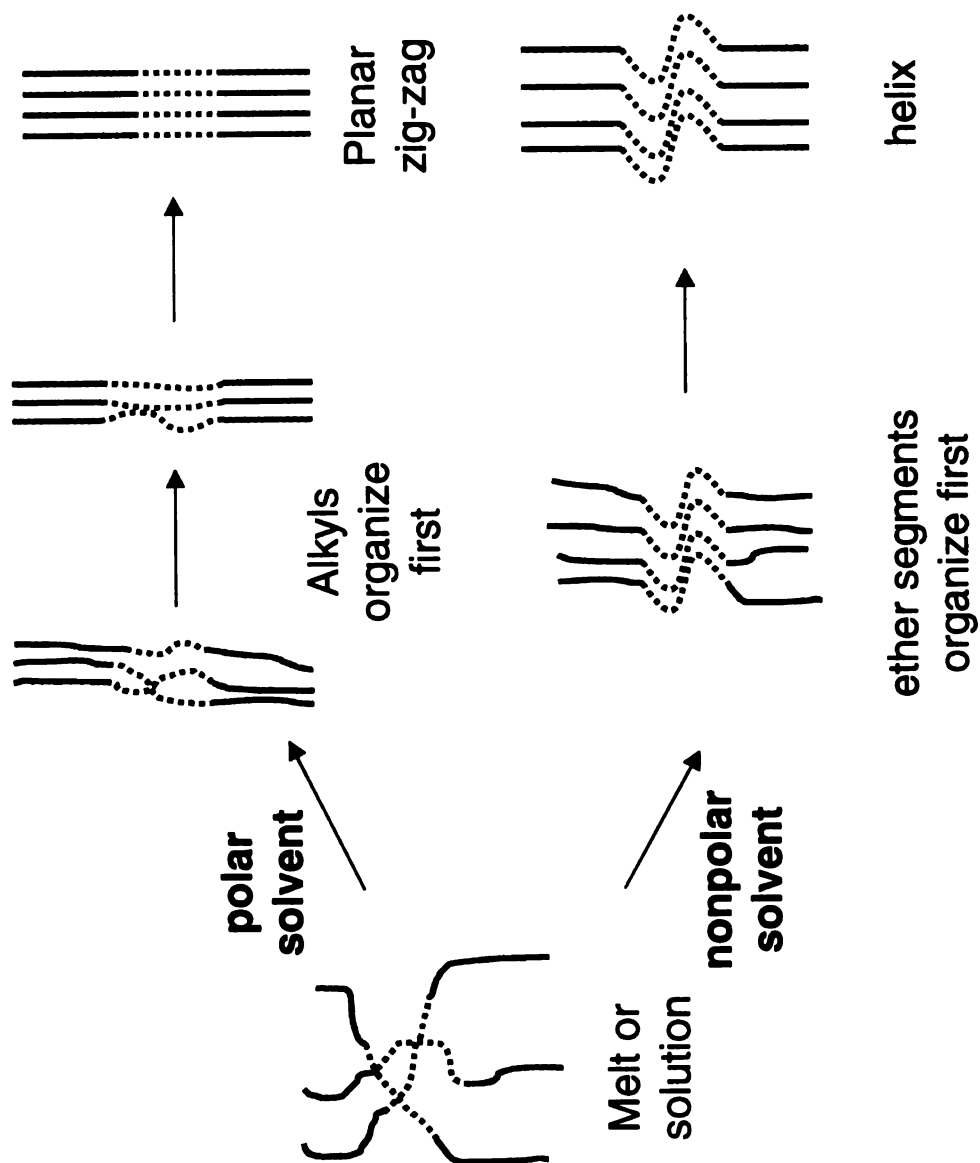


Figure 79. Oligomer $C_{14}EO_7C_{14}$ solvent crystallization mechanism

Solvent crystallization mechanism

To understand why we obtain either a helical or a trans conformation for the PEO core under different crystallization conditions, it is reasonable to consider a step-wise process for the crystallization of the ABA oligomers. In particular, we believe that given the amphiphilic nature of the oligomers, the A and B sub-units pre-organize before crystallization. Thus the outcome of the crystallization process should be governed by the relative solubilities of the A and B segments in a given solvent. As shown in **Figure 79**, in hydrophobic solvents the alkyl portions of the oligomers should be more soluble than the PEO core, and the less soluble PEO core should crystallize first and choose its most stable conformation, the 7_2 helix. When the alkyl fragments crystallize, they adopt their normal planar zigzag conformation, but tilt with respect to the PEO core axis to accommodate the helical structure of the PEO core and to increase the packing density. This situation should be reversed when hydrophilic solvents are used for crystallization. For example, crystallization from methanol should yield a pre-organized structure where the alkyl portions are poorly solubilized. Thus the alkyl portions of the oligomers should crystallize first in a trans zigzag conformation. When the PEO segments crystallize, they must conform to the structure defined by the alkyl segments and thus adopt a trans conformation. We note that this mechanism is not unlike that of protein folding, where the hydrophobic residues associate and help define the structure of the protein.

Even though spectral data show that ABA oligomers with PEO cores shorter than 7 repeat units all have planar zigzag conformations, the abrupt formation of a helical unit in these oligomers at $m = 7$ should not be surprising. To insert a stable helix into a polyethylene chain and retain high crystallinity requires that the junctions between the

PEO and PE chains have similar symmetries, a condition satisfied when the length of the PEO helix corresponds to one unit cell. This result points to a general strategy for incorporating stable crystalline polymer sub-units into materials. By using segment lengths that correspond to multiples of the polymer unit cell, such segments can be expected to self-assemble into crystalline sub-units that have the same structure as the parent polymer.

Melt crystallization of oligomers

When the oligomer $\text{C}_{14}\text{EO}_7\text{C}_{14}$ was crystallized from melt, it also gave different crystal structures depending on the crystallization conditions. The powder XRD results of a flash quenched sample which had been held at above its melting point for an extended time showed that the d-spacing is 54.6 Å (**Figure 31**). Annealing this sample at room temperature showed that its d-spacing gradually shifted to a higher value (**Figure 31**) within hours. The majority of the resulting crystal has a d-spacing corresponding to that of a fully extended conformation. If the sample was annealed at a higher temperature the conversion was faster. **Figure 35** shows that the crystal with the shorter d-spacing was mostly converted to that of the extended form within 14 minutes at the annealing temperature of 35 °C. Similar conversions at 35 °C were also seen in DSC experiments (**Figure 21**). These transformations were also noticeable in the wide angle XRD profiles (**Figure 32**), where the profile for the initially obtained crystal is very different from that after annealing. The wide angle XRD of the annealed sample resembles that of samples crystallized from methanol. Raman spectroscopy experiments showed the conformation changes of the PEO segment in this sample. With time, the melt quenched sample which had a helical PEO core, was converted to a planar zigzag conformation as evidenced from

bands emerging at 1498, 1150 and 1062 cm^{-1} . The oligomer $\text{C}_{14}\text{EO}_7\text{C}_{14}$ was also isothermally crystallized at equilibrium temperature since this should yield the most thermodynamically stable structure. The powder XRD of this sample showed a d-spacing corresponding to the fully extended molecular conformation, and this d-spacing did not change with time (**Figure 33**). The wide angle XRD of this sample (**Figure 34**) also looks very similar to that obtained from the sample crystallized from methanol.

From the information given above, we can infer that the melt quenched crystal has a helical PEO core and a planar zigzag alkyl chain. The structure is very similar to that obtained from hexane, but since the d-spacing is shorter, the alkyl chain tilt angle with respect to the PEO helix axis should be smaller. We estimate it to be about 10° . This conformation is not stable at room temperature and slowly transforms to the fully extended molecular conformation.

More interestingly, these samples seem to show a memory effect with respect to its conformations. When a planar zigzag sample was melted and then quenched to recrystallize the sample, the crystal form obtained was decided by the time the sample was held in the melt state. For short times, the crystal obtained had more planar zigzag molecules than helical PEO molecules. Longer holding times gave opposite results. If the sample was held at melt long enough, the quenched sample contained no extended molecules; all of the sample was converted to molecules with helical PEO cores. These differences can be quantified from DSC experiments by measuring the relative peak areas corresponding to the different crystal forms (see **Figure 20**). The higher temperature endotherm corresponds to the fully extended molecule and the lower temperature

endotherm to the helical form. In solvent crystallization experiments, memory effects were also observed. Systematic experiments are underway to study these behaviors.

The mechanism of the crystal formation from the melt can be explained as follows. When the sample is melted, both kinds of segments start to adopt their most stable conformation. Therefore, a helical PEO core and planar zigzag alkyl chains were always obtained. Crystals with this combination of conformations are kinetically favored since no reorganization is required. When these crystals are annealed at room temperature or higher, they were converted to the thermodynamically more stable conformations — the fully extended molecule with a planar zigzag conformation throughout the whole chain. It is not hard to see that this conformation is more uniform and has a higher degree of symmetry. The cross sections of the packed molecules are smaller because of this uniformity.

Summary of crystalline forms of triblock $C_xEO_7C_x$ oligomers

These triblock oligomers all crystallize in lamellar structures. The PEO core of this series of oligomers can adopt either helical or planar zigzag conformations depending on the crystallization conditions. When crystallized from polar solutions or isothermally crystallized close to the melt-crystallization equilibrium temperature, the oligomers adopt a fully extended structure with a trans zigzag conformation throughout the molecules. When crystallized from non-polar solvents or from the melt with large supercooling, the oligomers crystallize with the PEO core in the conformation of a 7_2 helix flanked by alkyl groups in their usual planar zigzag conformation. The alkyl chains are tilted with respect to the PEO helix axis. The tilt angle was 21° for crystal from hexane and 10° for crystals

formed by quenching from the melt. The fully extended crystal is the thermodynamically stable crystal.

3. ABA oligomers $C_xEO_yC_x$ with $y > 7$

Seven ethylene oxide units are needed to make the perfect 7_2 helix for the PEO core in the oligomers. Moreover, the geometry of the PEO structure also sets the two planar zigzag alkyl chains parallel to each other. The oligomers can be crystallized in a form that contains both helical and planar zigzag segments. When there are less than the 7 ethylene oxides needed to complete one 7_2 helix repeat unit, it is unfavorable for the PEO core to adopt a helical form since the two alkyl chain can not align parallel to each other. When the number of ethylene oxide units is > 7 , it is easy to form the helical conformation. Even for the oligomers with non-integer multiples of 7, the colinear problem can be easily accommodated by small adjustments of each PEO segment. Plotted in **Figure 80** are the d-spacings for a series of $C_{14}EO_yC_{14}$ oligomers measured by powder XRD. Also plotted in the figure are the calculated molecular end to end distances of the oligomers assuming either a helical or a planar zigzag conformation for the PEO core. The alkyl chains are adjusted to be colinear with the PEO helix axis for calculation of oligomers with helical PEO cores. From the figure, we can see that when $y \leq 7$, the d-spacings fit the calculated values for fully extended molecules, while when $y \geq 7$, the d-spacings fit the calculated curve of molecules with helical PEO. The transformation can be seen happening at 7 ethylene oxide units.

Raman spectroscopy also showed that all triblock oligomers with more than seven ethylene oxide units have a helical PEO core. The spectrum of oligomer $C_{14}EO_{14}C_{14}$ is shown in **Figure 81**. For comparison, spectra of stretched and unstretched PEO and

oligomer $\text{C}_{14}\text{EO}_7\text{C}_{14}$ (planar zigzag conformation for PEO) are also shown in the figure. Through this comparison, we can conclude that the PEO segments of $\text{C}_{14}\text{EO}_{14}\text{C}_{14}$ are in a helical conformation. A helical PEO conformation for oligomers with more than seven ethylene oxide units is stable. Unlike the oligomers with 7 ethylene oxide units, it does not convert to a planar structure when annealed at room temperature. The Raman spectra shown in **Figure 40** clearly indicated that this is true.

Therefore, the triblock oligomers with $y \geq 7$ adopt a structure with a 7_2 helical PEO core flanked by planar zigzag alkyl chains. Because of the good matches of the calculated end to end distances and the measured d-spacings, the alkyl chains have a very small tilt angle relative to the PEO helix axis if at all.

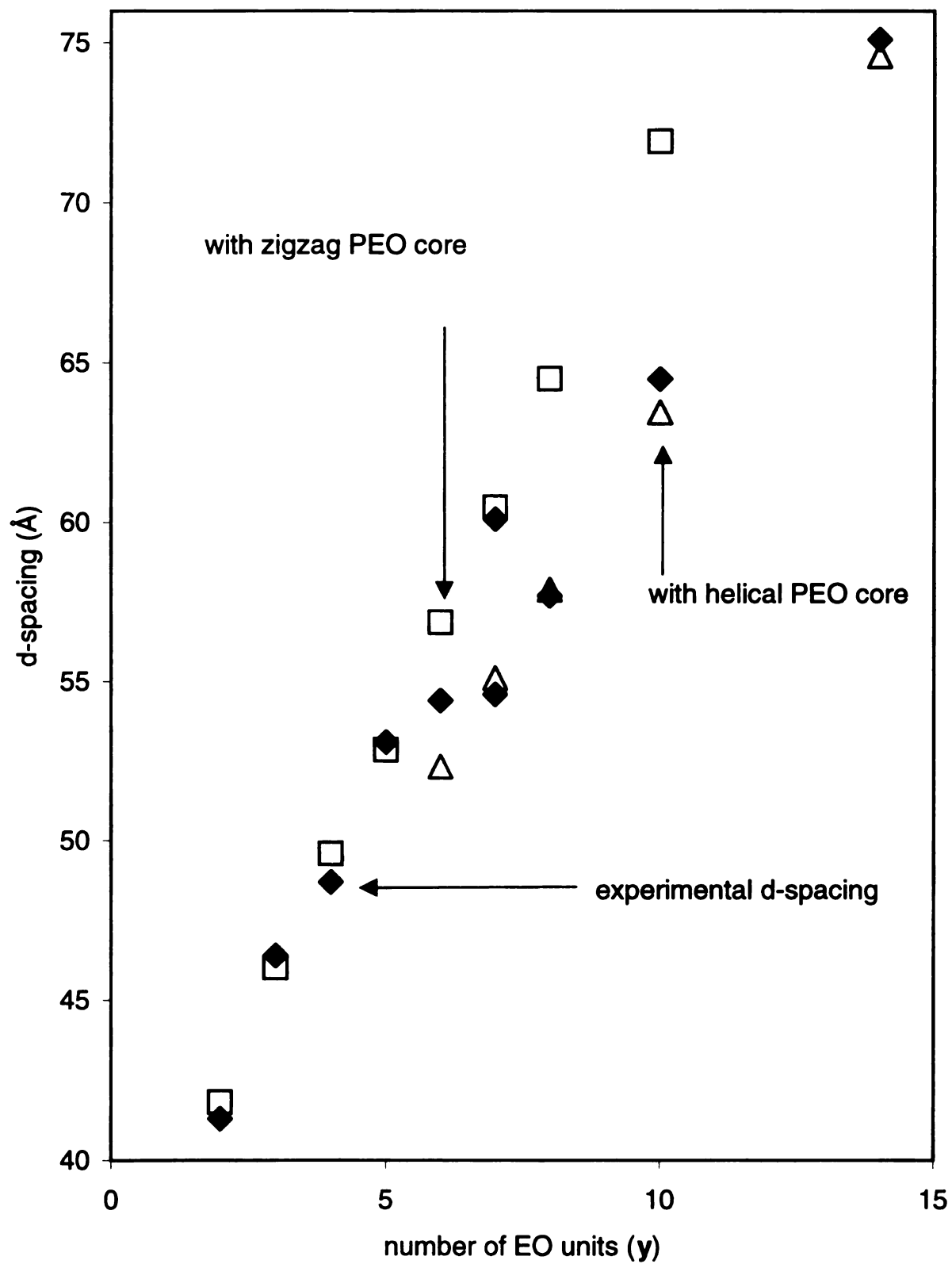


Figure 80. D-spacings of oligomer $C_{14}EO_yC_{14}$ measured by powder XRD compared to the calculated end-to-end distances.

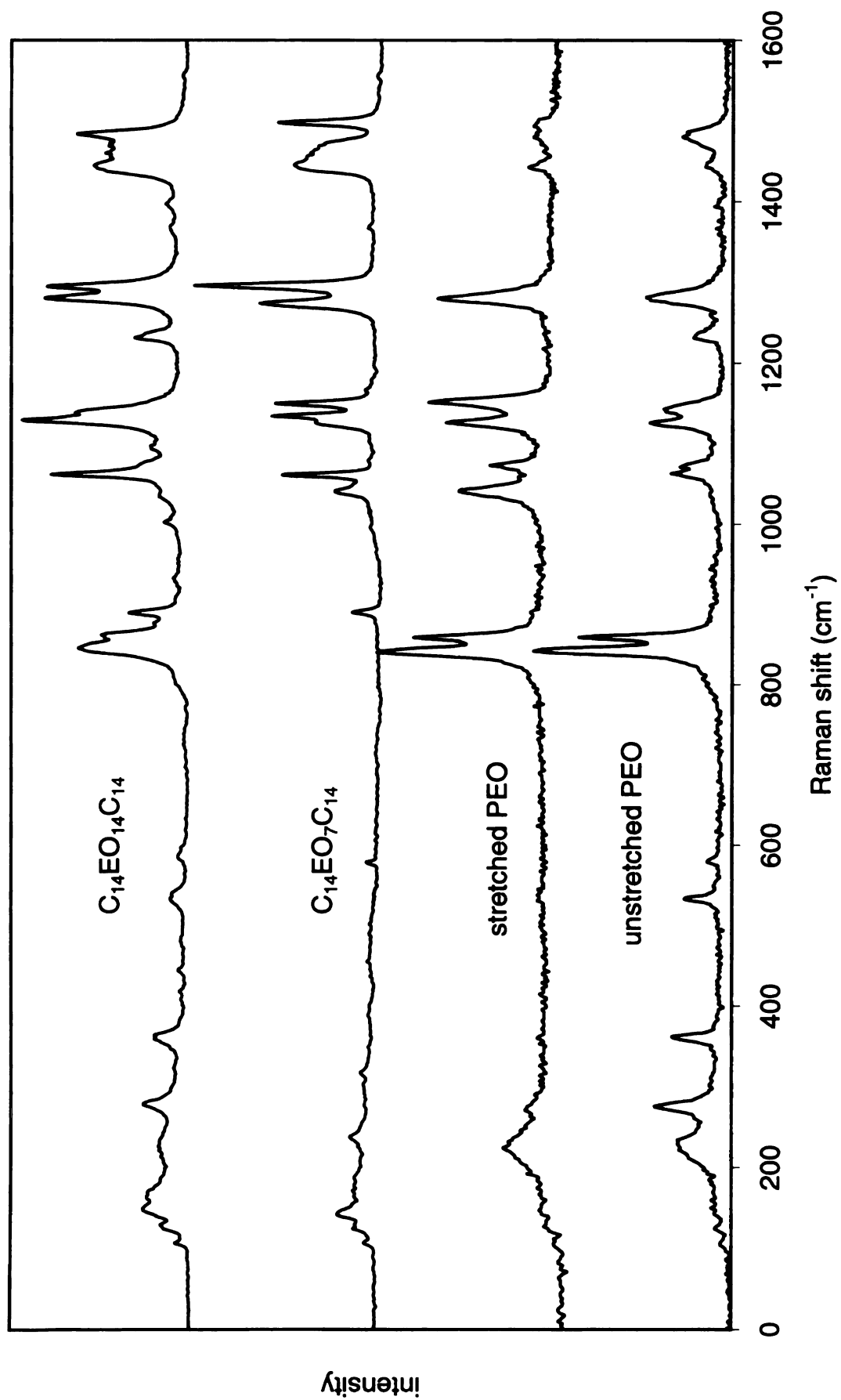


Figure 81. Raman spectra comparison between triblock oligomers and PEO.

4. Melting trends and odd-even effects in triblock oligomers

The melting points for the series of ABA triblock oligomers are plotted in **Figure 82**. For samples with more than one melting transitions, the highest melting transition temperature was used since it corresponds to the thermodynamically more stable crystal. For a given length of alkyl group, the melting points of a series of ABA amphiphiles show a weak dependence on the length of the PEG segment when $x \geq 10$. In contrast, increasing the length of the alkyl chain by two carbon atoms shifts the melting points for a series to higher temperatures due to the low PEO fraction in these oligomers. The trend in melting points is similar to that of the *n*-alkanes. For example, the melting points of $C_8EO_7C_8$ and $C_{10}EO_7C_{10}$ are 9 and 22 °C; the corresponding melting points for C_{16} and C_{20} are 18 and 38 °C. When ethylene oxide fraction is higher ($x \leq 8$), it will play a more important role in determining the oligomer's melting point. As the ethylene oxide segment becomes longer, the melting points of the oligomers with different alkyl chain length get closer. It is believed that when the ethylene oxide segment is long enough, the melting points will finally converge to a temperature that is very close to the melting point of pure PEO.

Another feature of the melting point data is the oscillation of the melting points within a series. ABA molecules with odd values of *y* have systematically higher melting points than those where *y* is even when $x \leq 12$ or $y \leq 6$. Odd even effects are commonly seen in the melting points of *n*-alkanes and molecules like liquid crystals, where chromophores or mesogens are linked with short alkyl chains in a planar zigzag conformation. In the ABA oligomers, the odd-even effect originates in the PEG segment, where an odd number of EO units correspond to an even number of oxygen atoms and a

relatively high melting point. The odd-even effect can be understood by treating the oxygen atoms in the chain as defects in a linear alkane caused by the difference in the C-O-C bond angle relative to that of the C-C-C bond angle. Because the ABA chains adopt a planar zigzag conformation when $y \leq 7$, successive oxygen atoms are *anti* to each other, effectively canceling the distortions. Thus, ABA amphiphiles with odd values of y are more linear and have higher melting points. When the alkyl chains are longer, the bending of the molecule can be better accommodated with a series of small distortions along the alkyl chain. The molecule looks more linear when the alkyl chains are longer. A calculated result is shown in **Figure 83**: oligomer $\text{C}_8\text{EO}_4\text{C}_8$ bends 3° throughout the molecule while oligomer $\text{C}_{16}\text{EO}_4\text{C}_{16}$ only bends 1° .

The odd-even effect can also be seen from trends in the heats of fusion for the oligomers. Theoretical heat of fusion values were estimated by a linear combination of PE and PEO's heat of fusion based on their mole fractions. The heat of fusion for PE is $7.70 \text{ kJ/mol}^{172}$ and the heat of fusion for PEO is $8.04 \text{ kJ/mol}^{172}$. Since no heat of fusion for planar zigzag PEO is available, we instead used the value for PEO. This may cause some error in the estimation, but the trend for the series should hold. The calculated and the measure heats of fusion are listed in **Table 16**. To better illustrate the odd-even effect trend, the percentage difference in the calculated and experimental heats of fusion values are plotted in **Figure 84** versus number of ethylene oxide units for oligomers $\text{C}_8\text{EO}_y\text{C}_8$ and $\text{C}_{14}\text{EO}_y\text{C}_{14}$. The odd-even effect in oligomers with 8 carbon alkyl chains is obvious. The experimental heats of fusion of oligomers with odd number ethylene oxide are closer to the calculated value than those with even numbers. This again can be explained by a planar zigzag PEO conformation in the oligomer. The

oligomers with odd number of ethylene oxide are more linear which enables them to pack better in the crystal structure, thus higher heats of fusion. This trend is lost for oligomers with longer alkyl chains because the long chains can achieve a linear structure through small changes in the bond angles of the alkyl chains.

Table 16. Calculated and measured heats of fusion* for $C_xEO_yC_x$ oligomers.
(kJ/mol)

	x					
y	6	8	10	12	14	16
2	55/27	70/35	85/62	101/79	116/89	132/105
3	63/47	78/57	93/67	109/94	124/105	140/124
4	71/38	86/54	101/65	117/93	132/111	148/105
5	79/45	94/70	110/78	125/103	140/117	156/127
6	87/37	102/57	118/81	133/103	148/121	164/123
7	95/48	110/68	126/87	141/95	156/118	172/142
8	103/44	118/65	134/91	149/107	164/117	180/88
10	119/86	134/80	150/100	165/106	181/128	196/107
14	151/102	166/98	182/118	197/120	213/132	228/145

* the value on top is calculated, while the bottom number is from DSC measurements.

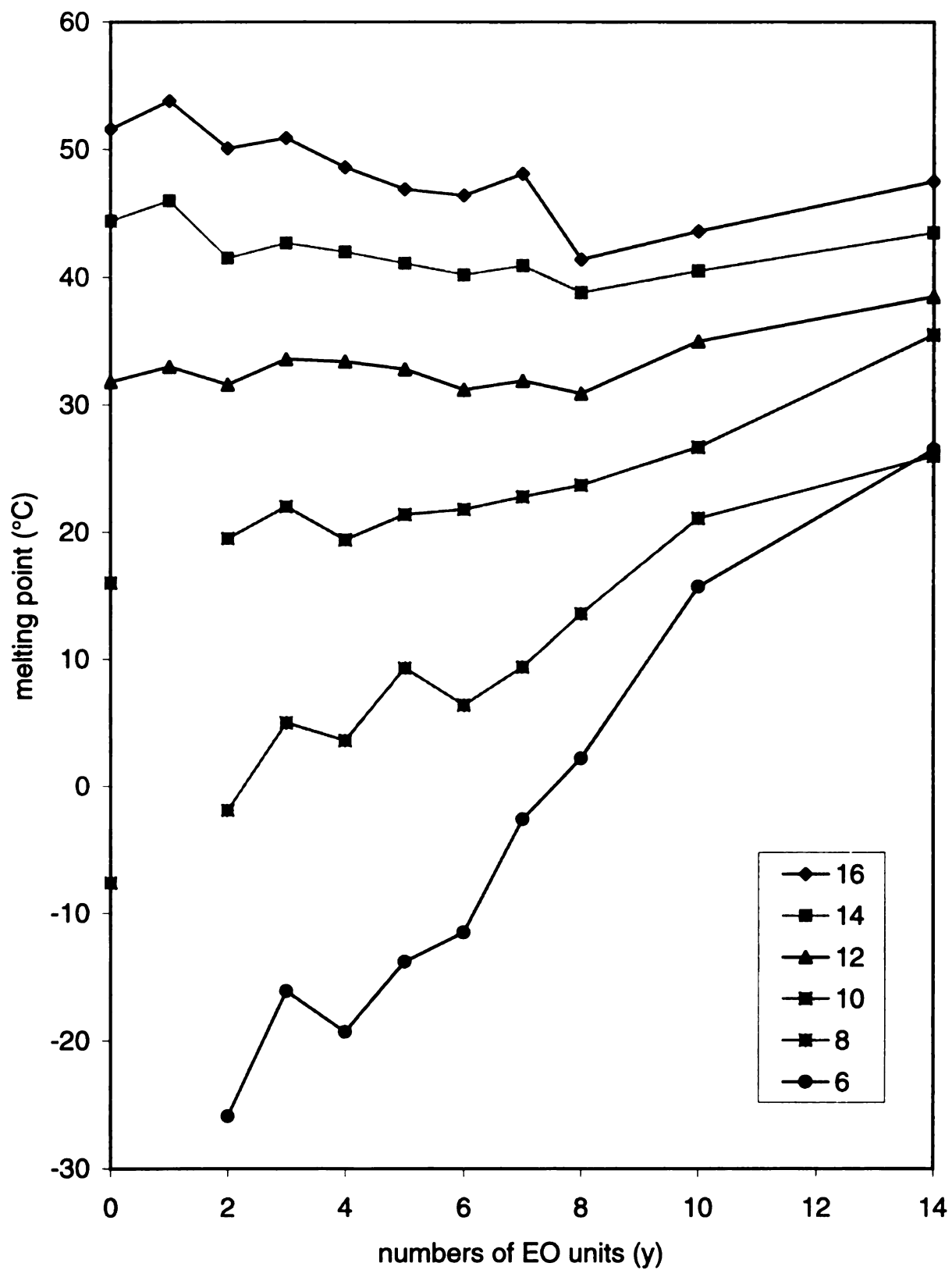


Figure 82. Melting points of $C_xEO_yC_x$ triblock oligomers. The numbers in the inset are the values of x for the compounds.



Oligomer $\text{C}_8\text{EO}_4\text{C}_8$ bend about 3° throughout the chain



Oligomer $\text{C}_{16}\text{EO}_4\text{C}_{16}$ bend about 1° throughout the chain

Figure 83. Bending of the triblock oligomers caused by the angle difference in C-C-C and C-O-C.

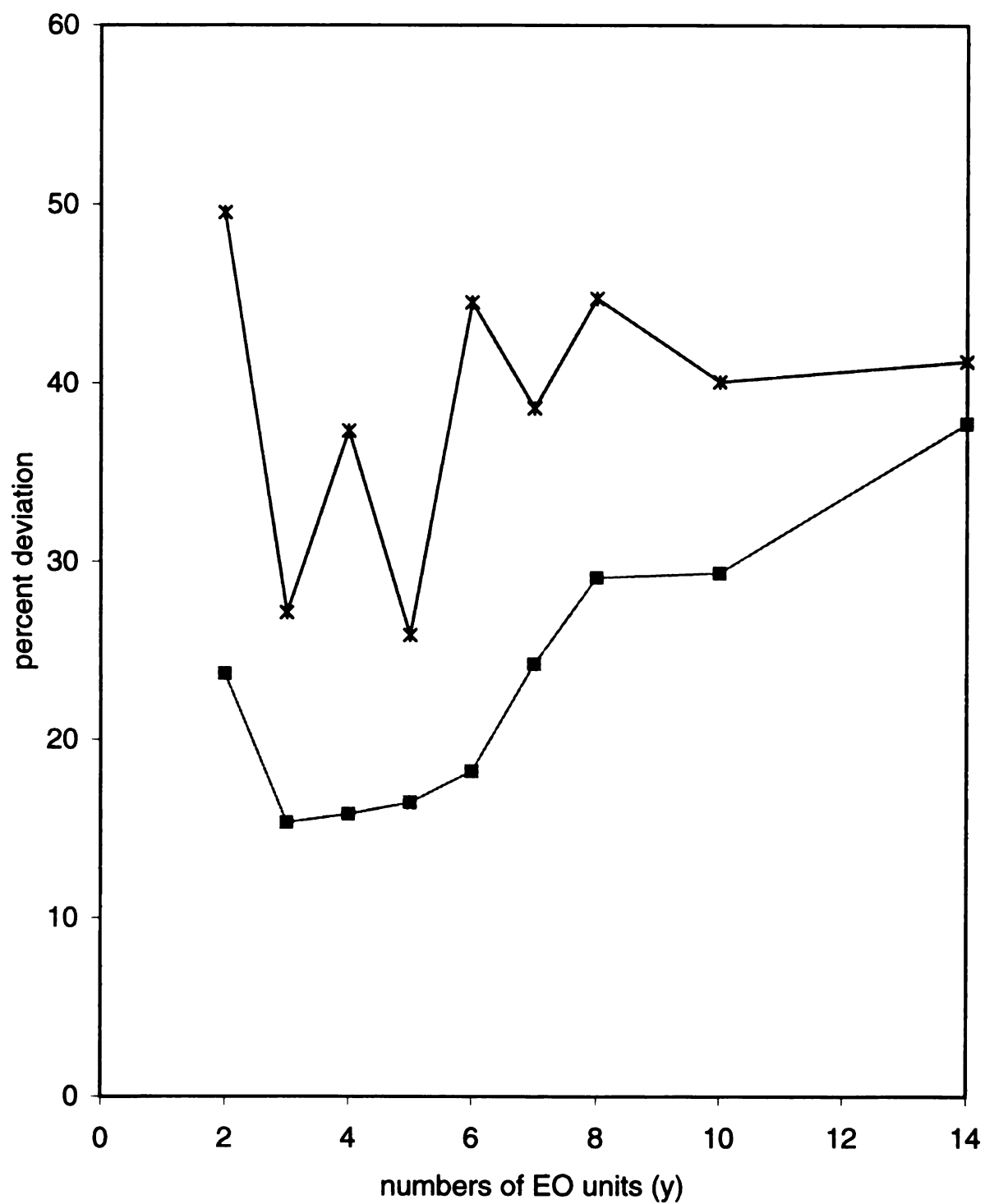


Figure 84. Percent heat of fusion deviation versus numbers of ethylene oxide units of oligomers $C_8EO_yC_8$ (top) and $C_{14}EO_yC_{14}$ (bottom).

III. Structure and properties of $(AB)_n$ microblock copolymers

1. Melting point trend compare to the triblock oligomers

In **Figure 85**, the melting points of polymer $(C_{10}EO_y)_n$ and its unsaturated analog $(C_4\pi C_4EO_y)_n$ are plotted together with model compounds $C_6EO_yC_6$ and $C_{10}EO_yC_{10}$. The melting points of unsaturated polymers with short ethylene oxide segment show an odd-even effect that tracks that of the model compounds, but deviate from the model compounds when the ethylene oxide segment is longer. On the other hand, the melting points of the saturated polymers deviate from the model compounds when $y = 2$ and 3 , but then follow closely the model compounds. A weak odd-even effect is seen to $y = 8$.

In the unsaturated polymers, the double bond is actually acting as a breaking point for the polymer repeat units since the regular molecular conformation is disrupted at the double bonds. The polymer can be thought of as a series of triblock oligomers with short alkyl chains linked by the carbon carbon double bonds. Therefore, the repeat unit looks more like $C_5EO_yC_5$. This explains why the unsaturated polymers behave more like the compounds $C_6EO_yC_6$ rather than like $C_{10}EO_yC_{10}$. By analogy, the unsaturated polymer with $y \leq 5$ should have conformation with a planar zigzag conformation in all the atoms but the double bond carbons. The odd-even effect originates from the trans PEO conformation. When the PEO segment is longer, the polymer melting points deviate from that of the model compounds, meaning that they may have different structures than the model compounds.

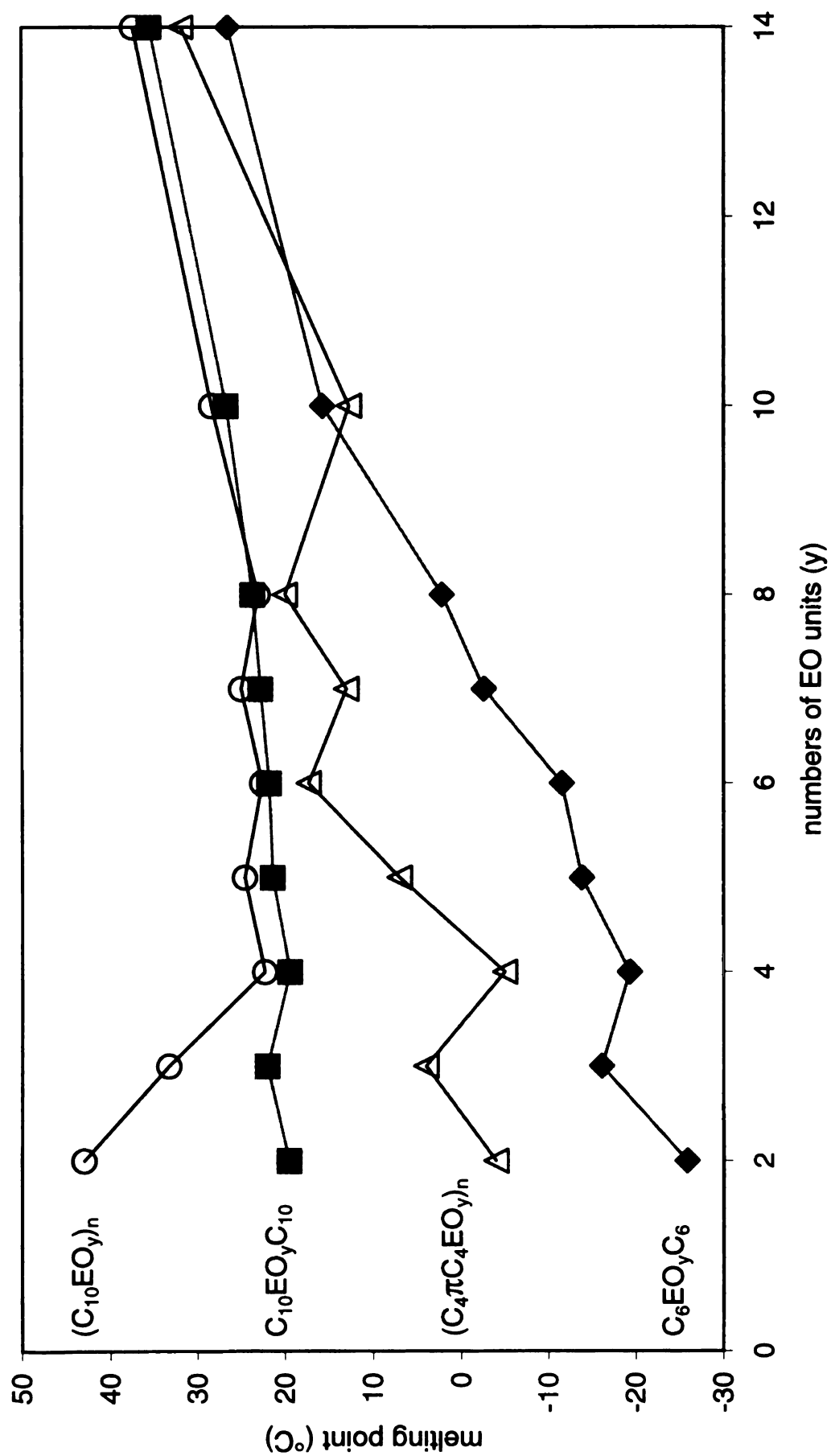


Figure 85. Melting points vs. numbers of ethylene oxide units of triblock oligomers and polymers.

In the saturated polymers, the double bonds are removed, and there are no defects in the molecules. The polymer chain can pack just like the model compounds. When the PEO segments are very short, they played a small role in crystallization, and the microblock copolymers behave more like a PE homopolymer. Therefore, the melting points of these polymers actually are more like those of long chain *n*-alkanes, which will be higher than those of the model compounds. When the ethylene oxide segment is longer, real diblock properties start to show. The polymers are more like a serial connection of the corresponding model compounds. The melting point trend now follows exactly that of the model compounds.

These resemblance of the polymers to model triblock oligomers validates our use of these oligomers to study the polymer properties. The properties of these oligomers can help explain the complicated properties of structurally similar crystalline $(AB)_n$ microblock copolymers and provide molecular design rules for the preparation of crystalline polymers with defined crystalline structures.

2. Polymer structure controls

Now that we know that the polymers resemble to a certain extent the triblock oligomers, we would like to see if we could use the same method to manipulate the PEO conformation in the polymers.

The unsaturated polymer $(C_9\pi C_9EO_y)_n$ was crystallized from the melt, methanol and hexane. The samples were studied with FTIR and XRD. The IR spectra shown in **Figure 47** for all samples are basically the same. The IR bands indicate that the PEO segments in this polymer are in a helical conformation. The XRD results (**Figure 58** and **59**) show that they all have very similar d-spacings, 42.4 Å, although the wide angle

XRD show some differences in details of the XRD pattern. It seems that the PEO conformation manipulations that were used in the model system failed for this unsaturated polymer.

The unsaturated polymer was then reduced to its saturated analog, $(C_{20}EO_7)_n$, and was crystallized from methanol and hexane. For this sample, XRD shows no long d-spacing feature. However, in IR spectra, we do observe distinct differences. As shown in **Figure 71**, both spectra have bands at 718 cm^{-1} , an indication of planar zigzag packing for PE. The major differences are the bands between 1185 and 1085 cm^{-1} . Samples crystallized from hexane show two equal intensity bands at 1144 and 1115 cm^{-1} , very similar to the absorptions in the unsaturated polymer and model compounds with a helical PEO conformation. Therefore, this sample should have helical PEO segments. For the sample crystallized from methanol, the peak at this region is basically a singlet, and the sample should have a planar zigzag PEO conformation.

To understand why the conformation control experiment could not get the desired result for the unsaturated polymer, we have to study the detailed structure of the polymer. Compared to the model compound, the major structural difference in this unsaturated polymer is that there is a double bond in the middle of every alkyl segment. Since this double bond can not have the same conformation as the rest of the alkyl chain, it acts as a defect for the alkyl segment packing. As shown in **Figure 86**, double bonds lead to some voids in the packing of the unsaturated polymer chains even if they are all in trans configuration. The polymer still has about 15% of the double bonds with a cis geometry, which can worsen the packing situation. Recall the mechanism for the crystallization of model compound in polar solution, where the alkyl chains crystallize first and then

provides a template that essentially locks the PEO into the planar zigzag conformation. It is impossible for that to happen in the unsaturated polymer with the poor packing caused by double bond defects. With the void in the system, the alkyl chains can not pack tightly and therefore when the PEO segments crystallize, there are enough spaces for them to adopt their preferred helical conformation. Not surprisingly, when the double bonds are removed, all the template effects work the same as in the model compounds and PEO segments with different conformation were obtained. The deviation caused by the unsaturation already showed in the comparison of their melting points with model compounds. When the PEO segments are longer than 6 repeat units, instead of increasing a little like in the model compounds, the melting points of the unsaturated polymers jumped to a new level that is closer to those in the model compounds with longer alkyl segments (**Figure 85**). It is believed that the PEO segments take charge of the crystal melting point when $y \geq 6$.

For all of the samples of $(C_9\pi C_9EO_y)_n$ crystallized with different methods, XRD showed a long d-spacing of 42.4 Å which indicated that there is some periodicity in this range. Since we already know that the PEO segments are in a 7_2 helix, we estimate the periodicity of the polymer chain given a helical PEO conformation. One of the obvious repeating periods in this molecule is the repeating pattern of the segments between two double bonds. The calculated distance from the first double bond carbon to the second double bond carbon in the next repeat unit is longer than the 42.4 Å d-spacing. We estimated the packing by treating the unsaturated polymer the same way as in the model compounds by tilting the alkyl chains with respect to the PEO helix axis. As shown in **Figure 87**, by tilting the alkyl chains 23° relative to PEO helix axis, the d-spacing agrees

well with the repeating distance of the polymer between two double bonds. It is also good to see that the tilt angle is very close to that in the model compound. The hypothetical packing model of the unsaturated polymers is shown in **Figure 88**. When the polymer is reduced, the periodicity of the double bonds is lost, and the d-spacing for the polymer should correspond to the lamellar thickness of the polymer crystal which is in the order of hundreds of angstroms. This distance is outside the range of the XRD measurement we used. No distinct feature in our measuring range can be ascribed to the long spacing.

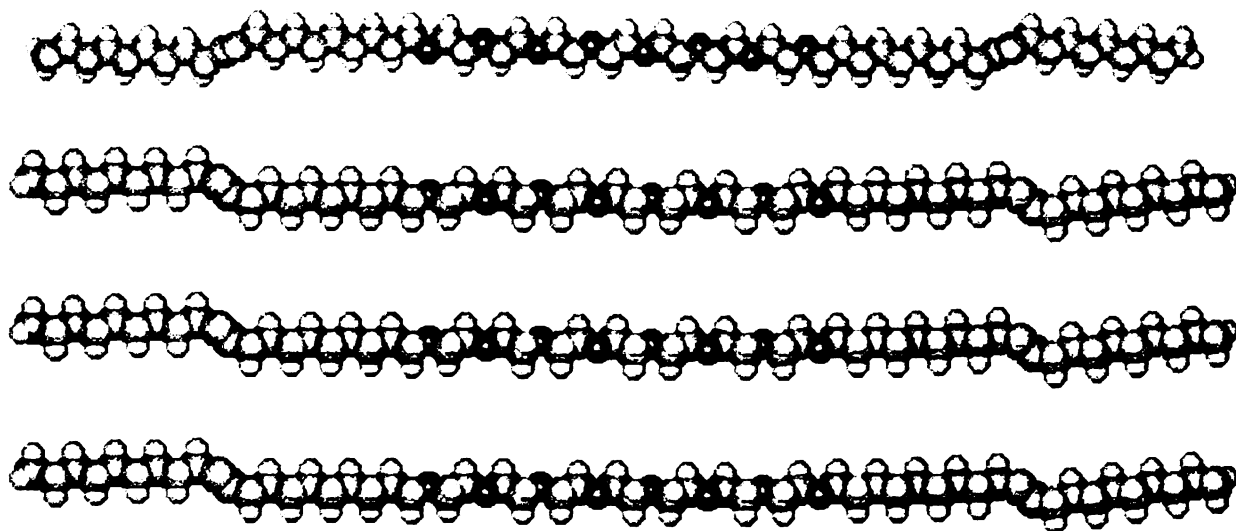


Figure 86. Packing of unsaturated polymers $(C_9\pi C_9EO_y)_n$ with a planar zigzag PEO conformation.

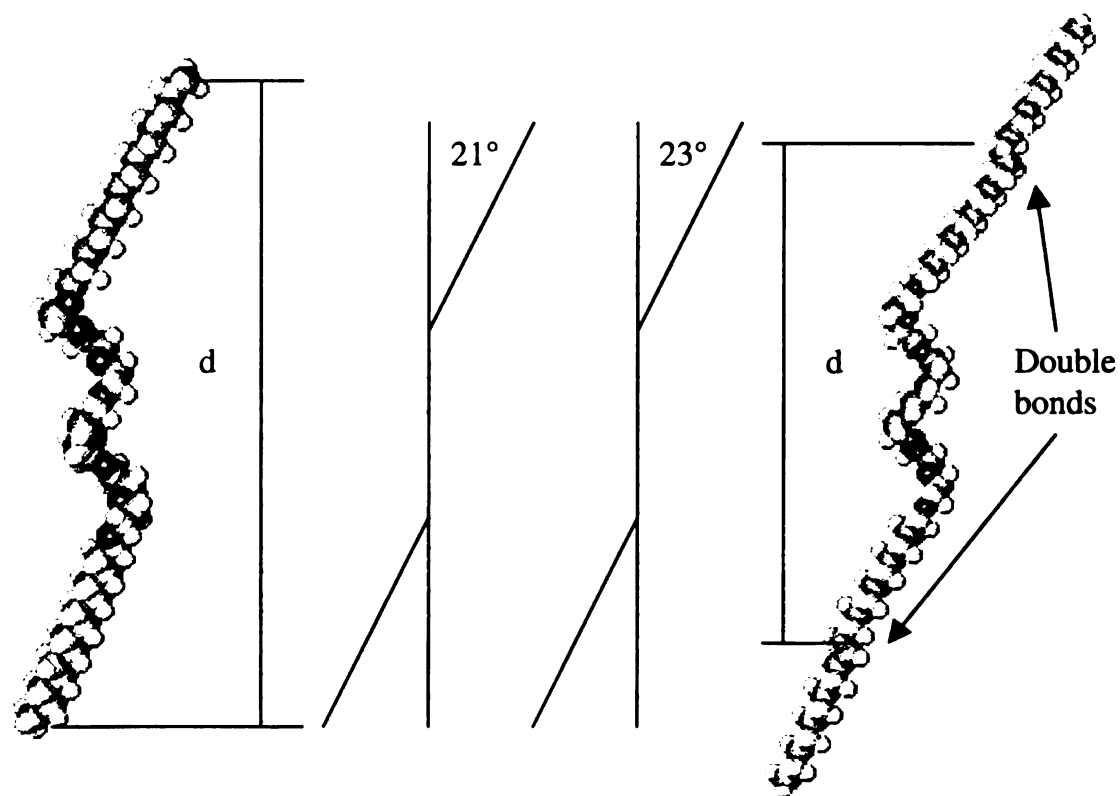


Figure 87. Comparison of model compound $C_{14}EO_7C_{14}$ and polymers $(C_9\pi C_9EO_y)_n$.

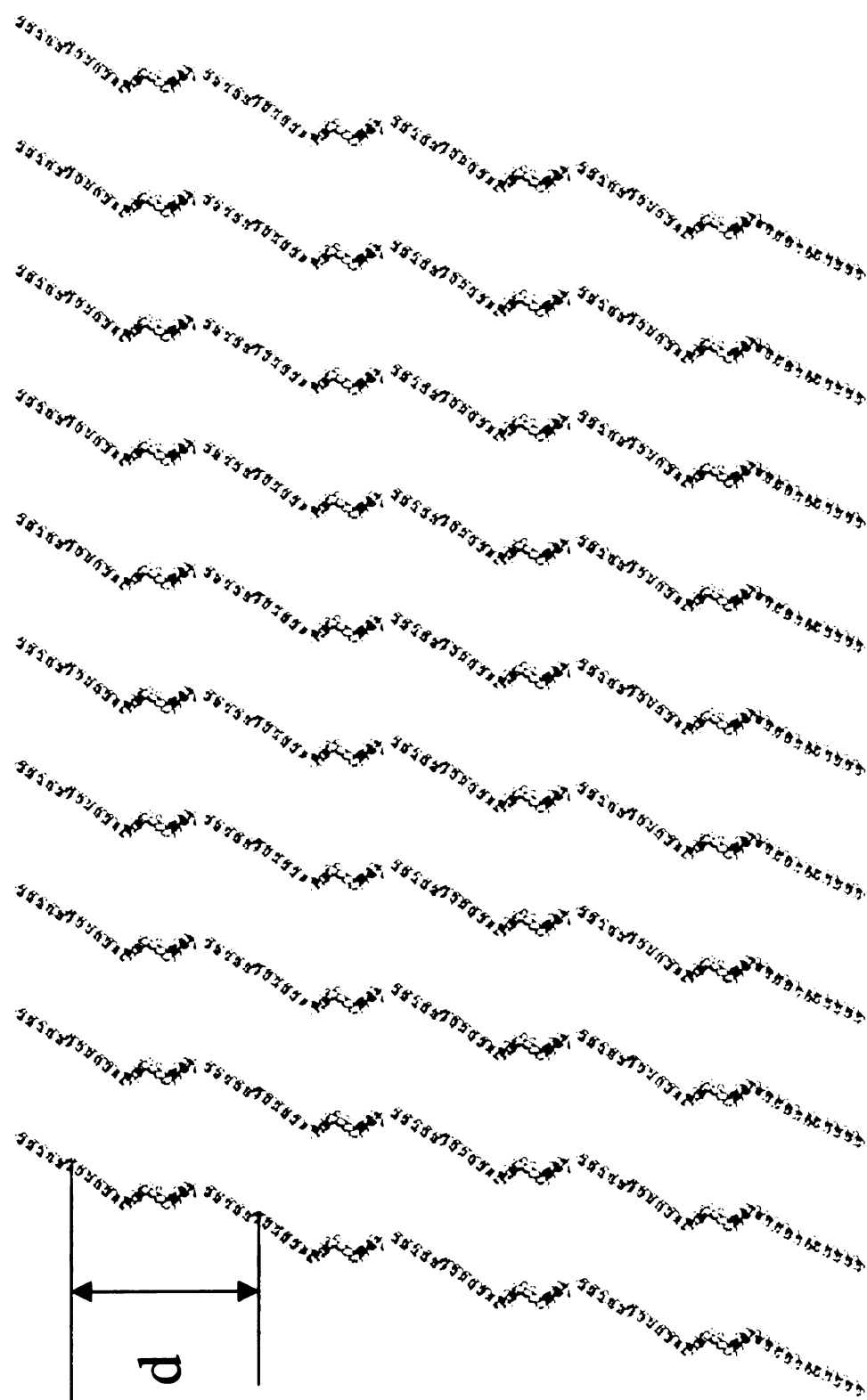


Figure 88. Packing model of unsaturated polymers $(C_9\pi C_9EO_y)_n$ in crystalline state

3. Multiple thermal transitions of the polymers

Multiple transitions are seen for both saturated and unsaturated polymers, especially when the PEO segments are short (see **Figures 48-51** collectively). For polymers, there are two possible explanations for this behavior—lamellae thickening and thinning caused by chain folding, and polymorphism.

Since the multiplicity of the DSC endotherms disappeared when the ethylene oxide segments become longer, it is likely that the multiple transitions are originated from the PEO segments. In our low temperature XRD experiments (**Figure 61 and 73**), we tried to observe changes for the polymers at different stages similar to the heating process in DSC experiments. Peaks emerged as crystallization occurred during the experiments. The peaks were similar in pattern to the PEO diffraction and the pattern remained the same throughout the heating process before melting with very small shifts in position. We think the crystal packing pattern is not changed significantly during the transitions. This may let us infer that the transitions belong to lamellae thickening or thinning since only they will substantially change the longer d-spacings without much effect on the packing patterns. The process could also belong to the transformation of non-integer folded to integer folded lamellae. One of the transformations in the annealing of polymer $(C_{10}EO_6)_n$ and $(C_{10}EO_7)_n$ can probably be ascribed to this change. For example, polymer $(C_{10}EO_7)_n$ shows (in **Figure 67**) a melting transition that peaks at 15 °C after cooling at 10 °C/min. However, during the annealing at 0 °C, this peak disappeared and was replaced by a transition at 9 °C. Annealing usually generates crystals with better packing and higher melting transition. Cheng *et al.*^{117-122,173} reported for a series of PEO samples, that mainly non-integer folded crystals were

generated during fast cooling or low temperature crystallization. These crystals can be annealed to integer folded crystals during annealing process. The lamellar thickness can either increase or decrease during this process. As the crystallization temperature increased, the formation of the higher melting crystal with least folding increased. However, at a certain crystallization temperature, formation of the high melting crystal was depressed which is very similar to our polymer case. We think that these transitions correspond to lamellar thinning or thickening. The crystal at 15 °C corresponds to a folded crystal that converted to a thinner lamellar thickness crystal that melts at 9 °C. We should be able to see the long d-spacing change during this process, however, the thickness of the polymer lamellae is outside the range of our XRD, and we were not able to see this shifting.

Polymorphism can not be excluded at this stage since in model compounds, crystals were in fact obtained with different melting points that originated from different conformations of the molecular structures. Giving the good resemblance of the melting point trends of the polymers and model compounds, similar transformations may also occur in the polymer. Further experiments are needed to fully clarify the nature of these transitions.

IV. Comparison to other structurally similar (AB)_n copolymers

The polymers prepared in this work are most closely related to the thioethylene-segmented polymers (C_xES_y)_n prepared by Mathias *et al.*^{144,145} which differ structurally only in that oxygen has been replaced by sulfur. For these polymers, a single exothermic transition was observed between two endothermic transitions, and polarized optical

microscopy indicated that at least some order was maintained up to the highest melting transition. A series of model compounds ($C_{10}ES_yC_{10}$) were prepared and studied to elucidate the structural transformations detected by DSC and microscopy. Vibrational spectroscopy studies of the model compound with the shortest thioethylene segment, $C_{10}ES_1C_{10}$, showed that it adopted a trans conformation for the thioethylene core, just as we observed for the oxygenated analogs. However, the remaining compounds reveal crucial differences between the oxyethylene and thioethylene systems. The x-ray diffraction patterns of the $C_{10}ES_yC_{10}$ series show no distinct low angle reflections that can be attributed to a lamellar structure, and thus the details of the packing arrangement must be different. In addition, two melting transitions are observed for the $C_{10}ES_3C_{10}$ and $C_{10}ES_4C_{10}$ model compounds. Based on solid state NMR experiments, planar structures were assigned for these models in the temperature range between the two melting transitions. At room temperature, (below the lowest melting transition), vibrational spectroscopy and NMR data indicate that the thioethylene segments are increasingly dominated by gauche conformations as the length of segments increase. Consistent with that assignment is the absence of an odd-even effect for the melting points of the polymers and model compounds, one of the signatures of the planar trans conformation seen in the oxygenated compounds. The greater tendency to form helical conformations in the thioethylene system has been ascribed to strong dipolar interactions between C-S-C groups in adjacent chains.¹⁴⁷

In contrast, the fluorinated $(AB)_n$ polymers of Griffin *et al.*^{160,161} exhibit fundamentally different physical characteristics. Studies of the polymers and model compounds¹⁶⁰ show that the fluorocarbon segments are stiff due to the steric

stabilization of a helical structure for the $(CF_2)_n$ segment. This rigidity leads to mesophase formation that extends from the melting point of the alkyl segments to the eventual melting (disordering) of the fluorocarbon segments. Thus, fluorinated $(AB)_n$ microblock copolymers correspond to a combination of hard and soft blocks analogous to thermoplastic polyurethanes, while the oxyethylene $(AB)_n$ system should be viewed as a combination of flexible blocks. The conformational issues of the thioethylene and oxyethylene $(AB)_n$ microblocks also are absent in the fluorinated systems; the methylenes adopt a planar trans zig-zag conformation as expected and because of the homogeneous character of the $(CF_2)_n$ segment, discussions about gauche conformations are replaced by those of helix formation and periodicity.

EXPERIMENTAL

I. General Details

Unless otherwise specified, ACS reagent grade starting materials were used as received from commercial suppliers. The reported melting points and boiling points are uncorrected. Glassware used for the synthesis of Schrock's molybdenum catalyst and ADMET polymerizations were soaked in a potassium hydroxide/ethanol base bath overnight, thoroughly rinsed with distilled water, and oven dried at 140 °C.

Proton and carbon nuclear magnetic resonance (^1H and ^{13}C NMR) analyses were carried out at room temperature in CDCl_3 on a Varian Gemini-300 spectrometer. The chemical shifts were calibrated using residual CHCl_3 in the solvent and are reported relative to tetramethylsilane. Infrared (IR) spectra for samples in solution were recorded as CCl_4 solutions under nitrogen at room temperature on a Nicolet IR/42 Fourier Transform IR spectrometer. The spectrum of each pure compound was obtained by subtracting the CCl_4 spectrum from that of the solution. Infrared spectra of solid samples were measured on films prepared by evaporating a solution to dryness on a polished (19.4 mm diameter, 1.8 mm thick) silicon disk. The spectrum for each pure sample was obtained by subtracting the silicon spectrum from that of the sample plus substrate.

Molecular weights of polymer samples were determined by gel permeation chromatography (GPC) using a PLgel 20m Mixed A column at room temperature with THF as eluting solvent at a flow rate of 1 mL/min. The concentration of the polymer

samples were 1 mg/mL. Detection was by a Waters R410 Differential Refractometer and the results were calibrated with monodisperse polystyrene standards.

1. Thermal characterization of model compounds and polymers.

Thermogravimetric analyses (TGA) of the polymers were obtained from a Perkin Elmer TGA 7 instrument at a heating rate of 10 °C/min, usually in the temperature range of 30 to 800 °C. DSC analyses of model compounds, monomers and polymers were performed in aluminum pans under a helium atmosphere on a Perkin Elmer DSC 7 instrument, two-point calibrated with indium and hexyl bromide standards. The coolant for the system was liquid nitrogen. Each sample was heated from room temperature to 100 °C at a rate of 10 °C/min, held at 100 °C for 5 minutes, quenched to -100 °C at a rate of 200 °C/min, heated to 100 °C at a rate of 10 °C/min, cooled to -100 °C at a rate of 10 °C/min, and heated to 100 °C at a rate of 10 °C/min. The glass transition temperature, T_g , was defined as midpoint temperature of the transition, and the melting point was taken as the onset of the peak of the melting endotherm. Sample crystallinity and melting points were studied by using a Nikon Optiphot2-POL polarizing optical microscope equipped with a Mettler FP82-HT hot stage. The reported melting point range from microscopy corresponds to the temperature where birefringence begins to be lost, and the temperature where the sample becomes isotropic. The latter temperature correlates well with the melting points determined by DSC. The heating rate used for melting point determination was 10°C/min. Heats of fusion were calculated from the endothermic peak using the accompanied functions of the DSC 7 software. Dynamic mechanical analyses of polymer samples were performed on a Perkin Elmer DMA 7 instrument, calibrated with an indium standard. DMA samples were held in a 8.5 mm diameter flat bottom

stainless steel cup and were probed with a 5 mm diameter flat top probe. DMA scans were run under a helium flow. The coolant for the system was a mixture of liquid nitrogen and dry ice.

XRD patterns were recorded on a Rigaku rotaflex 200B diffractometer equipped with a rotating anode, Cu K_{α} x-ray radiation ($\lambda = 1.541838 \text{ \AA}$) and a curved crystal graphite monochromator. The x-ray instrument was operated at 45 kV and 100 mA. Diffraction patterns were collected at 0.02° intervals between 1 and 15° values of 2θ at a scanning rate of 1° per minute and DS and SS slit widths of $1/6$, and between 15 and 45° values of 2θ at DS and SS slit widths of $1/2$. Powder samples were prepared by spreading solid samples on the window of the glass sample holder with a spatula, or by melting the sample directly on the window of the sample holder in an oven, and cooling the holder to crystallize the sample as a film. XRD samples for low temperature experiments were prepared by melting the polymer samples on the perforated copper sample holder and flash-cooling to low temperature by immersion into liquid nitrogen. The sample was installed while cold and the temperature was controlled at the desired value and the XRD was recorded for each temperature.

2. Solvents

Reagent grade diethyl ether was distilled from sodium benzophenone ketyl under nitrogen. Anhydrous dimethoxyethane (99.5%) was distilled from sodium benzophenone ketyl under nitrogen. Reagent grade pentane (4 L) was vigorously stirred over concentrated H_2SO_4 (300 mL), which was changed every 12 h until the acid remained colorless. The pentane was then stirred over a 500 mL solution of KMnO_4 (0.5 M) and H_2SO_4 (3.0 M) for one day. After separation from the aqueous phase, the pentane was

washed with distilled water (4×500 mL), saturated aqueous NaHCO₃ (500 mL) and distilled water (2×500 mL), and dried over anhydrous MgSO₄. The pentane was filtered and distilled from calcium hydride and then from sodium benzophenone ketyl under nitrogen. THF was dried first by distilling from calcium hydride and then from sodium benzophenone ketyl under nitrogen. Toluene was dried by distilling first from calcium hydride and then from sodium benzophenone ketyl under nitrogen.

3. Argon

Argon used in air-sensitive reactions was deoxygenated by passing it through a 60 cm (8 cm in diameter) Mn⁰/SiO₂ column. The raw column filling material is Mn(NO₃)₂ blended with silica gel (60 - 200 mesh). The quartz column was wrapped with a heating wire, filled with the raw filling material, and heated to at least 450 °C under a flow of hydrogen gas. The color of the filling material turned from black to brown to green, and moisture was evolved from the column. The generation process lasted about 10 h and was followed by switching the H₂ flow to argon for 2 h with continued heating. Traces of H₂O were removed by connecting the column to vacuum for 30 min. After it was used for a period of time, the filling material in the column turned from green to brown, and the column regeneration process was repeated.

4. Sodium mirrors

Sodium mirror coated Schlenk flasks were prepared by heating a piece of fresh sodium metal (0.2 g) inside a clean flask with a hot plate under high vacuum until the molten sodium vaporized and coated the walls of the flask.

5. Celite and Alumina packed funnel for monomer purification.

Celite[®] and Celite[®] acidic alumina mixtures (volume ratio 4/1) were dried in oven at 140 °C overnight. A Schlenk-style fritted funnel was packed with successive layers of Celite[®] (0.5 cm), Celite[®] and acidic alumina mixture (3 cm), Celite[®] (0.5 cm). The packed funnel was placed under vacuum until used.

II. Synthesis of chemicals in this project

1. Synthesis of ethylene glycol oligomer ditosylates

Diethylene glycol ditosylate [Ts(OCH₂CH₂)₂OTs, **2(2)**]. A solution of diethylene glycol (130 g, 1.22 mol) and *p*-toluenesulfonyl chloride (701 g, 3.66 mol) in THF (1.5 L) was placed in a 3 L three necked round bottom flask and stirred magnetically. The flask was cooled with an ice/water bath, and a solution of KOH (450 g, 8.00 mol) in water (500 mL) was added slowly over a period of 1h. The ice-water bath was removed and the system was stirred for additional 7h. The resulting suspension was poured into a mixture of 1 L CH₂Cl₂ and 500 mL ice water and the aqueous layer was extracted with 2 250 mL portions of CH₂Cl₂. The combined organic solutions were washed three times with distilled water, and dried over MgSO₄ overnight. After removal of MgSO₄ and solvent, the solid was recrystallized twice from methanol to give 89% yield of **2(3)** as a white crystalline product. ¹H NMR (300 MHz, CDCl₃) δ 7.76 (d, 4H), 7.33 (d, 4H), 4.07 (t, 4H), 3.59 (t, 4H), 2.43 (s, 6H). mp 87.5-88.5 °C. (lit.¹⁷⁴ 87-87.5 °C).

Triethylene glycol ditosylate [$\text{Ts}(\text{OCH}_2\text{CH}_2)_3\text{OTs}$, **2(3)**]. **2(3)** was prepared similarly to give 87% yield of a white crystalline solid. ^1H NMR (300 MHz, CDCl_3) δ 7.77 (d, 4H), 7.32 (d, 4H), 4.12 (t, 4H), 3.63 (t, 4H), 3.51 (s, 4H), 2.43 (s, 6H). mp 80-81 °C. (lit.¹⁷⁴ 80-81 °C).

Ditosylates for $y = 4 - 10$ [$\text{Ts}(\text{OCH}_2\text{CH}_2)_y\text{OTs}$, **2(y)**]. Ditosylates **2(y)** for $y = 4 - 10$ was prepared the same way as diethylene glycol ditosylate. After the reaction was finished, 200 mL ice water was added, the solution was separated and the aqueous layer was extracted with diethyl ether (3×100 mL). The combined organic solutions were washed with saturated aqueous NaCl solution (3×200 mL) and dried over MgSO_4 overnight. After removal of MgSO_4 and solvent, a clear colorless to light yellow viscous liquid was obtained. The product is pure enough for further use.

Tetraethylene glycol ditosylate [$\text{Ts}(\text{OCH}_2\text{CH}_2)_4\text{OTs}$, **2(4)**]. Yield 99%. Clear colorless oil.¹⁷⁵ ^1H NMR (300 MHz, CDCl_3) δ 7.78 (d, 4H), 7.32 (d, 4H), 4.12 (t, 4H), 3.65 (t, 4H), 3.57 (s, 4H), 3.54 (s, 4H), 2.43 (s, 6H).

Pentaethylene glycol ditosylate [$\text{Ts}(\text{OCH}_2\text{CH}_2)_5\text{OTs}$, **2(5)**]. Yield 99%. Clear colorless oil.¹⁷⁶ ^1H NMR (300 MHz, CDCl_3) δ 7.78 (d, 4H), 7.32 (d, 4H), 4.12 (t, 4H), 3.65 (t, 4H), 3.57 (s, 4H), 3.55 (s, 8H), 2.43 (s, 6H).

Hexaethylene glycol ditosylate [$\text{Ts}(\text{OCH}_2\text{CH}_2)_6\text{OTs}$, **2(6)**]. Yield 99%. Clear colorless oil.¹⁷⁷ ^1H NMR (300 MHz, CDCl_3) δ 7.78 (d, 4H), 7.32 (d, 4H), 4.12 (t, 4H), 3.65 (t, 4H), 3.58 (s, 4H), 3.55 (s, 12H), 2.43 (s, 6H).

Heptaethylene glycol ditosylate [Ts(OCH₂CH₂)₇OTs, 2(7)]. Yield 99%. Clear colorless oil. ¹⁷⁸ ¹H NMR (300 MHz, CDCl₃) δ 7.78 (d, 4H), 7.32 (d, 4H), 4.12 (t, 4H), 3.65 (t, 4H), 3.56 (m, 20H) 2.43 (s, 6H).

Octaethylene glycol ditosylate [Ts(OCH₂CH₂)₈OTs, 2(8)]. Yield 99%. Clear colorless oil. ¹⁶⁵ ¹H NMR (300 MHz, CDCl₃) δ 7.78 (d, 4H), 7.32 (d, 4H), 4.12 (t, 4H), 3.65 (t, 4H), 3.56 (m, 24H) 2.43 (s, 6H).

Decaethylene glycol ditosylate [Ts(OCH₂CH₂)₁₀OTs, 2(10)]. Yield 98%. Clear colorless oil. ¹H NMR (300 MHz, CDCl₃) δ 7.78 (d, 4H), 7.32 (d, 4H), 4.12 (t, 4H), 3.65 (t, 4H), 3.56 (m, 32H), 2.43 (s, 6H).

Tetradecaethylene glycol ditosylate [Ts(OCH₂CH₂)₁₄OTs, 2(14)]. Ditosylate 2(14) was prepared as described for tetraethylene glycol ditosylate except the reaction time was extended to 16 hours. After the reaction was finished, a mixture of 10/1 CH₂Cl₂ and ice water was added to the reaction mixture until the solids dissolved. The organic layer was separated, and the aqueous layer was extracted with CH₂Cl₂ (3 × 100 mL). The combined organic solutions were washed with saturated NaCl solutions (3 × 200 mL) and dried over Na₂SO₄ overnight. Removal of Na₂SO₄ and solvent gave a clear, colorless, viscous liquid product in 97% yield. ¹H NMR (300 MHz, CDCl₃) δ 7.78 (d, 4H), 7.32 (d, 4H), 4.12 (t, 4H), 3.65 (t, 4H), 3.56 (m, 48H), 2.43 (s, 6H).

2. Ethylene glycol oligomer monotritylates and ditritylates.

Diethylene glycol monotritylate [Tr(OCH₂CH₂)₂OH, 3(2)]. A 500 mL three neck round bottom flask equipped with a mechanical stirrer, thermometer, and nitrogen

inlet was charged with di(ethylene glycol) (106 g, 1.00 mol) and pyridine (11.9 g, 0.150 mol). With the mixture heated and maintained at 45°C, powdered trityl chloride (27.9 g, 0.100 mol) was added to the reaction mixture under vigorous stirring. After stirring at 45 °C for 16 h, the suspension was filtered and the white solid was washed with distilled water (5 × 50 mL). The crude product was recrystallized from isopropanol and twice from 2/1 EtOAc/hexanes to give a white crystalline solid. Yield 71%. ¹H NMR (300 MHz, CDCl₃) δ 7.46 (d, 6H), 7.25 (m, 9H), 3.58-3.77 (m, 6H), 3.24 (t, 2H), 2.06 (t, 1H). mp 113.0-114.5 °C (lit.¹⁶⁵ 112.7-114.5°C).

Triethylene glycol monotritylate [Tr(OCH₂CH₂)₃OH,]. **3(3)** was prepared as describe for diethylene glycol monotritylate. After the reaction was finished, the reaction mixture was poured into a separatory funnel and an equal volume of distilled water was added. The mixture was shaken vigorously, and allowed to settle for 2 hours. The bottom layer was separated from the aqueous solution, and the aqueous solution was extracted with toluene (3 × 50 mL). The product was dissolved in toluene and combined with the toluene extract. The toluene solution was washed with distilled and dried over MgSO₄ overnight. Removal of the solid and solvent gave a yellow viscous gel-like liquid¹⁷⁹ in 99% yield. The product was used for next reaction without further purification. ¹H NMR (300 MHz, CDCl₃) δ 7.46 (d, 6H), 7.25 (m, 9H), 3.59-3.75 (m, 10H), 3.22 (t, 2H), 1.70 (s, 1H).

Tetraethylene glycol monotritylate [Tr(OCH₂CH₂)₄OH,]. **3(4)** was prepared and purified as describe for **3(4)** to give a yellow viscous gel-like liquid¹⁸⁰ in 99% yield.

^1H NMR (300 MHz, CDCl_3) δ 7.46 (d, 6H), 7.20-7.45 (m, 9H), 3.25-3.15 (m, 12H), 3.12-3.08 (t, 2H), 3.26 (t, 2H), 2.35 (s, 1H).

General procedure for the preparation of ditritylates. Heptaethylene glycol ditritylate [$\text{Tr}(\text{OCH}_2\text{CH}_2)_7\text{OTr}$, **4(7)].** A 500 mL Schlenk flask with an argon inlet was charged with NaH (3.00 g, 0.125 mol). A solution of diethylene glycol monotritylate (34.8 g, 0.100 mol) in 200 mL THF was added dropwise and the mixture was stirred for 24 h. $\text{Ts}(\text{OCH}_2\text{CH}_2)_3\text{OTs}$ (23.0 g, 0.050 mol) in 150 mL THF was added dropwise, and the mixture was stirred for 96 h at room temperature. The solid was removed by filtration, and the organic filtrate was washed with saturated aqueous NaCl (3×150 mL), dried over MgSO_4 , and concentrated to give a quantitative yield of **4(7)** as a yellow gel-like liquid.¹⁶⁵ ^1H NMR (300 MHz, CDCl_3) δ 7.45 (d, 12H), 7.18-7.30 (m, 18H), 3.59-3.69 (m, 24H), 3.19-3.25 (t, 4H).

Hexaethylene glycol ditritylate [$\text{Tr}(\text{OCH}_2\text{CH}_2)_6\text{OTr}$, **4(6)].** A yellow gel-like liquid,¹⁶⁵ prepared by reacting $\text{Tr}(\text{OCH}_2\text{CH}_2)_2\text{OH}$ with $\text{Ts}(\text{OCH}_2\text{CH}_2)_2\text{OTs}$ in 100% yield. ^1H NMR (300 MHz, CDCl_3) δ 7.45 (d, 12H), 7.18-7.28 (m, 18H), 3.62 (m, 20H), 3.20 (t, 4H).

Octaethylene glycol ditritylate [$\text{Tr}(\text{OCH}_2\text{CH}_2)_8\text{OTr}$, **4(8)].** A yellow gel-like liquid,¹⁶⁵ prepared by reacting $\text{Tr}(\text{OCH}_2\text{CH}_2)_2\text{OH}$ with $\text{Ts}(\text{OCH}_2\text{CH}_2)_4\text{OTs}$ in 99% yield. ^1H NMR (300 MHz, CDCl_3) δ 7.48 (d, 12H), 7.18-7.23 (m, 18H), 3.60-3.78 (m, 28H), 3.20-3.30 (t, 4H).

Nonaethylene glycol ditritylate [$\text{Tr}(\text{OCH}_2\text{CH}_2)_9\text{OTr}$, **4(9)].** A yellow gel-like liquid, prepared by reacting $\text{Tr}(\text{OCH}_2\text{CH}_2)_3\text{OH}$ with $\text{Ts}(\text{OCH}_2\text{CH}_2)_3\text{OTs}$. Yield 98%. ^1H

NMR (300 MHz, CDCl_3) δ 7.45 (d, 12H), 7.18-7.30 (m, 18H), 3.58-3.69 (m, 32H), 3.19-3.25 (t, 4H).

Decaethylene glycol ditritylate [$\text{Tr}(\text{OCH}_2\text{CH}_2)_{10}\text{OTr}$, **4(10)**]. A yellow gel-like liquid, prepared by reacting $\text{Tr}(\text{OCH}_2\text{CH}_2)_4\text{OH}$ with $\text{Ts}(\text{OCH}_2\text{CH}_2)_2\text{OTs}$. Yield 99%. ^1H NMR (300 MHz, CDCl_3) δ 7.44 (d, 12H), 7.17-7.30 (m, 18H), 3.57-3.68 (m, 36H), 3.20 (t, 4H).

Tetradecaethylene glycol ditritylate [$\text{Tr}(\text{OCH}_2\text{CH}_2)_{14}\text{OTr}$, **4(14)**] was prepared by reacting $\text{Tr}(\text{OCH}_2\text{CH}_2)_4\text{OH}$ with $\text{Ts}(\text{OCH}_2\text{CH}_2)_6\text{OTs}$. Removal of the MgSO_4 and concentration of the solvent gave a brownish-yellow solution. The solution was refluxed with charcoal overnight and filtered to give a colorless to light yellow solution. Removal of the solvent gave a light yellow viscous gel-like liquid in 97% yield. ^1H NMR (300 MHz, CDCl_3) δ 7.44 (d, 12H), 7.17-7.30 (m, 18H), 3.57-3.68 (m, 52H), 3.20 (t, 4H).

3. Exact length ethylene glycol oligomers:

General procedure for the synthesis of exact length ethylene glycol oligomers.

Heptaethylene glycol [$\text{H}(\text{OCH}_2\text{CH}_2)_7\text{OH}$, **1(7)**]. A high pressure Monel bomb with a glass insert was charged with 36.6 g (45.0 mmol) heptaethylene glycol ditritylate, 150 mL CH_2Cl_2 , and 0.677g of 10% palladium on carbon. Hydrogenolysis was carried out at room temperature under 50 atm H_2 for 48 hours. Upon completion of the reaction, the catalyst (which can be reused) was filtered and washed with CH_2Cl_2 . The filtrate was concentrated to give a mixture of a white solid (triphenylmethane) and an oil. The

mixture was dissolved in boiling methanol and the majority of the triphenylmethane crystallized when the solution was cooled to 0 °C. The mixture was filtered and the filtrate was washed with hexanes (6 × 100 mL) to remove trace amounts of triphenylmethane. The solvent was removed to give a clear colorless oil. Yield 97%. bp 180-195 °C/50 mtorr. (lit.¹⁸¹ 200-208 °C/300 mtorr.) ¹H NMR (300 MHz, CDCl₃) δ 3.72-3.67 (t, 4H), 3.66-3.61 (m, 20H), 3.60-3.55 (t, 4H), 2.9 (s, 2H).

Hexaethylene glycol [H(OCH₂CH₂)₆OH, 1(6)]. A clear colorless oil. Yield 99%. ¹H NMR (300 MHz, CDCl₃) δ 3.72-3.67 (t, 4H), 3.66-3.61 (m, 16H), 3.60-3.55 (t, 4H), 2.9 (s, 2H). bp 197-205 °C/100 mtorr (lit.¹⁸² 201-205 °C/700 mtorr).

Octaethylene glycol [H(OCH₂CH₂)₈OH, 1(8)]. A clear colorless oil. Yield 97%. ¹H NMR (300 MHz, CDCl₃) δ 3.72-3.55 (m, 32H), 2.7 (s, 2H).

Nonaethylene glycol [H(OCH₂CH₂)₉OH, 1(9)]. A clear colorless oil. Yield 92%. ¹H NMR (300 MHz, CDCl₃) δ 3.72-3.55 (m, 36H), 2.7 (s, 2H).

Decaethylene glycol [H(OCH₂CH₂)₁₀OH, 1(10)]. A clear light yellow oil. Yield 96%. ¹H NMR (300 MHz, CDCl₃) δ 3.72-3.56 (m, 40H), 2.58 (s, 2H).

Tetradecaethylene glycol [H(OCH₂CH₂)₁₄OH, 1(14)]. A white waxy solid. Yield 96%. ¹H NMR (300 MHz, CDCl₃) δ 3.72-3.56 (m, 56H), 2.58 (s, 2H). mp 37-39 °C.

4. Model compound syntheses:

Preparation of model compounds $[\text{CH}_3(\text{CH}_2)_{x-1}(\text{OCH}_2\text{CH}_2)_y\text{O}(\text{CH}_2)_{x-1}\text{CH}_3, \text{C}_x\text{EO}_y\text{C}_x]$. Under Ar, the appropriate ethylene glycol oligomer (5.00 mmol) in 20 mL of dry THF was added dropwise to a 100 mL Schlenk flask charged with NaH (12.5 mmol). The reaction mixture was stirred for 24 h, and then the appropriate alkyl bromide (10.2 mmol) in 15 mL THF was added and stirred for 72 h at room temperature, or at reflux ($y = 2, 3$). Upon completion of the reaction, 5 mL of water were added slowly and the solution was stirred for 10 min. The layers were separated and the water layer was extracted with ether (3×20 mL). The combined organic solutions were washed with saturated NaCl solution (2×80 mL), dried over MgSO_4 , and concentrated. Hexyl and octyl derivatives ($y = 2, 3, 4, 5$) were distilled under vacuum to give clear colorless oils. All other compounds were recrystallized from acetone ($y = 2, 3$), or methanol ($y = 4, 5, 6, 7, 8, 10, 14$) at low temperature. Liquid products are clear colorless and solid products are white and crystalline. The melting points of all model compounds were determined by DSC.

$\text{C}_6\text{EO}_2\text{C}_6$. A clear colorless liquid. Yield 53%. ^1H NMR (300 MHz, CDCl_3) δ 3.62 (m, 4H), 3.57 (m, 4H), 3.42 (t, 4H), 1.49-1.59 (quintuplet, 4H), 1.20-1.34 (m, 12H), 0.86 (t, 6H). mp -25.9°C .

$\text{C}_8\text{EO}_2\text{C}_8$. Yield 52%. ^1H NMR (300 MHz, CDCl_3) δ 3.62 (m, 4H), 3.57 (m, 4H), 3.42 (t, 4H), 1.50-1.60 (quintuplet, 4H), 1.20-1.32 (m, 20H), 0.86 (t, 6H). mp -1.9°C .

$\text{C}_{10}\text{EO}_2\text{C}_{10}$. A clear colorless liquid. Yield 77%. ^1H NMR (300 MHz, CDCl_3) δ 3.62 (m, 4H), 3.57 (m, 4H), 3.41 (t, 4H), 1.20-1.60 (m, 32H), 0.86 (t, 6H). mp 19.5°C .

C₁₂EO₂C₁₂. A white crystalline solid. Yield 79%. ¹H NMR (300 MHz, CDCl₃) δ 3.62 (m, 4H), 3.57 (m, 4H), 3.42 (t, 4H), 1.20-1.60 (m, 40H), 0.86 (t, 6H). mp 31.6 °C.

C₁₄EO₂C₁₄. Yield 82%. ¹H NMR (300 MHz, CDCl₃) δ 3.63 (m, 4H), 3.57 (m, 4H), 3.42 (t, 4H), 1.20-1.60 (m, 48H), 0.86 (t, 6H). mp 41.5 °C.

C₁₆EO₂C₁₆. A white crystalline solid. Yield 85%. ¹H NMR (300 MHz, CDCl₃) δ 3.62 (m, 4H), 3.57 (m, 4H), 3.42 (t, 4H), 1.20-1.60 (m, 56H), 0.86 (t, 6H). mp 50.1 °C.

C₆EO₃C₆. A clear colorless liquid. Yield 55%. ¹H NMR (300 MHz, CDCl₃) δ 3.60-3.65 (m, 8H), 3.57 (m, 4H), 3.42 (t, 4H), 1.49-1.59 (quintuplet, 4H), 1.20-1.34 (m, 12H), 0.86 (t, 6H). mp -16.1 °C.

C₈EO₃C₈. A clear colorless liquid. Yield 53%. ¹H NMR (300 MHz, CDCl₃) δ 3.60-3.65 (m, 8H), 3.57 (m, 4H), 3.42 (t, 4H), 1.49-1.60 (quintuplet, 4H), 1.20-1.32 (m, 20H), 0.86 (t, 6H). mp 5.0 °C.

C₁₀EO₃C₁₀. A white crystalline solid. Yield 59%. ¹H NMR (300 MHz, CDCl₃) δ 3.60-3.65 (m, 8H), 3.57 (m, 4H), 3.42 (t, 4H), 1.20-1.60 (m, 32H), 0.86 (t, 6H). mp 22.0 °C.

C₁₂EO₃C₁₂. A white crystalline solid. Yield 72%. ¹H NMR (300 MHz, CDCl₃) δ 3.60-3.65 (m, 8H), 3.57 (m, 4H), 3.42 (t, 4H), 1.20-1.60 (m, 40H), 0.86 (t, 6H). mp 33.6 °C. (lit.¹⁸³ 35.7-36.2 °C)

C₁₄EO₃C₁₄. A white crystalline solid. Yield 85%. ¹H NMR (300 MHz, CDCl₃) δ 3.60-3.65 (m, 8H), 3.57 (m, 4H), 3.42 (t, 4H), 1.20-1.60 (m, 48H), 0.86 (t, 6H). mp 42.7 °C.

C₁₆EO₃C₁₆. A white crystalline solid. Yield 82%. ¹H NMR (300 MHz, CDCl₃) δ 3.60-3.65 (m, 8H), 3.57 (m, 4H), 3.42 (t, 4H), 1.19-1.60 (m, 56H), 0.86 (t, 6H). mp 50.9 °C.

C₆EO₄C₆. A clear colorless liquid. Yield 50%. ¹H NMR (300 MHz, CDCl₃) δ 3.59-3.66 (m, 12H), 3.57 (m, 4H), 3.42 (t, 4H), 1.49-1.59 (quintuplet, 4H), 1.20-1.34 (m, 12H), 0.86 (t, 6H). mp -21.9 °C.

C₈EO₄C₈. A clear colorless liquid. Yield 52%. ¹H NMR (300 MHz, CDCl₃) δ 3.59-3.66 (m, 12H), 3.57 (m, 4H), 3.42 (t, 4H), 1.50-1.60 (quintuplet, 4H), 1.20-1.32 (m, 20H), 0.86 (t, 6H). mp 3.6 °C.

C₁₀EO₄C₁₀. A clear colorless liquid. Yield 71%. ¹H NMR (300 MHz, CDCl₃) δ 3.62 (m, 12H), 3.57 (m, 4H), 3.41 (t, 4H), 1.20-1.60 (m, 32H), 0.86 (t, 6H). mp 19.4 °C.

C₁₂EO₄C₁₂. A white crystalline solid. Yield 84%. ¹H NMR (300 MHz, CDCl₃) δ 3.62 (m, 12H), 3.57 (m, 4H), 3.42 (t, 4H), 1.20-1.60 (m, 40H), 0.86 (t, 6H). mp 33.4 °C.
(lit.¹⁸⁴ 33-34 °C)

C₁₄EO₄C₁₄. A white crystalline solid. Yield 85%. ¹H NMR (300 MHz, CDCl₃) δ 3.60-3.65 (m, 12H), 3.57 (m, 4H), 3.42 (t, 4H), 1.20-1.60 (m, 48H), 0.86 (t, 6H). mp 42.0 °C.

C₁₆EO₄C₁₆. A white crystalline solid. Yield 82%. ¹H NMR (300 MHz, CDCl₃) δ 3.60-3.65 (m, 12H), 3.57 (m, 4H), 3.42 (t, 4H), 1.18-1.60 (m, 56H), 0.86 (t, 6H). mp 48.6 °C.

C₆EO₅C₆. A clear colorless liquid. Yield 46%. ¹H NMR (300 MHz, CDCl₃) δ 3.59-3.67 (m, 16H), 3.56 (m, 4H), 3.42 (t, 4H), 1.49-1.59 (quintuplet, 4H), 1.20-1.34 (m, 12H), 0.86 (t, 6H). mp -14.7 °C.

C₈EO₅C₈. A clear colorless liquid. Yield 52%. ¹H NMR (300 MHz, CDCl₃) δ 3.59-3.67 (m, 16H), 3.56 (m, 4H), 3.42 (t, 4H), 1.49-1.60 (quintuplet, 4H), 1.20-1.32 (m, 20H), 0.86 (t, 6H). mp 9.3 °C.

C₁₀EO₅C₁₀. A white crystalline solid. Yield 79%. ¹H NMR (300 MHz, CDCl₃) δ 3.59-3.67 (m, 16H), 3.56 (m, 4H), 3.42 (t, 4H), 1.20-1.60 (m, 32H), 0.86 (t, 6H). mp 21.4 °C.

C₁₂EO₅C₁₂. A white crystalline solid. Yield 81%. ¹H NMR (300 MHz, CDCl₃) δ 3.59-3.67 (m, 16H), 3.56 (m, 4H), 3.42 (t, 4H), 1.20-1.60 (m, 40H), 0.86 (t, 6H). mp 32.8 °C. (lit.¹⁸⁴ 33-34 °C)

C₁₄EO₅C₁₄. A white crystalline solid. Yield 91%. ¹H NMR (300 MHz, CDCl₃) δ 3.59-3.67 (m, 16H), 3.56 (m, 4H), 3.42 (t, 4H), 1.20-1.60 (m, 48H), 0.86 (t, 6H). mp 41.1 °C.

C₁₆EO₅C₁₆. A white crystalline solid. Yield 94%. ¹H NMR (300 MHz, CDCl₃) δ 3.59-3.67 (m, 16H), 3.56 (m, 4H), 3.42 (t, 4H), 1.20-1.60 (m, 56H), 0.86 (t, 6H). mp 46.9 °C.

C₆EO₆C₆. A clear colorless liquid. Yield 39%. ¹H NMR (300 MHz, CDCl₃) δ 3.59-3.66 (m, 20H), 3.57 (m, 4H), 3.42 (t, 4H), 1.49-1.59 (quintuplet, 4H), 1.20-1.34 (m, 12H), 0.86 (t, 6H). mp -11.5 °C.

C₈EO₆C₈. A clear colorless liquid. Yield 41%. ¹H NMR (300 MHz, CDCl₃) δ 3.59-3.66 (m, 20H), 3.57 (m, 4H), 3.42 (t, 4H), 1.49-1.60 (quintuplet, 4H), 1.20-1.32 (m, 20H), 0.86 (t, 6H). mp 6.4 °C.

C₁₀EO₆C₁₀. A white crystalline solid. Yield 78%. ¹H NMR (300 MHz, CDCl₃) δ 3.62 (m, 20H), 3.57 (m, 4H), 3.41 (t, 4H), 1.20-1.60 (m, 32H), 0.86 (t, 6H). mp 21.8 °C. (lit.¹⁸⁵ 30 °C)

C₁₂EO₆C₁₂. A white crystalline solid. Yield 90%. ¹H NMR (300 MHz, CDCl₃) δ 3.62 (m, 20H), 3.57 (m, 4H), 3.41 (t, 4H), 1.20-1.60 (m, 40H), 0.86 (t, 6H). mp 31.2 °C. (lit.¹⁸⁵ 33.5 °C)

C₁₄EO₆C₁₄. A white crystalline solid. Yield 90%. ¹H NMR (300 MHz, CDCl₃) δ 3.59-3.65 (m, 20H), 3.55 (m, 4H), 3.42 (t, 4H), 1.20-1.60 (m, 48H), 0.86 (t, 6H). mp 40.2 °C. (lit.¹⁸⁵ 43 °C)

C₁₆EO₆C₁₆. A white crystalline solid. Yield 92%. ¹H NMR (300 MHz, CDCl₃) δ 3.58-3.65 (m, 20H), 3.55 (m, 4H), 3.41 (t, 4H), 1.54 (quintuplet, 4H), 1.18-1.32 (m, 52H), 0.85 (t, 6H). mp 46.4 °C. (lit.¹⁸⁶ 43 °C)

C₆EO₇C₆. A clear colorless liquid. Yield 60%. ¹H NMR (300 MHz, CDCl₃) δ 3.59-3.65 (m, 24H), 3.55 (m, 4H), 3.42 (t, 4H), 1.49-1.59 (quintuplet, 4H), 1.20-1.34 (m, 12H), 0.86 (t, 6H). mp -2.6 °C.

C₈EO₇C₈. A clear colorless liquid. Yield 64%. ¹H NMR (300 MHz, CDCl₃) δ 3.59-3.65 (m, 24H), 3.55 (m, 4H), 3.42 (t, 4H), 1.49-1.60 (quintuplet, 4H), 1.20-1.32 (m, 20H), 0.86 (t, 6H). mp 9.4 °C.

C₁₀EO₇C₁₀. A white crystalline solid. Yield 80%. ¹H NMR (300 MHz, CDCl₃) δ 3.59-3.65 (m, 24H), 3.55 (m, 4H), 3.42 (t, 4H), 1.20-1.60 (m, 32H), 0.86 (t, 6H). mp 22.0 °C.

C₁₂EO₇C₁₂. A white crystalline solid. Yield 88%. ¹H NMR (300 MHz, CDCl₃) δ 3.59-3.65 (m, 24H), 3.55 (m, 4H), 3.42 (t, 4H), 1.20-1.60 (m, 40H), 0.86 (t, 6H). mp 32.3 °C. (lit.¹⁸⁷ 32.5 °C)

C₁₄EO₇C₁₄. A white crystalline solid. Yield 88%. ¹H NMR (300 MHz, CDCl₃) δ 3.59-3.65 (m, 24H), 3.55 (m, 4H), 3.42 (t, 4H), 1.20-1.60 (m, 48H), 0.86 (t, 6H). mp 41.3 °C.

C₁₆EO₇C₁₆. A white crystalline solid. Yield 91%. ¹H NMR (300 MHz, CDCl₃) δ 3.60-3.65 (m, 24H), 3.55 (m, 4H), 3.41 (t, 4H), 1.54 (m, 4H), 1.18-1.32 (m, 52H), 0.85 (t, 6H). mp 44.8 °C.

C₆EO₈C₆. A clear colorless liquid. Yield 62%. ¹H NMR (300 MHz, CDCl₃) δ 3.59-3.65 (m, 28H), 3.55 (m, 4H), 3.42 (t, 4H), 1.49-1.59 (quintuplet, 4H), 1.20-1.34 (m, 12H), 0.86 (t, 6H). mp 2.2 °C.

C₈EO₈C₈. A clear colorless liquid. Yield 62%. ¹H NMR (300 MHz, CDCl₃) δ 3.59-3.65 (m, 28H), 3.55 (m, 4H), 3.42 (t, 4H), 1.49-1.60 (quintuplet, 4H), 1.20-1.32 (m, 20H), 0.86 (t, 6H). mp 13.6 °C.

C₁₀EO₈C₁₀. A white crystalline solid. Yield 81%. ¹H NMR (300 MHz, CDCl₃) δ 3.59-3.65 (m, 28H), 3.55 (m, 4H), 3.42 (t, 4H), 1.20-1.60 (m, 32H), 0.86 (t, 6H). mp 23.7 °C.

C₁₂EO₈C₁₂. A white crystalline solid. Yield 87%. ¹H NMR (300 MHz, CDCl₃) δ 3.59-3.65 (m, 28H), 3.55 (m, 4H), 3.42 (t, 4H), 1.20-1.60 (m, 40H), 0.86 (t, 6H). mp 30.9 °C. (Lit.¹⁸³ 33.8-34.3 °C)

C₁₄EO₈C₁₄. A white crystalline solid. Yield 91%. ¹H NMR (300 MHz, CDCl₃) δ 3.59-3.65 (m, 28H), 3.55 (m, 4H), 3.42 (t, 4H), 1.20-1.60 (m, 48H), 0.86 (t, 6H). mp 38.8 °C.

C₁₆EO₈C₁₆. A white crystalline solid. Yield 89%. ¹H NMR (300 MHz, CDCl₃) δ 3.60-3.65 (m, 28H), 3.55 (m, 4H), 3.41 (t, 4H), 1.54 (m, 4H), 1.18-1.32 (m, 52H), 0.85 (t, 6H). mp 40.4 °C.

C₆EO₁₀C₆. A clear colorless liquid. Yield 70%. ¹H NMR (300 MHz, CDCl₃) δ 3.59-3.65 (m, 36H), 3.55 (m, 4H), 3.42 (t, 4H), 1.49-1.59 (quintuplet, 4H), 1.20-1.34 (m, 12H), 0.86 (t, 6H). mp 15.7 °C.

C₈EO₁₀C₈. A white crystalline solid. Yield 69%. ¹H NMR (300 MHz, CDCl₃) δ 3.59-3.65 (m, 36H), 3.55 (m, 4H), 3.42 (t, 4H), 1.49-1.60 (quintuplet, 4H), 1.20-1.32 (m, 20H), 0.86 (t, 6H). mp 21.1 °C.

C₁₀EO₁₀C₁₀. A white crystalline solid. Yield 78%. ¹H NMR (300 MHz, CDCl₃) δ 3.59-3.65 (m, 36H), 3.55 (m, 4H), 3.42 (t, 4H), 1.20-1.60 (m, 32H), 0.86 (t, 6H). mp 26.7 °C.

C₁₂EO₁₀C₁₂. A white crystalline solid. Yield 83%. ¹H NMR (300 MHz, CDCl₃) δ 3.59-3.65 (m, 36H), 3.55 (m, 4H), 3.42 (t, 4H), 1.20-1.60 (m, 40H), 0.86 (t, 6H). mp 35.0 °C. (Lit.¹⁸³ 36.5-37 °C)

C₁₄EO₁₀C₁₄. A white crystalline solid. Yield 85%. ¹H NMR (300 MHz, CDCl₃) δ 3.59-3.65 (m, 36H), 3.55 (m, 4H), 3.42 (t, 4H), 1.20-1.60 (m, 48H), 0.86 (t, 6H). mp 40.5 °C.

C₁₆EO₁₀C₁₆. A white crystalline solid. Yield 87%. ¹H NMR (300 MHz, CDCl₃) δ 3.60-3.65 (m, 36H), 3.55 (m, 4H), 3.41 (t, 4H), 1.54 (m, 4H), 1.18-1.32 (m, 52H), 0.85 (t, 6H). mp 43.6 °C.

C₆EO₁₄C₆. A white waxy solid. Yield 73%. ¹H NMR (300 MHz, CDCl₃) δ 3.59-3.65 (m, 52H), 3.55 (m, 4H), 3.42 (t, 4H), 1.49-1.59 (quintuplet, 4H), 1.20-1.34 (m, 12H), 0.86 (t, 6H). mp 26.5 °C.

C₈EO₁₄C₈. A white waxy solid. Yield 74%. ¹H NMR (300 MHz, CDCl₃) δ 3.59-3.65 (m, 52H), 3.55 (m, 4H), 3.42 (t, 4H), 1.49-1.60 (quintuplet, 4H), 1.20-1.32 (m, 20H), 0.86 (t, 6H). mp 26.0 °C.

C₁₀EO₁₄C₁₀. A white crystalline solid. Yield 80%. ¹H NMR (300 MHz, CDCl₃) δ 3.59-3.65 (m, 52H), 3.55 (m, 4H), 3.42 (t, 4H), 1.20-1.60 (m, 32H), 0.86 (t, 6H). mp 35.5 °C.

C₁₂EO₁₄C₁₂. A white crystalline solid. Yield 84%. ¹H NMR (300 MHz, CDCl₃) δ 3.59-3.65 (m, 52H), 3.55 (m, 4H), 3.42 (t, 4H), 1.20-1.60 (m, 40H), 0.86 (t, 6H). mp 38.5 °C.

C₁₄EO₁₄C₁₄. A white crystalline solid. Yield 84%. ¹H NMR (300 MHz, CDCl₃) δ 3.59-3.65 (m, 52H), 3.55 (m, 4H), 3.42 (t, 4H), 1.20-1.60 (m, 48H), 0.86 (t, 6H). mp 43.5 °C.

C₁₆EO₁₄C₁₆. A white crystalline solid. Yield 86%. ¹H NMR (300 MHz, CDCl₃) δ 3.60-3.65 (m, 52H), 3.55 (m, 4H), 3.41 (t, 4H), 1.54 (m, 4H), 1.18-1.32 (m, 52H), 0.85 (t, 6H). mp 47.5 °C.

5. General procedure for monomer syntheses and purification.

Hexaethylene glycol α,ω-dibutenyl ether [πC₂EO₆C₂π]. A 2 L round bottom flask equipped with an addition funnel with a N₂ inlet and outlet was charged with 95% NaH (6.19 g, 0.250 mol) in dry THF (200 mL). To the stirred slurry, a solution of 3-buten-1-ol (14.4 g, 0.200 mol) in 200 mL THF was added dropwise and stirred for 24 h, Hexaethylene glycol α,ω-ditosylate (58.0 g, 0.0980 mol) in 1 L THF was added. The addition funnel was replaced with a cold water condenser with an Ar inlet and outlet and the reaction mixture was refluxed for 5 days. The product was filtered and the clear brown solution was washed with saturated aqueous NaCl (4 × 150 mL) and dried over MgSO₄ overnight. Filtration and removal of the solvent gave a yellow oil which was further purified by column chromatography (75/25 EtOAc/hexanes). The resulting yellow oil product was dissolved in hexanes and stirred over a freshly made sodium mirror under Ar overnight. The mixture was filtered under Ar through a funnel packed with Celite and alumina. The process was repeated (2 to 3 times) until the filtrate was colorless. The solvent was removed from the filtrate in *vacuo* to give a 34% yield (13.0 g) of a clear colorless liquid. The purified monomer was stored in dry box under helium until used. ¹H NMR (300 MHz, CDCl₃) δ 5.88-5.70 (m, 2H), 5.10-4.98 (m, 4H), 3.65-3.60 (m, 20H), 3.59-3.52 (m, 4H), 3.52-3.47 (t, 4H), 2.37-2.27 (m, 4H). mp -10.1 °C.

All the other monomers were prepared in the same way. Since the monomers derived from tetradecaethylene glycol series are not soluble in hexanes, dry toluene was used in the sodium mirror process for this series.

$\pi\text{C}_3\text{EO}_6\text{C}_3\pi$. Isolated by column chromatography (silica gel, ethyl acetate) as a clear yellow liquid. Purified by sodium mirror to give a clear colorless liquid. Yield 24.2g (59%). ^1H NMR (300 MHz, CDCl_3) δ 5.86-5.70 (m, 2H), 5.04-4.90 (m, 4H), 3.65-3.59 (m, 20H), 3.58-3.53 (m, 4H), 3.47-3.41 (t, 4H), 2.13-2.03 (m, 4H), 1.71-1.60 (m, 4H). mp -13.9 °C.

$\pi\text{C}_4\text{EO}_6\text{C}_4\pi$. Isolated by column chromatography (silica gel, EtOAc : hexanes = 3 : 1) as a clear yellow liquid. Purified by sodium mirror to give a clear colorless liquid. Yield 23.0 g (53%). ^1H NMR (300 MHz, CDCl_3) δ 5.86-5.71 (m, 2H), 5.02-4.89 (m, 4H), 3.65-3.59 (m, 20H), 3.57-3.53 (m, 4H), 3.46-3.40 (t, 4H), 2.09-2.00 (m, 4H), 1.63-1.52 (m, 4H), 1.47-1.35 (m, 4H). mp -11.5 °C.

$\pi\text{C}_8\text{EO}_6\text{C}_8\pi$. Isolated by column chromatography (silica gel, EtOAc : hexanes = 1 : 1) as a clear yellow liquid. Purified by sodium mirror to give a clear colorless liquid. Yield 30.9 g (57%). ^1H NMR (300 MHz, CDCl_3) δ 5.86-5.71 (m, 2H), 5.01-4.87 (m, 4H), 3.65-3.59 (m, 20H), 3.57-3.53 (m, 4H), 3.45-3.39 (t, 4H), 2.06-1.96 (m, 4H), 1.60-1.49 (m, 4H), 1.40-1.20 (m, 20H). mp 3.6 °C.

$\pi\text{C}_9\text{EO}_6\text{C}_9\pi$. Isolated by column chromatography (silica gel, EtOAc : hexanes = 1 : 1) as a clear yellow liquid. Purified by sodium mirror to give a clear colorless liquid. Yield 23.8 g (41%). ^1H NMR (300 MHz, CDCl_3) δ 5.86-5.71 (m, 2H), 5.01-4.87 (m,

4H), 3.65-3.59 (m, 20H), 3.57-3.53 (m, 4H), 3.45-3.39 (t, 4H), 2.06-1.96 (m, 4H), 1.60-1.49 (m, 4H), 1.40-1.20 (m, 24H). mp 10.1 °C.

$\pi\text{C}_2\text{EO}_7\text{C}_2\pi$. Isolated by column chromatography (silica gel, ethyl acetate) as a clear yellow liquid. Purified by sodium mirror to give a clear colorless liquid. Yield 13.2 g (31%). ^1H NMR (300 MHz, CDCl_3) δ 5.87-5.71 (m, 2H), 5.01-4.98 (m, 4H), 3.64-3.60 (m, 24H), 3.59-3.53 (m, 4H), 3.52-3.47 (t, 4H), 2.37-2.28 (m, 4H). mp -5.3 °C.

$\pi\text{C}_3\text{EO}_7\text{C}_3\pi$. Isolated by column chromatography (silica gel, EtOAc : hexanes = 9 : 1) as a clear yellow liquid. Purified by sodium mirror to give a clear colorless liquid. Yield 26.8 g (59%). ^1H NMR (300 MHz, CDCl_3) δ 5.85-5.71 (m, 2H), 5.03-4.99 (m, 4H), 3.64-3.58 (m, 24H), 3.57-3.52 (m, 4H), 3.46-3.40 (t, 4H), 2.12-2.03 (m, 4H), 1.70-1.60 (m, 4H). mp -7.7 °C.

$\pi\text{C}_4\text{EO}_7\text{C}_4\pi$. Isolated by column chromatography (silica gel, EtOAc : hexanes = 9 : 1) as a clear yellow liquid. Purified by sodium mirror to give a clear colorless liquid. Yield 16.0 g (49%). ^1H NMR (300 MHz, CDCl_3) δ 5.86-5.71 (m, 2H), 5.01-4.87 (m, 4H), 3.65-3.59 (m, 24H), 3.57-3.53 (m, 4H), 3.46-3.40 (t, 4H), 2.09-2.00 (m, 4H), 1.63-1.52 (m, 4H), 1.47-1.35 (m, 4H). mp -5.4 °C.

$\pi\text{C}_8\text{EO}_7\text{C}_8\pi$. Isolated by column chromatography (silica gel, EtOAc : hexanes = 3 : 1) as a clear yellow liquid. Purified by sodium mirror to give a clear colorless liquid. Yield 28.8 g (49%). ^1H NMR (300 MHz, CDCl_3) δ 5.86-5.71 (m, 2H), 5.01-4.87 (m, 4H), 3.65-3.59 (m, 24H), 3.57-3.53 (m, 4H), 3.45-3.39 (t, 4H), 2.06-1.96 (m, 4H), 1.60-1.49 (m, 4H), 1.40-1.20 (m, 20H). mp 5.9 °C.

$\pi\text{C}_9\text{EO}_7\text{C}_9\pi$. Isolated by column chromatography (silica gel, EtOAc : hexanes = 3 : 1) as a clear yellow liquid. Purified by sodium mirror to give a clear colorless liquid. Yield 30.9 g (50%). ^1H NMR (300 MHz, CDCl_3) δ 5.86-5.71 (m, 2H), 5.01-4.87 (m, 4H), 3.65-3.59 (m, 24H), 3.57-3.53 (m, 4H), 3.45-3.39 (t, 4H), 2.06-1.96 (m, 4H), 1.60-1.49 (m, 4H), 1.40-1.20 (m, 24H). mp 16.0 °C.

$\pi\text{C}_2\text{EO}_8\text{C}_2\pi$. Isolated by column chromatography (silica gel, EtOAc : MeOH = 9 : 1) as a clear yellow liquid. Purified by sodium mirror to give a clear colorless liquid. Yield 14.0 g (30%). ^1H NMR (300 MHz, CDCl_3) δ 5.87-5.71 (m, 2H), 5.01-4.98 (m, 4H), 3.64-3.60 (m, 28H), 3.59-3.53 (m, 4H), 3.52-3.47 (t, 4H), 2.37-2.28 (m, 4H). mp 1.5 °C.

$\pi\text{C}_3\text{EO}_8\text{C}_3\pi$. Isolated by column chromatography (silica gel, EtOAc : MeOH = 9 : 1) as a clear yellow liquid. Purified by sodium mirror to give a clear colorless liquid. Yield 25.9 g (52%). ^1H NMR (300 MHz, CDCl_3) δ 5.85-5.71 (m, 2H), 5.03-4.99 (m, 4H), 3.64-3.58 (m, 28H), 3.57-3.52 (m, 4H), 3.46-3.40 (t, 4H), 2.12-2.03 (m, 4H), 1.70-1.60 (m, 4H). mp -1.1 °C.

$\pi\text{C}_4\text{EO}_8\text{C}_4\pi$. Isolated by column chromatography (silica gel, EtOAc : MeOH = 9 : 1) as a clear yellow liquid. Purified by sodium mirror to give a clear colorless liquid. Yield 24.3 g (46%). ^1H NMR (300 MHz, CDCl_3) δ 5.86-5.71 (m, 2H), 5.01-4.87 (m, 4H), 3.65-3.59 (m, 28H), 3.57-3.53 (m, 4H), 3.46-3.40 (t, 4H), 2.09-2.00 (m, 4H), 1.63-1.52 (m, 4H), 1.47-1.35 (m, 4H). mp 0.8 °C.

$\pi\text{C}_8\text{EO}_8\text{C}_8\pi$. Isolated by column chromatography (silica gel, EtOAc : hexanes = 9 : 1) as a clear yellow liquid. Purified by sodium mirror to give a clear colorless liquid.

Yield 37.0 g (58%). ^1H NMR (300 MHz, CDCl_3) δ 5.86-5.71 (m, 2H), 5.01-4.87 (m, 4H), 3.65-3.59 (m, 28H), 3.57-3.53 (m, 4H), 3.45-3.39 (t, 4H), 2.06-1.96 (m, 4H), 1.60-1.49 (m, 4H), 1.40-1.20 (m, 20H). mp 13.2 °C.

$\pi\text{C}_9\text{EO}_8\text{C}_9\pi$. Isolated by column chromatography (silica gel, EtOAc : hexanes = 3 : 1) as a clear yellow liquid. Purified by sodium mirror to give a clear colorless liquid. Yield 37.0 g (56%). ^1H NMR (300 MHz, CDCl_3) δ 5.86-5.71 (m, 2H), 5.01-4.87 (m, 4H), 3.65-3.59 (m, 28H), 3.57-3.53 (m, 4H), 3.45-3.39 (t, 4H), 2.06-1.96 (m, 4H), 1.60-1.49 (m, 4H), 1.40-1.20 (m, 24H). mp 17.5 °C.

$\pi\text{C}_2\text{EO}_{10}\text{C}_2\pi$. Isolated by column chromatography (silica gel, EtOAc : MeOH = 9 : 1) as a clear yellow liquid. Purified by sodium mirror to give a clear colorless liquid. Yield 22.0 g (40%). ^1H NMR (300 MHz, CDCl_3) δ 5.87-5.71 (m, 2H), 5.01-4.98 (m, 4H), 3.64-3.60 (m, 36H), 3.59-3.53 (m, 4H), 3.52-3.47 (t, 4H), 2.37-2.28 (m, 4H). mp 12.6 °C.

$\pi\text{C}_3\text{EO}_{10}\text{C}_3\pi$. Isolated by column chromatography (silica gel, EtOAc : MeOH = 9 : 1) as a clear yellow liquid. Purified by sodium mirror to give a clear colorless liquid. Yield 28.0 g (48%). ^1H NMR (300 MHz, CDCl_3) δ 5.85-5.71 (m, 2H), 5.03-4.99 (m, 4H), 3.64-3.58 (m, 36H), 3.57-3.52 (m, 4H), 3.46-3.40 (t, 4H), 2.12-2.03 (m, 4H), 1.70-1.60 (m, 4H). mp 10.7 °C.

$\pi\text{C}_4\text{EO}_{10}\text{C}_4\pi$. Isolated by column chromatography (silica gel, EtOAc : MeOH = 9 : 1) as a clear yellow liquid. Purified by sodium mirror to give a clear colorless liquid. Yield 31.6 g (52%). ^1H NMR (300 MHz, CDCl_3) δ 5.86-5.71 (m, 2H), 5.01-4.87 (m,

4H), 3.65-3.59 (m, 36H), 3.57-3.53 (m, 4H), 3.46-3.40 (t, 4H), 2.09-2.00 (m, 4H), 1.63-1.52 (m, 4H), 1.47-1.35 (m, 4H). mp 12.6 °C.

$\pi\text{C}_8\text{EO}_{10}\text{C}_8\pi$. Isolated by column chromatography (silica gel, EtOAc : Hexanes = 9 : 1) as a clear yellow liquid. Purified by sodium mirror to give a clear colorless liquid. Yield 34.4 g (48%). ^1H NMR (300 MHz, CDCl_3) δ 5.86-5.71 (m, 2H), 5.01-4.87 (m, 4H), 3.65-3.59 (m, 36H), 3.57-3.53 (m, 4H), 3.45-3.39 (t, 4H), 2.06-1.96 (m, 4H), 1.60-1.49 (m, 4H), 1.40-1.20 (m, 20H). mp 19.8 °C.

$\pi\text{C}_9\text{EO}_{10}\text{C}_9\pi$. Isolated by column chromatography (silica gel, EtOAc : Hexanes = 9 : 1) as a cloudy yellow liquid. Purified by sodium mirror to give a white crystalline solid. Yield 42.0 g (56%). ^1H NMR (300 MHz, CDCl_3) δ 5.86-5.71 (m, 2H), 5.01-4.87 (m, 4H), 3.65-3.59 (m, 36H), 3.57-3.53 (m, 4H), 3.45-3.39 (t, 4H), 2.06-1.96 (m, 4H), 1.60-1.49 (m, 4H), 1.40-1.20 (m, 24H). mp 24.6 °C.

$\pi\text{C}_2\text{EO}_{14}\text{C}_2\pi$. Isolated by column chromatography (silica gel, EtOAc : MeOH = 9 : 1) as a cloudy yellow liquid. Purified by sodium mirror to give a white waxy solid. Yield 20.5 g (28%). ^1H NMR (300 MHz, CDCl_3) δ 5.87-5.71 (m, 2H), 5.01-4.98 (m, 4H), 3.64-3.60 (m, 52H), 3.59-3.53 (m, 4H), 3.52-3.47 (t, 4H), 2.37-2.28 (m, 4H). mp 23.5 °C.

$\pi\text{C}_3\text{EO}_{14}\text{C}_3\pi$. Isolated by column chromatography (silica gel, EtOAc : MeOH = 9 : 1) as a cloudy yellow liquid. Purified by sodium mirror to give a white crystalline solid. Yield 31.6 g (42%). ^1H NMR (300 MHz, CDCl_3) δ 5.85-5.71 (m, 2H), 5.03-4.99 (m, 4H), 3.64-3.58 (m, 52H), 3.57-3.52 (m, 4H), 3.46-3.40 (t, 4H), 2.12-2.03 (m, 4H), 1.70-1.60 (m, 4H). mp 23.9 °C.

$\pi\text{C}_4\text{EO}_{14}\text{C}_4\pi$. Isolated by column chromatography (silica gel, EtOAc : MeOH = 9 : 1) as a cloudy yellow liquid. Purified by sodium mirror to give a white crystalline solid. Yield 36.6 g (47%). ^1H NMR (300 MHz, CDCl_3) δ 5.86-5.71 (m, 2H), 5.01-4.87 (m, 4H), 3.65-3.59 (m, 52H), 3.57-3.53 (m, 4H), 3.46-3.40 (t, 4H), 2.09-2.00 (m, 4H), 1.63-1.52 (m, 4H), 1.47-1.35 (m, 4H). mp 22.9 °C.

$\pi\text{C}_8\text{EO}_{14}\text{C}_8\pi$. Isolated by column chromatography (silica gel, EtOAc : MeOH = 95 : 5) as a yellow waxy solid. Purified by sodium mirror to give a white crystalline solid. Yield 36.8 g (41%). ^1H NMR (300 MHz, CDCl_3) δ 5.86-5.71 (m, 2H), 5.01-4.87 (m, 4H), 3.65-3.59 (m, 52H), 3.57-3.53 (m, 4H), 3.45-3.39 (t, 4H), 2.06-1.96 (m, 4H), 1.60-1.49 (m, 4H), 1.40-1.20 (m, 20H). mp 27.7 °C.

$\pi\text{C}_9\text{EO}_{14}\text{C}_9\pi$. Isolated by column chromatography (silica gel, EtOAc : MeOH = 95 : 5) as a yellow waxy solid. Purified by sodium mirror to give a white crystalline solid. Yield 39.1 g (43%). ^1H NMR (300 MHz, CDCl_3) δ 5.86-5.71 (m, 2H), 5.01-4.87 (m, 4H), 3.65-3.59 (m, 52H), 3.57-3.53 (m, 4H), 3.45-3.39 (t, 4H), 2.06-1.96 (m, 4H), 1.60-1.49 (m, 4H), 1.40-1.20 (m, 24H). mp 28.4 °C.

6. Schrock's Molybdenum Catalyst

$\text{Mo}(\text{CHCMe}_2\text{Ph})(\text{NAr})[\text{OCMe}(\text{CF}_3)_2]_2$, Schrock's molybdenum alkylidene catalyst was prepared starting from MoO_2 , using the five-step synthesis reported in the literature.

7. General procedure for the synthesis of ethylene oxide-segmented polymers

Polymer from hexaethylene glycol α , ω -di-3-pentenyl ether $[(C_3\pi C_3EO_6)_n]$. In a helium filled drybox, $\pi C_3EO_6C_3\pi$ (5.00 g, 12 mmol) was placed in a 30 mL Schlenk flask with a stir bar. Schrock's Mo catalyst (15 mg) was added and the mixture was vigorously stirred at room temperature as ethylene gas evolved from the liquid. The reaction vessel was removed from the drybox and high vacuum (<0.02 mtorr) was applied to the system to remove ethylene generated during the polymerization. After 6 h, the reaction temperature was raised to 50 °C by heating with a silicone oil bath. When the reaction mixture became too viscous to stir, toluene (10 mL) was added to the polymer. During the polymerization, the pressure was released occasionally by opening the reaction to vacuum. The polymerization was terminated after 10 days by exposing it to air or adding 1 mL of MeOH. Some reactions took longer times to reach the desired molecular weight. For these cases, a small amount of catalyst (5 mg) was occasionally added. After termination, 40 mL of toluene was added to dilute the polymerization solution, the solution was filtered through Celite[®], and the polymer was precipitated into hexanes. The cloudy suspension was centrifuged to separate the precipitate from the solution. The precipitate was dried in *vacuo* at 85 °C until constant weight was reached. The polymer samples were stored in a desiccator at room temperature. Yield 85% of a yellow tacky gel-like solid ($M_n = 25,500$, PDI = 1.71). ¹H NMR (300 MHz, CDCl₃) δ 5.40-5.38 (m, 2H), 3.65-3.59 (m, 20H), 3.58-3.53 (m, 4H), 3.47-3.41 (t, 4H), 2.13-2.03 (m, 4H), 1.71-1.60 (m, 4H).

$(C_4\pi C_4EO_6)_n$. The polymer was purified by precipitation from toluene into hexanes. Yield 97% of a yellow tacky gel-like solid ($M_n = 48,800$, PDI = 1.84). ¹H NMR

(300 MHz, CDCl₃) δ 5.40-5.38 (m, 2H), 3.65-3.59 (m, 20H), 3.57-3.53 (m, 4H), 3.46-3.40 (t, 4H), 2.09-2.00 (m, 4H), 1.63-1.52 (m, 4H), 1.47-1.35 (m, 4H).

(C₈πC₈EO₆)_n. The polymer was purified by precipitation from toluene into hexanes. The precipitate was dissolved in THF and re-precipitated into MeOH. The precipitate was dried in *vacuo* to give a white translucent solid (M_n = 58,500, PDI = 1.41) in 41% yield. Evaporation of the MeOH solution gave a yellow gel-like solid (M_n = 15,300, PDI = 1.59) in 43% yield. ¹H NMR (300 MHz, CDCl₃) δ 5.40-5.38 (m, 2H), 3.65-3.59 (m, 20H), 3.57-3.53 (m, 4H), 3.45-3.39 (t, 4H), 2.06-1.96 (m, 4H), 1.60-1.49 (m, 4H), 1.40-1.20 (m, 20H).

(C₉πC₉EO₆)_n. The polymer was purified by precipitation from toluene into hexanes. Yield 89% of a yellow tacky gel-like solid (M_n = 67,800, PDI = 1.56). ¹H NMR (300 MHz, CDCl₃) δ 5.40-5.38 (m, 2H), 3.65-3.59 (m, 20H), 3.57-3.53 (m, 4H), 3.45-3.39 (t, 4H), 2.06-1.96 (m, 4H), 1.60-1.49 (m, 4H), 1.40-1.20 (m, 24H).

(C₃πC₃EO₇)_n. The polymer was purified by precipitation from toluene into hexanes. Yield 98% of a yellow tacky gel-like solid (M_n = 26,400, PDI = 1.89). ¹H NMR (300 MHz, CDCl₃) δ 5.40-5.38 (m, 2H), 3.64-3.58 (m, 24H), 3.57-3.52 (m, 4H), 3.46-3.40 (t, 4H), 2.12-2.03 (m, 4H), 1.70-1.60 (m, 4H).

(C₄πC₄EO₇)_n. The polymer was purified by precipitation from toluene into hexanes. The precipitate was dissolved in THF and re-precipitated into *iso*-propanol. The precipitate was dried in *vacuo* to give a white translucent solid (M_n = 55,500, PDI = 1.79) in 78% yield. Evaporation of the *iso*-propanol solution gave a yellow gel-like solid (M_n = 25,100, PDI = 2.27) in 20% yield. ¹H NMR (300 MHz, CDCl₃) δ 5.40-5.38 (m,

2H), 3.65-3.59 (m, 24H), 3.57-3.53 (m, 4H), 3.46-3.40 (t, 4H), 2.09-2.00 (m, 4H), 1.63-1.52 (m, 4H), 1.47-1.35 (m, 4H).

(C₈πC₈EO₇)_n. The polymer was purified by precipitation from toluene into hexanes. The precipitate was dissolved in THF and re-precipitated into MeOH. The precipitate was dried in *vacuo* to give a white translucent solid ($M_n = 58,300$, PDI = 1.40) in 44% yield. Evaporation of the MeOH solution gave a yellow gel-like solid ($M_n = 22,300$, PDI = 1.47) in 37% yield. ¹H NMR (300 MHz, CDCl₃) δ 5.40-5.38 (m, 2H), 3.65-3.59 (m, 24H), 3.57-3.53 (m, 4H), 3.45-3.39 (t, 4H), 2.06-1.96 (m, 4H), 1.60-1.49 (m, 4H), 1.40-1.20 (m, 20H).

(C₉πC₉EO₇)_n. The polymer was purified by precipitation from toluene into hexanes. The precipitate was dissolved in THF and re-precipitated into MeOH. The precipitate was dried in *vacuo* to give a white translucent solid ($M_n = 40,600$, PDI = 1.41) in 58% yield. Evaporation of the MeOH solution gave a yellow gel-like solid ($M_n = 11,800$, PDI = 1.44) in 27% yield. ¹H NMR (300 MHz, CDCl₃) δ 5.40-5.38 (m, 2H), 3.68-3.59 (m, 24H), 3.58-3.52 (m, 4H), 3.46-3.39 (t, 4H), 2.00-1.90 (m, 4H), 1.60-1.50 (m, 4H), 1.40-1.20 (m, 24H).

(C₃πC₃EO₈)_n. The polymer was purified by precipitation from toluene into hexanes. Yield 95% of a yellow tacky gel-like solid ($M_n = 47,200$, PDI = 1.73). ¹H NMR (300 MHz, CDCl₃) δ 5.40-5.38 (m, 2H), 3.64-3.58 (m, 28H), 3.57-3.52 (m, 4H), 3.46-3.40 (t, 4H), 2.12-2.03 (m, 4H), 1.70-1.60 (m, 4H).

(C₄πC₄EO₈)_n. The polymer was purified by precipitation from toluene into hexanes. Yield 85% of a yellow tacky gel-like solid ($M_n = 19,400$, PDI = 1.61). ¹H NMR

(300 MHz, CDCl₃) δ 5.40-5.38 (m, 2H), 3.65-3.59 (m, 28H), 3.57-3.53 (m, 4H), 3.46-3.40 (t, 4H), 2.09-2.00 (m, 4H), 1.63-1.52 (m, 4H), 1.47-1.35 (m, 4H).

(C₈ π C₈EO₈)_n. The polymer was purified by precipitation from toluene into hexanes. The precipitate was dissolved in THF and re-precipitated into *iso*-propanol. The precipitate was dried in *vacuo* to give a white translucent solid (M_n = 65,700, PDI = 1.46) in 21% yield. Evaporation of the *iso*-propanol solution gave a yellow gel-like solid (M_n = 30,400, PDI = 1.62) in 73% yield. ¹H NMR (300 MHz, CDCl₃) δ 5.40-5.38 (m, 2H), 3.65-3.59 (m, 28H), 3.57-3.53 (m, 4H), 3.45-3.39 (t, 4H), 2.06-1.96 (m, 4H), 1.60-1.49 (m, 4H), 1.40-1.20 (m, 20H).

(C₉ π C₉EO₈)_n. The polymer was purified by precipitation from toluene into hexanes. The precipitate was dissolved in THF and re-precipitated into *iso*-propanol. The precipitate was dried in *vacuo* to give a white translucent solid (M_n = 60,100, PDI = 1.51) in 53% yield. Evaporation of the *iso*-propanol solution gave a yellow gel-like solid (M_n = 23,300, PDI = 1.52) in 38% yield. ¹H NMR (300 MHz, CDCl₃) δ 5.40-5.38 (m, 2H), 3.65-3.59 (m, 28H), 3.57-3.53 (m, 4H), 3.45-3.39 (t, 4H), 2.06-1.96 (m, 4H), 1.60-1.49 (m, 4H), 1.40-1.20 (m, 24H).

(C₃ π C₃EO₁₀)_n. The polymer was purified by precipitation from toluene into hexanes. The precipitate was dissolved in THF and re-precipitated into *iso*-propanol. The precipitate was dried in *vacuo* to give a white translucent solid (M_n = 54,500, PDI = 1.57) in 63% yield. Evaporation of the *iso*-propanol solution gave a yellow gel-like solid (M_n = 14,000, PDI = 2.10) in 34% yield. ¹H NMR (300 MHz, CDCl₃) δ 5.40-5.38 (m,

2H), 3.64-3.58 (m, 36H), 3.57-3.52 (m, 4H), 3.46-3.40 (t, 4H), 2.12-2.03 (m, 4H), 1.70-1.60 (m, 4H).

(C₄πC₄EO₁₀)_n. The polymer was purified by precipitation from toluene into hexanes. The precipitate was dissolved in THF and re-precipitated into *iso*-propanol. The precipitate was dried in *vacuo* to give a white translucent solid (*M_n* = 98,500, PDI = 1.38) in 24% yield. Evaporation of the *iso*-propanol solution gave a yellow gel-like solid (*M_n* = 28,300, PDI = 2.01) in 71% yield. ¹H NMR (300 MHz, CDCl₃) δ 5.40-5.38 (m, 2H), 3.65-3.59 (m, 36H), 3.57-3.53 (m, 4H), 3.46-3.40 (t, 4H), 2.09-2.00 (m, 4H), 1.63-1.52 (m, 4H), 1.47-1.35 (m, 4H).

(C₈πC₈EO₁₀)_n. The polymer was purified by precipitation from toluene into hexanes. The precipitate was dissolved in THF and re-precipitated into *iso*-propanol. The precipitate was dried in *vacuo* to give a white translucent solid (*M_n* = 41,300, PDI = 1.74) in 29% yield. Evaporation of the *iso*-propanol solution gave a yellow gel-like solid (*M_n* = 23,200, PDI = 1.64) in 70% yield. ¹H NMR (300 MHz, CDCl₃) δ 5.40-5.38 (m, 2H), 3.65-3.59 (m, 36H), 3.57-3.53 (m, 4H), 3.45-3.39 (t, 4H), 2.06-1.96 (m, 4H), 1.60-1.49 (m, 4H), 1.40-1.20 (m, 20H).

(C₉πC₉EO₁₀)_n. The polymer was purified by precipitation from toluene into hexanes. The precipitate was dissolved in THF and re-precipitated into *iso*-propanol. The precipitate was dried in *vacuo* to give a white translucent solid (*M_n* = 52,700, PDI = 1.46) in 28% yield. Evaporation of the *iso*-propanol solution gave a yellow gel-like solid (*M_n* = 16,500, PDI = 1.73) in 71% yield. ¹H NMR (300 MHz, CDCl₃) δ 5.40-5.38 (m,

2H), 3.65-3.59 (m, 36H), 3.57-3.53 (m, 4H), 3.45-3.39 (t, 4H), 2.06-1.96 (m, 4H), 1.60-1.49 (m, 4H), 1.40-1.20 (m, 24H).

$(C_3\pi C_3EO_{14})_n$. The polymer was purified by precipitation from toluene into hexanes. The precipitate was dissolved in THF and re-precipitated into *iso*-propanol. The precipitate was dried in *vacuo* to give a white translucent solid ($M_n = 17,400$, PDI = 2.00) in 46% yield. Evaporation of the *iso*-propanol solution gave a yellow gel-like solid ($M_n = 15,600$, PDI = 1.93) in 51% yield. 1H NMR (300 MHz, $CDCl_3$) δ 5.40-5.38 (m, 2H), 3.64-3.58 (m, 52H), 3.57-3.52 (m, 4H), 3.46-3.40 (t, 4H), 2.12-2.03 (m, 4H), 1.70-1.60 (m, 4H).

$(C_4\pi C_4EO_{14})_n$. The polymer was purified by precipitation from toluene into hexanes. The precipitate was dissolved in THF and re-precipitated into *iso*-propanol. The precipitate was dried in *vacuo* to give a white translucent solid ($M_n = 41,700$, PDI = 1.52) in 58% yield. Evaporation of the *iso*-propanol solution gave a yellow gel-like solid ($M_n = 13,200$, PDI = 1.81) in 40% yield. 1H NMR (300 MHz, $CDCl_3$) δ 5.40-5.38 (m, 2H), 3.65-3.59 (m, 52H), 3.57-3.53 (m, 4H), 3.46-3.40 (t, 4H), 2.09-2.00 (m, 4H), 1.63-1.52 (m, 4H), 1.47-1.35 (m, 4H).

$(C_8\pi C_8EO_{14})_n$. The polymer was purified by precipitation from toluene into hexanes. The precipitate was dissolved in THF and re-precipitated into *iso*-propanol. The precipitate was dried in *vacuo* to give a white translucent solid ($M_n = 21,100$, PDI = 1.87) in 57% yield. Evaporation of the *iso*-propanol solution gave a yellow gel-like solid ($M_n = 15,900$, PDI = 1.73) in 41% yield. 1H NMR (300 MHz, $CDCl_3$) δ 5.40-5.38 (m,

2H), 3.65-3.59 (m, 52H), 3.57-3.53 (m, 4H), 3.45-3.39 (t, 4H), 2.06-1.96 (m, 4H), 1.60-1.49 (m, 4H), 1.40-1.20 (m, 20H).

(C₉πC₉EO₁₄)_n. The polymer was purified by precipitation from toluene into hexanes. The precipitate was dissolved in THF and re-precipitated into *iso*-propanol. The precipitate was dried in *vacuo* to give a white translucent solid (M_n = 63,200, PDI = 1.64) in 38% yield. Evaporation of the *iso*-propanol solution gave a yellow gel-like solid (M_n = 59,200, PDI = 1.62) in 59% yield. ¹H NMR (300 MHz, CDCl₃) δ 5.40-5.38 (m, 2H), 3.65-3.59 (m, 52H), 3.57-3.53 (m, 4H), 3.45-3.39 (t, 4H), 2.06-1.96 (m, 4H), 1.60-1.49 (m, 4H), 1.40-1.20 (m, 24H).

8. General procedure for preparation of saturated polymers.

Preparation of (C₁₀EO₆)_n. A 70 mL Fisher-Porter bottle was charged with unsaturated polymer (C₄πC₄EO₆)_n (0.200 g), 20 mL CH₂Cl₂, and 0.010 g 10% palladium on carbon. Hydrogenation was carried out with stirring at room temperature under 5 atm hydrogen pressure for 2 hours. Upon completion of the reaction, the catalyst (which can be reused) was filtered and washed with CH₂Cl₂. The filtrate was concentrated and the resulting polymer was dissolved in THF. Precipitation in hexanes followed by drying in *vacuo* gave white saturated polymer (C₁₀EO₆)_n (M_n = 11,800, PDI = 1.64) in 97% yield. ¹H NMR (300 MHz, CDCl₃) δ 3.67-3.58 (m, 20H), 3.57-3.52 (m, 4H), 3.45-3.38 (t, 4H), 1.60-1.49 (m, 4H), 1.34-1.18 (m, 12H).

(C₁₀EO₇)_n. A white waxy solid (M_n = 15,800, PDI = 1.85) prepared by hydrogenation of polymer (C₄πC₄EO₆)_n in 98% yield. ¹H NMR (300 MHz, CDCl₃) δ

3.67-3.58 (m, 24H), 3.57-3.52 (m, 4H), 3.45-3.38 (t, 4H), 1.60-1.49 (m, 4H), 1.34-1.18 (m, 12H).

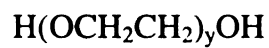
(C₁₀EO₈)_n. A white waxy solid (Mn = 13,200, PDI = 1.98) prepared by hydrogenation of polymer **(C₄πC₄EO₆)_n** in 98% yield. ¹H NMR (300 MHz, CDCl₃) δ 3.67-3.58 (m, 28H), 3.57-3.52 (m, 4H), 3.45-3.38 (t, 4H), 1.60-1.49 (m, 4H), 1.34-1.18 (m, 12H).

(C₁₀EO₁₀)_n. A white waxy solid (Mn = 24,100, PDI = 2.41) prepared by hydrogenation of polymer **(C₄πC₄EO₆)_n** in 99% yield. ¹H NMR (300 MHz, CDCl₃) δ 3.67-3.58 (m, 36H), 3.57-3.52 (m, 4H), 3.45-3.38 (t, 4H), 1.60-1.49 (m, 4H), 1.34-1.18 (m, 12H).

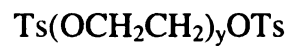
(C₁₀EO₁₄)_n. A white waxy solid (Mn = 8,500, PDI = 1.58) prepared by hydrogenation of polymer **(C₄πC₄EO₆)_n** in 99% yield. ¹H NMR (300 MHz, CDCl₃) δ 3.67-3.58 (m, 52H), 3.57-3.52 (m, 4H), 3.45-3.38 (t, 4H), 1.60-1.49 (m, 4H), 1.34-1.18 (m, 12H).

(C₂₀EO₇)_n. A white waxy solid (Mn = 9,900, PDI = 1.45) prepared by hydrogenation of polymer **(C₄πC₄EO₆)_n** in 99% yield. ¹H NMR (300 MHz, CDCl₃) δ 3.67-3.58 (m, 24H), 3.57-3.52 (m, 4H), 3.45-3.38 (t, 4H), 1.60-1.49 (m, 4H), 1.34-1.18 (m, 32H).

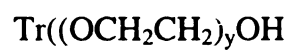
III. Number of Compounds



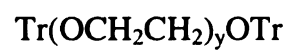
1(y)



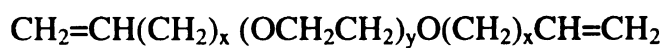
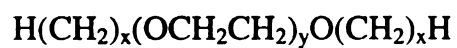
2(y)



3(y)



4(y)



APPENDIX

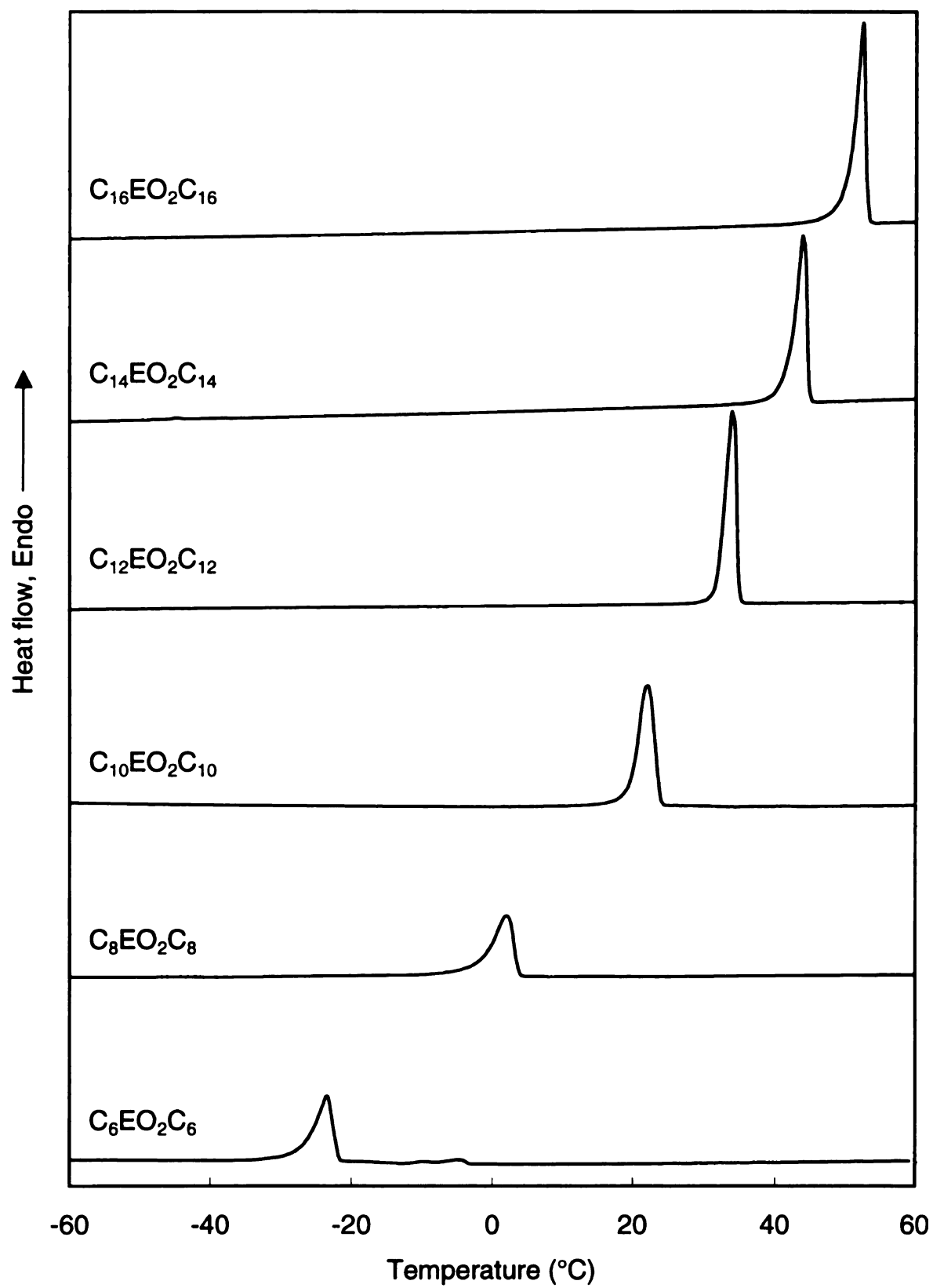


Figure 89. DSC heating scans of triblock oligomers $C_xEO_2C_x$

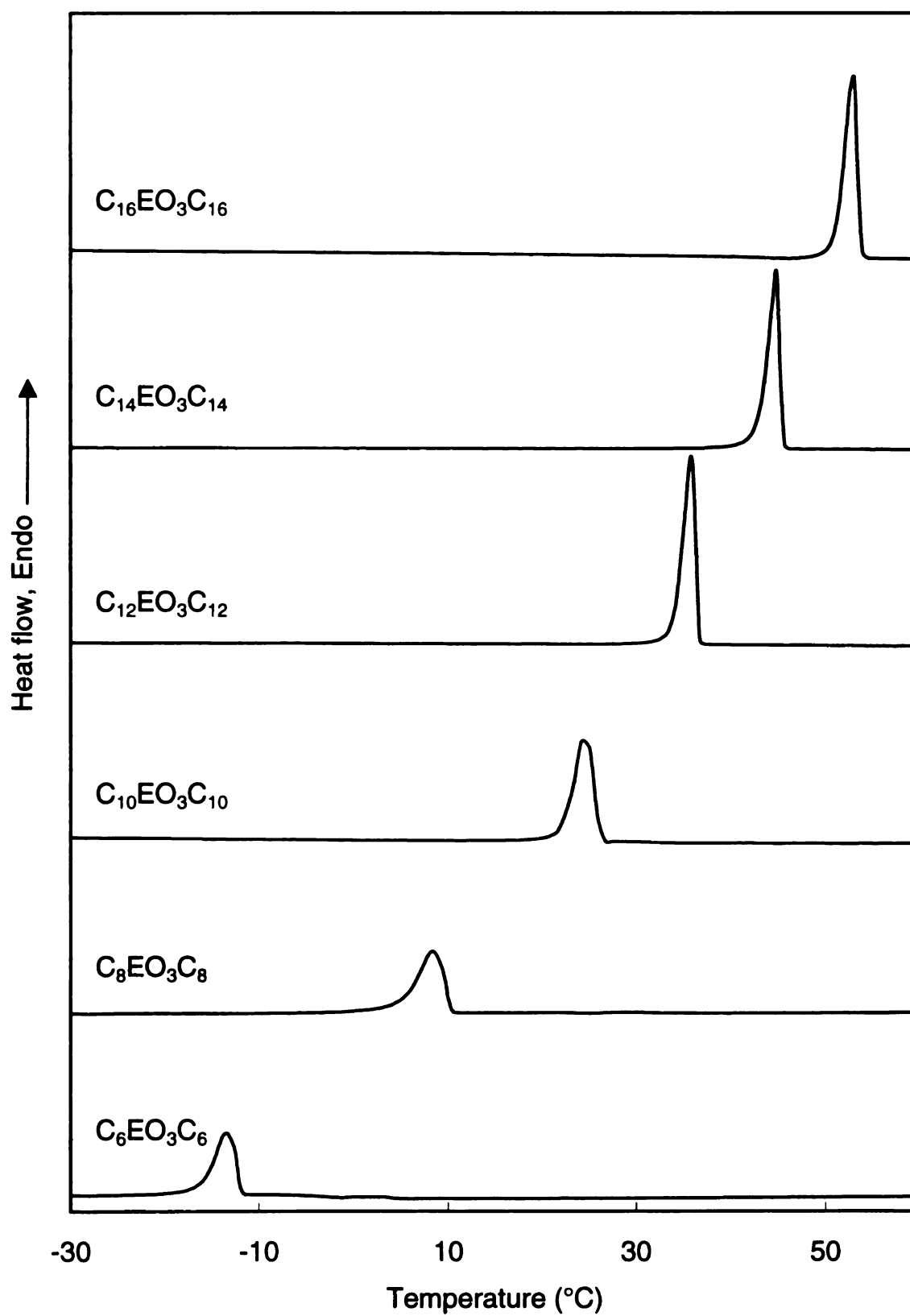


Figure 90. DSC heating scans of triblock oligomers $C_xEO_3C_x$

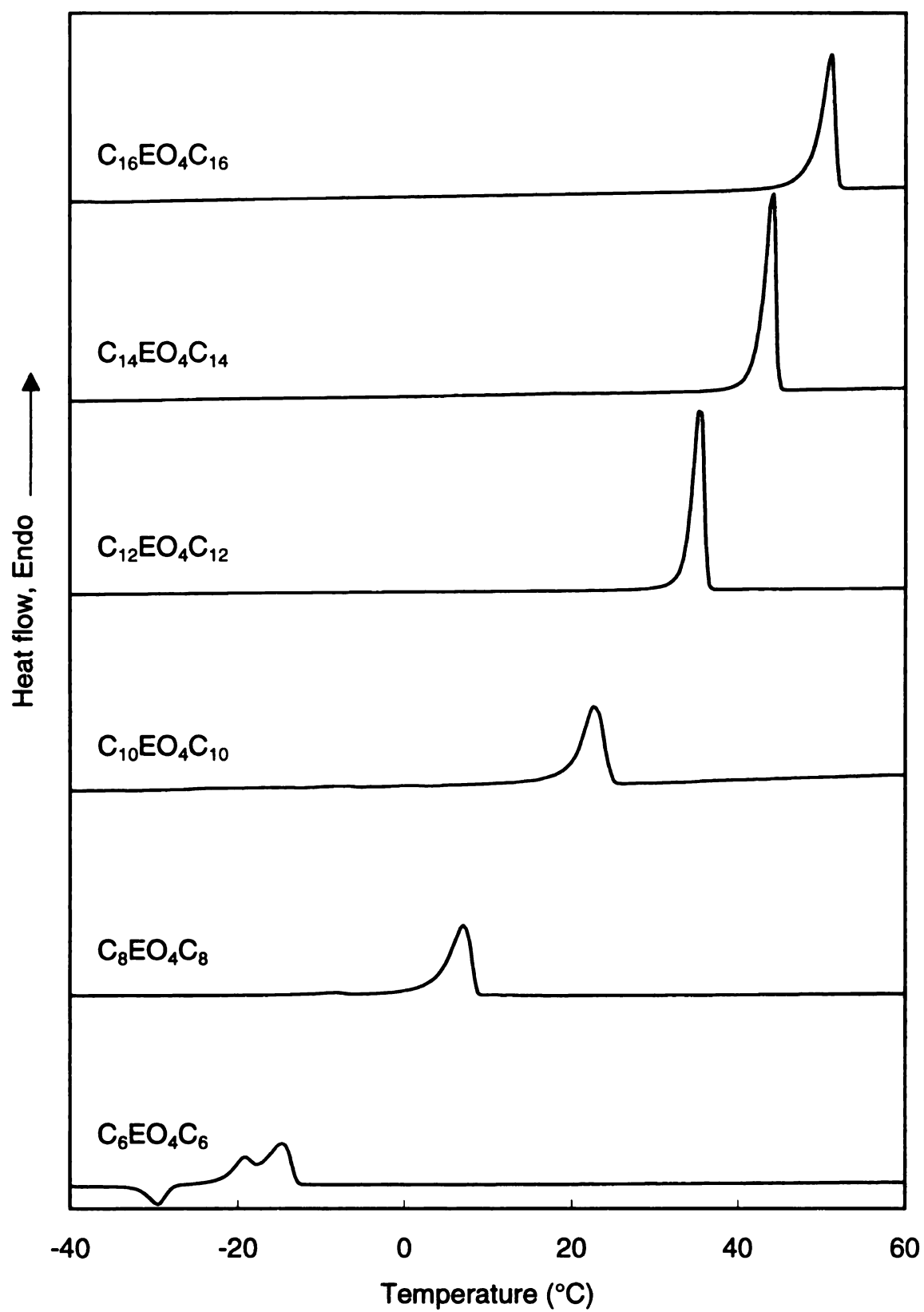


Figure 91. DSC heating scans of triblock oligomers $C_xEO_4C_x$

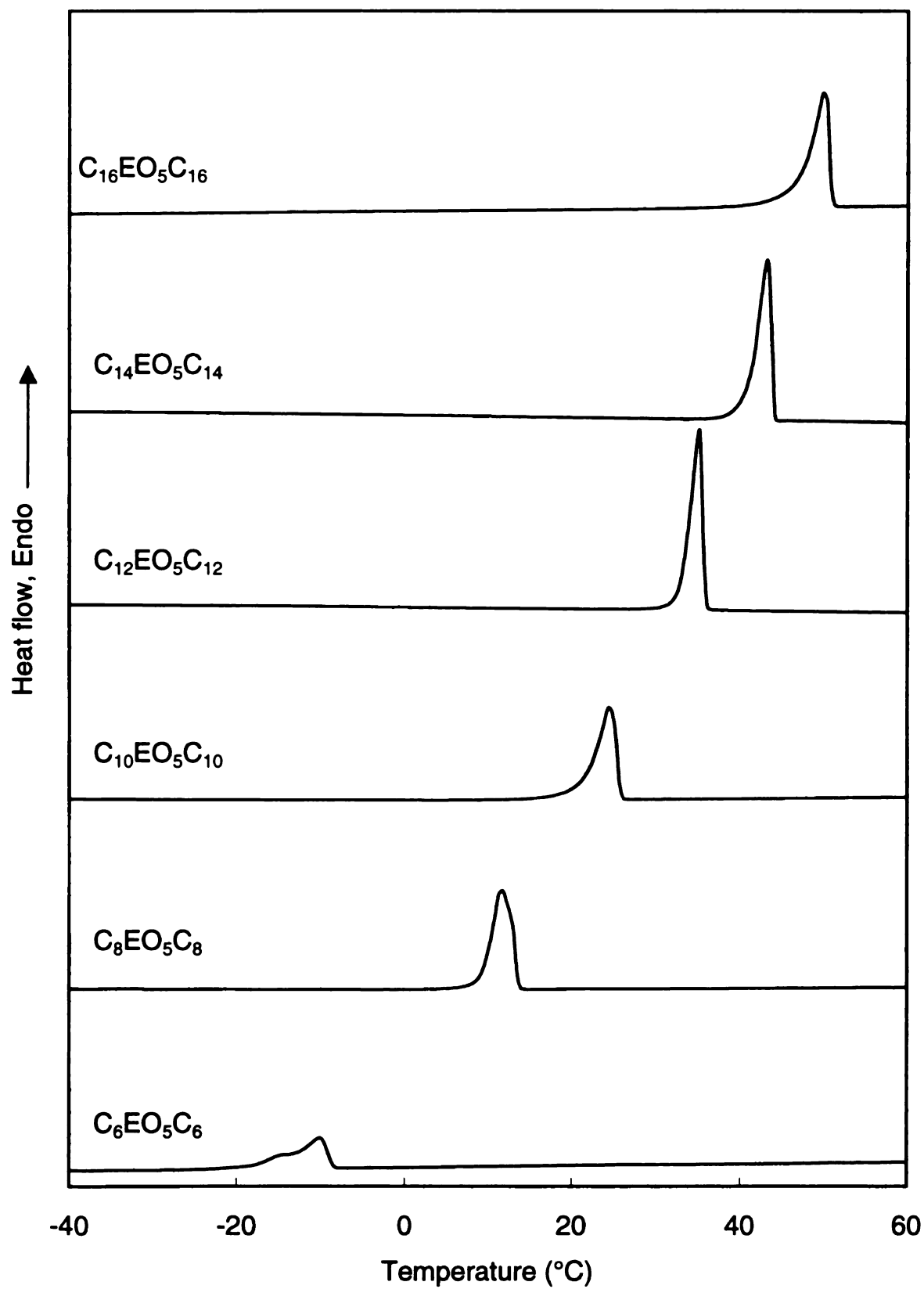


Figure 92. DSC heating scans of triblock oligomers $C_xEO_5C_x$

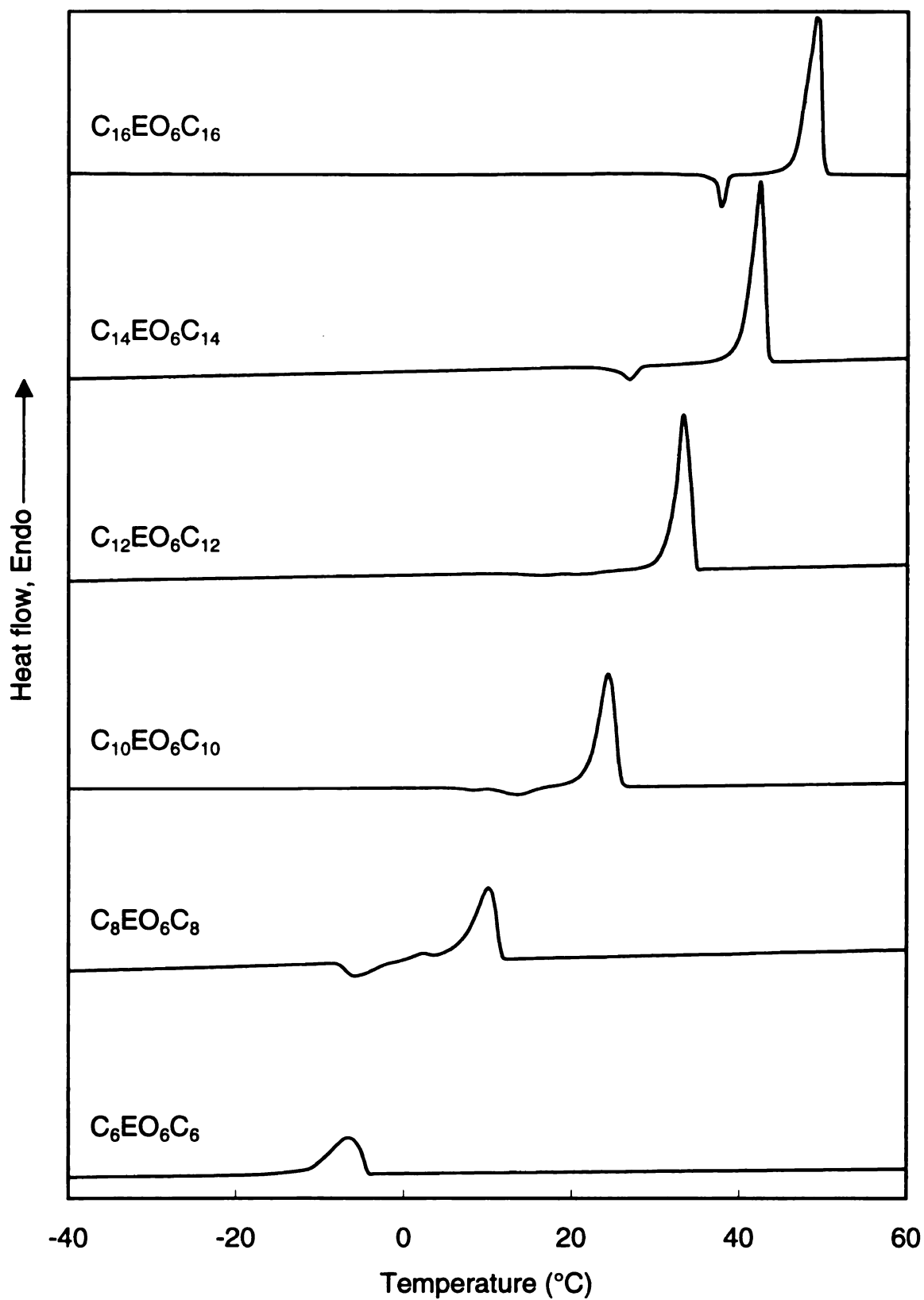


Figure 93. DSC heating scans of triblock oligomers $C_xEO_6C_x$

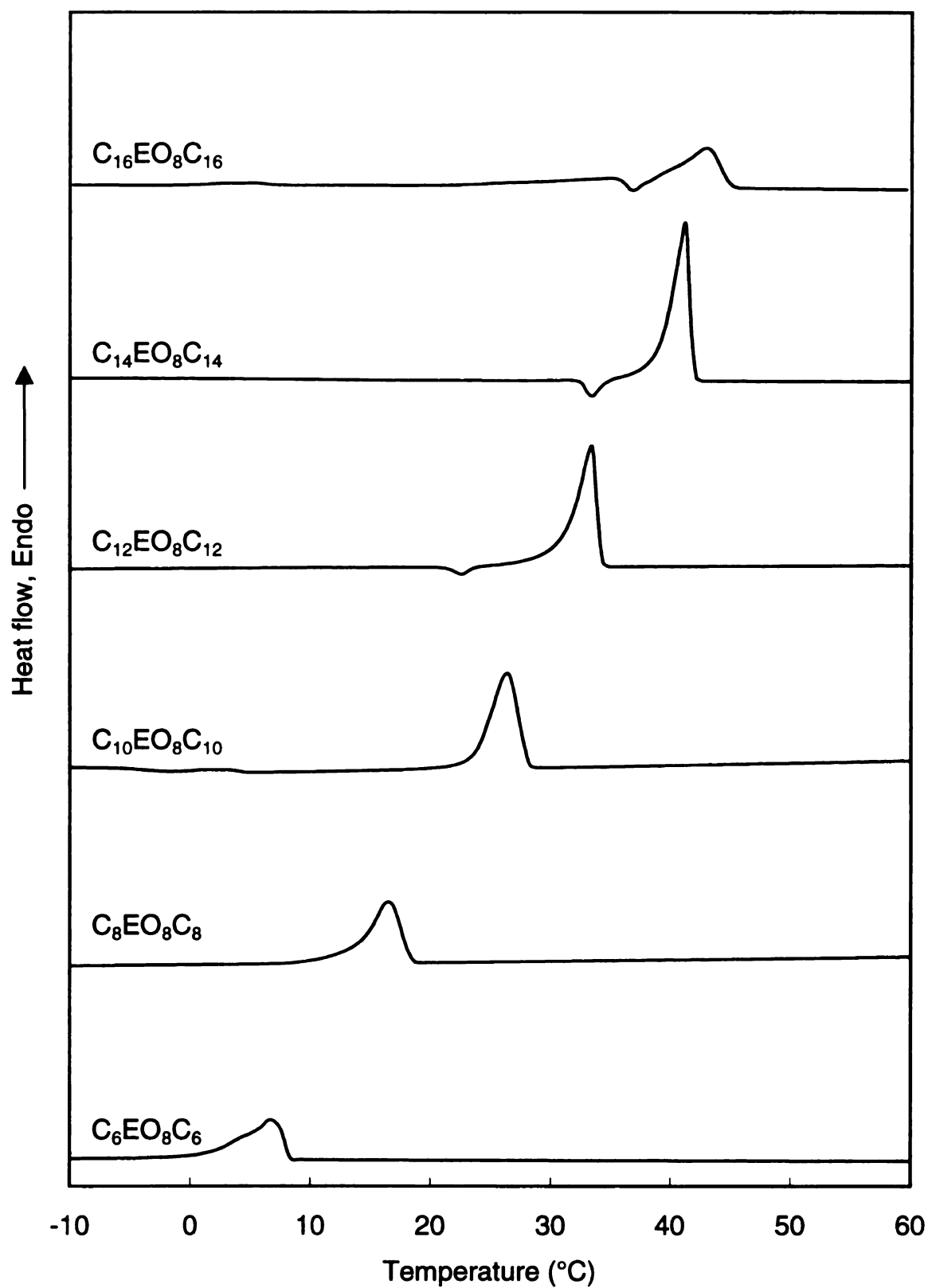


Figure 94. DSC heating scans of triblock oligomers $C_xEO_8C_x$

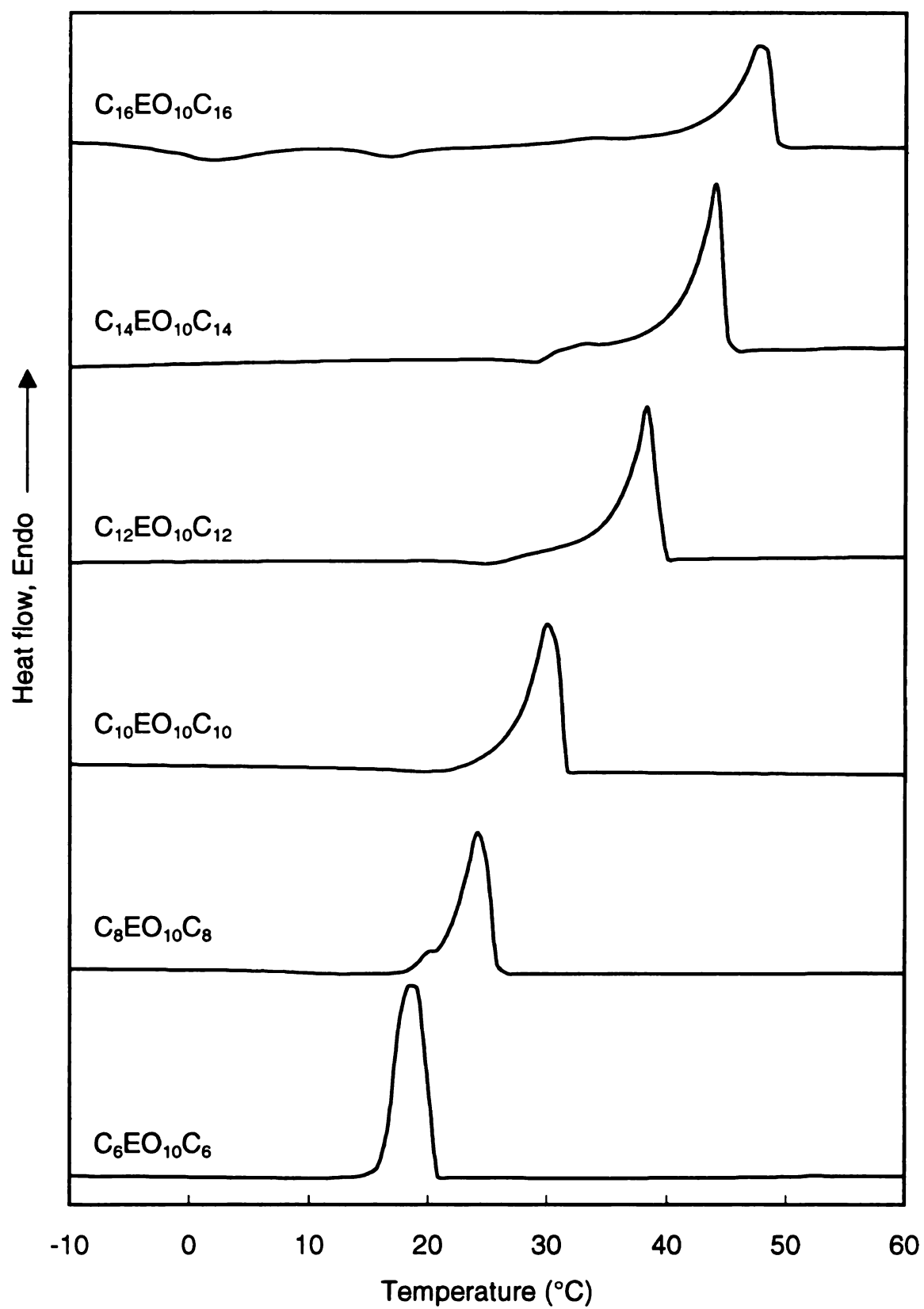


Figure 95. DSC heating scans of triblock oligomers $C_xEO_{10}C_x$

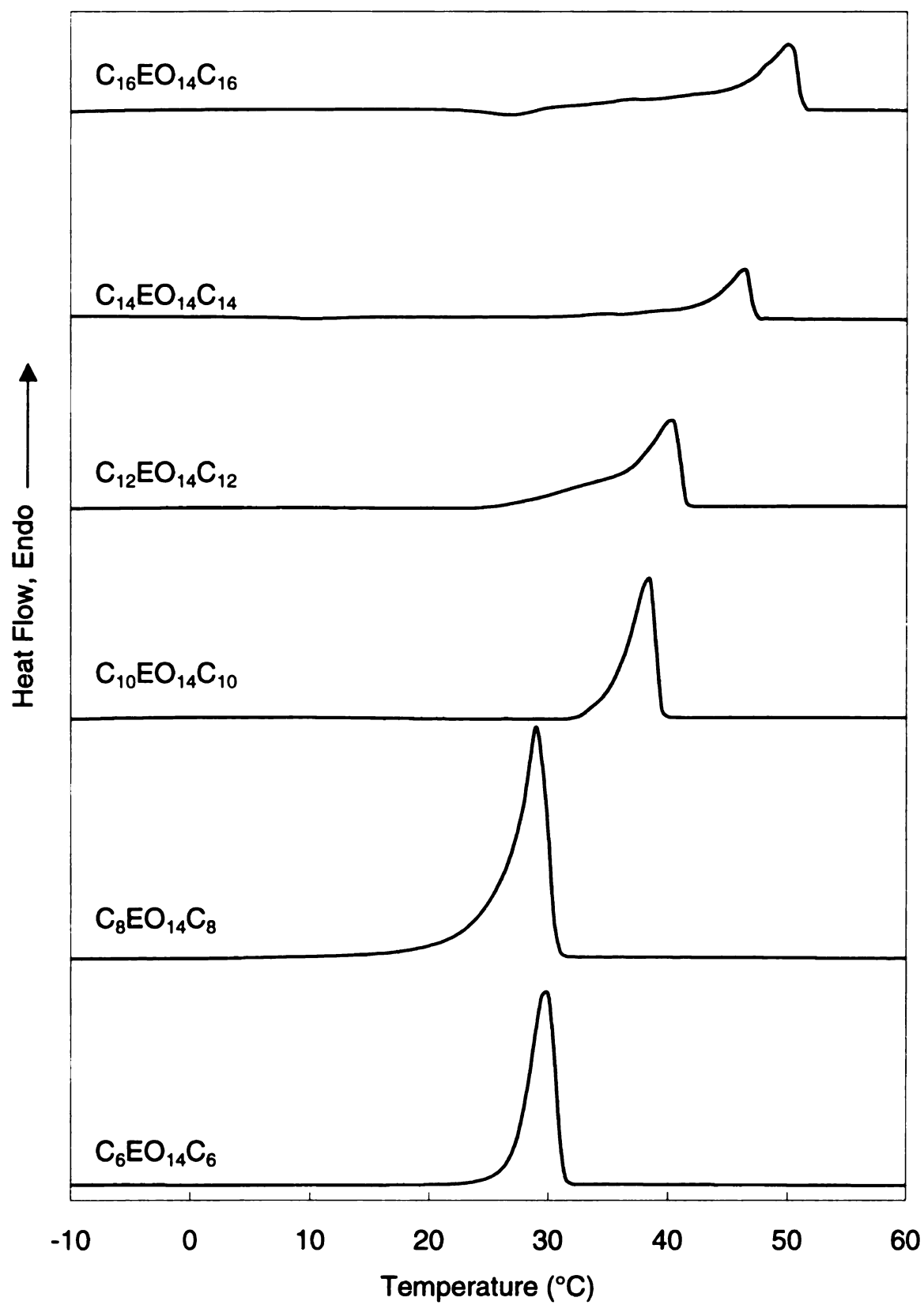


Figure 96. DSC heating scans of triblock oligomers $C_xEO_{14}C_x$

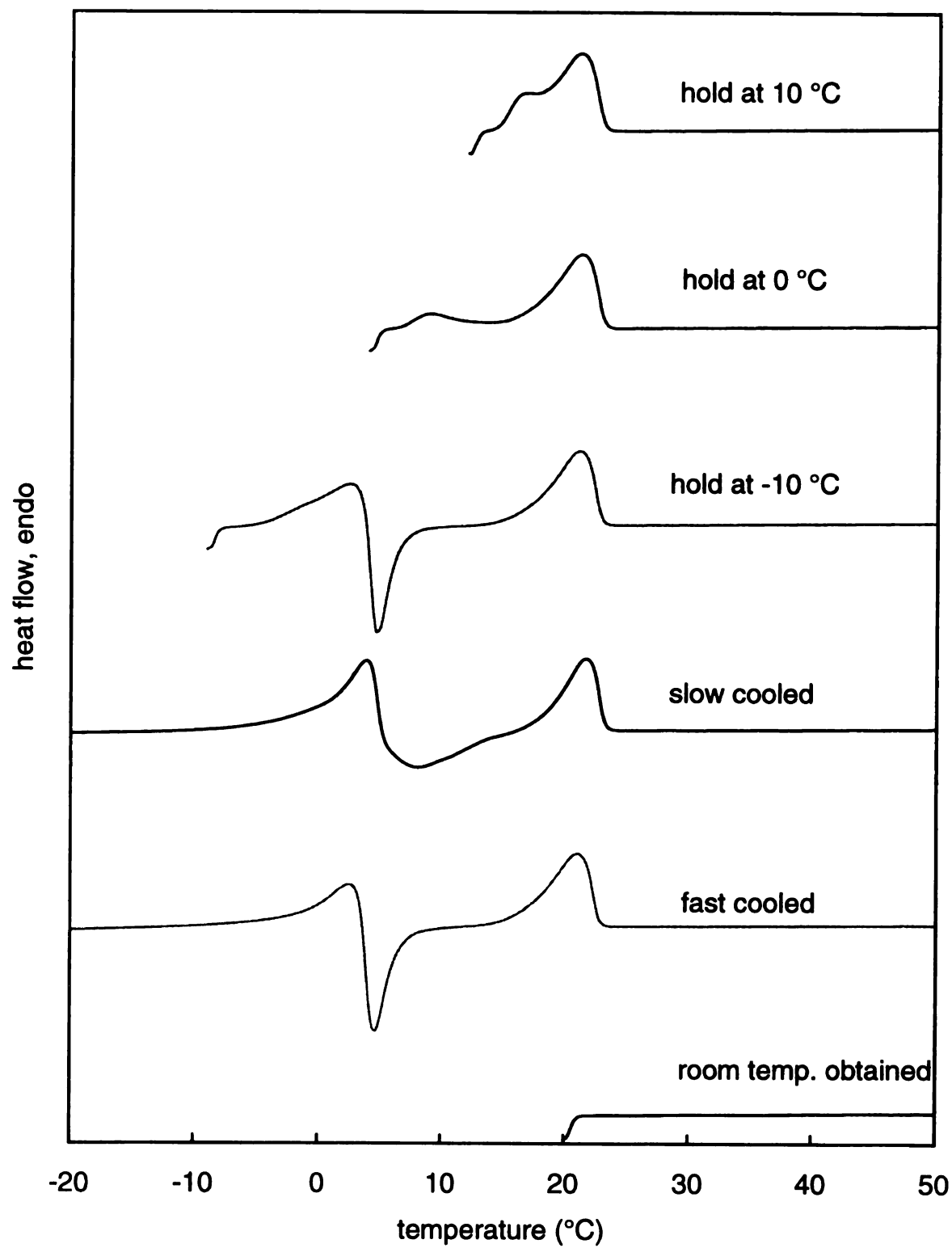


Figure 97. DSC heating scans of polymer $(C_4\pi C_4EO_6)_n$ with different crystallization histories.

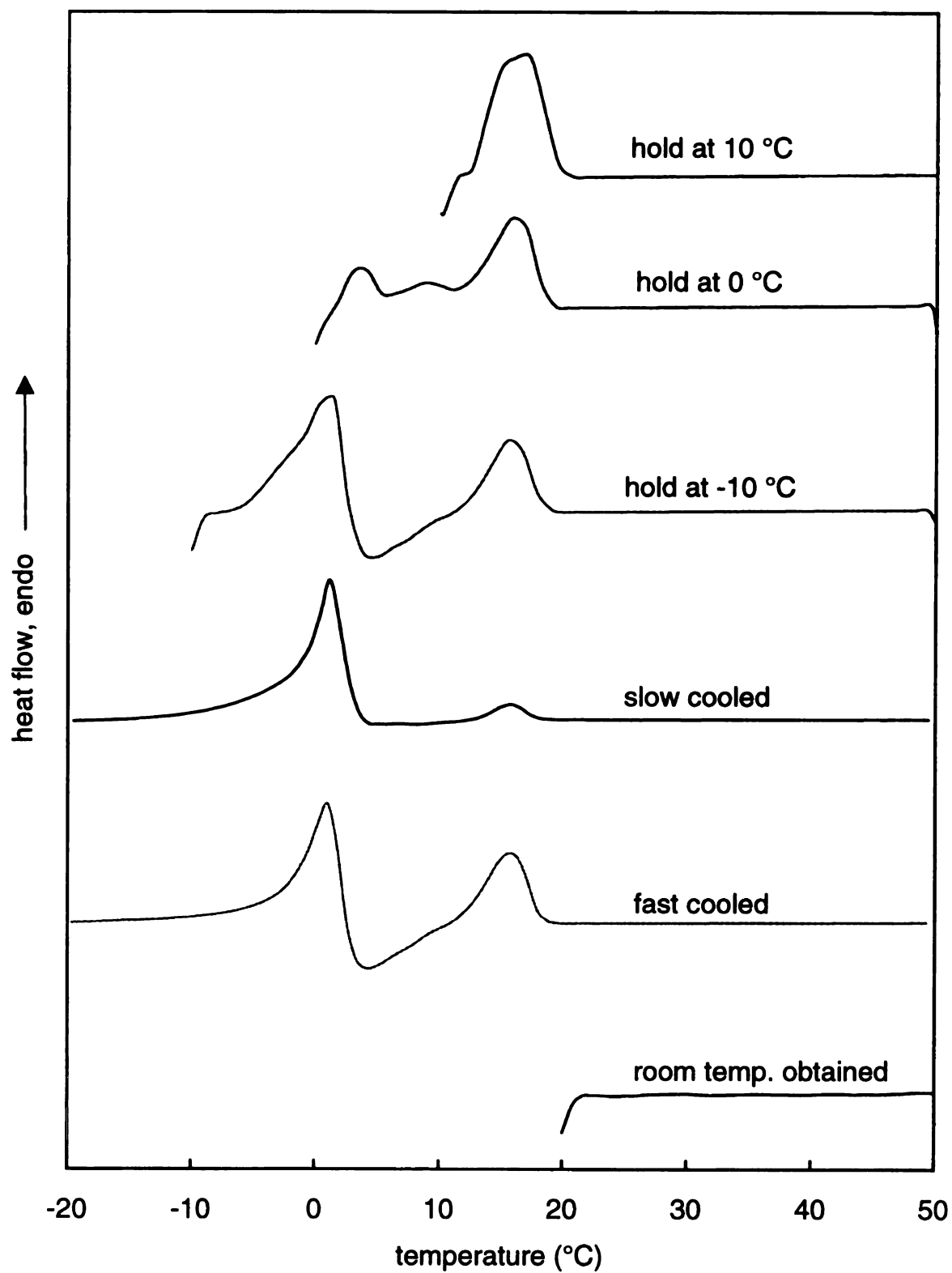


Figure 98. DSC heating scans of polymer $(C_4\pi C_4EO_7)_n$ with different crystallization histories.

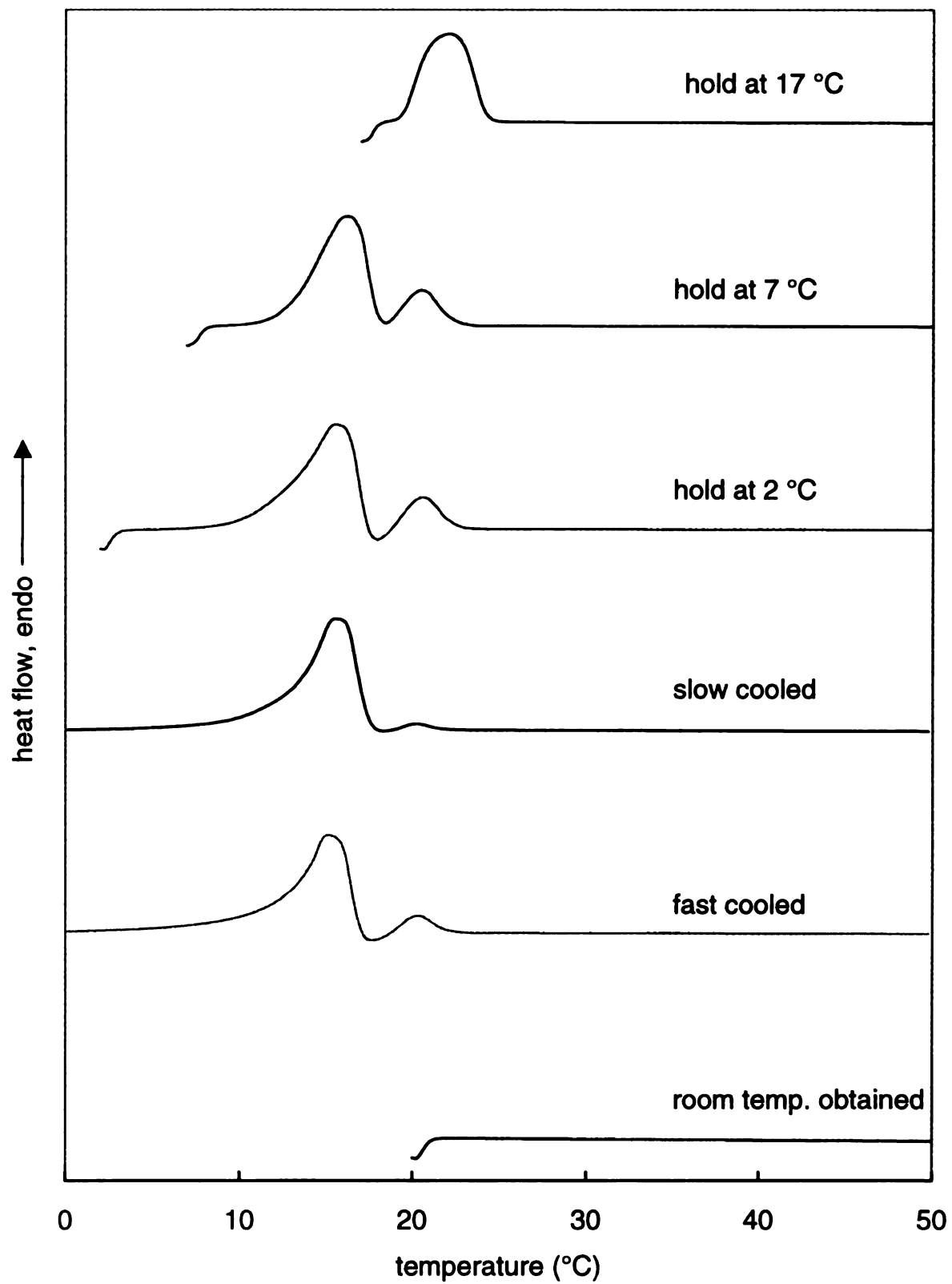


Figure 99. DSC heating scans of polymer $(C_4\pi C_4EO_8)_n$ with different crystallization histories.

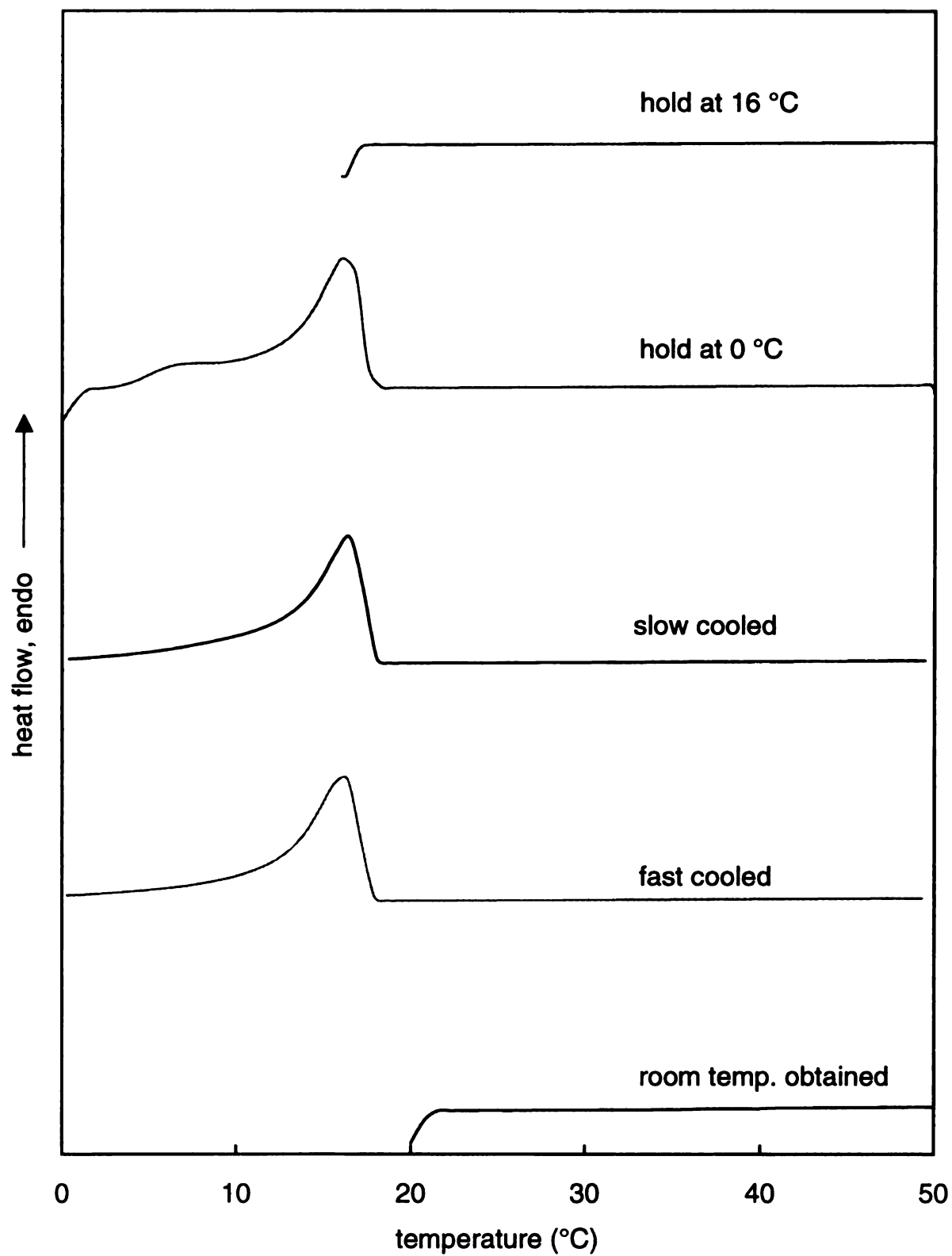


Figure 100. DSC heating scans of polymer $(C_4\pi C_4EO_{10})_n$ with different crystallization histories.

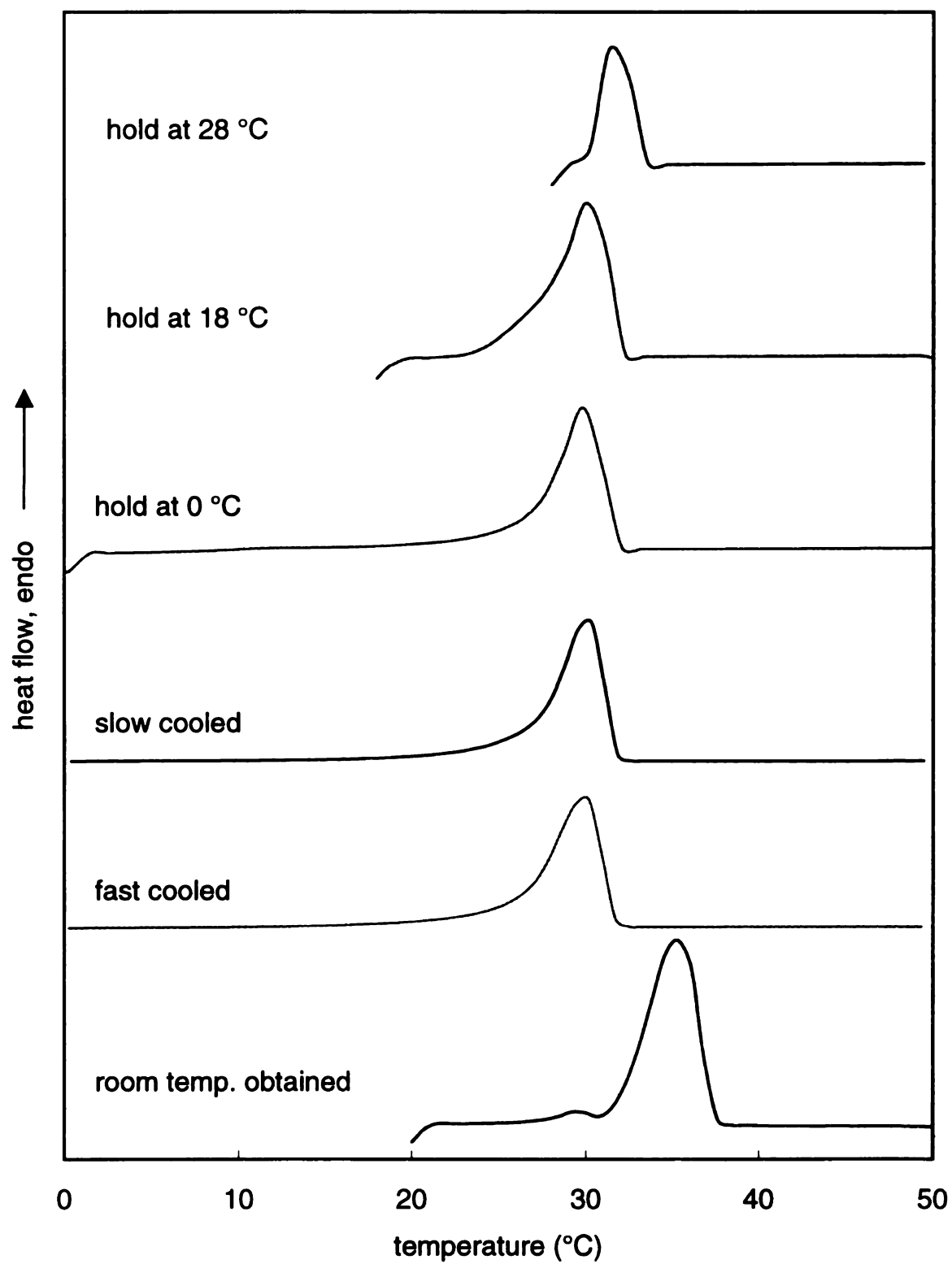


Figure 101. DSC heating scans of polymer $(C_4\pi C_4EO_{14})_n$ with different crystallization histories.

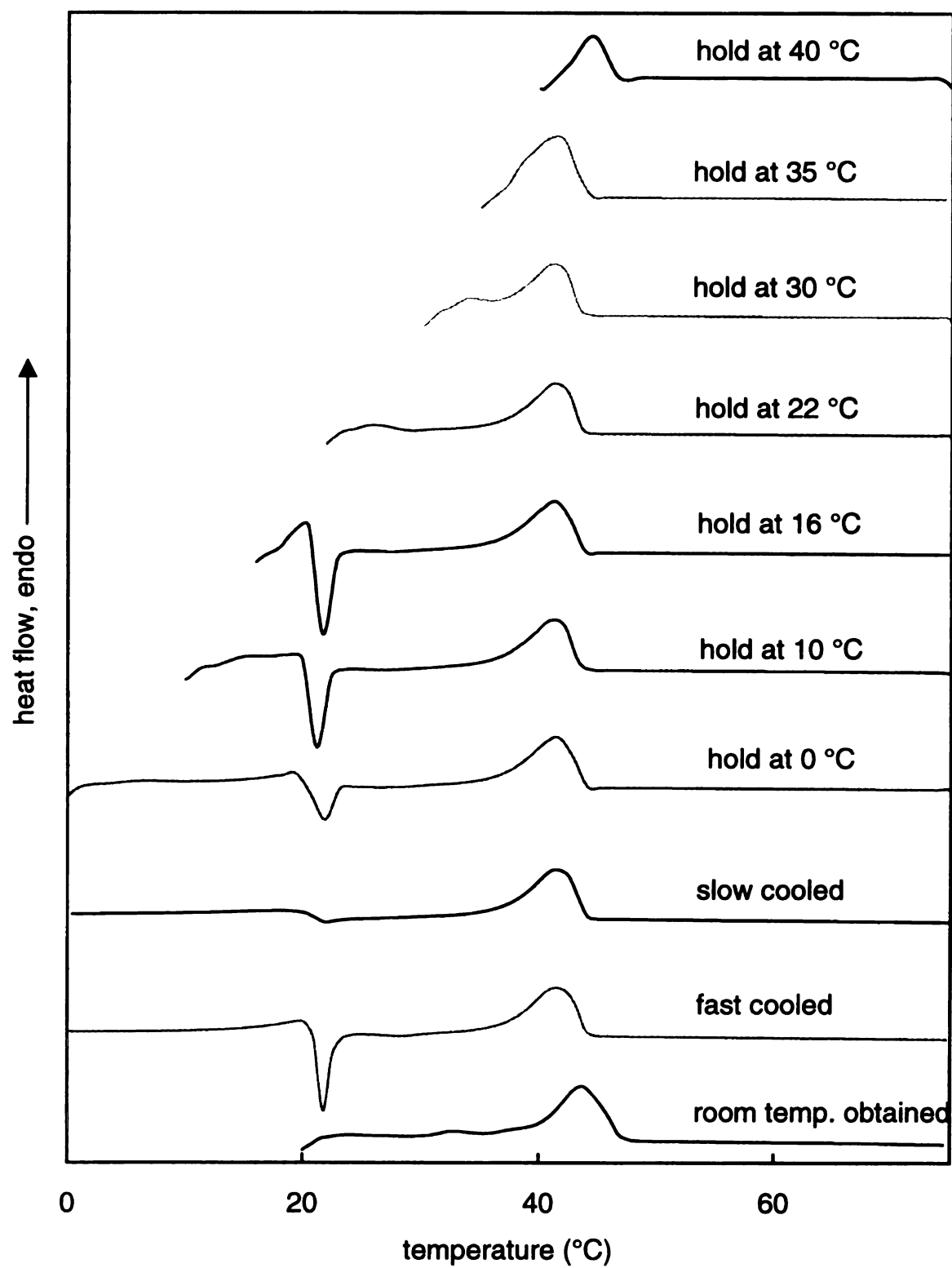


Figure 102. DSC heating scans of polymer $(C_8\pi C_8EO_6)_n$ with different crystallization histories.

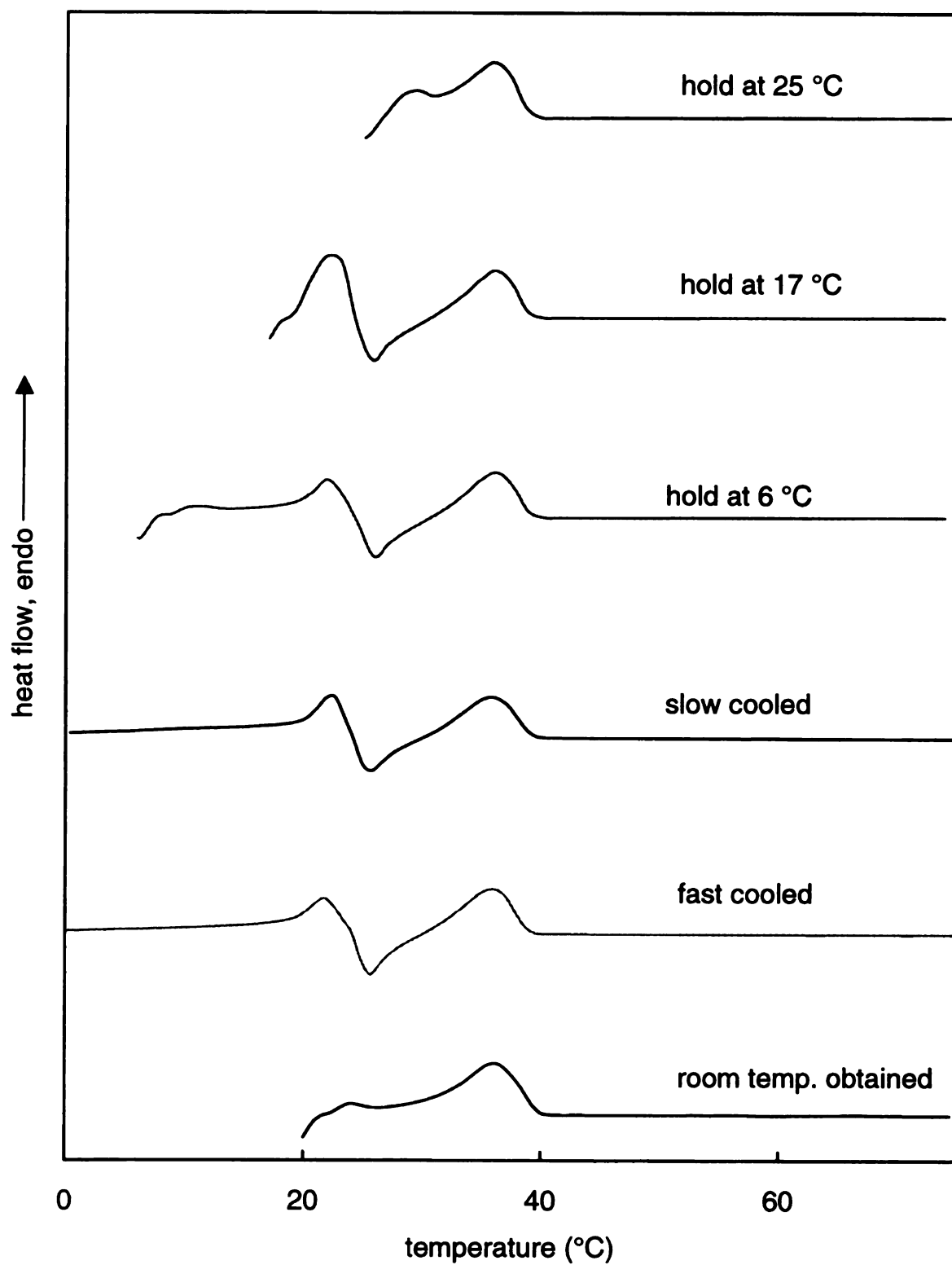


Figure 103. DSC heating scans of polymer $(C_8\pi C_8EO_7)_n$ with different crystallization histories.

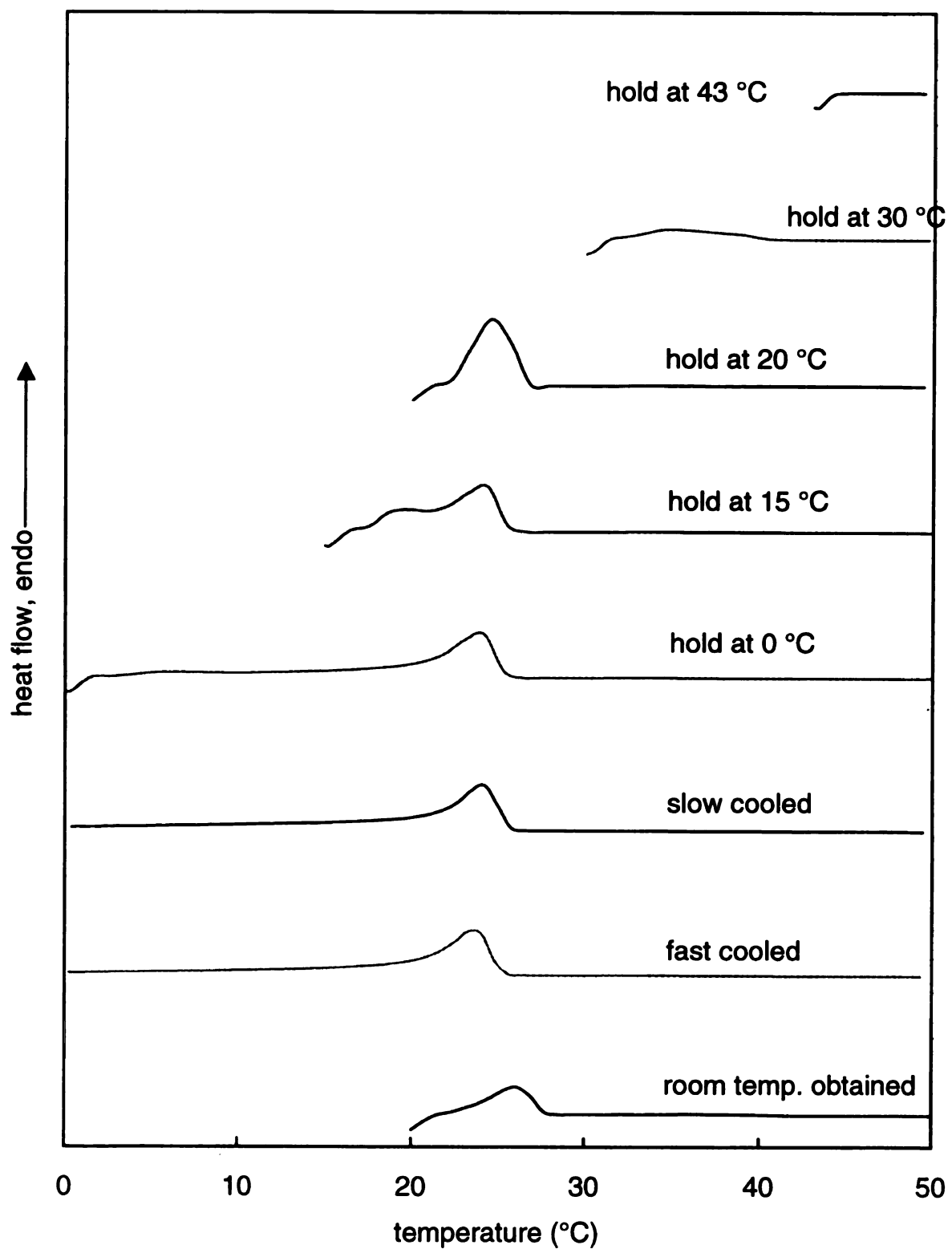


Figure 104. DSC heating scans of polymer $(C_8\pi C_8EO_8)_n$ with different crystallization histories.

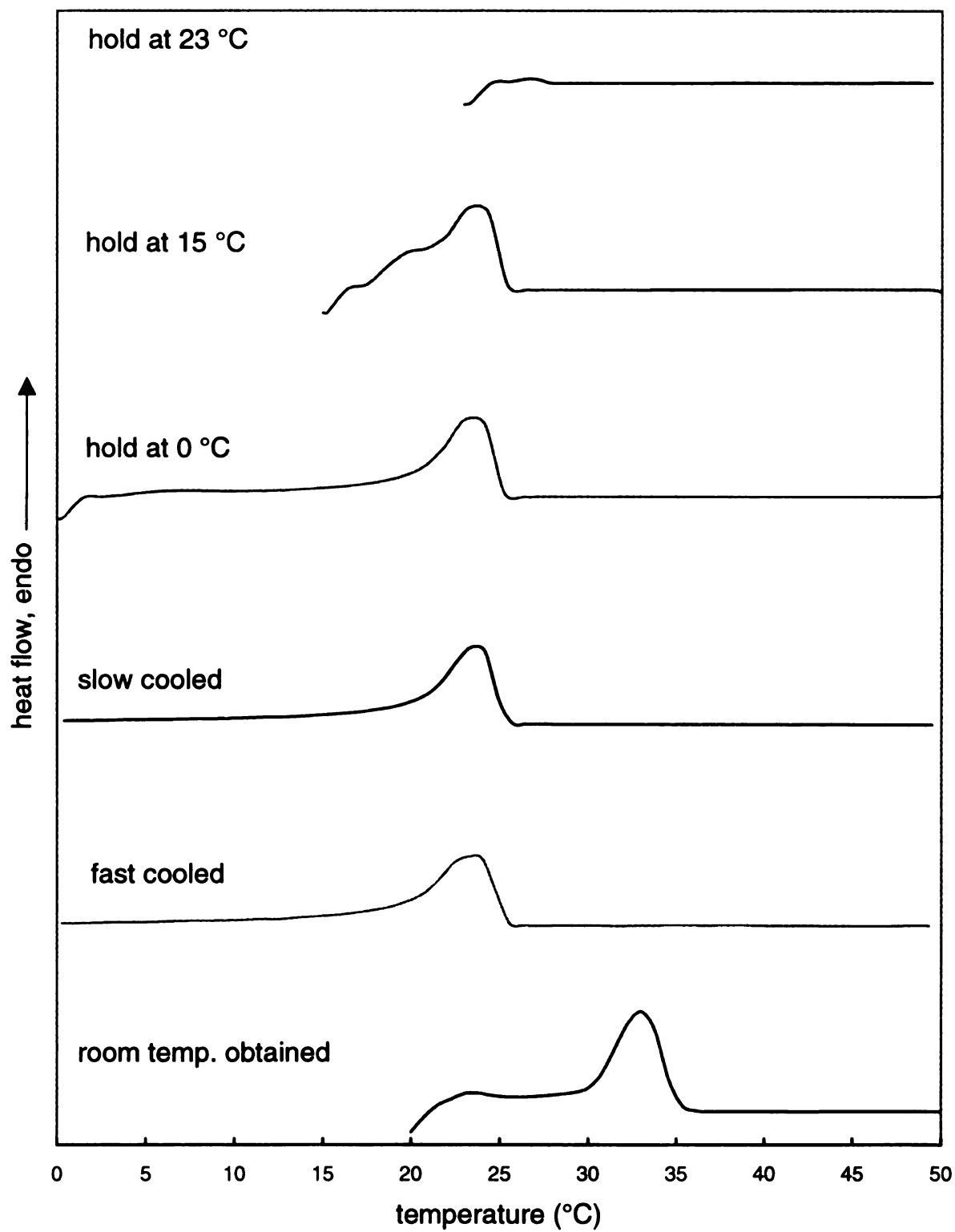


Figure 105. DSC heating scans of polymer $(C_8\pi C_8EO_{10})_n$ with different crystallization histories.

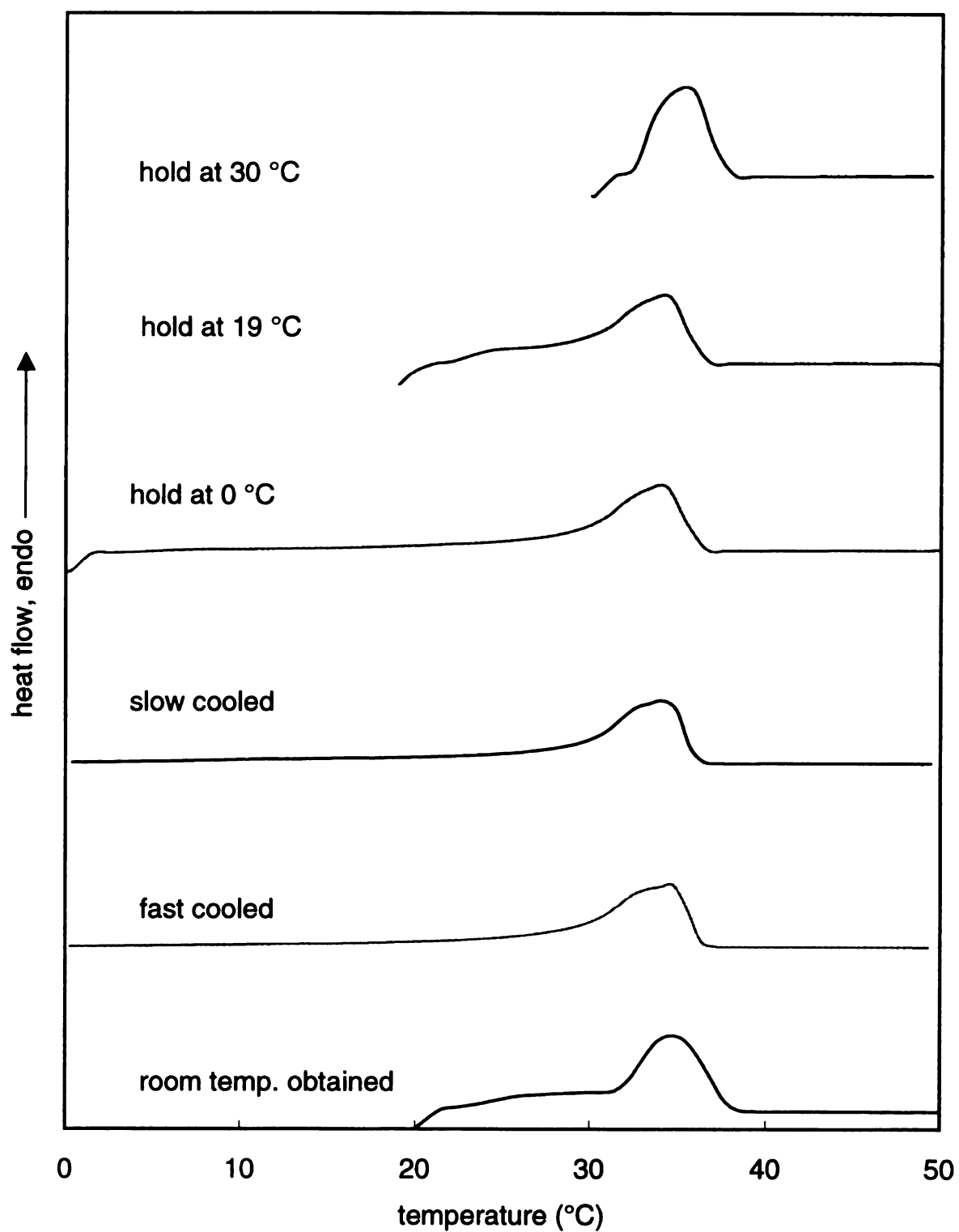


Figure 106. DSC heating scans of polymer $(C_8\pi C_8EO_{14})_n$ with different crystallization histories.

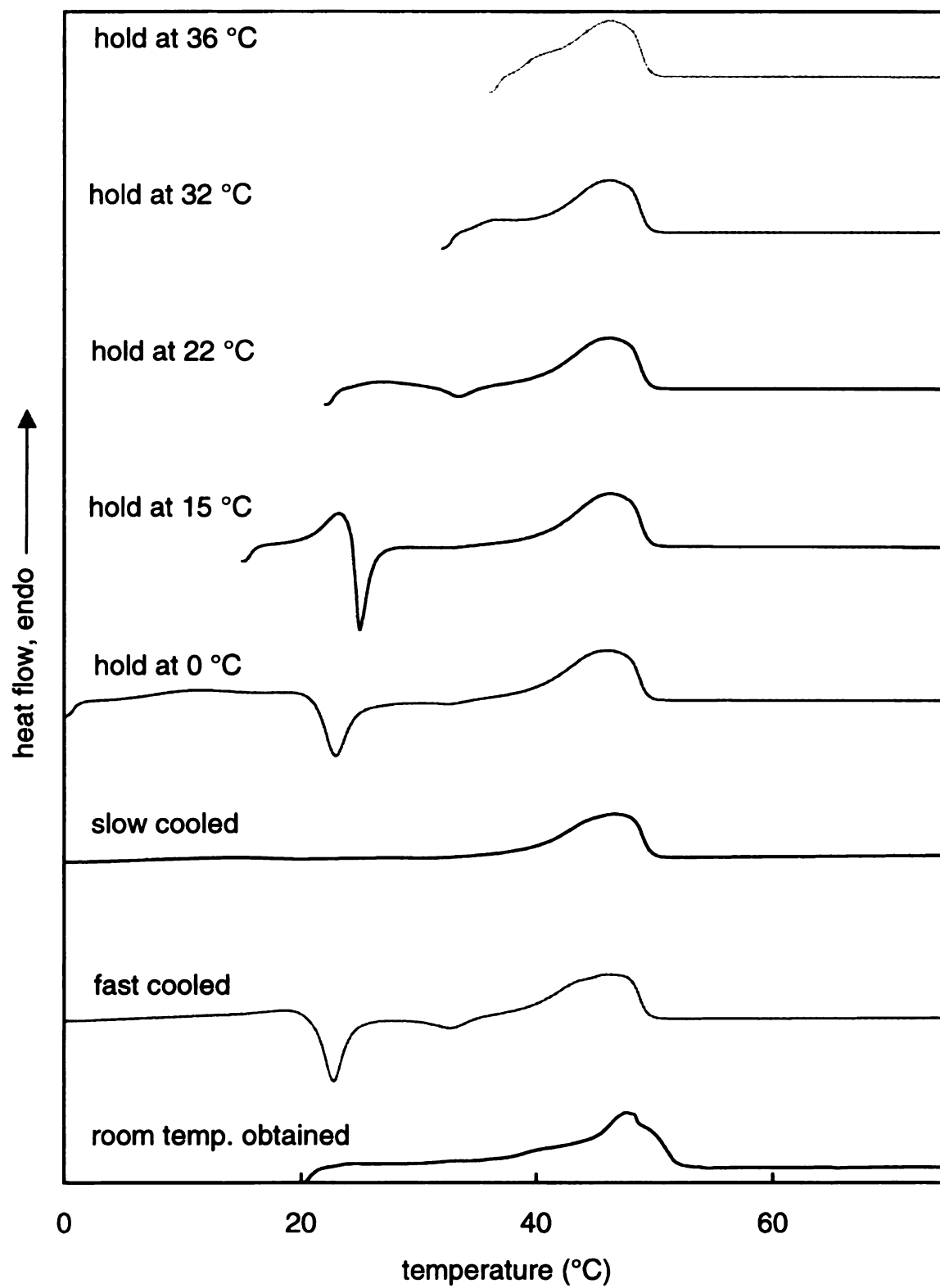


Figure 107. DSC heating scans of polymer $(C_9\pi C_9EO_6)_n$ with different crystallization histories.

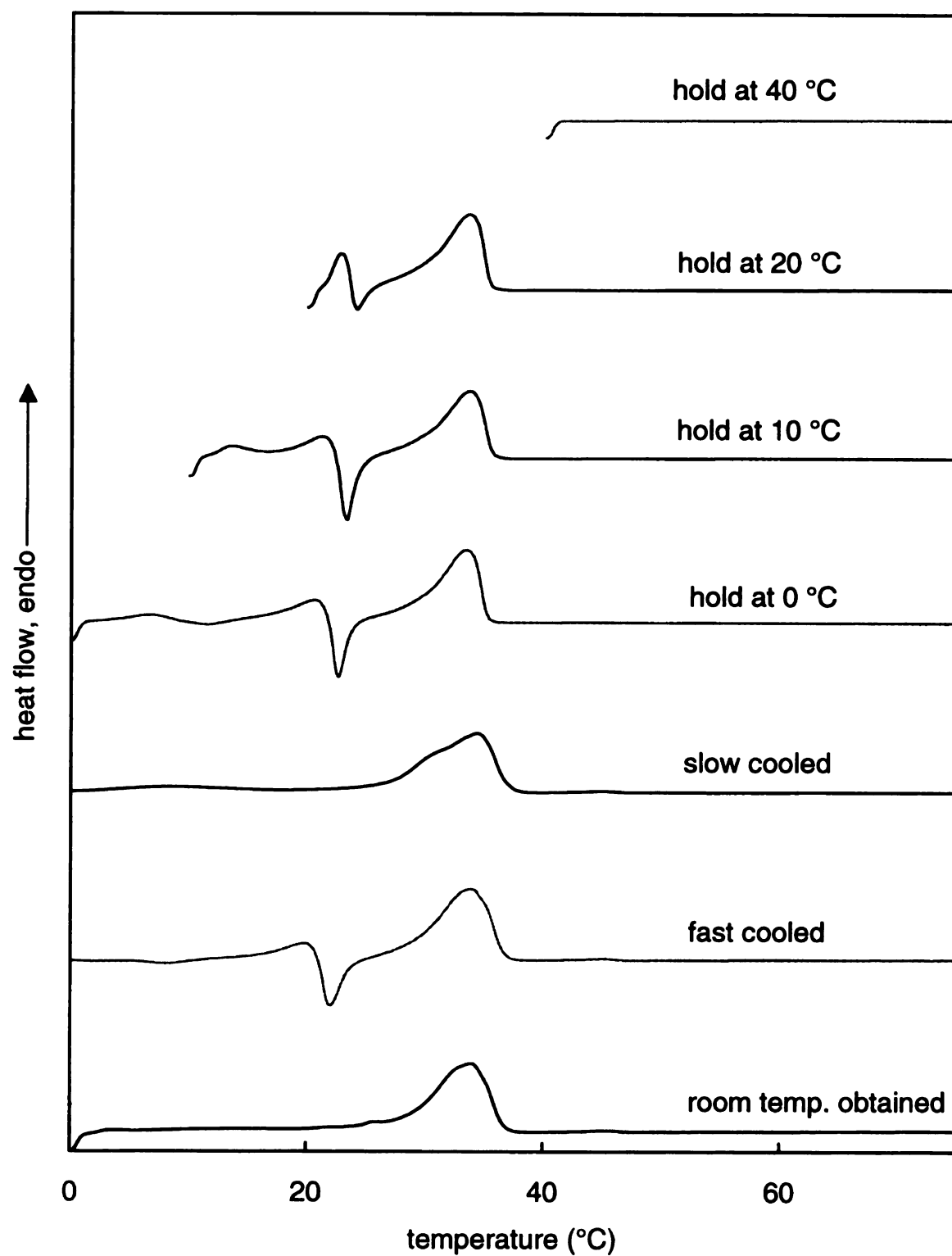


Figure 108. DSC heating scans of polymer $(C_9\pi C_9EO_7)_n$ with different crystallization histories.

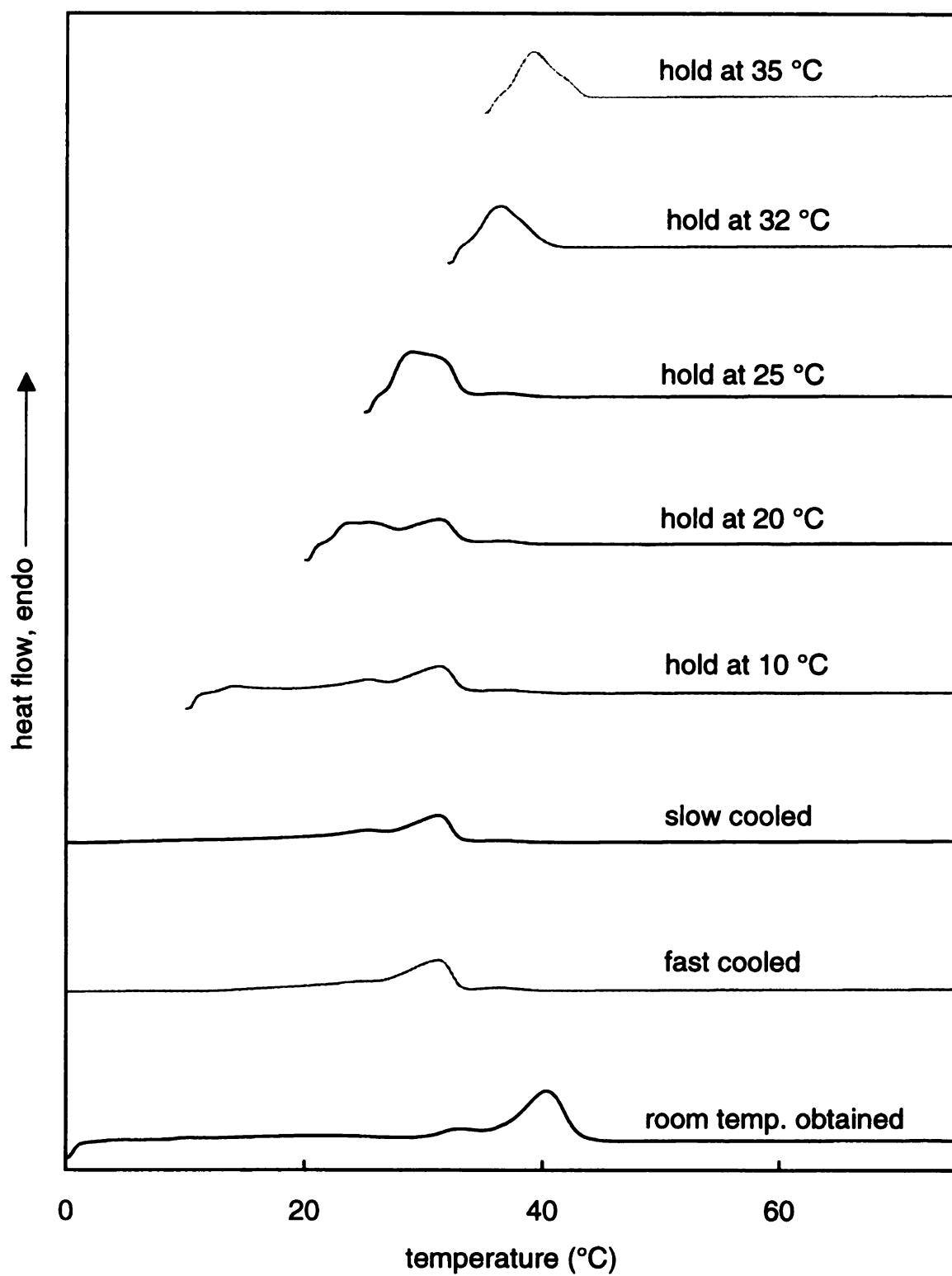


Figure 109. DSC heating scans of polymer $(C_9\pi C_9EO_8)_n$ with different crystallization histories.

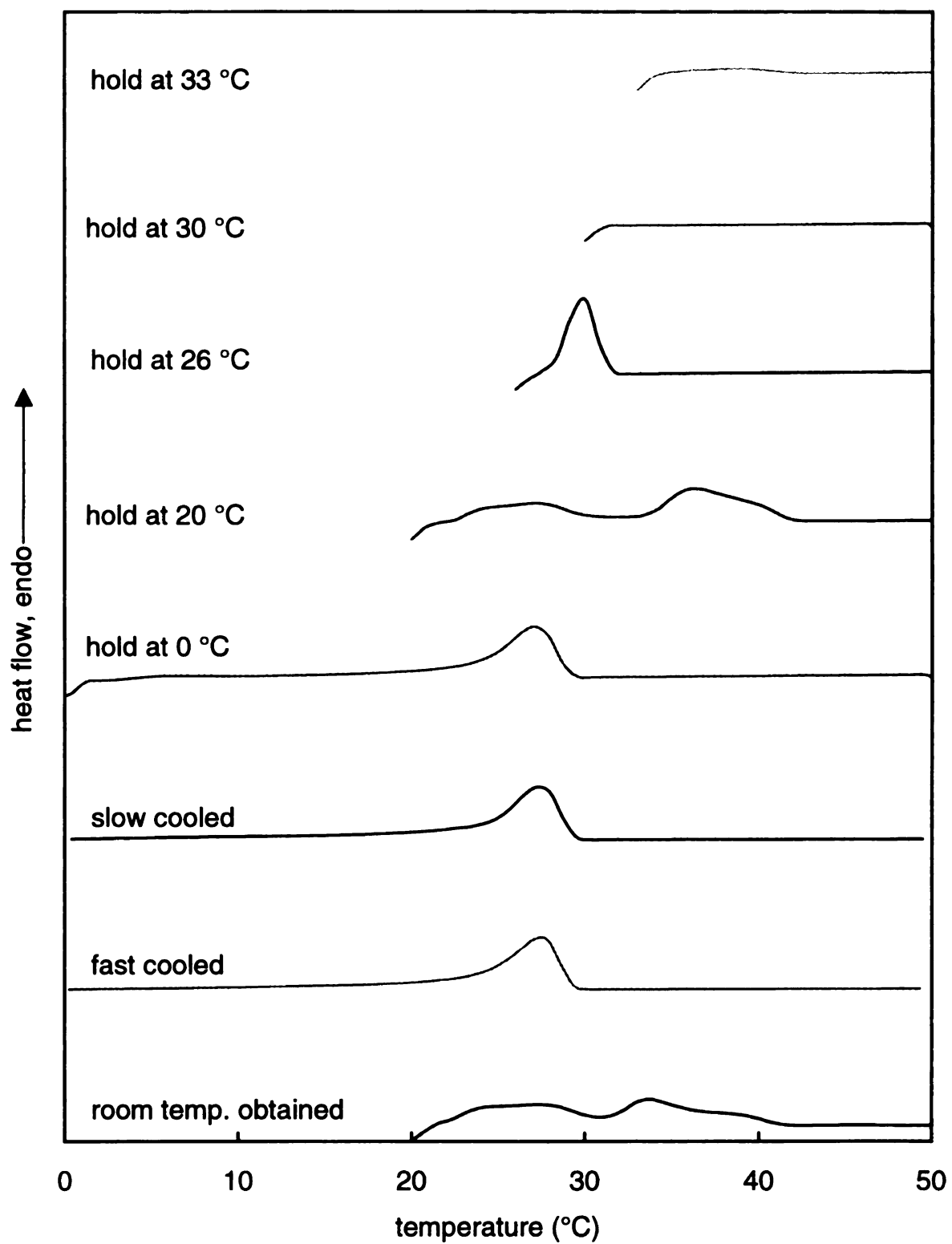


Figure 110. DSC heating scans of polymer $(C_9\pi C_9EO_{10})_n$ with different crystallization histories.

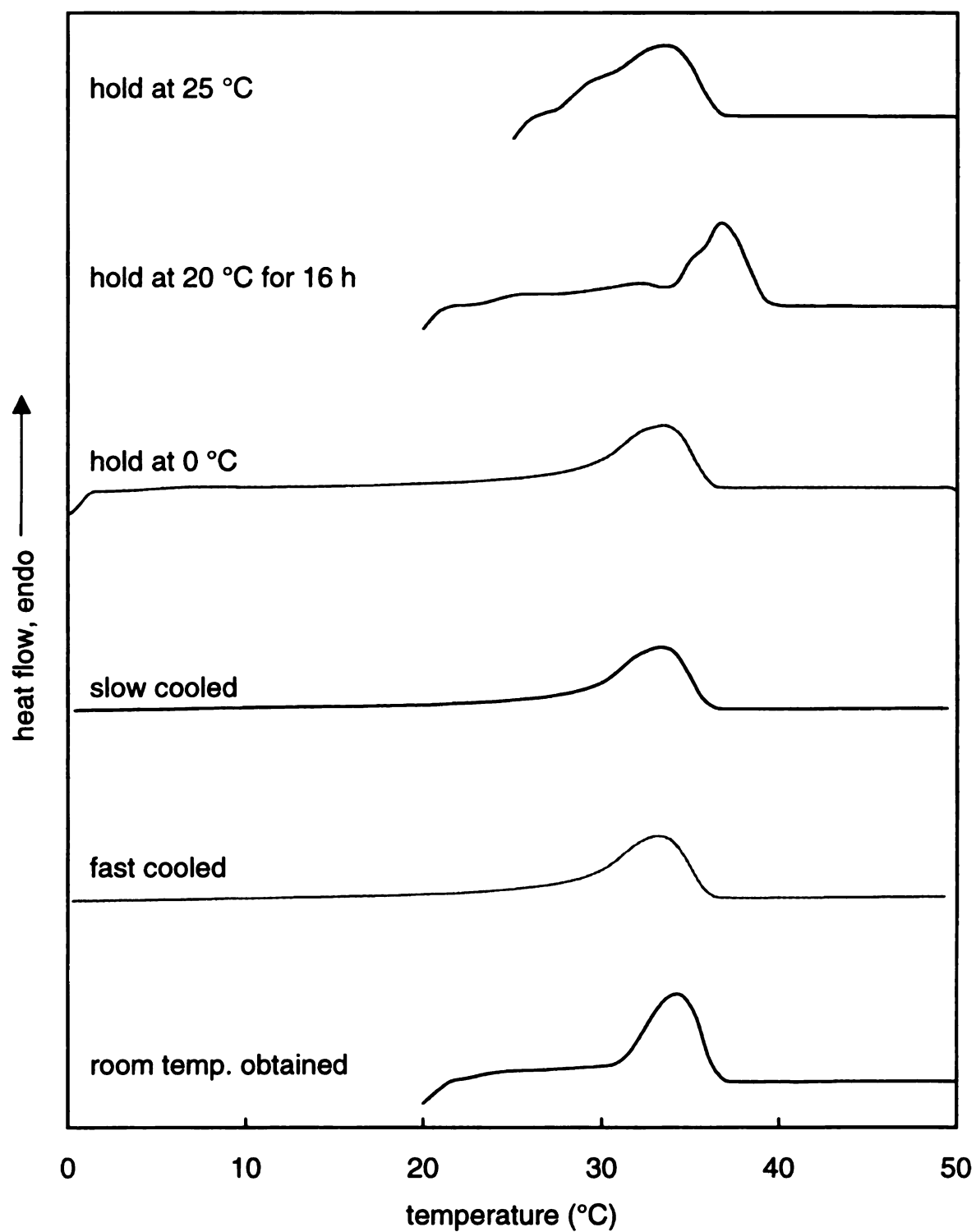


Figure 111. DSC heating scans of polymer $(C_9\pi C_9EO_{14})_n$ with different crystallization histories.

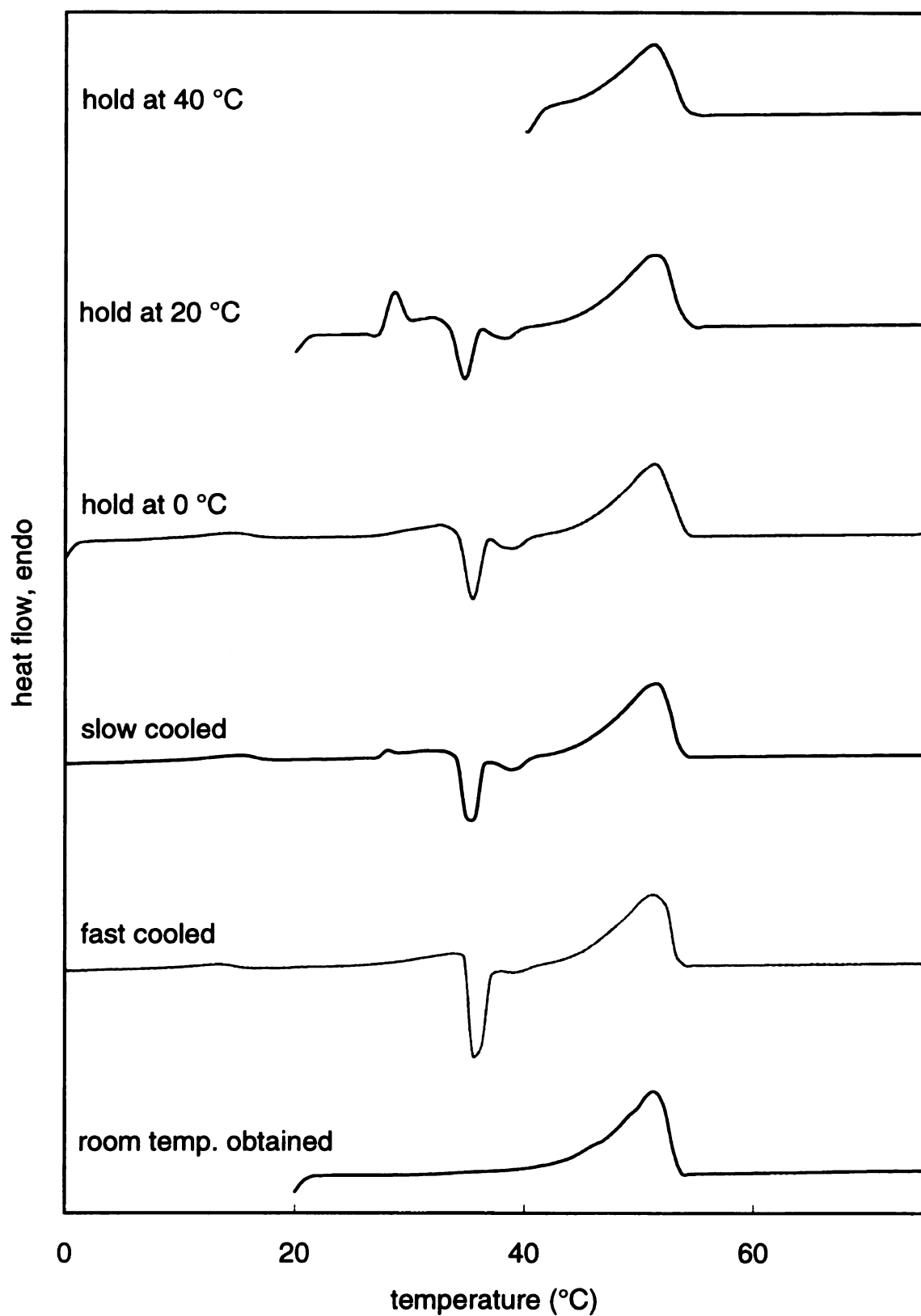


Figure 112. DSC heating scans of polymer $(C_{20}EO_7)_n$ with different crystallization histories.

BIBLIOGRAPHY

Bibliography

- 1) Morton, M. J. *Polym. Sci. Part C. Polym. Sym.* **1977**, 1-13.
- 2) Strobl, G. R. *The Physics of Polymers: Concepts for Understanding Their Structures and Behavior*; 2nd ed.; Springer-Verlag Berlin Heidelberg: New York, 1997.
- 3) Zhao, J.; Majumdar, B.; Schulz, M. F.; Bates, F. S.; Almdal, K.; Mortensen, K.; Hajduk, D. A.; Gruner, S. M. *Macromolecules* **1996**, 29, 1204-1215.
- 4) Sperling, L. H. *Introduction to Physical Polymer Science*; 2nd ed.; John Wiley & Sons, Inc.: New York, 1992.
- 5) Hasegawa, H.; Tanaka, H.; Yamasaki, K.; Hashimoto, T. *Macromolecules* **1987**, 20, 1651-1662.
- 6) Thomas, E. L.; Alward, D. B.; Kinning, D. J.; Martin, D. C.; Handlin, D. L.; Fetters, L. J. *Macromolecules* **1986**, 19, 2197-2202.
- 7) Forster, S.; Khandpur, A. K.; Zhao, J.; Bates, F. S.; Hamley, I. W.; Ryan, A. J.; Bras, W. *Macromolecules* **1994**, 27, 6922-6935.
- 8) Spontak, R. J.; Smith, S. D.; Ashraf, A. *Polymer* **1993**, 34, 2233-2236.
- 9) Spontak, R. J.; Smith, S. D.; Ashraf, A. *Macromolecules* **1993**, 26, 956-962.
- 10) Schulz, M. F.; Bates, F. S.; Almdal, K.; Mortensen, K. *Phys. Rev. Lett.* **1994**, 73, 86-89.
- 11) Hajduk, D. A.; Harper, P. E.; Gruner, S. M.; Honeker, C. C.; Kim, G.; Thomas, E. L.; Fetters, L. J. *Macromolecules* **1994**, 27, 4063-4075.
- 12) Phan, S.; Fredrickson, G. H. *Macromolecules* **1998**, 31, 59-63.
- 13) Matsushita, Y.; Nomura, M.; Watanabe, J.; Mogi, Y.; Noda, I.; Imai, M. *Macromolecules* **1995**, 28, 6007-6013.
- 14) Matsushita, Y.; Tamura, M.; Noda, I. *Macromolecules* **1994**, 27, 3680-3682.
- 15) Breiner, U.; Krappe, U.; Thomas, E. L.; Stadler, R. *Macromolecules* **1998**, 31, 135-141.

- 16) Auschra, C.; Stadler, R. *Macromolecules* **1993**, *26*, 2171-2174.
- 17) van Aert, H. A. M.; Sijbesma, R. P.; Fischer, H.; de Waal, B. F. M.; Gilberts, J.; Maas, J. H.; Broer, D.; Meijer, E. W. *Acta Polym.* **1998**, *49*, 18-26.
- 18) Stelzer, F.; Grubbs, R. H.; Leising, G. *Polymer* **1991**, *32*, 1851-1856.
- 19) Matsushita, Y.; Mogi, Y.; Mukai, H.; Watanabe, J.; Noda, I. *Polymer* **1994**, *35*, 246-249.
- 20) Zielinski, J. M.; Spontak, R. J. *Macromolecules* **1992**, *25*, 653-662.
- 21) Noshay, A.; McGrath, J. E. *Block Copolymers: Overview and Critical Survey*; Academic Press: New York, 1977.
- 22) Stupp, S. I.; LeBonheur, V.; Walker, K.; Li, L. S.; Huggins, K. E.; Keser, M.; Amstutz, A. *Science* **1997**, *276*, 384-389.
- 23) Zubarev, E. R.; Pralle, M. U.; Li, L. M.; Stupp, S. I. *Science* **1999**, *283*, 523-526.
- 24) Kanig, B. **1975**, *57*, 176.
- 25) el Maaty, M. I. A.; Hosier, I. L.; Bassett, D. C. *Macromolecules* **1998**, *31*, 153-157.
- 26) Vaughan, A. S.; Bassett, D. C. *Comprehensive Polymer Science*; Pergamon Press: New York, 1989; Vol. 2.
- 27) Li, W.; Yan, R. J.; Jiang, B. Z. *Polymer* **1992**, *33*, 889-892.
- 28) Ding, J. D.; Zhu, J. X.; Yang, Y. L. *Chem. J. Chin. Univ.-Chin.* **1996**, *17*, 498-499.
- 29) Hoffmann, J. D.; Frolen, L. J.; Ross, G. S.; Jr., J. I. L. *J. Res. NBS* **1975**, *79A*, 671.
- 30) Ergoz, E.; Fatou, J. G.; Mandelkern, L. *Macromolecules* **1972**, *5*, 147.
- 31) Barham, P. J.; Chivers, R. A.; Keller, A.; Martinezsalazar, J.; Organ, S. J. *J. Mater. Sci.* **1985**, *20*, 1625-1630.
- 32) Kovacs, A. J.; Straupe, C.; Gonthier, A. *J. Polym. Sci. Part C. Polym. Sym.* **1977**, *31-54*.
- 33) Tyagi, D.; Hedrick, J. L.; Webster, D. C.; McGrath, J. E.; Wilkes, G. L. *Polymer* **1988**, *29*, 833-844.
- 34) Lin, C. S.; Qutubuddin, S. *Polymer* **1994**, *35*, 4120-4126.
- 35) Lee, J. L.; Pearce, E. M.; Kwei, T. K. *Macromolecules* **1997**, *30*, 6877-6883.

- 36) Hashimoto, T.; Tsukahara, Y.; Tachi, K.; Kawai, H. *Macromolecules* **1983**, *16*, 648-657.
- 37) Ryan, A. J.; Fairclough, J. P. A.; Hamley, I. W.; Mai, S. M.; Booth, C. *Macromolecules* **1997**, *30*, 1723-1727.
- 38) Mai, S. M.; Fairclough, J. P. A.; Viras, K.; Gorry, P. A.; Hamley, I. W.; Ryan, A. J.; Booth, C. *Macromolecules* **1997**, *30*, 8392-8400.
- 39) Mortensen, K.; Talmon, Y.; Gao, B.; Kops, J. *Macromolecules* **1997**, *30*, 6764-6770.
- 40) Hamley, I. W.; Fairclough, J. P. A.; Ryan, A. J.; Bates, F. S.; TownsAndrews, E. *Polymer* **1996**, *37*, 4425-4429.
- 41) Seymour, R. W.; Estes, G. M.; Cooper, S. L. **1970**, *3*, 579.
- 42) Srichatrapimuk, V. W.; Cooper, S. L. *J. Macromol. Sci.-Phys.* **1978**, *B15*, 267-311.
- 43) Seymour, R. W.; Cooper, S. L. *J. Polym. Lett.* **1971**, *9*, 680.
- 44) Seymour, R. W.; Cooper, S. L. *Macromolecules* **1973**, *6*, 48.
- 45) Cerrada, M. L.; Perez, E.; Perena, J. M.; Benavente, R. *Macromolecules* **1998**, *31*, 2559-2564.
- 46) Wang, S.; Brisse, F. *Macromolecules* **1998**, *31*, 2265-2277.
- 47) Odian, G. *Principles of Polymerization*; 3rd Ed. ed.; John Wiley & Sons, Inc.: New York, 1991.
- 48) Xu, G. X. *Macromolecules* **1998**, *31*, 2395-2402.
- 49) Davis, F.; Hodge, P.; Towns, C. R.; Aliadib, Z. *Macromolecules* **1991**, *24*, 5695-5703.
- 50) Mormann, W.; Grimm, A. *Macromol. Chem. Phys.* **1997**, *198*, 1281-1291.
- 51) Yu, J. M.; Dubois, P.; Jerome, R. *Macromolecules* **1997**, *30*, 4984-4994.
- 52) Summers, G. J.; Quirk, R. P. *J. Polym. Sci. Pol. Chem.* **1998**, *36*, 1233-1241.
- 53) Mormann, W.; Tiemann, N.; Turuskan, E. *Polymer* **1989**, *30*, 1127-1132.
- 54) Finaz, G.; Rempp, P.; Parrod, J. *Bull. Soc. Chim. Fr.* **1962**, 262.
- 55) Fang, M. C.; Watanabe, A.; Matsuda, M. *Chem. Lett.* **1994**, 13-16.
- 56) Gibson, V. C. *Adv. Mater.* **1994**, *6*, 37-42.

- 57) Ivin, K. J. *Olefin Metathesis*; Academic Press: New York, 1983.
- 58) Grubbs, R. H.; Hoppin, C. R. *J. Chem. Soc.-Chem. Commun.* **1977**, 634-635.
- 59) Lindmarkhamberg, M.; Wagener, K. B. *Macromolecules* **1987**, 20, 2949-2951.
- 60) Nubel, P. O.; Lutman, C. A.; Yokelson, H. B. *Macromolecules* **1994**, 27, 7000-7002.
- 61) Schaverien, C. J.; Dewan, J. C.; Schrock, R. R. *J. Am. Chem. Soc.* **1986**, 108, 2771-2773.
- 62) Murdzek, J. S.; Schrock, R. R. *Organometallics* **1987**, 6, 1373-1374.
- 63) Schrock, R. R.; Depue, R. T.; Feldman, J.; Schaverien, C. J.; Dewan, J. C.; Liu, A. H. *J. Am. Chem. Soc.* **1988**, 110, 1423-1435.
- 64) Schrock, R. R.; Murdzek, J. S.; Bazan, G. C.; Robbins, J.; Dimare, M.; Oregan, M. *J. Am. Chem. Soc.* **1990**, 112, 3875-3886.
- 65) Fu, G. C.; Grubbs, R. H. *J. Am. Chem. Soc.* **1992**, 114, 5426-5427.
- 66) Nguyen, S. T.; Johnson, L. K.; Grubbs, R. H.; Ziller, J. W. *J. Am. Chem. Soc.* **1992**, 114, 3974-3975.
- 67) Fu, G. C.; Nguyen, S. T.; Grubbs, R. H. *J. Am. Chem. Soc.* **1993**, 115, 9856-9857.
- 68) Grubbs, R. H. *J. Macromol. Sci.-Pure Appl. Chem.* **1994**, A31, 1829-1833.
- 69) Lynn, D. M.; Kanaoka, S.; Grubbs, R. H. *J. Am. Chem. Soc.* **1996**, 118, 784-790.
- 70) Hillmyer, M. A.; Benedicto, A. D.; Nguyen, S. T.; Wu, Z.; Grubbs, R. H. *Macromol. Symp.* **1995**, 89, 411-419.
- 71) Walba, D. M.; Keller, P.; Shao, R. F.; Clark, N. A.; Hillmyer, M.; Grubbs, R. H. *J. Am. Chem. Soc.* **1996**, 118, 2740-2741.
- 72) Konzelman, J.; Wagener, K. B. *Macromolecules* **1996**, 29, 7657-7660.
- 73) Heroguez, V.; Gnanou, Y.; Fontanille, M. *Macromolecules* **1997**, 30, 4791-4798.
- 74) Heroguez, V.; Gnanou, Y.; Fontanille, M. *Macromol. Rapid Commun.* **1996**, 17, 137-142.
- 75) Heroguez, V.; Breunig, S.; Gnanou, Y.; Fontanille, M. *Macromolecules* **1996**, 29, 4459-4464.
- 76) Wolf, A.; Wagener, K. B. *Polym. Prepr.* **1991**, 31, 535.

- 77) Smith, D. W.; Wagener, K. B. *Macromolecules* **1993**, 26, 3533-3537.
- 78) Wagener, K. B.; Boncella, J. M.; Nel, J. G.; Duttweiler, R. P.; Hillmyer, M. A. *Makromol. Chem. Macro. Chem. Phys.* **1990**, 191, 365-374.
- 79) Wagener, K. B.; Boncella, J. M.; Nel, J. G. *Macromolecules* **1991**, 24, 2649-2657.
- 80) Ungar, G.; Stejny, J.; Keller, A.; Bidd, I.; Whiting, M. C. *Science* **1985**, 229, 386-389.
- 81) Boda, E.; Ungar, G.; Brooke, G. M.; Burnett, S.; Mohammed, S.; Proctor, D.; Whiting, M. C. *Macromolecules* **1997**, 30, 4674-4678.
- 82) Teare, P. W. *Acta Crystallogr.* **1959**, 12, 294.
- 83) Khoury, F.; Fanconi, B.; Barnes, J. D.; Bolz, L. H. *J. Chem. Phys.* **1973**, 59, 5849.
- 84) Kobayashi, M.; Kobayashi, T.; Itoh, Y.; Chatani, Y.; Tadokoro, H. *J. Chem. Phys.* **1980**, 72, 2024-2031.
- 85) Sullivan, P. K.; Weeks, J. J. *J. Res. NBS A* **1969**, 74, 203.
- 86) Reynhardt, E. C.; Fenrych, J.; Basson, I. *J. Phys.-Condes. Matter* **1994**, 6, 7605-7616.
- 87) Takamizawa, K.; Ogawa, Y.; Oyama, T. O. *Polym. J.* **1982**, 14, 441-456.
- 88) Kim, Y. S.; Strauss, H. L.; Snyder, R. G. *J. Phys. Chem.* **1989**, 93, 7520-7526.
- 89) Hagemann, H.; Strauss, H. L.; Snyder, R. G. *Macromolecules* **1987**, 20, 2810-2819.
- 90) Tashiro, K.; Sasaki, S.; Kobayashi, M. *Macromolecules* **1996**, 29, 7460-7469.
- 91) Jarrett, W. L.; Mathias, L. J.; Alamo, R. G.; Mandelkern, L.; Dorset, D. L. *Macromolecules* **1992**, 25, 3468-3472.
- 92) Mandelkern, L.; Alamo, R. G.; Sokolov, E. L.; Li, Y.; Chu, B. *Macromolecules* **1994**, 27, 2324-2326.
- 93) Dorset, D. L.; Alamo, R. G.; Mandelkern, L. *Macromolecules* **1992**, 25, 6284-6288.
- 94) Gray, F. M. *Solid Polymer Electrolytes--Fundamentals and Technological Applications*; VCH publishers, Inc.: New York, 1991.
- 95) Staudinger, H.; Lohmann, H. *Ann. Chim.* **1933**, 505, 41.
- 96) Hill, F. N.; Bailey, F. E.; Fitzpatrick, J. T. *Ind. Eng. Chem.* **1958**, 50, 5.

- 97) Tadokoro, H.; Chatani, Y.; Yoshihara, T.; Tahara, S.; Murahashi, S. *Makromol. Chem.* **1964**, *73*, 109-127.
- 98) Koenig, J. L.; Angood, A. C. *J. of Polymer Sci.: Part A-2* **1970**, *3*, 1787-1796.
- 99) Liu, K.-J.; Parsons, J. L. *Macromolecules* **1969**, *2*, 529-533.
- 100) Machida, K.; Miyazawa, T. *Spectr. Acta* **1964**, *20*, 1865-1873.
- 101) Matsuura, H.; Miyazawa, T. *Spectr. Acta* **1967**, *23A*, 2433-2447.
- 102) Matsuura, H.; Fukuhara, K. *J. Mol. Struct.* **1985**, *126*, 251-260.
- 103) Matsuura, H.; Fukuhara, K. *J. Polym. Sci. Pt. B-Polym. Phys.* **1986**, *24*, 1383-1400.
- 104) Yoshihara, T.; Tadokoro, H.; Murahashi, S. *J. Chem. Phys.* **1964**, *11*, 2902-2904.
- 105) Mullerplathe, F.; Vangunsteren, W. F. *Macromolecules* **1994**, *27*, 6040-6045.
- 106) Cooke, J.; Viras, K.; Yu, G. E.; Sun, T.; Yonemitsu, T.; Ryan, A. J.; Price, C.; Booth, C. *Macromolecules* **1998**, *31*, 3030-3039.
- 107) Viras, K.; Yan, Z. G.; Price, C.; Booth, C.; Ryan, A. J. *Macromolecules* **1995**, *28*, 104-109.
- 108) Yu, G. E.; Sinnathamby, P.; Sun, T.; Heatley, F.; Price, C.; Booth, C. *Macromol. Rapid Commun.* **1997**, *18*, 1085-1093.
- 109) Takahashi, Y.; Sumita, I.; Tadokoro, H. *J. of Polymer Sci.: Polymer Phys. Ed* **1973**, *11*, 2113-2122.
- 110) Tashiro, K.; Tadokoro, H. *Reports Prog. Poly. Phys. Jpn.* **1978**, *21*, 417-420.
- 111) Tadokoro, H.; Yoshihara, T.; Chatani, Y.; Murahashi, S. *J. Polym. Sci. B* **1963**, *2*, 363.
- 112) Delaite, E.; Point, J. J.; Damman, P.; Dosiere, M. *Macromolecules* **1992**, *25*, 4768-4778.
- 113) Iwamoto, R.; Saito, Y.; Ishihara, H.; Tadokoro, H. *J. of Polymer Sci.: Part A-2* **1968**, *6*, 1509-1525.
- 114) Yokoyama, M.; Ishihara, H.; Iwamoto, R.; Tadokoro, H. *Macromolecules* **1969**, *2*, 184-192.
- 115) Stone, F. W.; Stratta, J. J. *Encycloped. Polym. Sci. Technol.* **1967**, *6*, 103.
- 116) Beech, D. R.; Booth, C. *Polym. Lett.* **1970**, *8*, 731.

- 117) Cheng, S. Z. D.; Zhang, A. Q.; Barley, J. S.; Chen, J. H.; Habenschuss, A.; Zschack, P. R. *Macromolecules* **1991**, *24*, 3937-3944.
- 118) Cheng, S. Z. D.; Zhang, A. Q.; Chen, J. H.; Heberer, D. P. *J. Polym. Sci. Pt. B-Polym. Phys.* **1991**, *29*, 287-297.
- 119) Cheng, S. Z. D.; Chen, J. H. *J. Polym. Sci. Pt. B-Polym. Phys.* **1991**, *29*, 311-327.
- 120) Cheng, S. Z. D.; Chen, J. H.; Barley, J. S.; Zhang, A. Q.; Habenschuss, A.; Zschack, P. R. *Macromolecules* **1992**, *25*, 1453-1460.
- 121) Cheng, S. Z. D.; Chen, J.; Zhang, A.; Barley, J. S.; Habenschuss, A.; Zschack, P. R. *Polymer* **1992**, *33*, 1140-1149.
- 122) Cheng, S. Z. D.; Wu, S. S.; Chen, J. H.; Zhuo, Q. H.; Quirk, R. P.; Vonmeerwall, E. D.; Hsiao, B. S.; Habenschuss, A.; Zschack, P. R. *Macromolecules* **1993**, *26*, 5105-5117.
- 123) Talibuddin, S.; Bunt, J.; Liu, L. Z.; Chu, B. *Macromolecules* **1998**, *31*, 1627-1634.
- 124) Paternostre, L.; Damman, P.; Dosiere, M.; Bourgaux, C. *Macromolecules* **1996**, *29*, 2046-2052.
- 125) Chu, B.; Zhou, Z. in *Nonionic Surfactants: Polyoxyalkylene Block Copolymers*; Nace, V. M., Ed.; Marcel Dekker: New York, 1996; Vol. 60.
- 126) Sjoblom, J.; Stenius, P.; Danielsson, I. in *Nonionic Surfactants: Physical Chemistry*; Nace, V. M., Ed.; Marcel Dekker: New York, 1987; Vol. 23.
- 127) Fukuhara, K.; Matsuura, H. *Chem. Lett.* **1987**, 1549-1552.
- 128) Matsuura, H.; Fukuhara, K.; Masatoki, S.; Sakakibara, M. *J. Am. Chem. Soc.* **1991**, *113*, 1193-1202.
- 129) Matsuura, H.; Fukuhara, K. *J. Phys. Chem.* **1986**, *90*, 3057-3059.
- 130) Matsuura, H.; Fukuhara, K. *Chem. Lett.* **1984**, 933-936.
- 131) Corno, C.; Ghelli, S.; Perego, G.; Platone, E. *Colloid Polym. Sci.* **1991**, *269*, 1133-1139.
- 132) Dorset, D. L. *J. of Colloid and Interface Sci.* **1983**, *96*, 172-180.
- 133) Domszy, R. C.; Booth, C. *Makromol. Chem.* **1982**, *183*, 1051-1070.
- 134) Swales, T. G. E.; Teo, H. H.; Domszy, R. C.; Viras, K.; King, T. A.; Booth, C. *J. of Polymer Sci.: Polymer Phys. Ed.* **1983**, *21*, 1501-1511.

- 135) Swales, T. G. E.; Beddoes, R. L.; Price, C.; Booth, C. *Eur. Polym. J.* **1985**, *21*, 629-634.
- 136) Swales, T. G. E.; Domszy, R. C.; Beddoes, R. L.; Price, C.; Booth, C. *J. of Polymer Sci.: Polymer Phys. Ed.* **1985**, *23*, 1585-1595.
- 137) Teo, H. H.; Swales, T. G. E.; Domszy, R. C.; Heatley, F.; Booth, C. *Makromol. Chem.* **1983**, *184*, 861-877.
- 138) Yeates, S. G.; Teo, H. H.; Booth, C. *Makromol. Chem.* **1984**, *185*, 2474-2488.
- 139) Miesiac, I.; Merkwitz, H.; Szymanowski, J.; Beger, J. *J. of Colloid and Interface Sci.* **1986**, *114*, 425-431.
- 140) Fukuhara, K.; Masatoki, S.; Yonemitsu, T.; Matsuura, H. *J. Mol. Struct.* **1998**, *444*, 69-76.
- 141) Fukuhara, K.; Sakogawa, F.; Matsuura, H. *J. Mol. Struct.* **1997**, *405*, 123-131.
- 142) Fukuhara, K.; Sagawa, T.; Kihara, S.; Matsuura, H. *J. Mol. Struct.* **1996**, *379*, 197-204.
- 143) Masatoki, S.; Matsuura, H.; Fukuhara, K. *J. Raman Spectrosc.* **1994**, *25*, 641-645.
- 144) Muthiah, J.; Johnson, C. G.; Thompson, R. D.; Mathias, L. J. *Macromolecules* **1995**, *28*, 7796-7805.
- 145) Muthiah, J.; Mathias, L. J. *Macromolecules* **1995**, *28*, 7806-7816.
- 146) Zhang, T. H.; Litt, M. H.; Rogers, C. E. *J. Polym. Sci. Pol. Chem.* **1994**, *32*, 1323-1330.
- 147) Takahashi, Y.; Tadokoro, H.; Chatani, Y. *J. Makromol. Sci., Phys.* **1968**, *B2(2)*, 361.
- 148) Abe, A. *Macromolecules* **1980**, *13*, 546-549.
- 149) Rabolt, J. F.; Russell, T. P.; Twieg, R. J. *Macromolecules* **1984**, *17*, 2786-2794.
- 150) Russell, T. P.; Rabolt, J. F.; Twieg, R. J.; Siemens, R. L.; Farmer, B. L. *Macromolecules* **1986**, *19*, 1135-1143.
- 151) Mahler, W.; Guillon, D.; Skoulios, A. *Mol. Cryst. Liquid Cryst.* **1985**, *2*, 111-119.
- 152) Viney, C.; Russell, T. P.; Depero, L. E.; Twieg, R. J. *Mol. Cryst. Liquid Cryst.* **1989**, *168*, 63-82.
- 153) Viney, C.; Twieg, R. J.; Russell, T. P.; Depero, L. E. *Liq. Cryst.* **1989**, *5*, 1783-1788.

- 154) Hopken, J.; Moller, M. *Macromolecules* **1992**, *25*, 2482-2489.
- 155) Song, K.; Twieg, R. J.; Rabolt, J. F. *Macromolecules* **1990**, *23*, 3712-3714.
- 156) Twieg, R. J.; Rabolt, J. F. *Macromolecules* **1988**, *21*, 1806-1811.
- 157) Viney, C.; Twieg, R. J.; Gordon, B. R.; Rabolt, J. F. *Mol. Cryst. Liquid Cryst.* **1991**, *198*, 285-289.
- 158) Brace, N. O. *J. Am. Chem. Soc.* **1964**, *86*, 523.
- 159) Kostov, G. K.; Nikolov, A. T. *J. Appl. Polym. Sci.* **1995**, *55*, 1529-1536.
- 160) Wilson, L. M.; Griffin, A. C. *Macromolecules* **1993**, *26*, 6312-6314.
- 161) Davidson, T.; Griffin, A. C.; Wilson, L. M.; Windle, A. H. *Macromolecules* **1995**, *28*, 354-357.
- 162) Tanigami, T.; Yamaura, K.; Matsuzawa, S.; Ishikawa, M.; Mizoguchi, K.; Miyasaka, K. *Polymer* **1986**, *27*, 999-1006.
- 163) Tanigami, T.; Yamaura, K.; Matsuzawa, S.; Ishikawa, M.; Mizoguchi, K.; Miyasaka, K. *Polymer* **1986**, *27*, 1521-1528.
- 164) Farmer, B. L.; Lando, I. B. *J. Macromol. Sci. Phys. B* **1975**, *11*, 89.
- 165) Keegstra, E. M. D.; Zwikker, J. W.; Roest, M. R.; Jenneskens, L. W. *J. Org. Chem.* **1992**, *57*, 6678-6680.
- 166) Qiao, J. *Synthesis and Characterization of Ethylene Oxide-Segmented Polymers*; Michigan State University: East Lansing, 1996, pp 184.
- 167) Yu, G. E.; Sinnathamby, P.; Price, C.; Booth, C. *Chem. Commun.* **1996**, 31-32.
- 168) Small, P. A. **1953**, *3*, 71.
- 169) Brandrup, J.; Immergut, E. H. *Polymer Handbook*; 2nd ed.; Wiley-Interscience: New York, 1975.
- 170) Wagener, K. B.; Brzezinska, K. *Macromolecules* **1991**, *24*, 5273-5277.
- 171) Delgado, M.; Martin, J. D. *J. Org. Chem.* **1999**, *64*, 4798-4816.
- 172) Brandrup, J.; Immergut, E. H.; Grulke, E. A. *Polymer Handbook*; 4th ed.; John Wiley & Sons, Inc.: New York, 1999.
- 173) Lee, S.-W.; Chen, E.; Zhang, A.; Yoon, Y.; Moon, B. S.; Lee, S.; Harris, F. W.; Cheng, S. Z. D.; von Meerwall, E. D.; Hsiao, B. S.; Verma, R.; Lando, J. *Macromolecules* **1996**, *29*, 8816-8823.

- 174) Ouchi, M.; Inoue, Y.; Kanzaki, T.; Hakushi, T. *J. Org. Chem.* **1984**, *49*, 1408-1412.
- 175) Bartsch, R. A.; Liu, Y.; Kang, S. I.; Son, B.; Heo, G. S.; Hipes, P. G.; Bills, L. J. *J. Org. Chem.* **1983**, *48*, 4864-4869.
- 176) Fenton, D. E.; Parkin, D.; Newton, R. F. *J. Chem. Soc.-Perkin Trans. I* **1981**, 449-454.
- 177) Newcomb, M.; Moore, S. S.; Cram, D. J. *J. Am. Chem. Soc.* **1977**, *99*, 6405-6410.
- 178) Weber, E. *J. Org. Chem.* **1982**, *47*, 3478-3486.
- 179) Huszthy, P.; Bradshaw, J. S.; Zhu, C. Y.; Izatt, R. M.; Lifson, S. *J. Org. Chem.* **1991**, *56*, 3330-3336.
- 180) Kaatsrichters, V. E. M.; Zwikker, J. W.; Keegstra, E. M. D.; Jenneskens, L. W. *Synth. Commun.* **1994**, *24*, 2399-2409.
- 181) Warshawsky, A.; Kalir, R.; Deshe, A.; Berkovitz, H.; Patchornik, A. *J. Am. Chem. Soc.* **1979**, *101*, 4249-4258.
- 182) Newkome, G. R.; Nayak, A.; McClure, G. L.; Daneshkhoshboo, F.; Broussardsimpson, J. *J. Org. Chem.* **1977**, *42*, 1500-1508.
- 183) Gerhardt, W. *Monatsber. Dtsch. Akad. Wiss. Berlin* **1967**, 923-929.
- 184) Weber, E. **1983**, 770-801.
- 185) Gingras, B. A.; Bayley, C. H. *Can. J. Chem.* **1957**, *35*, 599-601.
- 186) Gingras, B. A.; Bayley, C. H. *Can. J. Chem.* **1958**, *36*, 1320.
- 187) Gloe, K.; Merkwitz, H.; Muhl, P.; Beger, J. *Z. Chem.* **1987**, *27*, 376-377.

MICHIGAN STATE UNIV. LIBRARIES



31293018230783